

## **INFORMATION TO USERS**

This manuscript has been reproduced from the microfilm master. UMI films the text directly from the original or copy submitted. Thus, some thesis and dissertation copies are in typewriter face, while others may be from any type of computer printer.

**The quality of this reproduction is dependent upon the quality of the copy submitted.** Broken or indistinct print, colored or poor quality illustrations and photographs, print bleedthrough, substandard margins, and improper alignment can adversely affect reproduction.

In the unlikely event that the author did not send UMI a complete manuscript and there are missing pages, these will be noted. Also, if unauthorized copyright material had to be removed, a note will indicate the deletion.

Oversize materials (e.g., maps, drawings, charts) are reproduced by sectioning the original, beginning at the upper left-hand corner and continuing from left to right in equal sections with small overlaps.

Photographs included in the original manuscript have been reproduced xerographically in this copy. Higher quality 6" x 9" black and white photographic prints are available for any photographs or illustrations appearing in this copy for an additional charge. Contact UMI directly to order.

ProQuest Information and Learning  
300 North Zeeb Road, Ann Arbor, MI 48106-1346 USA  
800-521-0600

**UMI<sup>®</sup>**



**UNIVERSITY OF OKLAHOMA  
GRADUATE COLLEGE**

**DEVELOPMENT OF A THREE-SEGMENT HYDRAULIC MODEL  
FOR CUTTINGS TRANSPORT IN HORIZONTAL AND DEVIATED  
WELLS**

**A DISSERTATION  
SUBMITTED TO THE GRADUATE FACULTY**

In partial fulfillment of the requirement for the  
Degree of

**Doctor of Philosophy**

By

**Hyun Cho**

**Norman, Oklahoma**

**2001**

UMI Number: 3025980

Copyright 2001 by  
Cho, Hyun

All rights reserved.

UMI<sup>®</sup>

---

UMI Microform 3025980

Copyright 2001 by Bell & Howell Information and Learning Company.

All rights reserved. This microform edition is protected against  
unauthorized copying under Title 17, United States Code.

---

Bell & Howell Information and Learning Company  
300 North Zeeb Road  
P.O. Box 1346  
Ann Arbor, MI 48106-1346

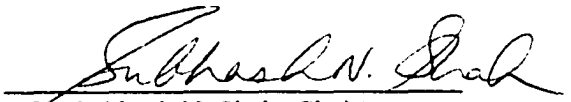
**© Copyright by Hyun Cho 2001**

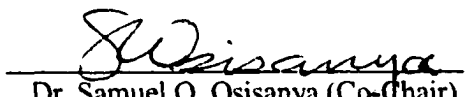
**All Rights Reserved.**

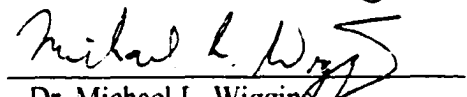
# **DEVELOPMENT OF A THREE-SEGMENT HYDRAULIC MODEL FOR CUTTINGS TRANSPORT IN HORIZONTAL AND DEVIATED WELLS**

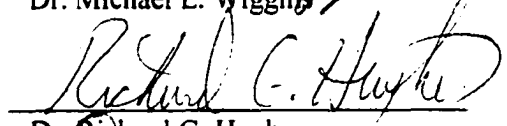
A Dissertation Approved for the  
Mewbourne School of Petroleum and Geological Engineering

BY

  
Dr. Subhash N. Shah (Chair)

  
Dr. Samuel O. Osisanya (Co-Chair)

  
Dr. Michael L. Wiggins

  
Dr. Richard G. Hughes

  
Dr. Daniel E. Resasco

## **DEDICATION**

This dissertation is dedicated to the memory of my father, Young-Chul, to my mother, Hoon, to my wife, Eun-Sook, and to my two boys, Yang-Hoon and Ji-Hoon for their love, sacrifices, and encouragement.

## **ACKNOWLEDGEMENTS**

I would like to express my sincere gratitude to Dr. Subhash N. Shah for his support in all matters related to the difficult challenge imposed by cuttings transport research. Dr. Shah provided me with the opportunity to know, work with, and learn from a group of excellent experts at the Well Construction Technology Center (WCTC) at the University of Oklahoma. Communication with them has greatly enriched my knowledge about the current industry's concerns as well as the state-of-the-art research. Without this precious experience and the generous support of Dr. Shah, the completion of this dissertation would not be possible.

I am also extremely grateful to Dr. Samuel O. Osisanya, the co-chair of my doctoral advisory committee, for his support and invaluable guidance throughout the course of this research. The author appreciates and is indebted to Dr. Michael L. Wiggins, Dr. Richard Hughes, and Dr. Daniel E. Resasco for their thorough reviews, helpful comments, and suggestions as members of my doctoral advisory committee. Many important technical concepts were acquired during the courses taken from them.

Special thanks are also due to Mr. Milt Bishop, Mr. Joe Flenniken, Mr. Max Mefford, Ms. C.K. Westbrook, and Dr. Joao Tadeu Vidal de Sousa at the WCTC for their friendly support and open door policy. I would like to thank Mr. Francis Tuedor, director of Network of Excellence in Training for his suggestions based on industry's concerns.

Many thanks are also extended to Dr. Naval Goel, Sudhakar D. Khade, and Ameet S. Raichurkar, my colleagues at the WCTC, for their suggestions and help. A special note



of gratitude is due to Ivan R. Gil, former officemate and classmate, whose contributions and suggestions have aided so much.

I would like to thank my family members; my mother, Hoon, who always loves me and has always been ready to help by praying; my elder brother, Une, who loves me in his own special way; and my elder sister, Jung-Hae, who supports me with her versatile mind and guides me in every aspect; my brother-in-law, Yun-Seok Suh, for his pray and support.

Finally, I give thanks to my wife, Eun-Sook, for her unfailing encouragement and love, and my two boys, Yang-Hoon and Ji-Hoon for their moments of joy. This work is dedicated to them with love.

Without all of this love, support, encouragement, understanding, sacrifice, and patience, the completion of this work would not have been possible.

Hyun Cho

Norman, Oklahoma

September 2001

## **ABSTRACT**

A new mathematical model is presented to overcome the limitations in existing hydraulic models used to predict cuttings transport when drilling a horizontal or deviated well. A new three-segment (a horizontal and near horizontal segment, a vertical and near vertical segment, and a transit segment) hydraulic model under two-phase (solid-liquid) flow in an annulus was developed to predict and interpret cuttings transport mechanisms. In particular, the model developed in this study advances a three-layer (a stationary bed layer of drilled cuttings at the bottom, a moving bed layer above it, and a heterogeneous suspension layer at the top) hydraulic model for the horizontal and near horizontal segment. An existing two-layer model was modified for a transit segment, and a one-layer model is used for the vertical and near vertical segment.

This study describes the model development for each segment, the combination of each model, the solution, and the simulation results of the combined three-segment model. To ensure a comprehensive understanding of the effects of the parameters affecting cutting transport efficiency, the simulation under drilling mode was performed. This involves build-up of cuttings-bed and the cuttings transport out of an existing cuttings-bed.

The concept of minimum anti-sliding velocity (MASV) of the cuttings-bed was developed for the transit segment. From a cuttings transport point of view, this segment is the most critical and difficult based on the inter-relationship between parameters. These parameters involve fluid rheology, wellbore deviation, interfacial friction between a suspension layer and a cuttings-bed, and in-situ fluid velocity in a suspension layer. For

this segment, the following were quantitatively analyzed: cuttings-bed distribution with its wellbore deviation, cuttings-bed movement and its direction, MASV, and pressure gradient.

In this study a user friendly simulator, CT-WellClean<sup>®</sup>, was developed based on the three-segment hydraulic model. This simulation program is capable of predicting the cuttings transport in coiled tubing while drilling under the following conditions: fluid pumping rate, fluid rheological characteristics, wellbore geometry, formation characteristics, and wellbore deviation. In addition, it is capable of providing solutions to problems related to selection of drilling fluids and prediction of frictional pressure losses of drilling hydraulic systems. This simulation program also allows drilling engineers to simulate all possible in-situ drilling conditions, resulting in the proper design of drilling programs and selection of fluid systems.

The simulation results of CT-WellClean<sup>®</sup> show how to obtain a reasonable pumping velocity, and how to optimize the rheology of drilling fluids for the lowest possible pressure gradient. These results can serve as an operational guideline for the design of a drilling program. Moreover, sensitivity analyses of the effects of the parameters that affect the efficiency of cuttings transport were performed. The results of the sensitivity analysis are compared with published experimental data. Finally, the observed agreement and discrepancies concerning these results are also discussed.

## **TABLE OF CONTENTS**

## **ACKNOWLEDGEMENTS**

## **ABSTRACT**

## **LIST OF TABLES**

## **LIST OF FIGURES**

## **CHAPTER**

### **I. FORMULATION OF THE PROBLEM**

1.1 Introduction .....	1
1.2 Literature Review .....	4
1.3 Objectives and Methodology .....	10
1.3.1 Objectives .....	10
1.3.2 Methodology .....	11

### **II. THEORETICAL BACKGROUND OF CUTTINGS TRANSPORT MECHANISM**

2.1 Introduction .....	14
2.2 Factors Affecting Cuttings Transport .....	15
2.3 Coiled Tubing Hydraulics .....	18
2.3.1 Background and Significance .....	18
2.3.2 Friction Pressure Losses in Straight Tubing .....	19
2.3.3 Friction Pressure Losses in Annuli .....	25

2.4 Cuttings Transport Mechanism .....	29
2.4.1 Classification of Cuttings Transport .....	29
2.4.2 Settling Velocity and Drag Coefficient .....	33
2.4.3 Lifting and Sliding/Rolling .....	41
2.4.4 Cuttings Volumetric Concentration .....	44
2.4.5 Suspension .....	51

### III. A THREE-LAYER MODEL FOR COILED-TUBING HORIZONTAL DRILLING

3.1 Introduction .....	59
3.2 Model Hypotheses and Descriptions .....	60
3.2.1 Model Hypothesis .....	60
3.2.2 Model Description .....	61
3.3 Model Development .....	63
3.3.1 Continuity Equations .....	64
3.3.2 Momentum Equations .....	66
3.3.3 Moving Bed Velocity .....	68
3.3.4 Summary of the Model .....	69
3.4 Solution of the Model .....	70
3.5 Model Simulation Results and Discussion .....	72
3.5.1 Effects of Nominal Annular Velocity in the Annulus .....	72
3.5.2 Analysis of Pressure Gradient .....	77
3.5.3 Effects of Drilling Fluid Rheology .....	81
3.5.4 Effects of Other Drilling Parameters .....	83

3.6	Summary .....	88
-----	---------------	----

#### IV. A THREE-SEGMENT HYDRAULIC MODEL

4.1	Introduction .....	89
4.2	Model Description .....	90
4.2.1	Basis for Model Development .....	90
4.2.2	Model Description .....	92
4.3	Model Development .....	95
4.3.1	Horizontal Segment .....	95
4.3.2	Transit Segment .....	99
4.3.3	Vertical Segment .....	102
4.3.4	Summary of the Model .....	103
4.4	Solutions .....	104
4.4.1	Horizontal Segment .....	104
4.4.2	Transit Segment .....	105
4.5	Model Simulation Results and Discussion .....	107
4.5.1	Effects of Nominal Annular Velocity in the Annulus .....	108
4.5.2	Analysis of Pressure Gradient .....	114
4.5.3	Effects of Fluid Rheology .....	121
4.5.4	Effects of Fluid Density .....	124
4.5.5	Effects of Borehole Size .....	129
4.5.6	Effects of Cuttings Specific Gravity .....	131
4.5.7	Effects of Rate of Penetration .....	134

4.5.8	Effects of Cuttings Size .....	139
4.6	Summary .....	142
 <b>V. CUTTINGS BED CHARACTERIZATION IN TRANSIT SEGMENT</b>		
5.1	Introduction .....	145
5.2	Model Description .....	146
5.3	Model Development .....	148
5.3.1	Continuity Equations .....	148
5.3.2	Momentum Equations .....	150
5.3.3	Suspension of Drilled Cuttings .....	151
5.3.4	Minimum Anti-Sliding Velocity .....	152
5.3.5	Cuttings-bed Movement .....	154
5.3.6	Fluid Flow Through Cuttings-Bed .....	156
5.4	Model Simulation Results and Discussion .....	157
5.4.1	Local Velocity Distribution .....	158
5.4.2	Forces Acting on Cuttings-Bed .....	158
5.4.3	Rheology Effects .....	166
5.4.4	Cuttings-Bed Movement .....	169
5.4.5	Fluid Flow Through a Porous Cuttings-Bed .....	173
5.5	Summary .....	178
 <b>VI. DEVELOPMENT PROCESS OF THE SIMULATION PROGRAM</b>		
6.1	Introduction .....	180

6.2	Development of the Simulation Program, ©CT Drilling .....	181
6.2.1	Selection of User Input Parameters .....	181
6.2.2	Development of Algorithm .....	189
6.2.3	Graphic Data Processing .....	192
6.3	Description of the Simulation Program .....	193
6.3.1	Program Description .....	193
6.3.2	Iteration Calculation .....	194
6.3.3	Integration of Simulation Results .....	197
6.3.4	Hydraulics Reference Module .....	198
6.4	Program Layout .....	202
6.5	User Interface.....	204
6.6	Summary .....	210
VII.	SUMMARY, CONCLUSIONS, AND RECOMMENDATIONS	
7.1	Summary and Conclusions .....	211
7.2	Recommendations .....	214
	<b>NOMENCLATURE .....</b>	<b>216</b>
	<b>REFERENCES .....</b>	<b>223</b>



## **APPENDIX**

<b>A</b>	<b>Drag Coefficient and particle Reynolds Number.....</b>	<b>232</b>
<b>B</b>	<b>Solution of Diffusivity Equation .....</b>	<b>237</b>
<b>C</b>	<b>Wellbore Geometry .....</b>	<b>241</b>
<b>D</b>	<b>Derivation of Minimum Moving Bed Velocity .....</b>	<b>250</b>
<b>E</b>	<b>Hierarchy Chart to Solve Cuttings-Bed Distribution .....</b>	<b>255</b>
<b>F</b>	<b>Hierarchy Chart for the Calculation of Cuttings-bed Velocity and its MASV .</b>	<b>257</b>
<b>G</b>	<b>Hierarchy Chart to Estimate Frictional Pressure Losses .....</b>	<b>259</b>

## LIST OF TABLES

2.1	Constants for Shah's correlation .....	22
2.2	Constants and equations for the Shah's roughness correction factor for $f$ ...	23
2.3	Two-factor factorial test design and results of the cuttings volumetric concentrations .....	48
2.4	ANOVA for cuttings volumetric concentrations .....	49
2.5	Statistical analysis of cuttings volumetric concentration.....	50
3.1	Selection of simulation parameters .....	72
3.2	Simulated data with the change of the annular nominal velocity for the base case .....	73
3.3	Simulation data of the gradient with the change of annular nominal Velocity (base case) .....	78
4.1	Fraction of each cuttings-bed layer (base case) .....	118
4.2	Fluid systems used in comparison .....	121
4.3	Fluid systems used in the comparison of fluid density effects.....	126
5.1	Effect of cuttings-bed movement on pressure gradient (base case).....	172
5.2	Effects of fluid flow in a porous cuttings-bed on frictional pressure gradient (base case, without gravitational force).....	176
6.1	Summary of simulation limitation of each parameters .....	191

## LIST OF FIGURES

2.1	Key variables affecting the cuttings transport .....	17
2.2	Typical eccentricity of coiled tubing in wellbore .....	27
2.3	Direction of cuttings slip related to carrier fluid direction .....	33
2.4	Comparison of particle Reynolds number and drag coefficient (Power-law model: $n = 0.68$ , $K = 0.006 \text{ lb}_f\text{s}^n/\text{ft}^2$ ) .....	38
2.5	Particle Reynolds number and settling shear rate (Power-law model: $n = 0.68$ , $K = 0.006 \text{ lb}_f\text{s}^n/\text{ft}^2$ ) .....	39
2.6	Cuttings settling velocity with the different nominal cutting diameters (Power-law model: $n = 0.68$ , $K = 0.006 \text{ lb}_f\text{s}^n/\text{ft}^2$ ) .....	40
2.7	Forces acting on a particle at the lower stratum .....	43
2.8	Cubic and rhombohedral packing/pore space with uniform spheres .....	45
2.9	Experimental apparatus for the measurement of cuttings volumetric Concentration.....	46
2.10	Wall shear stress vs. nominal shear rate for homogeneous and heterogeneous slurries.....	54
2.11	Critical resuspension velocity in slurry flow .....	54
2.12	Factors that affect cuttings suspension .....	55
3.1	Schematic illustration of different cuttings transport modes .....	63
3.2	Schematic diagram of the three-layer model; geometry, velocity, and shear stress .....	65
3.3	Forces acting on a particle at the lower stratum of a moving bed .....	70
3.4	Cuttings-bed distribution of each layer in horizontal well (base case) .....	74
3.5	Cuttings-bed height distribution of each layer (base case) .....	76
3.6	Comparison of pressure drop profile with a three-layer model (base case) .....	79

3.7	Relationship between the pressure gradient and the height of the stationary bed .....	80
3.8	Effects of fluid behavior index on the cuttings-bed area with 3.5 ft/s nominal annular velocity . ....	82
3.9	Cuttings concentrations in the suspension layer vs. nominal annular velocity (base case) .....	84
3.10	Average velocity profile of the suspension layer and the moving bed with the change in nominal annular velocity (base case) .....	85
3.11	Comparison of Total annular cuttings concentration and carrying capacity .....	87
4.1	Schematic diagram of the two-layer model for transit segment .....	94
4.2	Forces acting on particles at the vertical segment .....	95
4.3	Schematic diagram of a three-layer model for the horizontal segment .....	96
4.4	Forces acting on a particle at the lower stratum of the moving bed in a deviated wellbore .....	99
4.5	Cuttings-bed distribution with the wellbore deviation from the vertical position ( $U_a = 3$ ft/s) .....	109
4.6	Velocity of dispersed suspension layer at nominal annular velocity of 3 ft/s (base case) .....	110
4.7	Comparison of cuttings stationary bed area with experimental data (taken from Tomren <sup>17</sup> ) .....	112
4.8	Effect of nominal annular velocities on the cuttings-bed (base case).....	113
4.9	Effect of the wellbore deviation on particle concentration (experimental data taken from Tomren <sup>9</sup> ) .....	115
4.10	Comparison of pressure drop for horizontal section with different three-layer model (base case) .....	116
4.11	Effect of wellbore deviation on pressure gradient (base case) .....	119
4.12	Pressure gradient without gravitational effect of different nominal annular velocities (base case) .....	120

4.13	Effect of fluid rheology on the cuttings stationary bed area ( $U_a = 3$ ft/s).....	122
4.14	Effect of fluid rheology on pressure gradient ( $U_a = 3$ ft/s).....	123
4.15	Effects of fluid density on cuttings-bed distribution.....	125
4.16	Fluid density effects on critical fluid velocity vs. wellbore deviation (borehole: 5", drillpipe: 2-5/8", cutting size: 0.25", ROP: 55 ft/hr, experimental data taken from Hemphill and Larsen <sup>83</sup> ).....	127
4.17	Comparison of tube and annulus velocity profile of 4 lb <sub>m</sub> /Mgal HEC in 0.692-in. * 0.375-in. annulus (experimental taken from Zamora <sup>84</sup> ).....	129
4.18	Effects of the ratio of a wellbore diameter to a coiled tubing diameter (base case).....	132
4.19	Effects of borehole size on cuttings transport efficiency of horizontal Well (base case, $U_a = 3$ ft/s) .....	133
4.20	Effects of cuttings specific gravity on cuttings-bed distribution And pressure gradient of horizontal well.....	135
4.21	Comparison of ROP effects on cuttings-bed height for horizontal well (Fluid A, wellbore: 5", coiled tubing: 2-3/8-in, particle size: 0.025", experimental data taken from Li and Walker <sup>32</sup> ) .....	137
4.22	Effects of ROP on cuttings transport efficiency with wellbore deviation ....	138
4.23	Effects of particle size on cuttings transport efficiency in horizontal Segment (base case, $U_a = 3$ ft/s) .....	140
4.24	Effects of particle size on cuttings-bed distribution and pressure Gradient (base case, $U_a = 3$ ft/s) .....	141
5.1	Cuttings-bed velocity profile with its area fraction (base case) .....	159
5.2	Hydrodynamic friction force acting on the cuttings-bed (base case, $U_a = 3$ ft/s) .....	160
5.3	Forces acting on cuttings-bed (base case and $U_a = 3$ ft/s) .....	161
5.4	Comparison of $F_b$ and $F_{hf}$ with nominal annular velocity of 3 ft/s (base case) .....	163
5.5	Comparison of $F_b$ and $F_{hf}$ with nominal annular velocity of 4 ft/s (base case) .....	164

5.6	Minimum anti-sliding velocity with the different nominal annular velocity (base case) .....	165
5.7	Effect of rheology on minimum anti-sliding velocity ( $U_a = 3$ ft/s) .....	167
5.8	Comparison of $F_b$ and $F_{hf}$ with fluid A ( $U_a = 3$ ft/s) .....	168
5.9	Effects of fluid density on MASV (base case, $U_a = 3$ ft/s).....	170
5.10	Cuttings-bed velocity with different nominal annular velocity (base case) .	171
5.11	Effects of fluid flow in a porous cuttings-bed on pressure loss (base case).....	174
5.12	Comparison of frictional pressure drop with and without the effects of fluid flow in a porous cuttings-bed (base case, $U_a = 2.5$ ft/s).....	175
5.13	Comparison of frictional pressure drop of fluids flow in a porous Cuttings-bed (base case, $U_a = 3$ ft/s).....	177
6.1	Wellbore geometry for the angle build and hold .....	187
6.2	The user interface for a calculation of frictional pressure .....	188
6.3	The user interface for the hydraulic reference module .....	202
6.4	Program Layout of CT - WellClean® .....	204
6.5	The user interface for the selection of simulation methods .....	205
6.6	The user interface for input angles.....	206
6.7	The user interface for fluid data.....	207
6.8	The user interface for general input data .....	208
6.9	Graphical output of a simulation result.....	209

# **CHAPTER ONE**

## **FORMULATION OF THE PROBLEM**

### **1.1 Introduction**

It has been recognized for many years that the removal of the cuttings from a wellbore during the drilling of horizontal and deviated wells poses special problems. Insufficient hole cleaning leads to accumulation of cuttings in the annulus especially of a deviated wellbore. As the cuttings settle in the drilling fluid, a cuttings-bed is formed along the bottom of the hole. This may cause severe drilling problems including excessive over-pull on trips, high drag and torque, stuck pipe, hole pack-off, wellbore steering problems, excessive equivalent circulating density, formation break down, premature bit wear, slow ROP, and difficulty in running casing and logs.<sup>1</sup>

Drilled cuttings tend to settle out of drilling fluids on the lower side of the wall in annulus because of the density difference between the solids and the carrier fluid. Knowledge of the dynamics of cuttings transport mechanism and cuttings settling is essential to the design of effective transport systems. These systems involve pumping rates of drilling fluid, rheological properties, and ROP for a given wellbore configuration.

An investigation by Amoco<sup>2</sup> showed that 70% of lost time, due to unscheduled events, was associated with the sticking of the drilling string in deviated wells. A case study by Hopkins<sup>3</sup> showed that one third of all stuck pipe problems are due to insufficient wellbore cleaning. A single stuck pipe incident may cost over one million dollars depending on the situation.<sup>1</sup> Bradley et al.<sup>4</sup> reported that stuck pipe costs for the oil and gas industry were in the range of 100 to 500 million US dollars per year.

In an attempt to avoid such problems, drilling operators often include such practices as washing and reaming as the drilling fluid is circulated and the drilling bit is intruded into the wellbore; and back reaming, wherein the drilling fluid is circulated and the bit is withdrawn from the wellbore. Other operations, such as a wiper trip, are often performed to attempt to control the amount of cuttings accumulated in the wellbore.<sup>1</sup> All these operations require time and can significantly add to the costs of drilling horizontal and deviated wells.

In the last two decades, considerable efforts have been made to solve cuttings transport problems in horizontal and highly deviated wellbores. These efforts can be categorized into two main approaches. One is an empirical approach in which researchers begin with experimental work to obtain data from scale-up models and then correlate this data by dimensional analysis or semi-theoretical reasoning. The other approach is a theoretical study in which researchers develop sets of mathematical equations by analyzing the forces, stresses, and momentum acting during the cuttings transport process. They then solve these equations with certain physical or mathematical assumptions(boundary conditions).<sup>5</sup>



There are numerous mathematical (analytical and numerical) and empirical models for the prediction and interpretation of hydraulics of cuttings transport mechanism. Common problems with most of these cuttings transport models include inaccurate predictions, when compared with the experimental results or in-situ drilling results, and discrepancy between the models<sup>6</sup> There seem to be two main reasons for these problems. First, researchers make ambitious attempts to develop comprehensive models that cover a wide range of conditions (from vertical to horizontal) simply as a function of wellbore deviation. Azar and Sanchez<sup>6</sup> noted that researchers used the same methodology for different physical phenomena that occur under different conditions. Second, researchers make too many assumptions or neglect certain observed phenomena.

Thus, a new mathematical model is necessary to overcome some of the limitations of the existing hydraulic models.

## **1.2 Literature Review**

Since researchers were interested mainly in vertical wells, attention was focused on prediction of the rheology effects and flow rates on drilling operations by knowing the slip velocity of the cuttings.<sup>6</sup> By the end of the 70's, several studies<sup>7,8</sup> developed correlations for slip velocity, related to cuttings transport efficiency in vertical wells, between fluid rheology and physical characteristics of drilled cuttings.

The advent of horizontal and deviated well drilling, due to economic benefits, has led to various attempts to resolve cuttings transport problems. Horizontal wells are drilled to exploit reservoirs exhibiting thin pay zones. resolve problems with water and gas

coning, obtain greater drainage area, and maximize the productive potential in naturally fractured reservoirs. However, a major deterrent to horizontal drilling is the removal of drilled cuttings. Several cuttings transport models (mathematical and empirical) have been developed.<sup>9-17</sup> Reviewing these works can enhance understanding of how researchers approach this problem and what other problems they might have.

Tomren<sup>9</sup> performed one of the first practical studies on cuttings transport in deviated wellbores. He identified the existence of three different layers that might occur during the flow of drilling fluid and cuttings in a wellbore: a stationary bed, a sliding bed and a heterogeneous suspension layer. Ford et al.<sup>10</sup> later confirmed these observations. These experimental observations were used as a basis for a two-layer flow model presented by Gavignet and Sobey.<sup>11</sup> They assumed that the cuttings fell to the lower part of the deviated wellbore, and formed a cuttings-bed that slid up the annulus. Above this cuttings-bed, a second layer of pure drilling fluid exists. Consideration of the momentum balance for each of the two layers enabled the deposit bed thickness to be estimated as a function of nominal annular velocity and fluid rheology. Neither the cuttings suspension nor the stationary bed's effects on the transport mechanism were considered in the model.

Walton<sup>12</sup> developed a mathematical model to describe the suspension mechanism of drilled cuttings. He introduced a concept of particle diffusion in the fluid flow zone over the cuttings-bed. He solved a diffusivity equation for the particle concentration in a suspension layer. This mathematical model was developed based on analysis of forces and stresses acting on a cuttings-bed and a suspension layer. His model consists of a stationary bed at the bottom and suspension layer at the top. The rolling/sliding mechanisms of cuttings transport found in a horizontal segment were not considered in

this model. Solids suspension under strong turbulent eddies is the only transport mechanism in this model.

Researchers at the University of Tulsa carried out some of the earliest experimental studies of cuttings transport in directional drilling. Tomren, Iyoho, and Azar<sup>13</sup> studied effects of pipe rotation and eccentricity, wellbore deviation, drilling mud type, and flow regimes on cuttings transport performance. They found that a hole deviation angle of 40° to 50° was critical for cuttings transport, due to the downward sliding of a cuttings-bed. Pipe rotation has less effect on cuttings transport performance than that of pipe eccentricity, which was found to have a significant impact on cuttings removal. Okrajini and Azar<sup>14</sup> performed an experimental study of the effects of field-measured mud rheological properties (e.g. the ratio of yield point to plastic viscosity: YP/PV ratio) on cuttings transport in directional well drilling. They noted that the effects of mud yield were insignificant in high-angle wells (>55°). Becker, Azar, and Okrajini<sup>15</sup> correlated rheological properties, including yield point, plastic viscosity, Power-law exponent, consistency index. These were developed with 180 tests of cuttings transport performance. They indicated that the data with low-shear-rate parameters correlated better with annular cuttings concentration in steady-state flow.

Clark and Bickham<sup>16</sup> used a mechanistic model to describe hole cleaning. This model considers the various mechanisms involved in the cuttings transport out of a well (i.e., rolling, lift, and particle settling). Clark and Bickham's paper concurs with industrial opinion classifying flow rate as the most important factor in hole cleaning, and it considers fluid density and rheology as the most important drilling fluid properties that affect hole cleaning. The Herschel-Bulkley rheological model was used in their paper

with the fluid's yield stress being the dominant factor. The influences of the other rheological parameters (i.e. consistency index and fluid behavior index) were unclear.

Rasi<sup>17</sup> investigated the rate of cuttings-bed development. This researcher focused on predictions of cuttings-bed height in an eccentric wellbore. In an undefined manner, he used a dimensionless friction factor (which included factors for fluid rheology), well geometry and design, and pump rate. The plastic viscosity ( $\mu_p$ ), the yield point ( $\tau_y$ ), and the viscometer 6-rpm term (which approaches the yield stress term  $\tau_y$  in the Herschel Bulkley model) were considered as input parameters.

Recognizing the role of fluid velocity in cleaning an annulus where the drillpipe is off-center or eccentric, others have studied the distribution of annular point velocities.<sup>18-20</sup> Sophisticated computer models have been developed to calculate the magnitude of these velocities, both above and below the eccentric drillpipe. These researchers have all recognized that the flow index,  $n$ , (from the Herschel-Bulkley and Power-law rheological models) controls the flow distribution in an annulus when the inner pipe is eccentric. They also recognized that flow distribution at the bottom part in a highly eccentric annulus showed very low or almost zero velocity.

Sanchez et al.<sup>21</sup> investigated the effect of drill pipe rotation on hole cleaning while drilling directional wells. The results showed that the drill pipe rotation had a considerable effect on hole cleaning, and that the dynamic behavior of the drill pipe (vibration, turning, etc.) played a significant role in improving hole cleaning. They quantified the effects of drillpipe rotation on cuttings transport through the sensitivity analysis of numerous data from experiments with and without drillpipe rotation.

Martins and Santana<sup>22</sup> presented a two-layer model that was more versatile than

Gavignet and Sobey's model.<sup>11</sup> This model allows particles to be in suspension in the upper layer. The mean particle concentration in this layer was calculated from a concentration profile that was obtained by solving a diffusion equation. This approach was based on earlier works by Doron et al.<sup>23</sup> on slurry transport.

Recently, Doron et al.<sup>23</sup> introduced a three-layer model for solid-liquid flow in horizontal and inclined pipes using continuity and momentum equations to define fluid dynamics. This model was designed to overcome the limitations of the two-layer model, which was developed earlier for pipe flow. However, the applications of this model also have some limitations. This model does not consider annulus flow, rheology of the carrier fluid, and the rolling/lifting mechanism in solid transport.

Iyoho and Takahashi<sup>24</sup> proposed a three-layer, two-phase flow model to predict flow characteristics that include the formation of dunes, coupled with velocity and pressure fluctuations. Energy balance and pressure fluctuations are the basis of the model. Their model predicts the dune's thickness only when the pressure fluctuation is known, and vice-versa.

Nguyen and Rahman<sup>5</sup> published a mathematical model based on a three-layer flow concept for cuttings transport and hole cleaning in horizontal wells. This model did not specify the boundary conditions of each flow mode. Furthermore, the model did not consider the effects of changes in the drilling fluid rheology and cuttings sphericity. This model was developed only for horizontal well applications. The unit used for defining force balance on each layer has no consistency in this model. However, they explained effectively how a three-layer mode became a two-layer mode with changes in nominal annular velocities of the drilling fluid.

Cho et al.<sup>25</sup> extended the Doron and Barnea<sup>23</sup> mathematical model (horizontal pipe flow to annulus flow) with an additional consideration of drilling fluid rheology, drilled cuttings shape, cuttings concentration, and wellbore geometry with eccentricity of coiled tubing drilling. This model uses a three-layer concept in annuli: i.e., a cuttings stationary bed at the bottom; a cuttings moving bed above it; and a heterogeneous dispersed suspension layer at the top. The effects of the cuttings stationary bed are well defined in this model. Local velocity as a function of cuttings-bed and nominal annular velocity terms were used for the analysis of the transport mechanism. Cho et al.<sup>26</sup> pointed out that the conventional mechanistic models, which handle cuttings transport from vertical to horizontal as a function of wellbore deviation, could not properly characterize the cuttings transport mechanism. The dominant factors controlling cuttings transport are different depending on the wellbore deviation. They further extended a three layer horizontal model to cuttings transport in deviated wellbores.

A detailed review of the published experimental data reveals that the characteristics of cuttings transport varies with a change in the deviated wellbore angles. Some researchers<sup>27-29</sup> reported from their experimental works that the cuttings-bed in annuli is unstable under a certain range of wellbore deviation. The most unstable and difficult region for cuttings transport in a deviated well is reported as 30° to 60° from a vertical position.<sup>30-32</sup> In addition, the cuttings-bed sometimes slides down toward the bottom hole. However, the existing models, which can handle cuttings transport in highly deviated to horizontal wells, do not consider these characteristics for this region. One set of the mathematical model based on wellbore deviation only cannot properly characterize the cuttings transport mechanism in horizontal and highly deviated wellbores.

## **1.3 Objectives and Methodology**

A new three-segment mathematical model was developed to overcome the limitations in the existing hydraulic models by considering characteristics of wellbore deviation on cuttings transport in annuli. This model consists of three segments: horizontal and near horizontal segment ( $60^\circ$  to  $90^\circ$ ), vertical and near vertical segment ( $0^\circ$  to  $30^\circ$ ), and transit segment ( $60^\circ$  to  $90^\circ$ ).<sup>26</sup> Three different layer models can characterize the dominant factors that affect cuttings transport in each segment. In particular, the model developed in this study advances a three-layer flow model for the horizontal and near horizontal section (this section will now be called horizontal segment). The existing two-layer model was modified for the transit section (this section will now be called transit segment), and the one layer vertical model was used for the vertical and near vertical section (this section will now be called vertical segment).

### **1.3.1 Objectives**

There are three major objectives in this study and they are as follows:

1. To characterize the cuttings transport mechanism as a function of wellbore deviation and drilling parameters. These parameters involve drilling fluid flow rate, fluid rheological characteristics, wellbore configuration (wellbore and coiled tubing diameters), formation characteristics (sphericity and cuttings density), wellbore deviation, and the ROP. The cuttings transport mechanism in coiled tubing drilling is analyzed to develop a flow layer model for each segment in wellbore deviation.
2. To develop a mathematical model based on forces, stresses, and momentum balances acting on each flow layer. The mathematical model consists of three-segments, where

each segment uses a different flow layer model. The results of the mathematical model simulation were compared with the published data.

3. To develop the computer simulation program, CT-WellClean<sup>®</sup>. This program can be a useful tool for drilling engineers to simulate all possible in-situ drilling conditions, resulting in the proper design of drilling programs and selection of fluid systems.

### **1.3.2 Methodology**

The methodology of this study was to develop a mathematical model (a three-segment hydraulic model) for the accurate prediction and estimation of cuttings transport in coiled tubing drilling. Wellbore deviation was divided into three-segments based on a wellbore deviation: a vertical segment, a horizontal segment, and a transit segment. Each segment used a different flow layer model. In the development of the mathematical model, factors affecting cuttings transport described in Chapter 2.2 were included.

A simulation program, CT-WellClean<sup>®</sup>, has been developed based on the mathematical model developed in this study. This simulation program was developed to predict cuttings-bed area distribution, bed heights, pressure gradient, moving-bed velocity, and MASV with changes in drilling parameters that affect cuttings transport efficiency. These parameters include wellbore configuration, nominal annular velocities, fluid rheology, ROP, coiled tubing used in drilling, cuttings size and density, ROP, and wellbore deviation angle.

This program also included the development of a reference hydraulic module for the estimation of drilling hydraulics for the inside of coiled tubing and annular section (formed with a wellbore and coiled tubing). In this hydraulic reference module, the



horizontal sections of coiled tubing and annulus were considered without the effects of gravitational force. The magnitude of hydrostatic pressures inside coiled tubing and annulus is the same, but their directions are different. Therefore, these pressures can be offset in the calculation of pump capacity. This study also included simulations of this program with the various in-situ drilling conditions. These simulation results with the similar conditions used in other researcher's experiments were compared with their published experimental data. The analysis of these comparison results verified the appropriateness of this simulation program.

## **1.4 Organization of the Dissertation**

The most prevalent factors that affect cuttings transport in horizontal and deviated wells while drilling with coiled tubing are discussed in Chapter 2. This chapter also discusses frictional pressure loss in both straight tubing, as a drilling fluid conduit, and annuli. The various correlations for the prediction of frictional pressure loss are discussed. The correlations used in the computer hydraulic simulation program are specified. The effects of wellbore deviation in cuttings transport mechanism are discussed with the principles and the background theories related to this mechanism.

Chapter 3 discusses the development of a three-layer hydraulic model for horizontal wellbores. The details of the model hypotheses, model development, solution, and simulation results are discussed. This three-layer model is used for further development of the deviated three-layer model for highly deviated wells (horizontal segments).

Chapter 4 discusses the development of each segment of the three-segment hydraulic model. Each segment: a vertical segment ( $0 - 30^\circ$ ), a horizontal segment ( $60 - 90^\circ$ ), and transit segment ( $30 - 60^\circ$ ), uses a different hydraulic layer model. The characteristics of each segment in cuttings transport mechanism are discussed in this chapter. The treatment and combination of boundaries between segments are also described. The sensitivity analysis based on computer simulation with the various parameters is performed and these simulation results are compared with published data.

Chapter 5 discusses the development of a mathematical model to predict the minimum anti-sliding velocity (MASV) in transit segment. The cuttings-bed at the transit segment is unstable in view of cuttings transport and cuttings-bed movement. This chapter focuses on the characterization of transit segment for predicting both the MASV and additional frictional pressure loss in drilling fluid hydraulics due to a cuttings-bed movement and fluid flow through a cuttings-bed.

Chapter 6 discusses the basis of the simulation program. The details for the three-segment model solution, development, and user interface are described.

Finally, conclusions and recommendation are discussed in Chapter 7 based on this study.

# **CHAPTER TWO**

## **THEORETICAL BACKGROUND OF CUTTINGS TRANSPORT MECHANISM**

### **2.1 Introduction**

Since its formal introduction into the petroleum industry, coiled tubing has undergone many applications, such as fracturing, cementing, logging, sidetracking, and coiled tubing drilling. These applications have dramatically improved coiled tubing's capabilities. Today, coiled tubing is applied in almost every area of the petroleum industry. Coiled tubing technology has been applied to a wide variety of oilfield applications including, but not limited to, horizontal and directional drilling, electric wireline well logging, cementing, completion, tubing conveyed perforating, remedial work, acidizing and stimulation, side tracking, foam fracturing, sand control, and production.

One of the primary uses of coiled tubing is in the cleanout of a deviated wellbore, which is similar to cuttings transport during drilling.<sup>34,35</sup> Coiled tubing technology, along

with mud motors, has revolutionized the drilling industry and has dramatically changed the way horizontal and directional wells are drilled. This technology also allows for underbalanced drilling of some wells. The operation involves circulation of fluid through the coiled tubing down to the drilled cuttings filled in the wellbore. The fluid mixes with cuttings by large turbulent eddies and carries cuttings up to the surface through the annulus between the coiled tubing and the casing (wellbore). This chapter discusses and summarizes the basic theories adopted in this dissertation, which affect cuttings transport in coiled tubing drilling.

## **2.2 Factors Affecting Cuttings Transport**

There are many parameters that affect the cuttings transport in horizontal and deviated wells while drilling with coiled tubing. The most prevalent factors are as follows:

- 1) Annular drilling fluid velocity
- 2) Drilling fluid properties
  - Density
  - Rheology
- 3) Wellbore configuration
  - Coiled tubing eccentricity
  - Wellbore deviation angle
  - Hole size and coiled tubing size
- 4) Rate of penetration

- Bulk volume generated by the bit
- Cuttings concentration

5) Physical characteristics of cuttings

- Cuttings specific gravity
- Cuttings size and its distribution

6) Others

- Coiled tubing movement
- Coiled tubing vibration
- Wellbore surface smoothness

The effects of the main parameters on cuttings transport efficiency were analyzed through sensitivity studies by the theoretical simulation that will be discussed in later chapters. Figure 2.1 illustrates a graphical summary of the major parameters that influence cuttings transport in relation to their ease of control in the field. Practical use of these parameters to control cuttings transport is, however, very much dependent on their controllability in the field.<sup>1</sup> For example, drillpipe eccentricity has a strong influence on the cuttings transport. However, it is difficult to control the degree of eccentricity during coiled tubing drilling. As shown in Fig. 2.1, the flow rate of drilling fluid and rheology are the two main parameters. This would strongly influence cuttings transport while their control in the field is relatively easy. In other words, to ensure efficient transport of cuttings, one may depend on the optimum combination of drilling parameters.

The movement of the coiled tubing while drilling may affect cuttings transport. However, its movement is quite small. For example, the rates of movement of coiled tubing are 0.014 – 0.056 ft/s based on 50 – 200 ft/hr of the RCP. When these velocities

are compared with 3 - 10 ft/s of local velocities ( $U$ ), their relative velocities are very small and their effects may be insignificant.

The vibration of coiled tubing during drilling may also affect cuttings transport. As a result of a transferred energy reaction between a drilling bit and a rock formation, the downhole motors will generate some vibration in coiled tubing. The coiled tubing vibration may enhance cuttings to rebound in the fluid flow regime for cuttings diffusion. This vibration may also break some of the cuttings into fine particles, which can then be easily lifted into a fluid flow regime. However, this effect, which is quite difficult to quantify, is much smaller than that of a drilling string rotation.

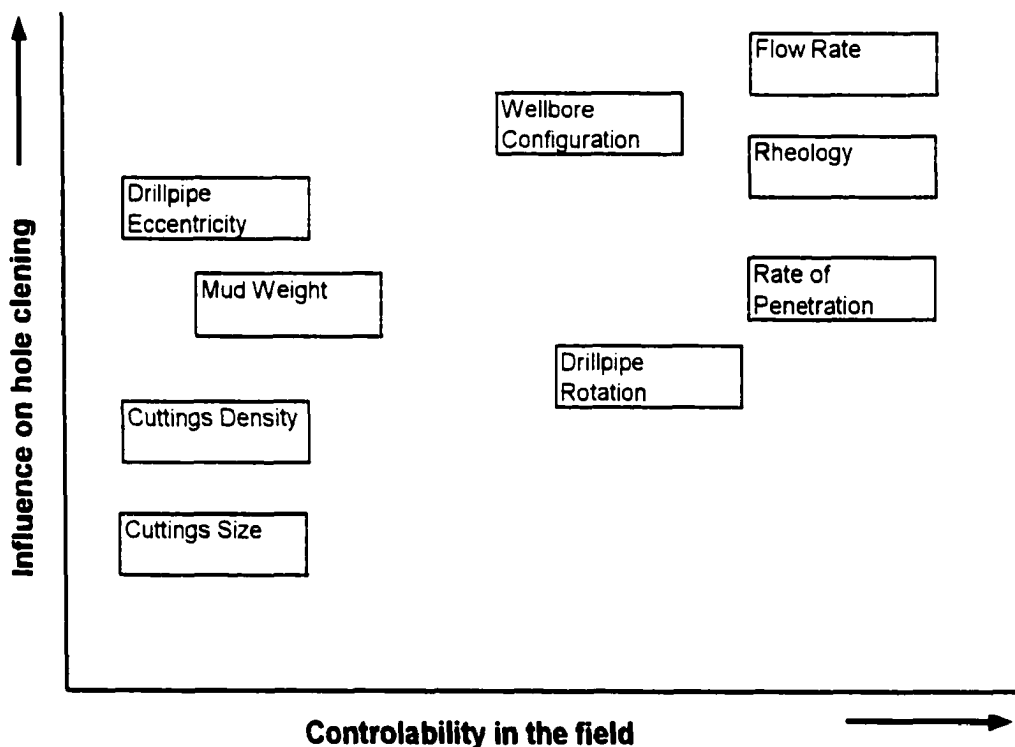


**Fig. 2.1 – Key variables affecting the cuttings transport<sup>1</sup>**

Actual wellbore drilling is neither sleek nor smooth. A wellbore drilling will be affected by various factors, such as formation types, coiled tubing methods, coiled tubing vibration, drilling personnel skills, bit wearing/balling, ROP, and the drilling fluid hydraulics. Surface smoothness of the wellbore clearly affects cuttings transport; however, its degree is quite arbitrary and may not be as severe as other parameters. Therefore, these items were considered only qualitatively in cuttings transport.

## **2.3 Coiled Tubing Hydraulics**

### **2.3.1 Background, Scope, and Significance**

The bottomhole pressure and the maximum allowable working pressure of the coiled tubing are the critical parameters in coiled tubing drilling applications. An accurate estimation of frictional pressure loss plays a crucial role in determining the horsepower requirement for pumping fluids through the coiled tubing. Frictional pressure loss calculations are not only useful in determining horsepower requirements, but also in estimating the allowable hydraulic forces for downhole motors.

Flow conditions inside the coiled tubing are quite different from the annulus. The fluids inside coiled tubing can be regarded as homogeneous.<sup>15</sup> At a lower concentration of drilling solids, the increase in friction pressure loss is not significant. Above 2% volumetric concentration of drilling solids, friction pressure loss becomes important.<sup>16</sup> Coiled tubing inside a wellbore is not a straight form. Helical buckling occurs easily in coiled tubing operations. Since the effects of helical buckling on a hydraulic calculation

have not been clearly studied yet, coiled tubing was assumed as a straight pipe in the wellbore in a hydraulic calculation.

The working fluid is not only pumped through the straightened segment of the reeled tubing as it flows down the well, but it is introduced there by the entire length of tubing left on the reel. Flow through coiled tubing is uniquely different from that in a straight pipe because of the secondary flow pattern induced by the imbalance between the forces acting in the radial direction of the pipe coil. This secondary flow pattern is composed of counter-rotating vortices, commonly called Dean vortices, which cause an increase in frictional pressure loss.<sup>37</sup> The frictional pressure loss in the reeled tubing can have a major impact on the drilling or fracturing operations. Frictional pressure loss in reeled tubing has been shown on to be 200% higher than for the same fluid in straight tubing.<sup>37</sup> The friction pressure loss in annulus between the coiled tubing and casing is more complicated. A mathematical model was derived from the relationships between the forces, stresses, and momentum acting on the fluid layers and the cuttings-bed. This is described in later chapters.

### **2.3.2 Friction Pressure Loss in Straight Tubing**

One of the important roles of coiled tubing while drilling is circulating drilling fluid from the surface to the downhole. This operation generates frictional pressure loss. Frictional pressure loss is defined as the energy lost in transporting a fluid through a pipe, due to the friction between the fluid and pipe wall.<sup>38</sup> Mathematically, the friction pressure loss can be expressed in terms of Fanning friction factor,  $f$ , defined as:

$$f = \frac{\tau_w}{1/2 \rho_L U^2} \quad (2.1)$$



where,  $\rho_L$  is fluid density,  $U$  is fluid velocity inside the coiled tubing, and the shear stress at the wall ( $\tau_w$ ) is calculated by using the following expression.

$$\tau_w = \frac{d_i \Delta P}{4L} \quad (2.2)$$

where,  $d_i$  is the inner diameter of coiled tubing,  $\Delta p$  is the frictional pressure loss across the coiled tubing length ( $L$ ). Friction factors have been correlated with Reynolds number.

Generalized forms of Reynolds numbers used for non-Newtonian fluids are as follows:

$$N_{Reg} = \frac{d_i^n U^{2-n} \rho_L}{K 8^{n-1}} \left( \frac{4n}{3n+1} \right)^n \quad (\text{for Power-law model}) \quad (2.3)$$

$$N_{Reg} = \frac{928 \rho_L U d_i}{\mu_p} \quad (\text{for Bingham-plastic model}) \quad (2.4)$$

where,  $n$  and  $K$  are the flow behavior index and flow consistency index for Power-law fluids and  $\mu_p$  is the plastic viscosity for Bingham-plastic fluid.

Separate analysis of friction factors versus the generalized Reynolds number is necessary for each fluid in any flow regime because their friction factors are different for the same Reynolds number. Friction pressure for laminar flow of drilling fluid in coiled tubing can be predicted assuming the Power-law model:

$$\frac{d_i \Delta P}{4L} = K \left( \frac{8U}{d_i} \right)^n \quad (2.5)$$

This equation is equivalent to:

$$f = \frac{16}{N_{Reg}} \quad (2.6)$$

where,  $f$  and  $N_{Reg}$  are the Fanning friction factor and the generalized Reynolds number, respectively.

To predict friction factors for the transition and turbulent flow regimes, Shah<sup>39</sup> developed a semi-analytical correlation for linear Hydroxypropyl Guar (HPG) fluids in smooth pipes using an equation of the following form:

$$f = f_{\infty}(n) + A(n) \left( N_{\text{Reg}} \right)^{B(n)} \quad (2.7)$$

where,  $f_{\infty}(n)$  is the infinite friction factor and  $A(n)$  and  $B(n)$  are empirical fluid parameters. The relationships between these empirical fluid parameters and flow behavior index ( $n$ ) are determined using experimental data. This equation works well for several other non-Newtonian fluids, such as Xanthan and Hydroxyethyl Cellulose (HEC) based fluid.<sup>40</sup> Shah<sup>41</sup> also studied the effects of coiled tubing roughness on friction pressure loss. Table 2.1 shows the values for  $f_{\infty}(n)$ ,  $A(n)$ , and  $B(n)$  with their respective values of  $n$ . The Arabic numerals represent different fluids that have not been disclosed for proprietary reasons. Table 2.2 presents the Shah<sup>41</sup> roughness correction to be used in increasing the value of the friction factor as a function of the generalized Reynolds number and apparent fluid viscosity at  $170 \text{ s}^{-1}$ . Apparent viscosity ( $\mu_a$ ) of the Power-law fluid in centi-poise unit can be defined as follows:

$$\mu_a = 47880 K_p \left( \dot{\gamma}_w \right)^{(n-1)} \quad (2.8)$$

where,  $K_p$  is the consistency index for pipe flow ( $\text{lb}_f \text{s}^n / \text{ft}^2$ ) and  $\left( \dot{\gamma}_w \right)$  is the wall shear rate ( $\text{s}^{-1}$ ).

The Shah<sup>39</sup> correlation (Eq. 2.7) and the effect of coiled tubing roughness are used for the hydraulic calculations of coiled tubing in the hydraulic reference module developed in this study.

Recently, Willingham and Shah<sup>42</sup> developed a new correlation to predict frictional pressure losses in straightened coiled tubing by extensive experimental work and analysis with different fluid systems at the Well Construction Technology Center (WCTC). They used a multiple regression method to specify the Fanning friction factor as a function of generalized Reynolds number for polymeric fluids as follows:

$$\sqrt{f} = a + \frac{b}{\sqrt{N_{\text{Re g}}^{(1-R)}}} \quad (2.9)$$

where,  $R$  represents coiled tubing curvature and is zero for straight tubing. Experimental constants,  $a$  and  $b$ , are functions of coiled tubing inner diameter ( $d_i$ ) and apparent viscosity ( $\mu_a$ ). Equation 2.9 can be applied to both straight and reeled tubing as a function of generalized Reynolds number, apparent viscosity, and coiled tubing inner diameter.

**Table 2.1 Constants for the Shah<sup>39</sup> correlation**

Fluid	n	K lb <sub>f</sub> s <sup>n</sup> /ft <sup>2</sup>	f <sub>∞</sub> (n)	A(n)	B(n)
Water	1	1.84x10 <sup>-5</sup>	1.40x10 <sup>-3</sup>	0.125	0.32
# 1	0.715	5.60x10 <sup>-4</sup>	3.80x10 <sup>-4</sup>	1.96	0.701
# 2	0.607	2.80x10 <sup>-3</sup>	4.01x10 <sup>-4</sup>	2.96	0.787
# 3	0.47	1.70x10 <sup>-2</sup>	5.10x10 <sup>-4</sup>	6.44	0.911
# 4	0.35	8.10x10 <sup>-2</sup>	6.04x10 <sup>-4</sup>	14.4	1.012
# 5	0.272	1.90x10 <sup>-1</sup>	6.19x10 <sup>-4</sup>	18.5	1.036

**Table 2.2 Constants and equations for the Shah<sup>41</sup> roughness correction factor for  $f$** 

$\mu_a$ @ 170 s <sup>-1</sup> (cp)	a	B	% increase of $f$
5	33.717	-312.982	$(a + b/\ln(N_{Reg}))^2$
10	30.680	-285.388	“
15	27.833	-258.302	“
20	25.818	-240.265	“
30	22.681	-211.424	“
40	-50.069	0.492	$a + b(\ln(N_{Reg}))^2$
50	-43.919	0.424	“
60	-39.999	0.377	“
80	-89.099	8.362	$a + b(\ln(N_{Reg}))$

The frictional pressure loss associated with the turbulent flow of a Bingham-plastic fluid is affected primarily by density and plastic viscosity. While the yield point of the fluid affects both the frictional pressure loss in laminar flow and the fluid velocity at which turbulence begins, at higher shear rates corresponding to a fully turbulent flow pattern, the yield point is no longer a significant parameter.<sup>43</sup> It has been found empirically that the frictional pressure loss associated with the turbulent flow of a Bingham-plastic fluid can be predicted using the equations developed for Newtonian fluids, if the plastic viscosity is substituted for the Newtonian viscosity. This substitution can be made in Reynolds number used in the Colebrook<sup>44</sup> function defined by:

$$\frac{1}{\sqrt{f}} = -4 \log \left( 0.269 \varpi / d_i + \frac{1.255}{N_{Re,g} \sqrt{f}} \right) \quad (2.10)$$

where,  $\varpi$  is absolute roughness.

The generalized Reynolds number in terms of fluid velocity ( $U$ : ft/s), and coiled tubing inner diameter ( $d_i$ : in.) yields:

$$N_{Reg} = \frac{928 \rho_L U d_i}{\mu_a} \quad (2.11)$$

where,  $\mu_a$  is apparent viscosity (cp),  $\rho_L$  is fluid density (lb<sub>m</sub>/gal).

The most commonly used turbulence criterion involves the calculation of a representative viscosity that can be used in Reynolds number criterion developed for Newtonian fluid. The apparent viscosity is given as:

$$\mu_a = \mu_p + \frac{6.66 \tau_y d_i}{U} \quad (2.12)$$

where,  $\mu_p$  and  $\tau_y$  are plastic viscosity (cp) and yield point (lb<sub>f</sub>/100ft<sup>2</sup>), respectively.

This apparent viscosity can be used in place of the Newtonian viscosity in Reynolds number formula. A turbulence criterion for fluids that follows the Bingham-plastic model was presented by Hanks.<sup>45</sup> He introduced Hedstrom number ( $N_{He}$ ), which is given as follows:

$$N_{He} = \frac{37100 \rho_L \tau_y d_i^2}{\mu_p^2} \quad (2.13)$$

He found that Hedstrom number could be correlated with the critical Reynolds number.  $N_{Rec}$  – Reynold number above which the flow pattern is turbulent.

The absolute roughness ( $\varpi$ ) is the average depth of the coiled tubing-wall irregularities. The Fanning friction factor, defined in Eq. 2.10, is a function of the generalized Reynolds number,  $N_{Reg}$ , and a term called the relative roughness,  $\varpi d_i$ . The Fanning friction factor,  $f$ , appears on both the left hand side and the right hand side of the

log term of Colebrook's<sup>44</sup> equation, requiring an iterative solution technique. The selection of an appropriate absolute roughness,  $\varepsilon$ , for a given applications is often difficult. Cullender and Smith<sup>46</sup> noted that the absolute roughness was 0.00065-in. for clean steel pipe. Bourgoyne et al.<sup>43</sup> suggested that the absolute roughness is usually less than 0.0004-in. for most drilling applications. For these conditions, the Fanning friction factors for smooth coiled tubing (zero roughness), Eq. 2.10 can be reduced to:

$$\frac{1}{\sqrt{f}} = 4 \log(N_{Reg} \sqrt{f}) - 0.395 \quad (2.14)$$

### 2.3.3 Frictional Pressure Loss in Annuli

An effective diameter concept for the flow of drilling fluid through annuli (between wellbore and drillstring) was introduced as a function of annular geometry and fluid rheology by Reed and Pilehvari.<sup>47</sup> They showed that this new criterion provides the link between Newtonian pipe flow and non-Newtonian flow through concentric annuli. They were able to correlate turbulent friction factors by using the generalized Reynolds number ( $N_{Reg}$ ), the effective diameter ( $D_{eff}$ ), and apparent viscosity ( $\mu_a$ ). The relationship between friction factor and the generalized Reynolds number for annular flow in laminar region remains the same as the classical Eqs. 2.1 to 2.4, but the substitution of the effective diameter ( $D_{eff}$ ) and apparent viscosity ( $\mu_a$ ) is required for the diameter and viscosity, respectively.

Shah<sup>39</sup> presented an important study corresponding to friction pressure loss of fracturing fluids. He developed a correlation for smooth pipes that has been widely used for the rheological characterization of non-Newtonian fluids. The friction factor was expressed as a function of the generalized Reynolds number and three constants, which

were obtained experimentally (Table 2.1). Later, Shah<sup>41</sup> extended his work, introducing the effects of pipe roughness on friction pressure for fracturing fluids (Table 2.2). Although this expression was developed for pipes, it is very useful in annular flow when the equivalent diameter criterion is applied.<sup>48</sup>

It is now well established that frictional pressure loss depends significantly on the exact value of eccentricity for uniformly eccentric annuli. Hacıislamoglu and Cartalos<sup>49</sup> showed that eccentricity effects on annular pressure loss calculations are quite important, while dependence on fluid rheology and diameter ratio (the ratio of coiled tubing diameter to the spool diameter) is less pronounced. Johnson and Sparrow<sup>50</sup> found experimentally that eccentricity influenced the onset and extent of laminar-turbulent transition.

Recently, Silva and Shah<sup>48</sup> demonstrated that the annular pressure in a fully eccentric annulus could be as low as 40% of the value in concentric annulus. They also observed that the effect of eccentricity is more evident as the polymer concentration increases. Eccentricity is a function of the decentralization of the coiled tubing inside the wellbore. Figure 2.2 illustrates the typical coiled tubing eccentricity ( $e$ ), which is defined as:

$$e = \frac{2\delta}{D - d} \quad (2.15)$$

where,  $\delta$  is distance between center points of wellbore and coiled tubing,  $D$  and  $d$  are inner diameter of wellbore (or casing) and outer diameter of coiled tubing, respectively.

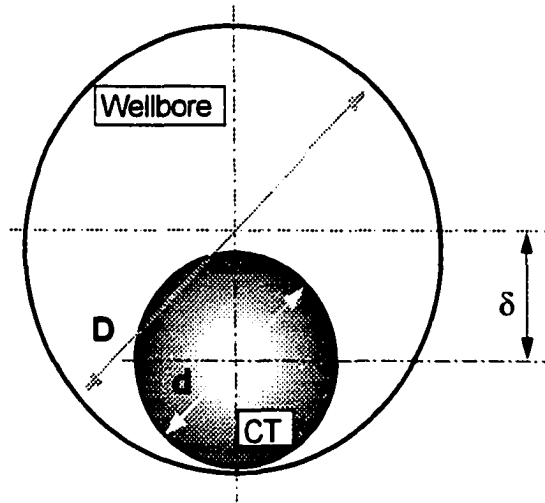


**Fig. 2.2 – Typical eccentricity of coiled tubing in wellbore**

The Fanning friction factor and the generalized Reynolds number for non-Newtonian fluids through an annulus can be described by applying the equivalent diameter concept into commonly used expressions for the pipe flows. These variables can be defined by the following expressions:

$$f = 154.65 \frac{(D-d)(D^2 - d^2)^2 \Delta p}{L \rho_L Q^2} \quad (2.16)$$

$$N_{Re_g} = 378.79 \frac{\rho_L Q}{(D+d)\mu_a} \quad (2.17)$$

where,  $\mu_a$  is the apparent fluid viscosity (cp) at a given shear rate,  $Q$  is flow rate (gal/min) and  $\rho_L$  is the fluid density (lb<sub>m</sub>/gal). The apparent viscosity of the non-Newtonian fluids is represented by the following equation:

$$\mu_a = 47880 * K_a \left( \dot{\gamma}_w \right)^{n-1} \quad (2.18)$$



where,  $K_a$  is the flow consistency index for annulus flow ( $\text{lb}_f \text{s}^n/\text{ft}^2$ ),  $\dot{\gamma}_w$  is the wall shear rate ( $\text{s}^{-1}$ ) given by the following expression:

$$\dot{\gamma}_w = 39.21 \left[ \frac{Q}{(D-d)(D^2-d^2)} \right] \quad (2.19)$$

The consistency index,  $K_v$ , obtained from the viscometer or rheometry data, can be converted into the annulus  $K_a$  by using the following relation:

$$K_a = K_v \left( \frac{2n+1}{3n\lambda} \right)^n \quad (2.20)$$

where,  $\lambda$  is a constant and is defined as follows:

$$\lambda = \frac{1 - \Omega^2}{n(1 - \Omega^{2+n})} \quad (2.21)$$

where,  $\Omega$  is the ratio of the bob to sleeve radius.

Recently, Silva and Shah<sup>48</sup> developed new correlations to predict friction losses in annuli. They performed extensive experimental work with fluids with different polymer concentrations. They also developed a generalized Fanning friction factor equation for concentric and eccentric annuli under laminar flow conditions as follows:

$$f = \frac{\omega}{N_{\text{Reg}}} \quad (2.22)$$

where,  $\omega$  is a constant, determined by experimental data, for annulus eccentricity (between wellbore and coiled tubing) and apparent viscosity.

A separate analysis of the friction factor versus the generalized Reynolds number is necessary for each fluid in a turbulent flow because they show significant differences. By comparing experimental results for different concentrations of polymer solutions,

Silva and Shah<sup>48</sup> observed that the ratio of frictional pressure losses in eccentric and concentric annuli decreases as the fluid behavior index decreases. The effects of eccentricity were more evident as the polymer concentration increased. They proposed the following equation for the Fanning friction factor for both concentric and eccentric annuli.

$$f = f_{\infty} + B(N_{Reg})^{-1.0} \quad (2.23)$$

where,  $f$  is the Fanning friction factor,  $N_{Reg}$  is the generalized Reynolds number. Both  $f_{\infty}$ , the infinite friction factor, and  $B$  are constants determined experimentally for each fluid concentration and type of fluid flow (concentricity and eccentricity).

The annular friction losses, estimated by the correlations, are compared with the friction losses estimated by the mathematical model derived from the relationship between forces, stresses, and momentum acting on the flow layer. The details of the derivation and comparison are described in later chapters.

## 2.4 Cuttings Transport Mechanism

### 2.4.1 Classification of Cuttings Transport

One of the primary functions of the drilling fluids in the coiled tubing drilling process is to clean rock fragments from beneath the bit and transport these cuttings to the surface. Cuttings generated by a bit are transported to the surface by several different mechanisms as they move along the wellbore. The basic principle underlying a particle settling velocity,  $v_p$ , is derived by the sum of the forces acting on a particle. The

gravitational force acts on the solid in the direction of the fall, and both the buoyancy force and the drag force act in the opposing direction due to fluid motion. The net force acting on a particle is the result of the gravitational force subtracted from the two upward forces (buoyancy force and drag force).

In the vertical segment, cuttings transport in the annulus occurs when upward velocity of the drilling fluid exceeds the fall velocity (settling velocity) of the cuttings. The average net upward velocity of the transported cuttings is the difference between the average velocity of the drilling fluid and the settling velocity of the cuttings in the annulus. Fluid rheology, particle size, shape, and wellbore geometry govern this settling velocity. The particle settling velocity is the dominant parameter in cuttings transport in the vertical segment. The carrying capacity of the fluid is also affected by the velocity profile in the annulus. Particle slip direction in a vertical well is opposed by the carrier fluid flow, as a result, the particle will be lifted out of the well, if the mud velocity is greater than the slip velocity.

The transport ratio, as defined by Sifferman et al.<sup>49</sup>, is the average transport velocity of the cuttings divided by the average annular velocity. They suggest that the transport ratio should exceed 0.5 for a satisfactory hole cleaning. Walton<sup>12</sup> noted that the annular velocity should be twice the settling velocity of the cuttings. This is generally accepted as a rule of thumb for cuttings transport in a vertical segment, during which cuttings transport is usually not a problem.

In a transit segment, the direction of cuttings settling is still vertical, but the fluid velocity has a reduced vertical component. This decreases the fluid carrying capacity of suspended drilled cuttings, resulting in faster particle settling time at higher values of

wellbore deviation. There is a tendency for cuttings to fall to the lower side of the wellbore (or casing) and form a cuttings-bed. If a sufficiently high annular velocity is available, the cuttings are transported as a pseudo-homogeneous mixture.<sup>51</sup> However, this situation rarely exists operationally.

The axial velocity increases with a reduction in wellbore deviation in a transit segment. The increased axial velocity can support cuttings more than in a horizontal segment. Therefore, cuttings can be in suspension for a long time in a suspension layer than in a horizontal segment. Lifting and suspending are the dominant transport mechanisms in a transit segment. It has been well recognized that solid particles can go a long distance by suspending particles in a suitably designed liquid. The flow behavior of liquid/solid systems depends on the basic physical properties of solids (size, density, and shape) and fluid (density and viscosity), wellbore configuration, and the pump rate.<sup>12</sup> Depending on the values of these parameters, particles may be conveyed in several different ways. Throughout this study, the term “particle” is used to denote a drilled cutting.

The velocity at the bottom part of the wellbore, at which coiled tubing is located in horizontal or transit segment, is lower than at the top part in the annulus.<sup>20</sup> An increase in eccentricity causes an increase in the flow through the annuli, thus increasing the average flow velocity. This increase is not uniform and the bulk of the increase in flow is through the wider section. In the case of high eccentricities, the narrow regions have a very small gap width. Thus, the flow regime in the narrow regions remains laminar even at high flow rates and the contribution of these regions to the total volumetric flow rate is not

significant.<sup>10</sup> Therefore, the cuttings easily settle at the low-side of the wellbore under the normal pumping rate (within nominal annular velocities of 1 to 3 ft/s).<sup>25</sup>

In a horizontal segment, cuttings are no longer fully supported by the fluid drag, and it is inappropriate to make predictions of cuttings transport from the techniques based on the settling velocity of the cuttings. The cuttings transport is significantly different from that in a vertical segment. The direction of the cuttings settling is still vertical, but the fluid velocity has a considerably reduced vertical component except those due to turbulent eddies. This decreases the drilling fluids capabilities to suspend drilled cuttings and results in faster particle settling time at highly deviated wellbores. Particle trajectory (influenced by axial fluid movement and downward particle movement) is such that particles slip through the fluid, having little distance to travel before settling to the low-side of the wellbore.<sup>27</sup> Local fluid velocities near the bottom wall are small,<sup>20</sup> which reduces further particle movement. Figure 2.3 shows the direction of cuttings slip relative to carrier fluid direction.

Ford et al.<sup>10</sup> and Gao et al.<sup>31</sup> reported two distinctly different cuttings transport mechanisms in the horizontal segment: rolling/sliding and the suspension mechanisms. The suspension mechanism requires a higher fluid velocity than the rolling/sliding mechanism. The settling tendency of particles creates a skewed distribution of particle density, with more particles moving toward the bottom of the annulus.<sup>12</sup> This was qualitatively confirmed by analysis of visual records for experiments of wellbore cleanout tests at the WCTC.

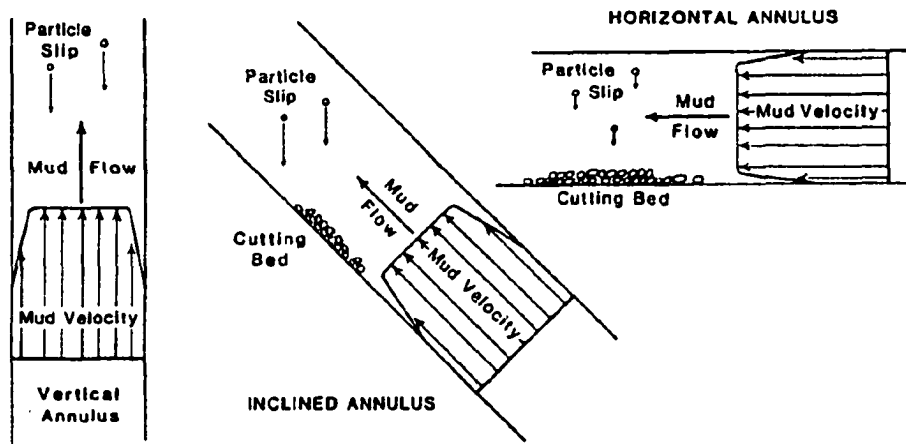


**Fig. 2.3 – Direction of cuttings slip related to carrier fluid direction<sup>52</sup>**

## **2.4.2 Settling Velocity and Drag Coefficient**

A cutting particle, because of its higher density, tends to settle out of the drilling fluid at a constant rate known as the terminal settling velocity. The settling velocity of any particle depends upon its density, shape, and roughness. The area of the particle projected surface at right angles to the direction of the relative fluid solid movement also affects the settling velocity. The fluid properties (density and viscosity) are important parameters that affect the settling velocity.

When a cutting is transported to the surface, there are three forces acting upon it; the downward force due to gravity, the upward buoyancy force, and the upward force due to viscous drag. Once the cutting reaches its terminal settling velocity, the net effect of gravity and buoyancy must be equal to the frictional force on the cutting due to the viscous drag. These relations can be expressed for the Newtonian fluid with the following equation:

$$V_p^2 = \frac{4d_p}{3C_D} \left( \frac{\rho_s}{\rho_L} - 1 \right) g \quad (2.24)$$

where,  $V_p$  is particle settling velocity,  $C_D$  is drag coefficient,  $d_p$  is particle diameter, and  $g$  is gravitational acceleration. Particle density and fluid density are represented by  $\rho_s$  and  $\rho_L$ , respectively.

Equation 2.24 can be rewritten as:

$$C_D = \frac{4d_p}{3V_p^2} \left( \frac{\rho_s}{\rho_L} - 1 \right) g \quad (2.25)$$

Particle Reynolds number,  $N_{Re p}$ , for the non-Newtonian fluid is defined as:

$$N_{Re p} = \frac{0.1617 \rho V_p^{2-n} d_p^n}{K(36)^{n-1}} \quad (2.26)$$

Note that the terminal settling velocity is presented in the equations for  $C_D$  and  $N_{Re p}$ .

Hence, to obtain a settling velocity from the drag coefficient and the particle Reynolds number, one needs to perform a trial-and-error procedure.<sup>53</sup>

In most practical applications, the particles involved are irregularly shaped. The irregular shape changes the settling behavior, unlike smooth and symmetrical particles.<sup>54</sup> Spheres have a sphericity of 1.0. However, in most practical applications of drilling, the cuttings involved are irregularly shaped. Drilled cuttings have sphericities<sup>54,55</sup> between 0.75 and 0.85. The sphericity ( $\phi$ ) represents a degree of deviation between a cutting shape from a spherical shape. It is the ratio of surface area of the sphere of the same volume to the surface area of the particle. It can be defined as:

$$\phi = \frac{\text{surface area of a sphere of the same volume as the particle}}{\text{surface area of the particle}} \quad (2.27)$$

The drag coefficient for spheres is less than that for cuttings, implying that spheres settle faster than non-spherical objects under similar conditions.<sup>54</sup>

Another practical consideration is that the drilling fluid is a typically non-Newtonian fluid. Chien<sup>55</sup> proposed a correlation between the drag coefficient and the particle Reynolds number of irregularly shaped particles. This correlation uses the cutting shape factor and the effective viscosity of the non-Newtonian fluid at the settling shear rate.

$$V_p'^2 + 0.45 \exp(5.03\phi) \left( \frac{\mu_e}{d_p \rho_L} \right) V_p' - 19.45 \exp(5.03\phi) d_p \left( \frac{\rho_s}{\rho_L} - 1 \right) = 0 \quad (2.28)$$

where,  $\mu_e$  is an effective viscosity. Chabra<sup>56</sup> suggested using an effective viscosity at a shear rate equal to annular velocity divided by the nominal particle diameter. Chien<sup>55</sup> showed that the settling shear rate of the laminar slip regime, where the viscosity of the fluid has a dominant role, is in the range from 0.1 to 50 s<sup>-1</sup>, and is usually less than 25 s<sup>-1</sup>. The effective viscosity at various shear rates will depend on the constitutive equation of the fluid, or the relationship between the shear stress and the shear rate of the fluid. Effective viscosity of the two popular drilling fluid rheological models, Bingham-plastic model and Power-law model, are summarized below:

$$\mu_e = \left( \frac{\tau_y d_p}{V_p'} \right) + \mu_p \quad (\text{Bingham - plastic model}) \quad (2.29)$$

$$\mu_e = K \left( \frac{V_p'}{d_p} \right)^{n-1} \quad (\text{Power - law model}) \quad (2.30)$$

Shah<sup>57,58</sup> proposed a generalized correlation for the settling velocity and the drag coefficient as a function of the flow behavior index ( $n$ ) of non-Newtonian fluids. He



noted that a flow behavior index,  $n$ , had a significant effect on proppant settling velocity at a low particle Reynolds number. This effect also diminished at a higher particle Reynolds number. He plotted  $N_{Re\ p}$  vs.  $\sqrt{C_D^{2-n} N_{Re\ p}^2}$  for non-Newtonian pseudo-plastic fluids based on dimensionless analysis. This generalized plot results in family of curves that are functions of the pseudo-plasticity index,  $n$ .

Peden and Luo<sup>59</sup> proposed the generalized drag coefficient correlation for Power-law fluids in laminar and transit regimes. They developed a generalized model for predicting settling velocities of various shaped particles in both Newtonian and Power-law fluids for all flow regimes. Equation 2.31 describes the model proposed by Peden and Luo.<sup>59</sup>

$$V_p^* = \left[ \frac{4}{3} g \frac{d_p^{1+h_1 n}}{a_l C_\phi K^{h_1} \rho_L^{1+h_1}} \right]^{\frac{1}{2-h_1(2-n)}} \quad (2.31)$$

where, experimental constants,  $a_l$  and  $h_l$ , are proposed as functions of the flow behavior index depending on flow regime.  $C_\phi$  represents shape factor (dimensionless).

Recently, Fang<sup>60</sup> proposed the settling velocity for intermediate flow ( $N_{Re\ p} < 100$ ) as follows:

$$V_p^* = 0.302 \left[ \frac{d_p^{1.667} (\rho_s - \rho_L)^{0.889}}{\mu_e^{0.778} \rho_L^{0.111}} \right] \quad (2.32)$$

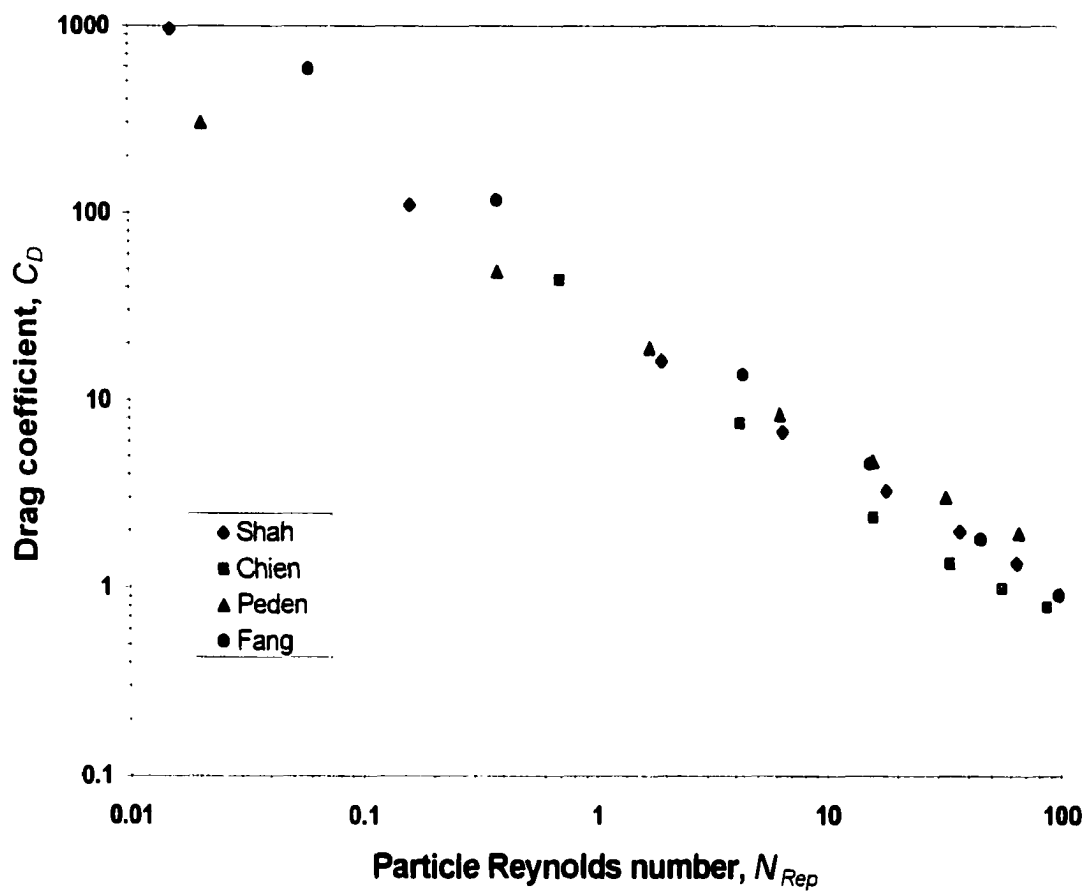
He assumed that nearly all of the particle Reynolds number for drilling applications were smaller than 100. When  $N_{Re\ p}$  approaches 100, the drag coefficient approaches a constant value of unity.

Figure 2.4 illustrates the relationship between particle Reynolds number and drag coefficient. All the models show the same trend that drag coefficient decreases with an increase in a particle Reynolds number. Estimated data points show a wide band in the Stokes' region, which is below a particle Reynolds number of 2.0 in Fig. 2.4. A Power-law fluid model ( $n = 0.68$  and  $k = 0.006 \text{ lbf s}^n/\text{ft}^2$ ) was used to calculate settling velocities.

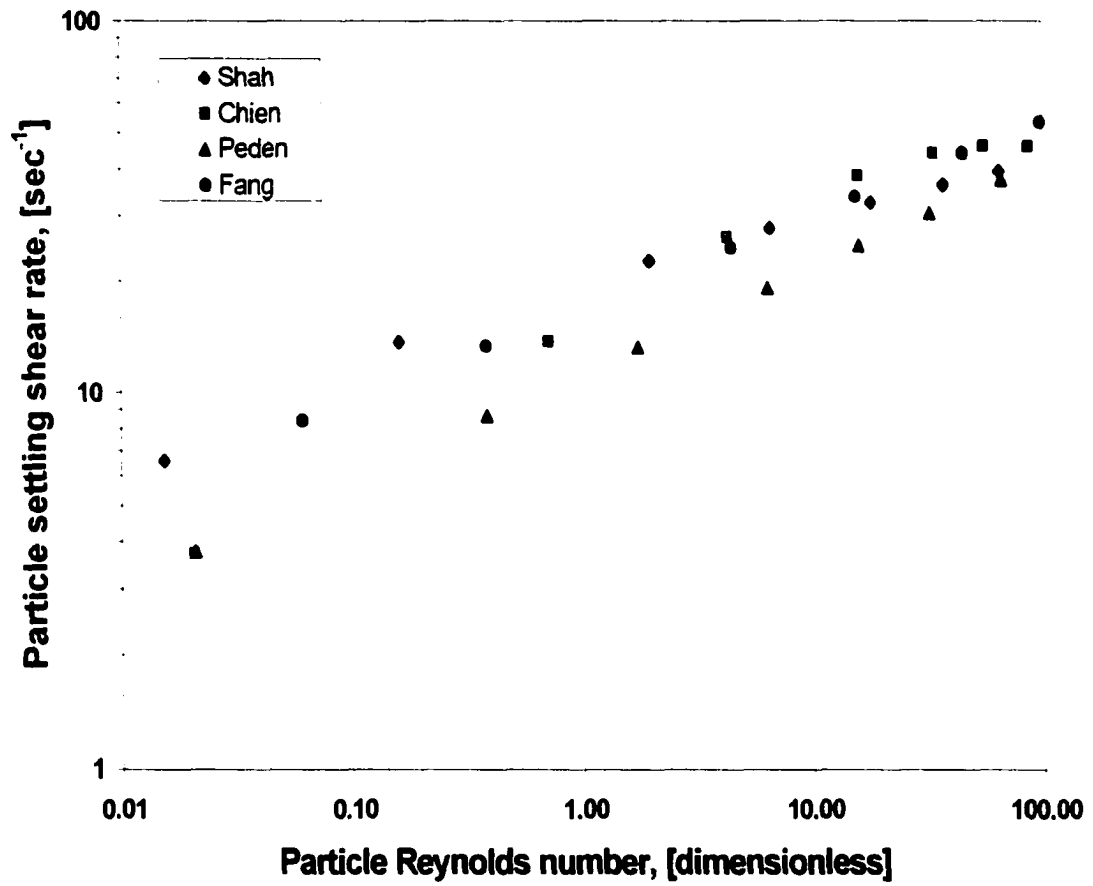
Figure 2.5 illustrates the relationship between particle Reynolds number and particle settling shear rate. The Shah model<sup>57</sup> shows a high shear rate and the Peden model<sup>59</sup> shows a low shear rate in the Stoke's region. The range of particle settling shear rate is  $0.1$  to  $70 \text{ s}^{-1}$  for the range of particle sizes ( $0.5 \text{ mm}$  to  $12.25 \text{ mm}$ ).

Figure 2.6 shows a comparison of the particle settling velocities with different nominal particle diameters. The settling velocities estimated by Chien<sup>55</sup> and Shah<sup>57</sup> are very close among the various models. The settling velocities estimated by Fang<sup>60</sup> show higher than other models. The Chien model<sup>55</sup> considers the particle shape factor as a sphericity, specified in Eq. 2.27. Therefore, Chien's correlation<sup>55</sup> was used in this study. The Shah's method<sup>57</sup> was also used for checking the appropriateness of the determined settling velocity. The equations relating the drag coefficient,  $C_D$ , and the particle Reynolds number,  $N_{Re p}$ , for Newtonian and non-Newtonian fluid flow around a smooth spherical particle in three regions (Stokes or creeping, intermediate, and Newton or turbulent) are presented in Appendix A.

When the particle volumetric concentration in the drilling fluid is less than  $0.5 \%$ , the individual particles are so far apart they do not affect each other (i.e., no particle - particle interaction) as they move through a laminar fluid.<sup>61</sup> The practical range of cuttings volumetric concentrations is generally  $0.5$  to  $5 \%$ .<sup>13,28,30</sup>



**Fig. 2.4 – Comparison of particle Reynolds number and drag coefficient (Power-law model:  $n = 0.68$ ,  $K = 0.006 \text{ lbrs}^n/\text{ft}^2$ )**



**Fig. 2.5 – Particle Reynolds number and settling shear rate (Power-law model:  $n = 0.68$  and  $K = 0.006 \text{ lb}_r\text{s}^n/\text{ft}^2$ )**

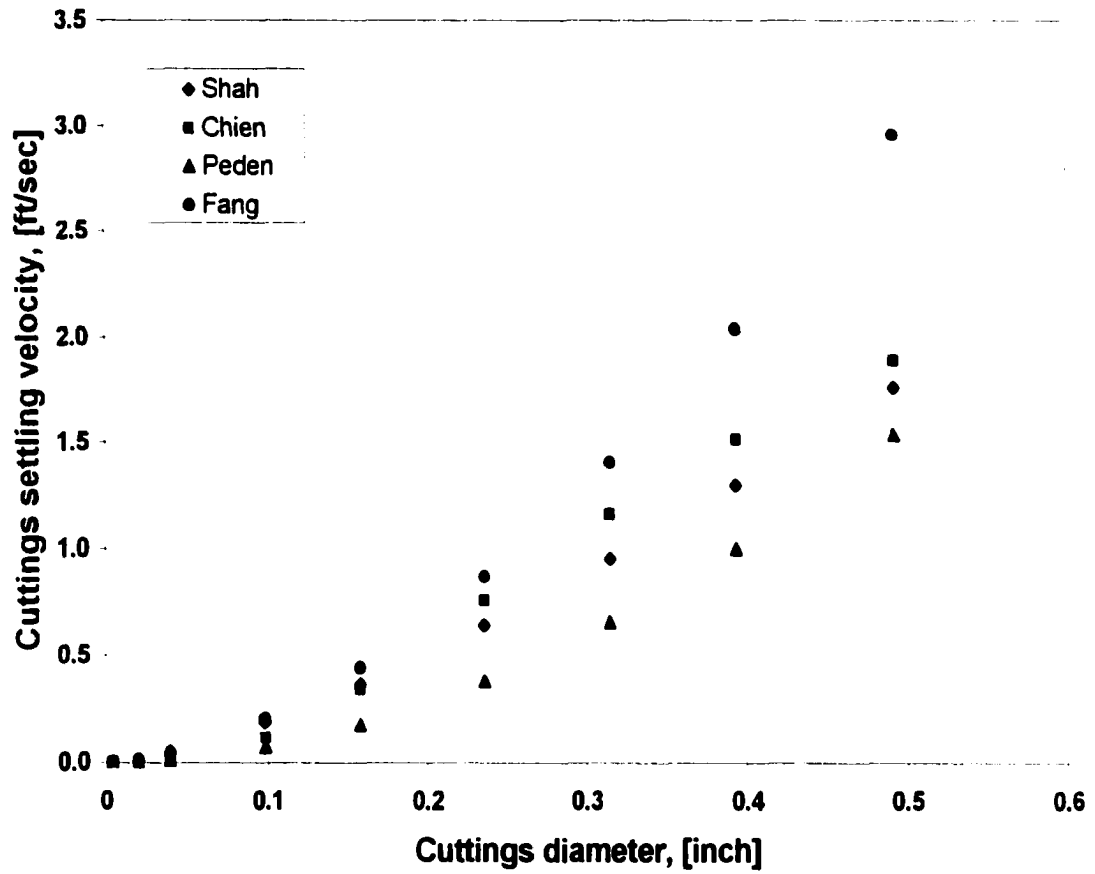


**Fig. 2.6 – Cuttings settling velocity with the different nominal cutting diameters (Power-law fluid:  $n = 0.68$ ,  $K = 0.006 \text{ lb}_r\text{s}^n/\text{ft}^2$ )**

As the solids concentration in the dispersed suspension increases, inter-particle distance during transport becomes smaller and the particles start to interfere with each other. The annulus flow conditions of a drilling fluid were also considered as turbulent regime, where the possibilities for particles to interact with each other increases.

If the particles are not uniformly distributed, the effect may be a net increase in settling velocity, because the return flow due to displaced volume will predominate in cluster formation. Salama and Mikura<sup>61</sup> noted that the cluster formation effect was significant only in suspensions that were nearly mono-dispersed. They also concluded that most suspensions were poly-dispersed and the clusters in such suspensions were short-lived.

Hindered settling behavior can be defined as a function of the particle volumetric concentration. Since the drilled cuttings suspension consists of clusters of many particles, the hindered settling velocity was considered in this study. The hindered settling velocity can be described as a Stoke's law correction by introducing a multiplying factor. For hindered settling, the correlation developed by Thomas<sup>62</sup> was used in this study.

$$V_h = V_p e^{-5.74C_s} \quad (2.33)$$

where,  $V_h$  is hindered settling velocity and  $C_s$  is cuttings volumetric concentration in a suspension layer.

### 2.4.3 Lifting and Sliding/Rolling

Apart from gravity and hydrostatic pressure, the bed particles are also subjected to forces caused by the fluid flow. These forces could be resolved into three components:

(1) the frictional force, which acts tangentially along the bottom of the stream; (2) the hydraulic lift, which has its largest effect on the top layer of the particles forming the bed; and (3) a buoyancy force, which acts to lift the particles by the weight of volume excluded by the particles.

At a small velocity the pressure at the front of the particle is nearly the same as that at the back. The drag force acting upon a particle is due to the viscous tangential stress along that part of the surface, which is exposed to the flow. El-Samni<sup>63</sup> noted that, at high velocities, the drag force due to tangential stress becomes unimportant compared to the drag due to the pressure differences caused by asymmetric pressure distribution at the front and at the rear of the particle. The second force is the hydraulic lift, which results from the pressure difference caused by the velocity distribution along the surface of the particle.<sup>63</sup>

El-Samni<sup>63</sup> and Einstein et al.<sup>14</sup> presented results of the dynamic forces due to a flowing stream acting on rocks protruding above a sediment bed. Their studies focused on a turbulent water stream flowing over a bed of rocks. Clark and Bickham<sup>16</sup> introduced El-Samni's equation<sup>63</sup> for the calculation of a lift coefficient for a sphere resting on a streambed. They presented the lift coefficient ( $C_L$ ) as follows:

$$C_L = 5.82 \left( \frac{\alpha_p}{N_{Re\ p}} \right)^{1/2} \quad (2.34)$$

$$\text{where, } \alpha_p = \frac{d_p}{2U} \left| \frac{du}{dr} \right| \quad (2.35)$$

The lift force ( $F_L$ ) can then be defined as:

$$F_L = C_L \frac{\pi d_p^2}{8} \rho_L U^2 \quad (2.36)$$

Figure 2.7 illustrates force diagram acting on a particle sitting on the surface of a cuttings-bed. It will likely be positioned in an interstice of several neighboring cuttings held stationary by the bed. The particle was assumed to be at the edge of a rolling and smooth sphere. The following equation represents the summation of the moment acting on point “A”.

$$F_D L_D + (F_L + F_B) L_G \geq F_G L_G \quad (2.37)$$

where,  $F_D$  is a drag force,  $F_B$  is a buoyancy force,  $F_G$  is a gravitational force.  $L_D$  is acting distance of drag force and  $L_G$  is acting distance of  $F_L$ ,  $F_B$ , and  $F_G$ .

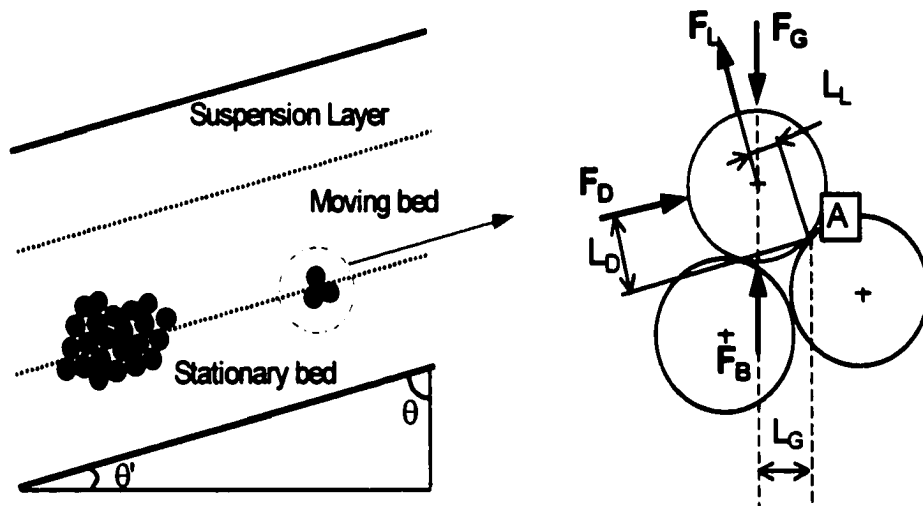


**Fig. 2.7– Forces acting on a particle at the lower stratum**

The first two terms give the driving moment and the last term is the opposing moment. When the driving moment, which arises from the drag exerted by the viscous fluid, is greater than the opposing torque (which arises from the weight of the particle acting on moving point A) the particle begins to move. A particle moves in the same direction as



the carrier fluid when the lift force is not strong enough. This is the sliding mechanism. When the lift force is strong enough to lift it up, the particle is lifted into the fluid. As it is de-accelerated by a decrease in the fluid velocity due to reduction of cuttings-bed area (an increase of flow path area), it will start to settle back in the wellbore due to particle settling.

#### **2.4.4 Cuttings Volumetric Concentration**

Early investigations of porosity effect were conducted by investigators in the fields of ground-water geology, petroleum geology, and petrophysics. Collins<sup>25</sup> considered six different packings of uniform spheres. The porosity of these various packings fell between the limiting values of 0.2595 for rhombohedral packing and 0.4764 for cubic packing. Figure 2.8 shows packing of uniform spheres. It is difficult to duplicate a natural packing existing in the wellbore by simply pouring spheres in a container. In addition, the cuttings involved are irregular shaped during drilling operations.

Knowledge of a cuttings volumetric concentration ( $C_b$ ) of a drilled cuttings-bed and its porosity ( $\phi$ ) are important in view of a fluid flow path and force balances. The cuttings volumetric concentration and its porosity have not been thoroughly investigated. Cuttings volumetric concentration affects forces and momentum balances, as well as the suspension rate in a dispersed suspension layer. Most recent studies<sup>12,22,23</sup> have considered that cuttings were the same size and were spherical in shape. They assumed that the cuttings used in their simulation were spheres with cubic packing: cuttings volumetric concentration was approximately 52%.

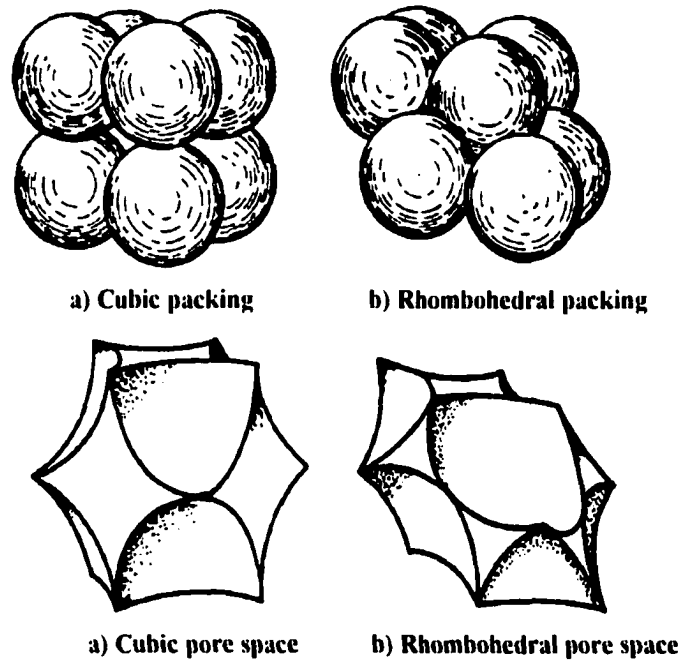


**Fig. 2.8 - Cubic and rhombohedral packing / pore space with uniform spheres<sup>66</sup>**

For naturally occurring drilled cuttings of non-uniform grain size, the porosity is dependent on the distribution of grain size. A variety of grain sizes permits smaller grains to fill the pores formed by large cuttings. This results in lower porosities. During the settling and movement of cuttings, saltation may exist above the cuttings-bed. This may result in the consolidation of cuttings packing. Conversely, a cuttings-pack usually consists of small regions of irregular packing in which “bridging” has occurred. In the bridging regions, the porosity is invariably greater than regular packing.<sup>65, 66</sup> Therefore, the following experimental work was performed to estimate the cuttings volumetric concentration, as well as the porosity of a cuttings-bed.

#### 2.4.4.1 Experimental Apparatus

The experimental apparatus shown in Fig. 2.9 was used to measure voids of a cuttings-bed. Eight percent (8%) of Potassium Chloride (*KCl*) solution was used to measure the voids in order to avoid any dispersion and swelling problems of shale cuttings during measurements. Generally, the cuttings size distribution is a function of formation types, ROP, torque, bit shape, and weight on bit (WOB). To obtain the generalized cuttings size distribution is a quite difficult matter. However, Aremu<sup>67</sup> noted that the drilled cuttings size distribution is US mesh size 4 to 8, which is generally accepted by the oil and gas industry. These are equivalent to 0.09 – 0.19-in. (2.36 to 4.75 mm).

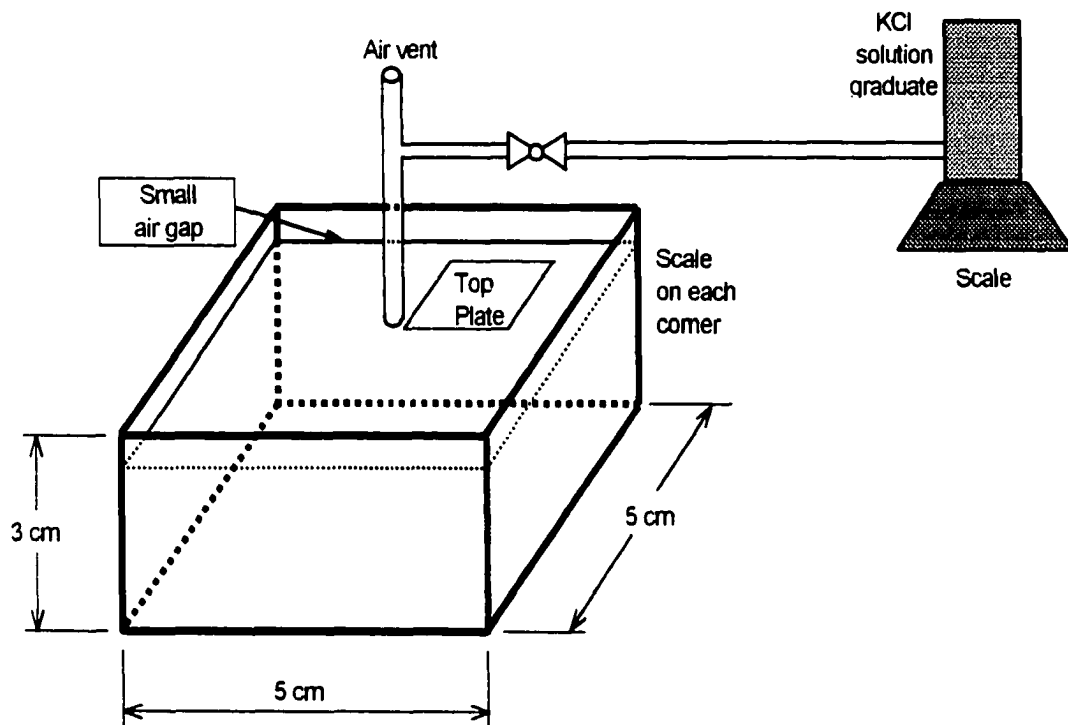


**Fig.2.9 - Experimental apparatus for the measurement of cuttings volumetric concentration**

#### 2.4.4.2 Experimental Procedure

The apparatus was filled with 4 – 8 US mesh drilled cuttings. The cuttings volume was carefully measured without shaking the apparatus. The 8 % KCl solution was used to fill up the voids formed by cuttings until the solution level reached the top plate. The weight of the KCl solution used in each test was recorded. Then the required volume of KCl was calculated. These tests were repeated, properly shaking the apparatus in order to revive the effects of cuttings transport at the bed surface on the cuttings consolidation. Cuttings-bed porosity can be obtained by the following equation:

$$\psi = \frac{\text{Volume of KCl solution}}{\text{Cuttings packing volume}} \quad (2.38)$$

Volumetric concentration of drilled cuttings ( $C'_b$ ) can then be calculated by the following equation:

$$C'_b = 1 - \psi \quad (2.39)$$

The porosity of a naturally settled cuttings-bed during drilling operation is assumed to be between the values measured, with or without shaking the cuttings packing.

#### 2.4.4.3 Experimental Results

A statistical analysis was performed using the “SAS Program” in order to determine if the two test-methods (shaking and without shaking the cuttings packing) were significantly different from each other. This experiment was designed as a two-factor (test methods and rock cuttings sources) factorial design with three replications. The test design and results are shown in Table 2.3. Two different test methods (shaking and

without shaking) are tested on cuttings volumetric concentration of rock cuttings sources (Berea sandstone, and Shale samples: Wapanuka, Atoka, and Wilcox).

**Table 2.3 – Two-factor factorial test design and results of cuttings volumetric concentrations**

Cuttings Source	Test Methods	
	Shaking	Without Shaking
Berea Sandstone	0.4775	0.4127
	0.4596	0.4074
	0.4854	0.4150
Wapanuka	0.5305	0.4483
	0.5019	0.4353
	0.5188	0.4489
Atoka	0.5197	0.4422
	0.5111	0.4502
	0.5142	0.4455
Wilcox	0.4470	0.4380
	0.4848	0.4408
	0.4781	0.4358

#### **2.4.4.4 Data Analysis of Cuttings Volumetric Concentration**

The analysis of variance (ANOVA) test results shows that the “F test” value is 31.15 with less than 0.0001 of “P value” (Table 2.4). This analysis shows that there are significant mean differences between the test methods. The test with shaken cuttings shows mean volumetric concentration,  $\bar{C}_{b1} = 0.4966$  with a standard deviation of 0.0223, while the test without shaking shows mean volumetric concentration,  $\bar{C}_{b2} = 0.4349$  with a

standard deviation of 0.0149. As expected, the test with a shaken cuttings sample shows higher mean scores than the test without shaking.

**Table 2.4 – ANOVA for cuttings volumetric concentrations**

Source	Degree of freedom	ANOVA Sum of Square	Mean Square	F value	P value
Cuttings sample	3	0.00602	0.00201	31.15	<0.0001
Test methods	1	0.02272	0.02272	352.89	<0.0001
Sample×method	3	0.00086	0.00029	4.48	0.0182
Error	16	0.00103	0.00006		
Total	23	0.03064			

Actual cuttings volumetric concentration was considered intuitively to be between the mean values of  $\overline{C_{h1}}$  and  $\overline{C_{h2}}$ . The actual cuttings volumetric mean concentration (0.4805) was obtained by estimating the mean parameter (average between upper confidence limit for shaking method and low confidence limit for without shaking method), and thus this value was used in this study. The details are described in Table 2.5. The volumetric concentration in a cuttings-bed with a 95 % confidence interval is shown in Table 2.5, regardless of rock sources.

**Table 2.5 – Statistical analysis of cuttings volumetric concentrations**

**a) Mean concentration of each test method**

<b>Level of test</b>	<b>No. of sources</b>	<b>Mean</b>	<b>Std. Deviation</b>
With shaking	12	0.4966	0.0223
Without shaking	12	0.4350	0.0149

**b) Mean concentration of each cuttings source**

<b>Level of sample</b>	<b>No. of sources</b>	<b>Mean</b>	<b>Std. Deviation</b>
Sandstone	6	0.4805	0.0380
Wapanuka	6	0.4429	0.0353
Atoka	6	0.4806	0.0412
Wilcox	6	0.4590	0.0232

**c) Estimation of mean value with a 95 % confidence interval for the shaking method**

<b>Parameter</b>	<b>Estimate</b>	<b>LCL</b>	<b>UCL</b>
Mean	0.4966	0.4824	0.5107
Std. Deviation	0.0223	0.0158	0.0378
Variance	0.0005	0.0002	0.0014

LCL: Low Confidence Limit, UCL: Upper Confidence Limit

**d) Estimation of mean value with a 95 % confidence interval for the without shaking method**

Parameter	Estimate	LCL	UCL
Mean	0.4658	0.4503	0.4812
Std. Deviation	0.0365	0.0284	0.0512
Variance	0.0013	0.0008	0.0026

## **2.4.5 Suspension**

### **2.4.5.1 Classification of Flow Behavior**

Suspensions are quite important and wide spread in the petroleum industry. In fact, suspensions may be encountered throughout each of the stages of petroleum recovery and processing, as shown in the following list<sup>68</sup>:

- Migration of fines during secondary and enhanced recovery
- Dispersions of asphalt in crude oils
- Production of solids in oil recovery at well-head
- Suspensions of drilled cuttings in drilling mud
- Stimulation and fracturing
- Well cementing slurries

A suspension is a special kind of dispersion. Dispersions can take different forms, depending on the dispersion medium and particle characterizations. The term suspension refers to the dispersion of solids in a continuous liquid phase. Dispersions can be formed with mechanical energy input via some form of fluid agitation, such as strong turbulent eddies of drilling fluid. The term aerosol is conventionally used to refer to dilute



suspensions of fine particles in a gas and the term emulsion is used to identify suspensions of particles in a gas or liquid in the field of fluidization.<sup>65</sup>

Walton<sup>12</sup> classified suspensions into the possible flow regimes described below. One is a homogeneous suspension (symmetric), which occurs when the fluid velocity is extremely high. Such high velocities will only rarely be encountered in cleanout operations and the gravitational settling of the particles will be negligible compared with the mixing generated by the fluid turbulence. All of the particles are carried in suspension and are uniformly distributed over the cross section of the wellbore. A uniform concentration profile is usually obtained when particles having low settling velocities are used. Such low settling velocities are encountered when the density of the solid particles approaches that of fluid.<sup>61</sup>

The other is a heterogeneous (asymmetric) suspension. At lower velocities than the ones for the symmetric suspension case, particles can also be carried in suspension.<sup>80</sup> However, the settling tendency of the particles creates a skewed distribution of particle density, with more of the particles settling at the bottom of the hole. The particle settling velocity in this case is high.

The pressure drop and pumping requirements for transportation of fluids with particles (slurry) depend on the type of slurry. Shah<sup>53</sup> noted that the flow curve (shear stress versus shear rate) is also a strong function of the slurry type. Figure 2.10 shows the variation of the wall shear stress as a function of the nominal shear rate for homogeneous and heterogeneous slurry flow in a horizontal pipe. At high shear rates, heterogeneous fluid response (curve A) tends to parallel homogeneous fluid response (Curve B). However, at low shear rates, the vertical solids concentration gradient increases until

either a stationary or slowly moving bed of deposited particles appears along the pipe bottom as the slurry velocity decreases.<sup>53</sup> The slurry velocity at which a bed of particles forms is defined as the critical deposition velocity,  $V_D$ . A further decrease in the slurry velocity below  $V_D$  leads to an increase in friction loss and may also result in pipe plugging.

Curve *B* of Fig. 2.10 shows the flow curve of homogeneous slurry. At high shear rates, a steep linear turbulent flow regime occurs. As the slurry velocity is decreased in the turbulent regime, a sudden transition to laminar flow regime occurs. The transition velocity,  $V_T$ , corresponds to this change in flow regime and remains the same whether approached from turbulent or laminar flow directions.<sup>53</sup> With an increasing shear rate, the wall shear stress decreases until a minimum value is reached in Fig. 2.11. The fluid velocity that corresponds to this minimum shear stress is the critical re-suspension velocity,  $V_r$ . Figure 2.11 shows that a particle re-suspension velocity is greater than a particle critical deposition velocity.

#### **2.4.5.2 Factors Affecting Suspension**

Suspension behavior is largely dependent on particle interactions or the degree of flocculation or aggregation.<sup>68</sup> There are several parameters that affect dispersion of drilled cuttings in a drilling fluid. Figure 2.12 illustrates the major factors affecting suspension in a drilling fluid. The drilled cutting size distribution, shape, and surface characterization are important factors in suspension.

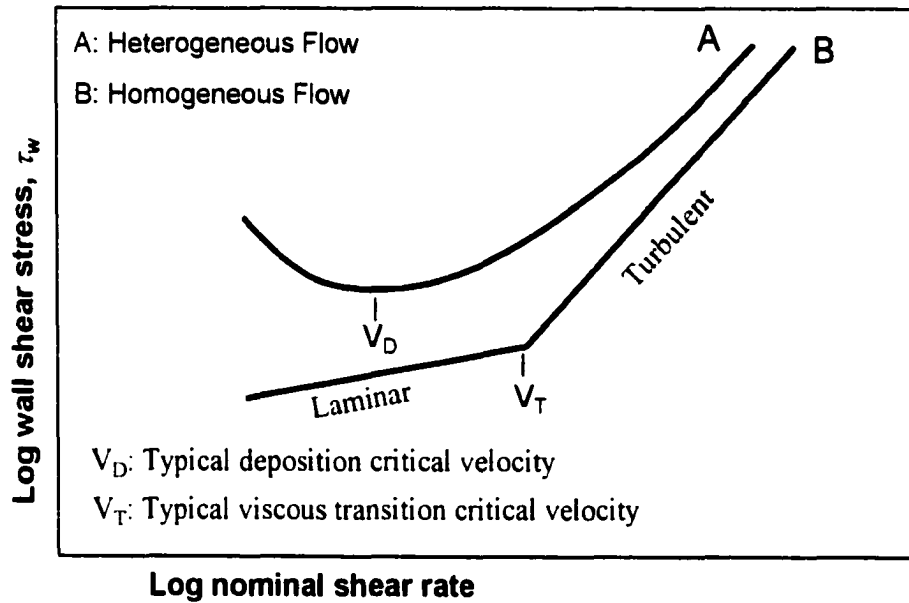


Fig. 2.10 – Wall shear stress vs. nominal shear rate for homogeneous and heterogeneous slurries<sup>53</sup>

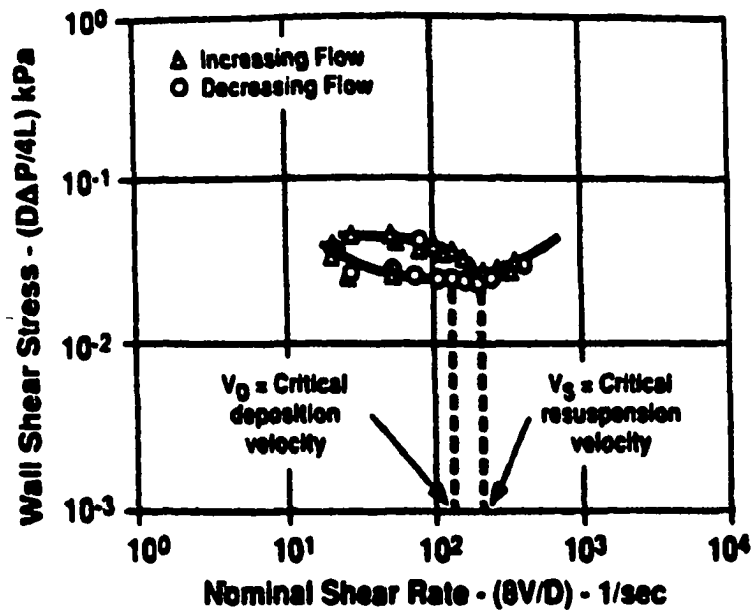
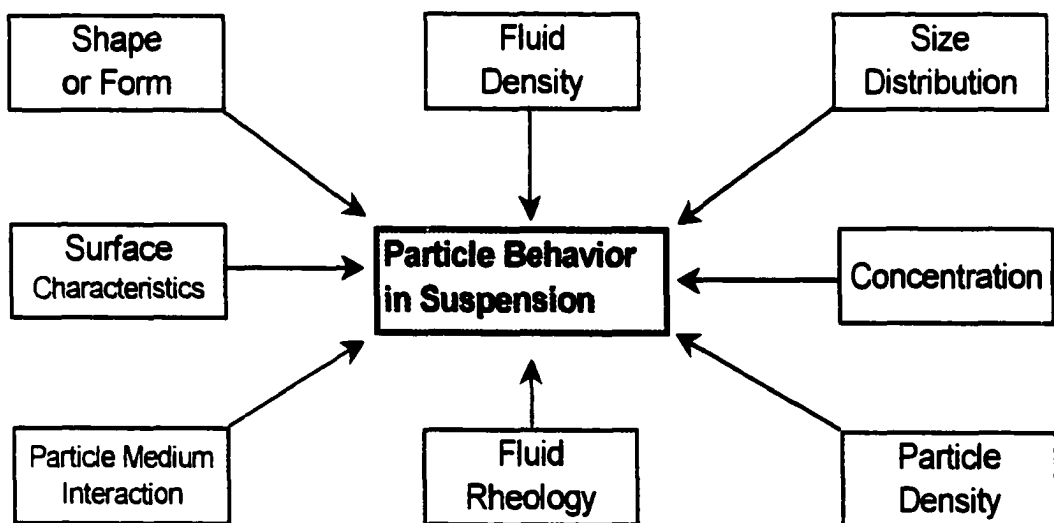


Fig. 2.11 – Critical re-suspension velocity in slurry flow<sup>53</sup>

Most drilled cuttings are of irregular size and shape. The shape of drilled cuttings is characterized by the degree of sphericity, as defined in Eq. 2.27. However, the cuttings size distribution varies from location to location, drilled bit size and types, rotation speed of bit, and ROP. In this study, the size range of drilled cuttings distribution used was 4 to 8 US mesh.

Suspensions are also strongly influenced by fluid rheology as a function of the shear rate. The shear rate at the drilling bit nozzle is about  $10,000 - 100,000 \text{ s}^{-1}$ , which is about 100 times larger than while circulating.<sup>70,71</sup> A highly viscous fluid may prevent cuttings settling out of the fluid. However, the longer supporting time is not relatively important in the horizontal segment because the settling distance for cuttings in the borehole wall is short. Moreover, a high viscous fluid makes it difficult to maintain a high turbulency, and increases the resistance to fluid flow. However, a highly viscous fluid is useful for suspending and carrying cuttings in a vertical segment. Other main factors affecting suspensions are cuttings concentration and density of both cuttings and drilling fluid.



**Fig. 2.12 – Factors that affect drilled cuttings suspension**

### 2.4.5.3 Suspension Mechanism

It is generally accepted that particles remain in suspension at a sufficiently high flow rate because of the effect of the turbulent eddies. These turbulent eddies are sufficiently strong to overcome the tendency of the particles to settle out. Theoretical models describe the suspension process variously in the following terms: (1) the turbulent energy required to support the particles; (2) forces on the particles due to the turbulent eddies, which balances the gravity force; and (3) balance between a downward drift, caused by gravity and diffusion by turbulence against the induced particle concentration distribution.<sup>72</sup>

Particles are held in suspension against the force of gravity by a combination of viscous resistance and diffusion by turbulent eddies. The mechanism, which governs the dispersion of solid particles in the upper layer is represented by the well-known diffusion equation:

$$\varepsilon_p \frac{d^2 C'}{dy^2} + V_h \frac{dC'}{dy} = 0 \quad (2.40)$$

where,  $C'$  is the local volumetric cuttings concentration (fraction) of a particle,  $y$  is the vertical coordinate (perpendicular to the pipe axis),  $\varepsilon_p$  is the diffusion coefficient, and  $v_h$  is the hindered settling velocity obtained from Eq. 2.33. The volumetric cuttings concentration,  $C'$ , is defined as the percent volume of the annulus that is occupied by cuttings. Over 5 % of cuttings volumetric concentration in vertical holes have been found to cause problems on cuttings transport in the field.<sup>73,74</sup> Cuttings volumetric concentration in a transit and a horizontal segment is relatively higher than a vertical segment because of cuttings-bed formation. By treating both  $\varepsilon_p$  and  $v_h$  as constants, Eq. 2.40 can be rewritten as:

$$\frac{d^2C}{dy^2} + \frac{V_h}{\varepsilon_p} \frac{dC}{dy} = 0 \quad (2.41)$$

Eq. 2.41 is a second-order, linear, homogeneous equation with constant coefficients and can be integrated to obtain

$$C(y) = C_1 + C_2 \exp\left(-\frac{V_p}{\varepsilon_p} y\right) \quad (2.42)$$

where,  $C_1$  and  $C_2$  are constants of integration. This integration can be solved by assuming that the particle volumetric concentration in suspension is equal to the particle bed at the interface between the bed and suspension as a boundary condition. The detail derivation is described in Appendix B. The solution of the diffusivity equation by integration gives the following concentration profile in the upper layer of a horizontal annulus:

$$C(y) = C_{sb} \exp\left[\frac{-V_p}{\varepsilon_p} (y - y_{mb} - y_{sb})\right] \quad (2.43)$$

where,  $C$  was to be replaced by  $C_{sb}$  (cuttings volumetric concentration in the stationary bed), which was obtained by statistical data analysis ( $C_{sb} = 0.4805$ ), and  $y$  is the height of the bed. This cuttings volumetric concentration obtained from the experiments was similar to a maximum cubic packing of deposited particle ( $C_{sb} = 0.52$ ), which were used by other researchers.<sup>12,23</sup> A boundary condition that  $C_{mb} = C_{sb}$  at the interface between the bed and the flowing suspension was utilized in the solution of Eq. 2.43.

The average cuttings volumetric concentration ( $C_{sd}$ ), by integration of Eq. 2.43, over the cross section of the upper layer can be found in the Reference 20.

$$\frac{C_{sd}}{C_{mb}} = \frac{(D^2 - d^2)}{4A_{sd}} \int_{(\pi-\alpha'-\alpha)}^{\pi/2} \left\{ \exp\left(\frac{-V_p(D-d)(\sin\gamma - \sin(\pi-\alpha'-\alpha))}{2\varepsilon_p}\right) \cos^2\gamma \right\} d\gamma \quad (2.44)$$

where,  $\alpha$  and  $\alpha'$  are the central angles to the edges of the moving bed and the stationary bed layers, respectively (Appendix C: Wellbore Geometry).

The particle diffusivity,  $\varepsilon_p$ , depends on the physical properties of the particle, the fluid type, a concentration of particles in suspension, and an in-situ velocity of the suspension,  $U_{sd}$ . Walton<sup>12</sup> proposed that the particle eddy diffusivity is a function of Reynolds number of the fluid in a suspension layer, which was given as:

$$\varepsilon_p = 0.014 \varepsilon_o d_p U_{sd} N_{Re f}^{1/3} \quad (2.45)$$

where,  $U_{sd}$  is a local velocity of a dispersed suspension layer and the cuttings particle diffusion coefficient is defined as:

$$\varepsilon_o = \left( \frac{C}{0.12} \right)^{0.25} \quad \text{if } C > 0.05 \quad (2.46)$$

$$\varepsilon_o = 1.24 \left( \frac{C}{0.12} \right)^{0.5} \quad \text{if } C < 0.05 \quad (2.47)$$

## **CHAPTER THREE**

# **A THREE-LAYER HYDRAULIC MODEL FOR COILED-TUBING HORIZONTAL DRILLING**

### **3.1 Introduction**

Over the last 30 years, substantial progress has been made in understanding the mechanism of cuttings transport and also in developing empirical or semi-analytical formulae for transport capacity and friction pressure loss for practical applications. The present two-layer model: a cuttings stationary bed and a suspension layer (or a stationary bed and a moving bed), does not properly characterize the cuttings transport mechanism in horizontal wells. Doron et al<sup>75</sup> argued that the two-layer model fails in many cases to predict the existence of a stationary bed, which was indeed observed experimentally.

In this study, the Doron and co-workers mathematical models<sup>23,76</sup> in horizontal pipe flow were extended to annular flow with the additional consideration of drilling fluid rheology, drilled cuttings shape, cuttings volumetric concentration, and wellbore



geometry including eccentricity of coiled tubing. These extended mathematical models have proven to overcome the limitations of existing two-layer models. This enables an efficient prediction of cuttings transport during horizontal drilling using coiled tubing. In particular, the model described in this study formulates a transport process and includes the relevant parameters, such as rheological characteristics of the drilling fluid, cuttings size/sphericity/concentration, wellbore geometry, eccentricity of the coiled tubing, and pumping rate of the drilling fluid.

The objective of this study was to develop a mathematical model to predict the effects of the parameters and to evaluate their effects, which affect cuttings transport in coiled tubing horizontal drilling. In order to accomplish the objective, various fluid velocities, concentrations of cuttings (change of ROP), fluid rheology, size and sphericity of cuttings, and wellbore geometry were incorporated in the model. The flow mode concepts of Nguyen and Rahman<sup>5</sup> were improved and the boundary conditions for different flow modes were specified.

## **3.2 Model Hypotheses and Description**

### **3.2.1 Model Hypotheses**

The following hypotheses were considered in the development of the mathematical model so as to simplify it within the range that would not deteriorate its accuracy:

(1) Flow phase and state

- The flow pattern in annulus was defined as a steady-state and a two-phase solid-liquid incompressible mixture.

#### (2) Cuttings

- Cuttings size, sphericity ( $\varphi = 0.8$ ),<sup>24,55</sup> and distribution were assumed uniform.
- Volumetric concentration of drilled cuttings in the upper layer (heterogeneous fluid layer) was relatively small.

#### (3) Carrier fluid

- The Ostwald de Waele (Power-law) fluid model was considered.
- Carrier fluid density and rheological properties were constant.

#### (4) Pipe rotation

- Rotation effect of the drill string was not considered since the coiled tubing does not rotate while drilling.

#### (5) Other hypotheses

- There was no slip between the solid and liquid states in each of the layers.
- An isothermal process was assumed.

### 3.2.2 Model Description

The hydraulic transport of the heterogeneous mixture of liquid and solid through the annulus is a complex physical phenomenon, which has been analyzed over the years by various researchers.<sup>5,28,75</sup> As a result, ranges of basic flow patterns have been identified. These flow patterns depend on a number of variables, which involve particle concentration, settling characteristics, slurry flow velocity, and pressure gradient.<sup>10</sup>

Transport process can be categorized into the following flow patterns and are schematically illustrated in Fig. 3.1:

- (1) If the fluid flow rate is high enough, resulting in high turbulence, all solid particles will be suspended (Fig. 3.1A). As the pumping rate decreases, which results in a decrease in turbulent intensity, the settling forces acting on the particles become significant. Solid particles, whose density is higher than that of the carrier fluid, tend to settle and agglomerate at the bottom of the annulus. This forms a stationary deposit, above which a heterogeneous mixture flows (Fig. 3.1B).
- (2) As the pump rate is further reduced, the bed height increases to a certain height until the in-situ velocity reaches the critical deposition velocity. Then, the interface between the contact point of a surface stationary bed and a carrier fluid is in pseudo-equilibrium (Fig. 3.1C). Reduction in flow area due to the continuous settling of particles on the stationary bed over the pseudo-equilibrium height increases the in-situ velocity (Fig 3.1D). An increase in the in-situ velocity (due to the reduced flow path area) increases the energy available for particle clusters in a moving bed layer to tumble around on the bed surface. A separated cuttings-bed is formed above the stationary bed called a moving bed layer (Fig. 3.1E). The cuttings at the surface of the bed travel forward, while the cuttings inside the bed remain stationary, so that the cuttings-bed looks as if it is rolling or sliding forward as a whole.<sup>28</sup>
- (3) Continuous reduction in the pump rate causes a reduction in the strength of turbulent eddies, as a result, it eventually reaches the two-layer flow (Fig. 3.1G). According to the two-layer model, the bed becomes stationary when the sum of the driving forces acting on the bed is lower than the sum of the forces opposing the bed's motion.<sup>75</sup>

(4) As the pump rate is further reduced, the stationary bed height increases (Fig. 3.1H).

It is reasonable that particles at the bottom get "stuck" and cannot be "dragged" by the bed at a low bed velocity.<sup>23</sup> These are the basic descriptions of a three-layer flow model used in this study, where the annulus is composed of three layers, i.e. a stationary bed at the bottom, a moving bed above it, and a heterogeneous mixture at the top in a horizontal segment.

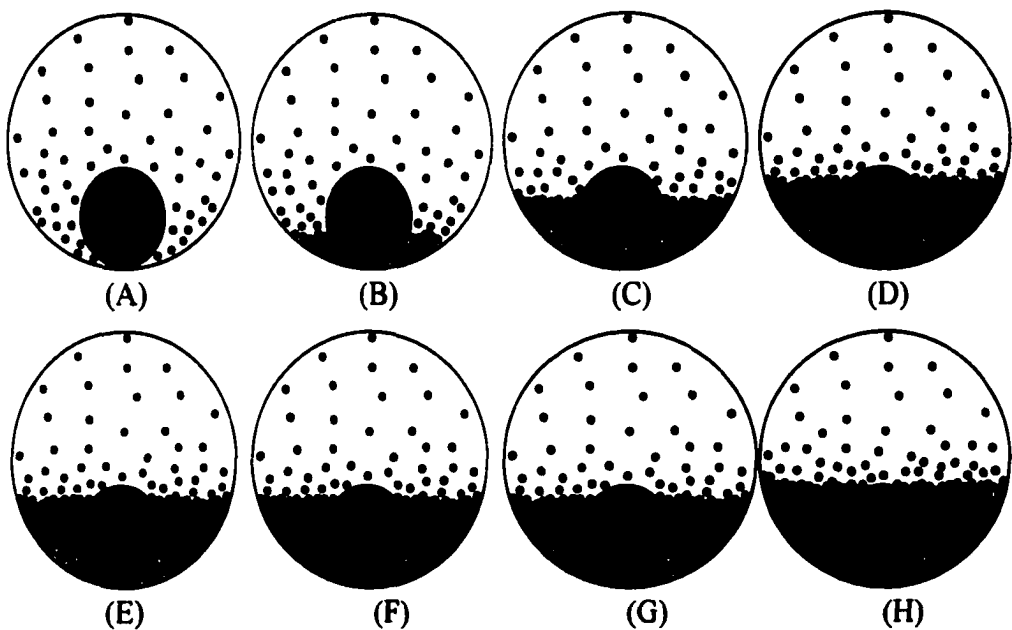


**Fig. 3.1- Schematic illustration of different cuttings transport modes**

### 3.3 Model Development

A mathematical model was developed based on the fact that cuttings–drilling fluid flows in a horizontal well at a flow rate such that there exists three layers in the annulus.

### 3.3.1 Continuity Equations

The carrier fluid flow with drilled cuttings can be considered as a stream tube bounded by a streamline. The continuity equation can be derived by equating the net mass flow rate into a stream tube of elemental length ( $dL$ ) and area  $A_i$  to the rate of change of mass within the elemental control volume. Thus, the steady state, mass transport equation for a one-dimensional (horizontal), two-phase and incompressible flow (neglecting any inter-phase mass transfer) for these three sections under consideration can be written as;

$$\frac{\partial}{\partial t}(A_i C_i \rho_i dL) = \rho_i C_i U_i \bullet A_i - \left[ \rho_i C_i U_i \bullet A_i + \frac{\partial}{\partial L}(\rho_i C_i U_i \bullet A_i) dL \right] \quad (3.1)$$

Dividing by  $dL$  (an elemental length), gives:

$$\frac{\partial}{\partial t}(A_i C_i \rho_i) + \frac{\partial}{\partial L}(\rho_i C_i U_i \bullet A_i) = 0 \quad (3.2)$$

The area  $A_i$  is a vector whose magnitude is equal to the magnitude of the area, and whose direction is normal to the plane of the area. Thus, the dot product of the area and the velocity indicates that the velocity component normal to the plane of the area and parallel to the vector  $A_i$  representing the area is multiplied by the magnitude of the area to get a scalar product, which represents the volumetric flow rate. Whenever the product of a scalar velocity and a scalar area is given as  $U_i A_i$ , the dot product  $U_i \bullet A_i$  is implied.

For steady-state flow, the first term is zero, thus, the second term is also zero, so that

$$\frac{\partial}{\partial L}(\rho_i C_i U_i A_i) = 0 \quad (3.3)$$

Where,  $C$  is the volume fraction,  $\rho$  is density,  $A$  is the cross sectional area of the flow path,  $U$  is the velocity, and the subscript  $i$  represents any one of the species in the flow.

### 3.3.1.1 For Solid Phase

Assuming no slip between the solid and fluid phase in the cuttings-bed, the continuity equation for the fluid and solid particles is written as:

$$\frac{\partial}{\partial L}(C_{sd}U_{sd}A_{sd} + \rho_{mb}C_{mb}U_{mb}A_{mb} + \rho_{sb}C_{sb}U_{sb}A_{sb}\rho_{sd}) = 0 \quad (3.4)$$

Here, the subscripts "sb", "mb", and "sd" refer to the stationary bed layer, the moving bed layer, and the dispersed suspension layer, respectively. The density of each layer at a certain point between 1 and 2 in the flow system in Fig. 3.2 can be regarded as constant under the steady-state flow conditions. Equation 3.4 was integrated to obtain:

$$A_{sd}C_{sd}U_{sd} + A_{mb}C_{mb}U_{mb} + A_{sb}C_{sb}U_{sb} = A_dC_tU_d \quad (3.5)$$

The relevant relation can be described as follows:

$$A_{sb} + A_{mb} + A_{sd} = A_d \quad (3.6)$$

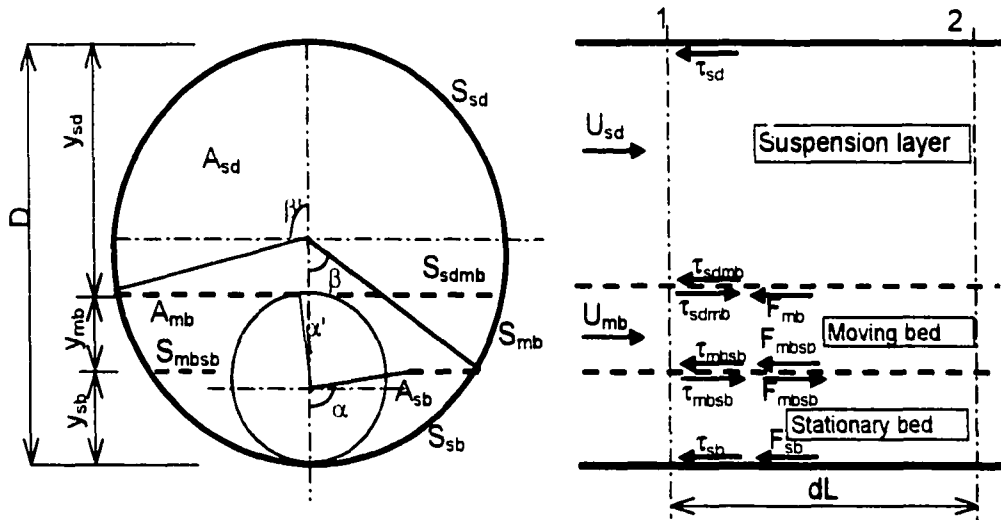


**Fig. 3.2 – Schematic diagram of the three-layer model; geometry, velocity, and shear stress**

### 3.3.1.2 For Liquid Phase

$$U_{sd}(1 - C_{sd})A_{sd} + U_{mb}(1 - C_{mb})A_{mb} + U_{sb}(1 - C_{sb})A_{sb} = U_a(1 - C_t)A_a \quad (3.7)$$

Under a steady-state flow condition, volumetric flow rate of cuttings ( $U_s C_s A_s$ ) is equal to the volume of cuttings generated at the drill bit per unit of time. Cuttings concentration can then be specified as a function of average rate of penetration (ROP):

$$C_t = \frac{ROP}{ROP + U_a \left( \frac{D_t^2 - d^2}{D_t^2} \right)} \quad (3.8)$$

where,  $D_t$  is the nominal diameter of the drill bit and  $d$  is the outer diameter of the coiled tubing.

## 3.3.2 Momentum Equations

### 3.3.1.1 Upper Dispersed Suspension Layer

The upper dispersed suspension layer is a relatively clean fluid or heterogeneous turbulent suspension, depending upon the flow conditions. Under a steady-state flow condition, the sum of the forces acting on the fluid flow zone should be:

$$A_{sd} \frac{\Delta P}{L} = \tau_{sd} S_{sd} + \tau_{sdmb} S_{sdmb} \quad (3.9)$$

where,  $\Delta P/L$  is the pressure gradient, and  $\tau_{sd}$  and  $\tau_{sdmb}$  are the upper layer shear stress and the interfacial shear stress acting on the wetted perimeters  $S_{sd}$  and  $S_{sdmb}$ , respectively. The relationships between each cuttings-bed area and the wetted-perimeter are described in Appendix C, Wellbore Geometry. The shear stress at the pipe circumference ( $\tau_{sd}$ ) is

$$\tau_{sd} = \frac{1}{2} \rho_{sd} U_{sd}^2 f_{sd} \quad (3.10)$$

where,  $f_{sd}$  is Fanning friction factor for a dispersed suspension layer. The shear stress at the interface between the upper layer and the moving bed is

$$\tau_{sdmb} = \frac{1}{2} \rho_{sd} (U_{sd}^2 - U_{mb}^2) f_{sdmb} \quad (3.11)$$

where,  $f_{sdmb}$  is friction coefficient between a suspension layer and a moving bed and  $\rho_{sd}$  is the effective density of the upper dispersed suspension layer. It is defined as:

$$\rho_{sd} = \rho_s C'_{sd} + \rho_L (1 - C'_{sd}) \quad (3.12)$$

where,  $\rho_s$  and  $\rho_L$  are the density of the cuttings and carrier fluid, respectively.

The Reynolds number,  $N_{Rej}$ , was calculated by using a hydraulic diameter. In the case of non-Newtonian fluids, the determination of Reynolds number is more complex, and many methods have been proposed. Most of these methods depend on the particular rheology of the fluid being used. The generalized Reynolds number for a Power-law fluid was used in this study. It is noted that the eccentricity has no effect on the calculation of Reynolds number because it uses only the hydraulic diameter of the annulus.<sup>19</sup> The following correlations for the friction factor of the dispersed suspension layer and interfacial friction factor were used in this study:

$$f_{sd} = 0.00454 + 0.645 N_{Rej}^{-0.7} \quad (\text{Doron et al.}^{23}) \quad (3.13)$$

$$f_{sdmb} = h N_{Rej}^p n^q \left( \frac{d_p}{D_{sd}} \right)^t \quad (\text{Martin et al.}^{77}) \quad (3.14)$$

where,  $h = 0.966368$ ,  $p = -1.07116$ ,  $q = 2.360211$ , and  $t = -2.34539$ . For both  $f_{sd}$  and  $f_{sdmb}$ , Reynolds number of the suspension layer was used.



### 3.3.2.2 Moving Bed Layer

Summing up all the forces acting on this region (Fig. 3.2) gives:

$$A_{mb} \frac{\Delta P}{L} = \left( \frac{F_{smb}}{L} \right) - \tau_{smb} S_{smb} + \left( \frac{F_{mbsb}}{L} \right) + \tau_{mbsb} S_{mbsb} \quad (3.15)$$

where,  $F_{mbsb}$  is the frictional force between the continuous moving and the associated stationary bed;  $\tau_{mbsb}$  is the hydrodynamic shear stress acting on the interface between a moving bed and a stationary bed; and  $\tau_{mh}$  is the hydrodynamic shear stress acting on the surface of a moving bed. The shear stress at the interface between a moving bed and a stationary bed is

$$\tau_{mbsb} = \frac{1}{2} \rho_{mb} U_{mb}^2 f_{mbsb} \quad (3.16)$$

where,  $\rho_{mb}$  is the effective density of the upper moving bed layer, and it is defined as:

$$\rho_{mb} = \rho_s C_{mb} + \rho_L (1 - C_{mb}) \quad (3.17)$$

The following correlation developed by Doron et al.<sup>23</sup> is used for the calculation of the moving bed friction coefficient,  $f_{mbsb}$ :

$$f_{mbsb} = 0.046 N_{Re f}^{-0.02} \quad (3.18)$$

where, Reynolds number of a moving bed is used.

### 3.3.3 Moving Bed Velocity

Figure 3.3 shows a momentum balance on a particle at the upper part of the stationary bed. When the driving torque (which arises from the drag exerted by the moving bed layer on the particle) is larger than the opposing torque (which arises from

the weight of the particle on the moving bed), the particle begins to move.<sup>31</sup> This is the dominant mechanism for cuttings transport in a moving-bed in this study. When the magnitudes of both moments are equal, the particle is in stationary status. This approach was useful for finding the mean velocity of a moving bed. The summation of moments around the acting point “A” is given as:

$$F_D L_D + (F_L + F_B) L_G - F_G L_G \geq 0 \quad (3.19)$$

where,  $F_D$  is the drag force,  $F_L$  is the lift force,  $F_G$  is the gravity force, and  $F_B$  is the buoyancy force. They were assumed to act through the center of gravity of the particle.<sup>23,75</sup>

The auxiliary equations used to calculate the related forces and derivation of the minimum moving bed velocity are described in Appendix A. Equating the driving moment and the opposing moment due to gravitational force gives:

$$U_{mb} = \sqrt{\frac{0.131(\rho_s - \rho_L)g \left[ C_{mb} \frac{y_{mb}}{d_p} \right]}{\rho_L (0.1651C_D + 0.0982C_L)}} \quad (3.20)$$

### 3.3.4 Summary of the Model

The three-layer model was described by a set of six equations. They are: Eqs. 2.43, 3.5, 3.7, 3.9, 3.15, and 3.20. The six unknowns with the given operating conditions were  $U_{sd}$ ,  $U_{mb}$ ,  $C_{sd}$ ,  $y_{mb}$ ,  $y_{sb}$ , and  $\Delta P / dL$  (the annular pumping velocities of the upper dispersed layer and of the moving bed, respectively, the average concentration of the upper dispersed layer, the heights of the moving bed, the heights of the stationary bed, and the pressure gradient). The other sets of equations were the auxiliary equations derived or directly imported from other works.<sup>12,23,77</sup>

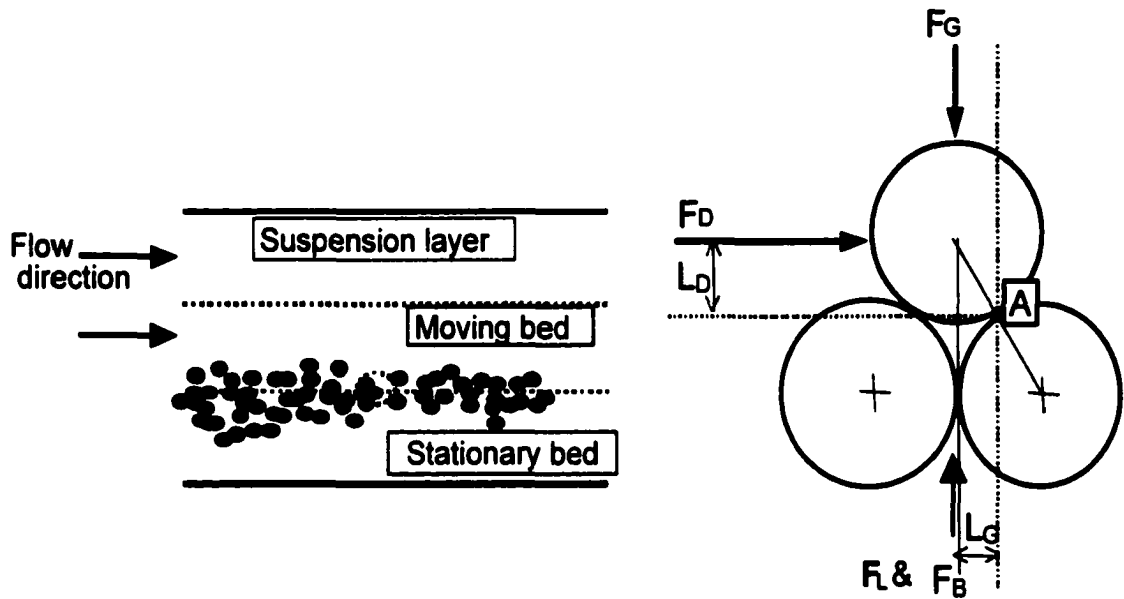


**Fig. 3.3 – Forces acting on a particle at the lower stratum of the moving bed**

### 3.4 Solution of the Model

The continuity equation for solid, Eq. 3.5, and for liquid, Eq. 3.7, may be further simplified by assuming that the velocity of the stationary bed ( $U_{sb}$ ) is almost zero (since it is not moving as specified in the model description). Hence, Eqs. 3.5 and 3.7 become the following:

$$A_{mb}C_{mb}U_{mb} + A_{sd}C_{sd}U_{sd} = A_aC_iU_a \quad (3.21)$$

$$U_{sd}(1 - C_{sd})A_{sd} + U_{mb}(1 - C_{mb})A_{mb} = U_a(1 - C_i)A_a \quad (3.22)$$

Adding Eqs. 3.21 and 3.22, it becomes:

$$U_{sd}A_{sd} + U_{mb}A_{mb} = U_aA_a \quad (3.23)$$

Equation 3.23 can be rewritten for a mean velocity of the suspension layer,  $U_{sd}$  as follows:

$$U_{sd} = U_a \left( \frac{A_a}{A_{sd}} \right) - U_{mb} \left( \frac{A_{mb}}{A_{sd}} \right) \quad (3.24)$$

Substituting for  $U_{sd}$  in Eq. 3.21 gives the following:

$$A_{mb} C_{mb} U_{mb} + A_a C_{sd} U_a - A_{mb} C_{sd} U_{mb} = A_a U_a C_t \quad (3.25)$$

Rearrange Eq. 3.25 gives a solid concentration of the dispersed layer ( $C_{sd}$ ) as follows:

$$C_{sd} = \frac{A_a C_t U_a - A_{mb} C_{mb} U_{mb}}{A_a U_a - A_{mb} U_{mb}} \quad (3.26)$$

All terms at the right-hand side of Eqs. 3.25 and 3.26 are functions of the unknowns  $y_{mh}$ ,  $y_{sh}$ , and  $U_{mh}$ , which are dependent on the operational conditions.

By applying the momentum equations, Eqs. 3.9 and 3.15, and eliminating the pressure gradient from these equations, Eq. 3.27 is obtained and written as follows:

$$\frac{A_{mb}}{A_{sd}} (\tau_{sd} S_{sd} + \tau_{sdmb} S_{sdmb}) = \frac{F_{mbsh}}{L} + \tau_{mbsh} S_{mbsh} + \frac{F_{mb}}{L} + \tau_{mb} S_{mb} - \tau_{sdmb} S_{sdmb} \quad (3.27)$$

Eq. 3.27 is rearranged into:

$$\frac{\tau_{sd} S_{sd} + \tau_{sdmb} S_{sdmb}}{A_{sd}} = \frac{\left( \frac{F_{mbsh}}{L} \right) + \tau_{mbsh} S_{mbsh} + \left( \frac{F_{mb}}{L} \right) + \tau_{mb} S_{mb} - \tau_{sdmb} S_{sdmb}}{A_{mb}} \quad (3.28)$$

Solving these equations simultaneously is quite complicated. An analytical iterative solution was used. The hierarchy flow chart for step-by-step calculation is provided in Appendix E.

### 3.5 Model Simulation Results and Discussion

In order to compare the simulation results with published experimental results, the simulation conditions were reviewed and compared, as shown in Table 3.1. From this comparison, the most reasonable range of simulation parameters was selected as a base case used in this study. The effect of the various parameters, such as fluid rheology, nominal annular velocity ( $U_a$ ) and cuttings concentration on cuttings transport efficiency were simulated and investigated with the base case listed in Table 3.1. The following sections are the simulation results showing the effects of changes in the parameters:

**Table 3.1 – Selection of simulation parameters**

Sources	Nguyen <sup>5</sup> (SPE 36383)	Martins <sup>22</sup> (SPE 23643)	Base case in this study
Fluid type	Low-vis bentonite	Low-vis bentonite	Low-vis bentonite
$n$	0.68	0.698	0.68
$K$ (lb <sub>r</sub> s <sup>n</sup> /ft <sup>2</sup> )	0.00566	0.00615	0.006
D (ID of wellbore)	5.0-in.	5.0-in.	5.0-in.
d (OD of CT)	1.9-in.	1.9-in.	1.9-in.
density of solid	2.62 g/cm <sup>3</sup>	2.62 g/cm <sup>3</sup>	2.62 g/cm <sup>3</sup>
density of fluid	8.41 lb/gal	9.2 lb/gal	9.2 lb/gal
mean dia. of solid	0.25-in.	0.248-in.	0.25-in. (0.63 cm)

#### 3.5.1 Effects of Nominal Annular Velocity in the Annulus

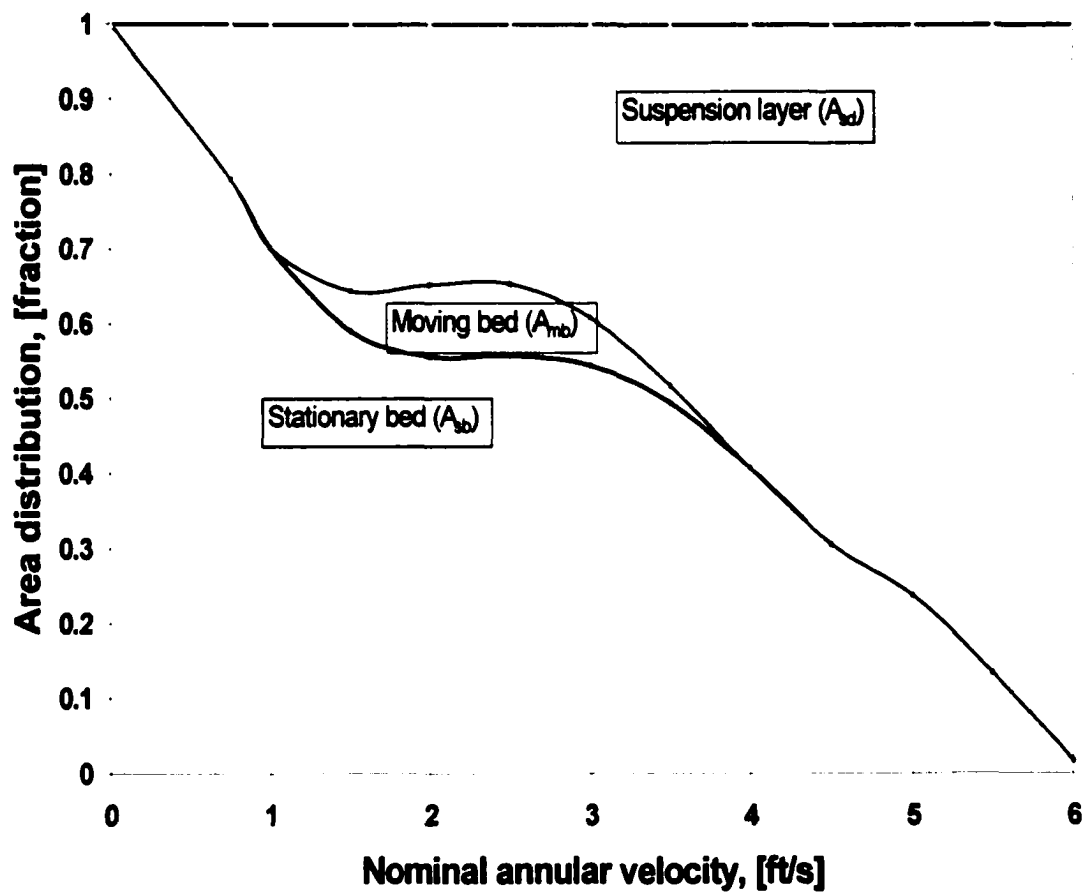
The simulation results for the base case are presented in Figs. 3.4 and 3.5. Figure 3.4 shows the area distribution of each layer in the annulus with changes of the nominal

annular velocity. The moving bed layer is plotted with its area distribution above the stationary bed. Similarly, the suspension layer is also plotted in the same manner. An increase in the nominal annular velocity,  $U_a$ , decreases the stationary bed up to 2 ft/s and then almost constant up to 3 ft/s. The stationary bed then dramatically reduces for flow velocity greater than 3 ft/s.

The simulation results with the different velocities for the base case are shown in Table 3.2. At the nominal annular velocity of 2.5 ft/s, the area of the moving bed begins to decrease. This means that the dispersed suspension criterion is satisfied, resulting in the top most particles being lifted into the suspension layer, and carried by the turbulent eddies. From the calculation, the turbulent suspension criterion is between 2.5 ft/s and 3 ft/s of the nominal annular velocity. This is in agreement with the result of Nguyen and Rahman (2.5 ft/s).<sup>5</sup>

**Table 3.2 – Simulated results with changes in the annular nominal velocity for the base case**

$U_a$ (ft/s)	$U_{mb}$ (ft/s)	$U_{sd}$ (ft/s)	$Y_{sb}$ (in.)	$Y_{mb}$ (in.)	$Y_{sd}$ (in.)	$A_{sb}$ (in. <sup>2</sup> )	$A_{mb}$ (in. <sup>2</sup> )	$A_{sd}$ (in. <sup>2</sup> )
0.75	0.00	4.13	3.93	0.00	1.07	13.73	0.00	3.07
1	0.19	3.63	3.56	0.01	1.42	12.14	0.00	4.66
2	1.07	5.84	3.06	0.32	1.61	9.78	1.51	5.51
3	0.85	7.83	3.02	0.20	1.77	9.58	0.94	6.28
4	0.00	6.89	2.52	0.00	2.49	7.04	0.00	9.76
5	0.00	6.62	1.92	0.00	3.08	4.10	0.00	12.71
6	0.00	6.08	0.11	0.00	4.89	0.17	0.00	16.63



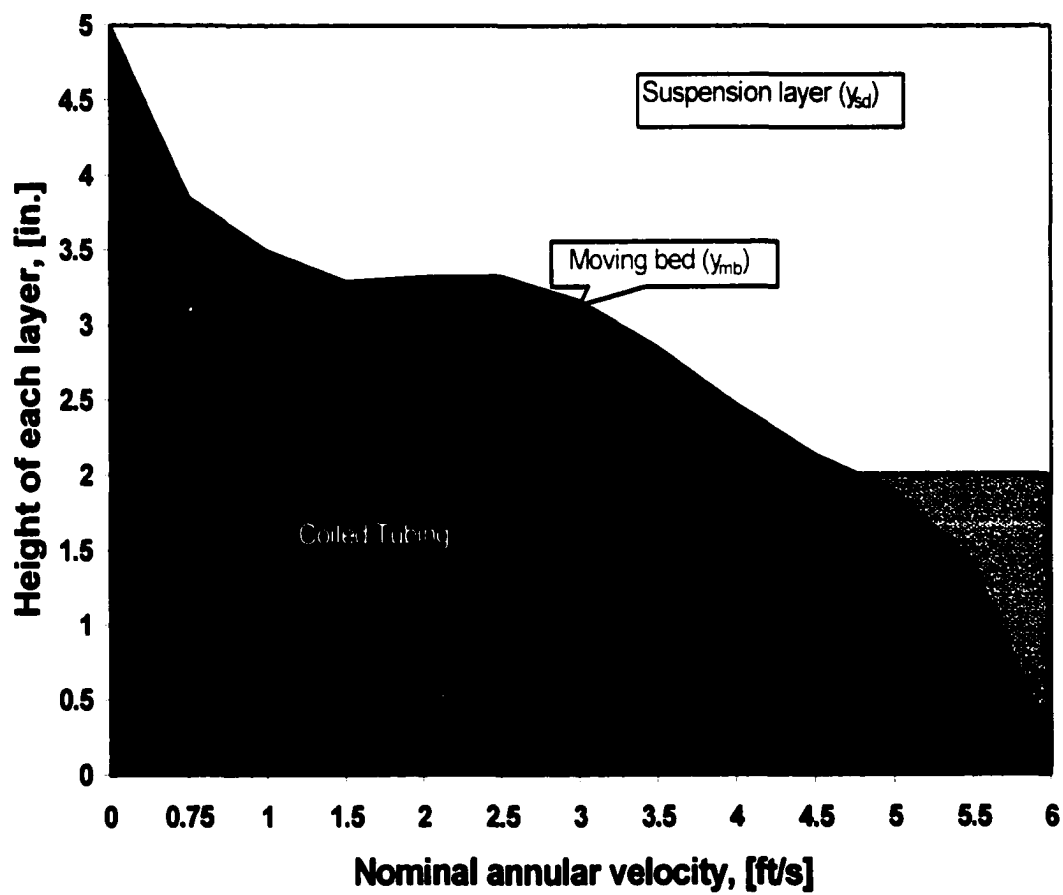
**Fig. 3.4 – Area distribution of each layer on the annulus with base case**

Figure 3.5 presents the height distribution of each layer in the annulus. It is quite apparent from Fig. 3.5 that the drilling fluid annular velocity plays a significant role in cuttings transport. With increased nominal annular velocity ( $U_a$ ) over 3 ft/s, the areas of the moving bed and the stationary bed are decreased. With further increase in  $U_a$ , more and more particles are lifted out of the moving bed and the stationary bed into the suspension region. This simulation shows that the critical deposition velocity ( $V_D$ ) defined in the previous chapter is 6 ft/s for the base case.

The cuttings-bed slightly increases or remains almost constant with an increase in the nominal annular velocity from 2 ft/s to 3 ft/s. This range can be classified as a pseudo-equilibrium status during which the in-situ velocity reaches resuspension velocity. In order for the cuttings-bed to be eroded, the cuttings should be resuspended by the strong turbulent eddies. The increase in nominal annular velocity and the reduced flow path area (due to slightly increased or almost constant stationary bed area) lead to a sufficient resuspension velocity.

With an increase in turbulent force, the moving bed vanishes after 4 ft/s of nominal annular velocity, after which, the flow pattern changes to two-layer flow regimes. In this study the critical velocity of a moving bed is defined as the maximum nominal annular velocity at which the cuttings are entirely suspended into the suspension layer and the moving bed vanishes. The simulation results show that the critical velocity of a moving bed is between the annular pumping velocities of 4 to 5 ft/s. When any layer vanishes, there is no solution to Eq. 3.20, which is a physical constraint of the three-layer model. The flow consists of only two layers (stationary bed and suspension layer). In this case, the two-layer model is used. The appropriate two-layer model is described in the next section.





**Fig. 3.5 – Cuttings-bed height distribution of each layer (base case)**

Pilehvari et al.<sup>78</sup> noted that for steady hole cleaning, (without increasing the stationary bed) 4 to 5 ft/s of fluid velocity was required from a large scale laboratory study (with no rotation effect). These simulation results are in good agreement with their laboratory study. It is also worthwhile to note that, according to the concept of Minimum Transport Velocity (MTV) introduced by Ford et al.<sup>10</sup>, at which all the cuttings are suspended and transported together with the transport medium,  $U_d$  of 174.5 cm/s (5.72 ft/s) corresponds to the result of this study (about 6 ft/s).

### **3.5.2 Analysis of Pressure Gradient**

Simulation results for the pressure gradient with different nominal annular velocities for the base case are presented in Figs. 3.6 and 3.7. An increase in the nominal annular velocity up to 2.8 ft/s increases the pressure gradient, which later sharply decreases until it reaches 4.5 ft/s. Simulation data of the pressure gradient with the change of nominal annular velocity is shown in Table 3.3. The Nguyen and Rahman model<sup>5</sup> shows the same pattern, but the peak point of the pressure gradient and its relevant velocity point are slightly different (the discrepancy is about 0.3 ft/s). However, the basic pattern of high-pressure gradient at about 2.5 – 3.0 ft/s is the same. The pressure gradient when the Power-law fluid is pumped without cuttings in the annulus is also shown in Fig. 3.6. It shows that the pressure gradient of the fluid without solids is a function of nominal annular velocity.

**Table 3.3 – Simulation data of the pressure gradient with the change of annular nominal velocity (base case)**

Mean $U_a$ (ft/s)	Fluid Only	With cuttings transportation			
	psi/ft	psi/ft	$U_{sd}$ (ft/s)	$A_{sb}$ (in. <sup>2</sup> )	$A_{mb}$ (in. <sup>2</sup> )
1	0.0029	0.035	3.63	12.14	0.00
2	0.0047	0.060	5.84	9.78	1.51
3	0.0061	0.091	7.83	9.58	0.94
4	0.0075	0.057	6.89	7.04	0.00
5	0.0088	0.042	6.62	4.10	0.00
6	0.011	0.026	6.08	0.17	0.00

The relationship between the pressure gradient and the stationary bed height is shown in Fig. 3.7. As previously explained, the moving bed is plotted as fractional height above the stationary bed. Similarly, the suspension layer is also plotted in the same manner for a better visual understanding (Figs. 3.7 and 3.8). The pressure gradient is the highest when the summed height of both the moving bed and the stationary bed reach the highest value.

Generally, from the drilling engineering point of view, it is desirable to minimize the stationary bed of drilled cuttings in the annulus. Low frictional pressure loss in drilling fluid circulation is also required in the design of a drilling program. Finding the optimum point means to compromise between parameters affecting cuttings-bed accumulation and frictional pressure drop. From this point of view, a reasonable drilling fluid velocity range should be nominal annular velocity between 3.5 and 4.5 ft/s from Fig. 3.7.

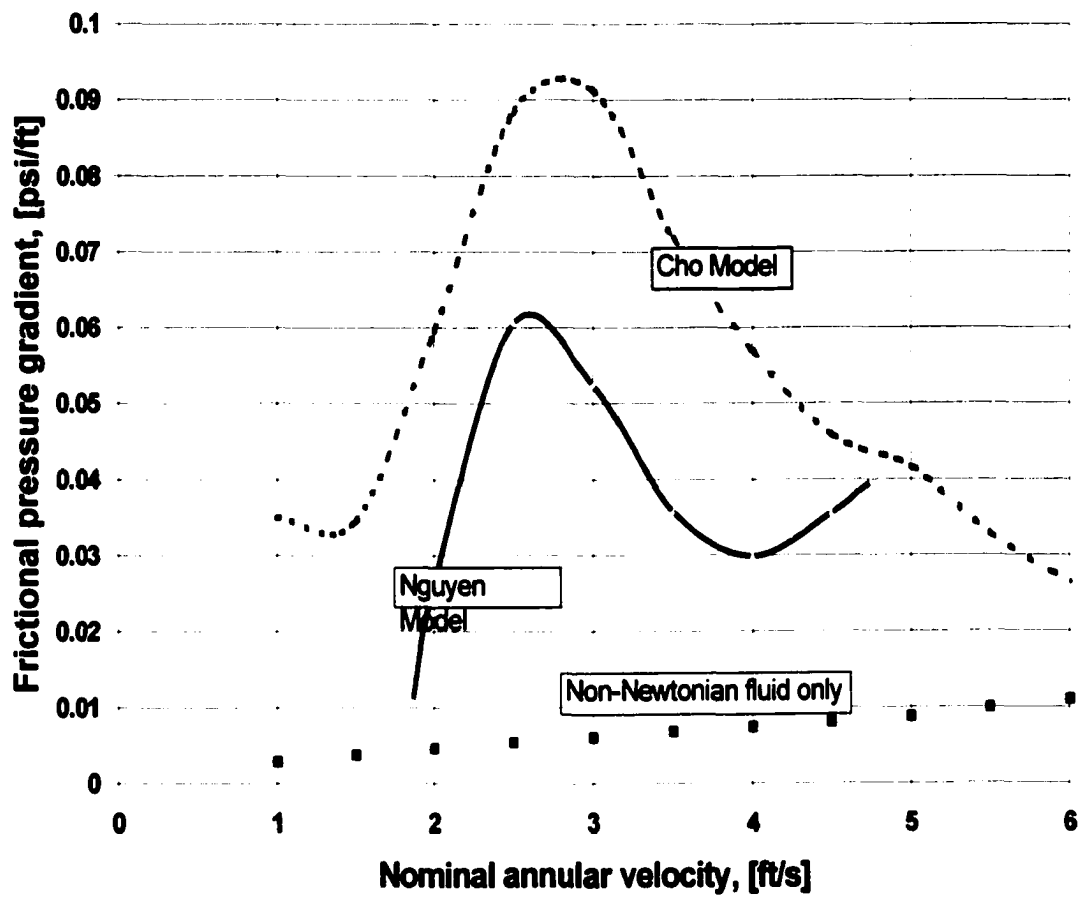


**Fig. 3.6 – Comparison of pressure drop profile with different three-layer model (base case)**

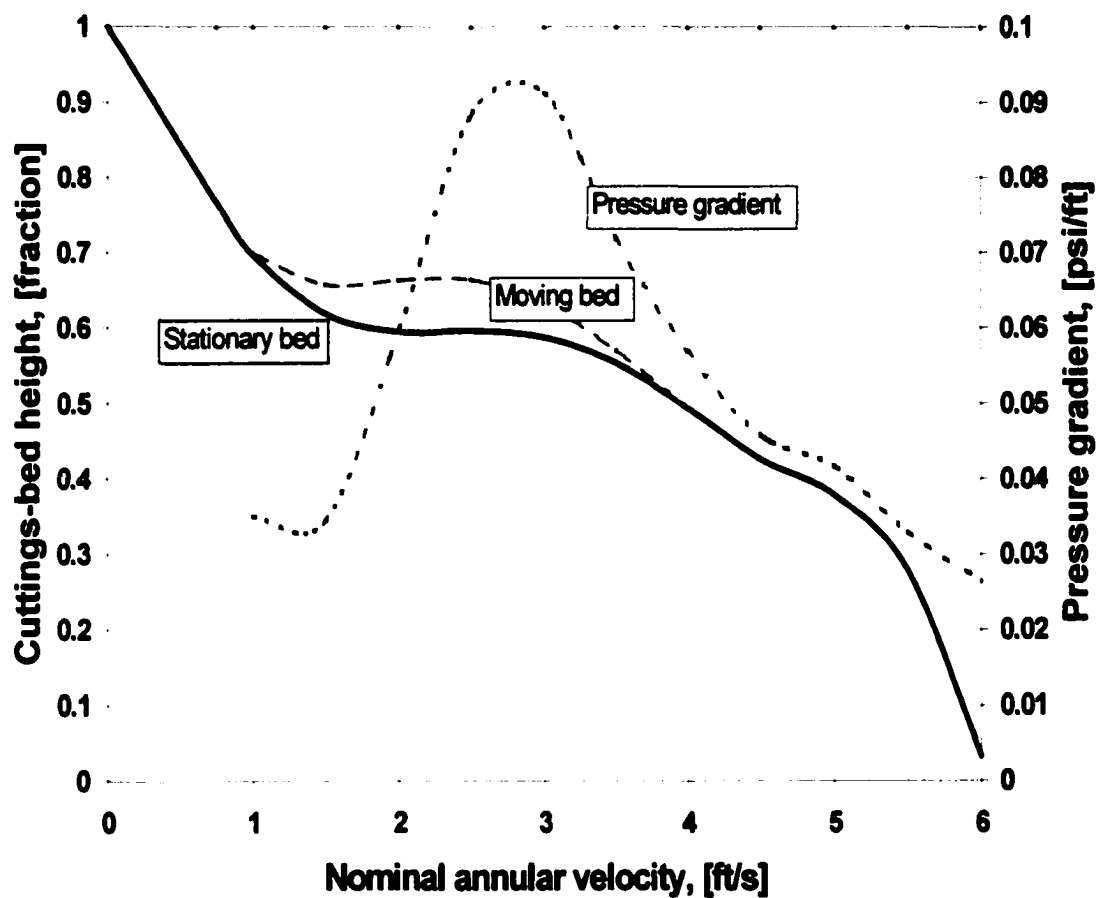


**Fig. 3.7 – Relationship between the pressure gradient and the height of the stationary bed (base case)**

Peden et al.<sup>28</sup> recommended 3.3 ft/s minimum transport velocity for the cuttings sliding forward. Their recommended velocity was obtained from an experiment with drilling rotation at 50 rpm. The effect of drillpipe rotation is equivalent to 30% of nominal annular velocity for this case.<sup>21</sup> Therefore, considering the drillpipe rotation effect on cuttings transport, Peden's recommended velocity is equivalent to 4.3 ft/s. This recommendation is in good agreement with the optimum point obtained from the simulation results.

### 3.5.3 Effects of Drilling Fluid Rheology

The effects of drilling fluid rheology were simulated for the different fluid systems. Fluid A used in simulation is a less viscous fluid ( $n = 0.76$  and  $K = 0.001 \text{ lb}_f \text{ s}^n/\text{ft}^2$ ) and Fluid B is a more viscous fluid ( $n = 0.502$  and  $K = 0.028 \text{ lb}_f \text{ s}^n/\text{ft}^2$ ). Figure 3.8 shows the effects of the fluid rheology on cuttings-bed area. Simulation results show that Fluid B decreases the cuttings-bed area in horizontal well.

Generally, a more viscous fluid has better suspension and transportation. However, the distance traveled by the cuttings in a horizontal well is significantly different from a vertical well as shown in Fig. 2.3. Even though a more viscous fluid can suspend the particles longer than a less viscous fluid, the suspension time alone does not improve cuttings transport efficiency in a horizontal well. Moreover, a more viscous fluid gives a less turbulent regime than a less viscous fluid under the same pump rate. Cuttings transport efficiency is a strong function of fluid rheology and turbulence. This might be the reason for small differences in cuttings-bed area between Fluid A and Fluid B.

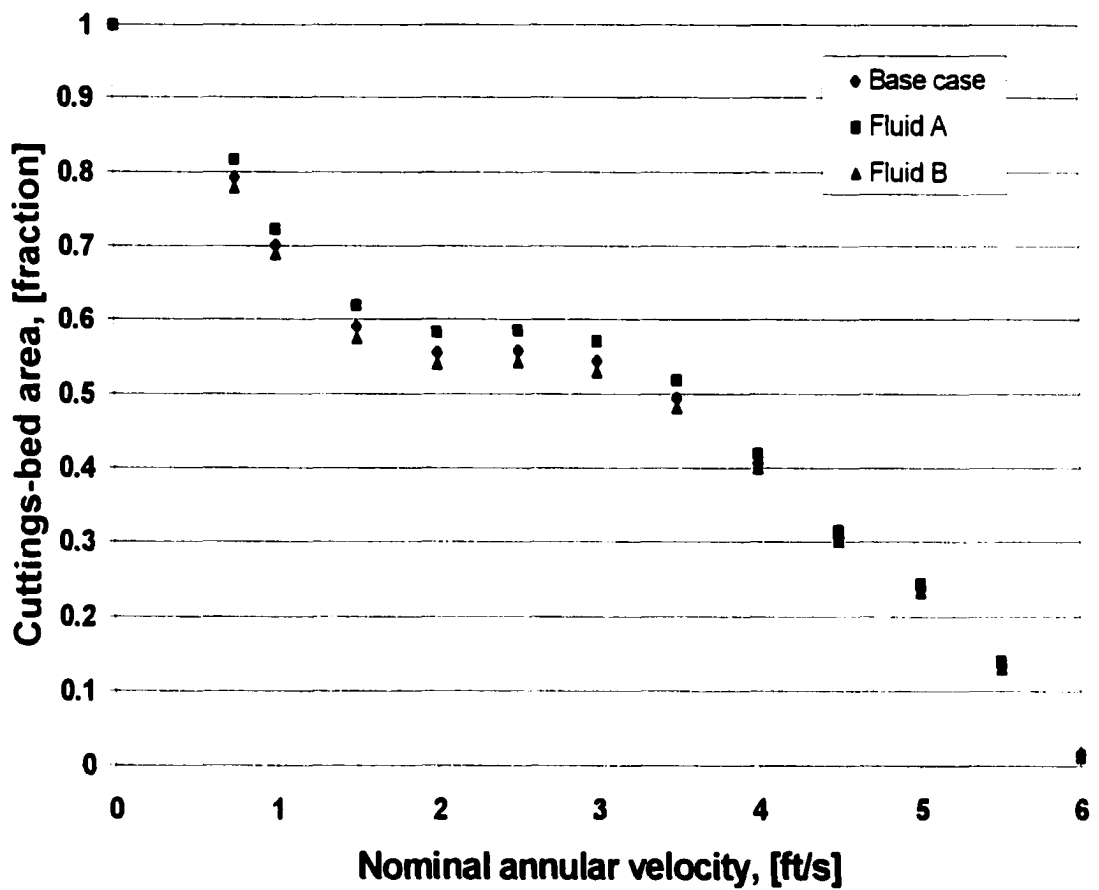


**Fig. 3.8 – Effects of fluid behavior index on the area of each layer distribution with the nominal annular velocity of 3.5 ft/s**

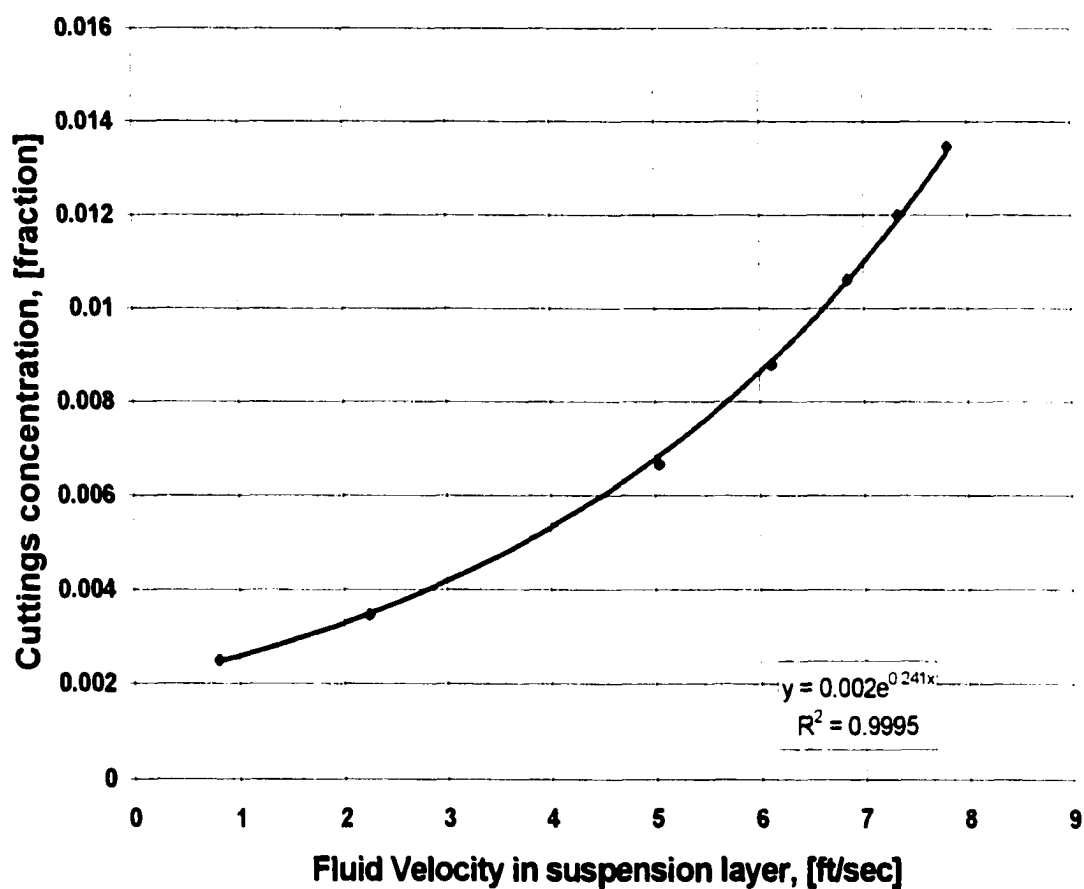
In addition, it was found that the simulation results with very low flow behavior index ( $n < 0.35$ ) and low pump rate sometimes did not have the positive moving bed areas, at which there is no solution to Eq. 3.20. In this case, a two-layer model was used to avoid any physical constraints in the simulation program.

### **3.5.4 Effects of Other Drilling Parameters**

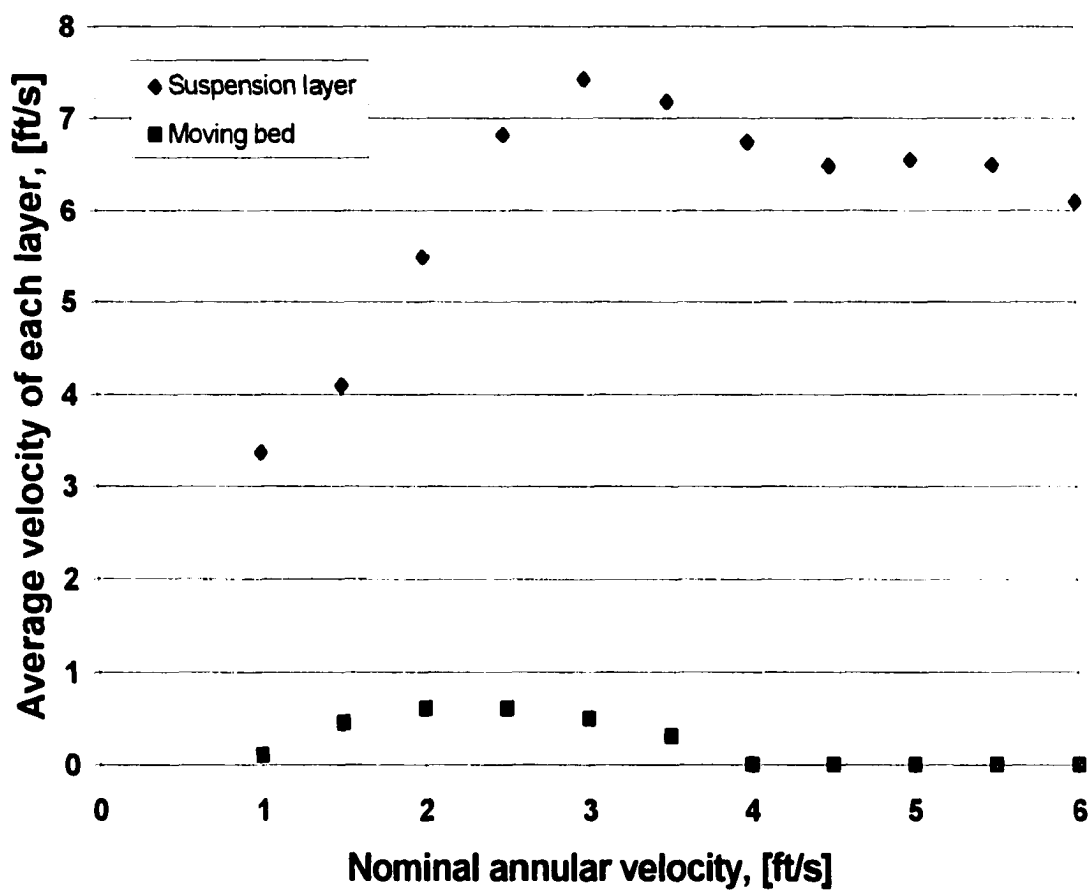
The effect of the suspension layer velocity on the cuttings concentration in the suspension layer was also simulated. The relationship between the velocity and the cuttings concentration for the base case can be defined analytically. High velocity in the suspension area, due to the increase in the moving and stationary bed, increases the cuttings concentration. The increased cuttings concentration has enough energy to lift up the cuttings from the moving bed. This will lead to an equilibrium condition in the horizontal annulus within a certain area of each flow layer. The correlation between the concentration in a suspension layer and nominal annular velocity is shown in Fig 3.9. Velocity of a suspension layer increases with an increase in fluid pumping rate.

The highest velocity of the suspension layer is obtained when the nominal annular velocity is about 3 ft/s (Fig. 3.10). Frictional pressure loss of the suspension layer at the nominal annular velocity of 3 ft/s is greater than other nominal annular velocities with the base case drilling data. The change in velocities of the moving bed is not high with an increasing in nominal velocities. The moving bed velocity is almost zero when the nominal annular velocity is over 4 ft/s because the moving bed disappears over this nominal annular velocity.





**Fig. 3.9 – Cuttings concentration in the suspension layer vs. nominal annular velocity (base case)**



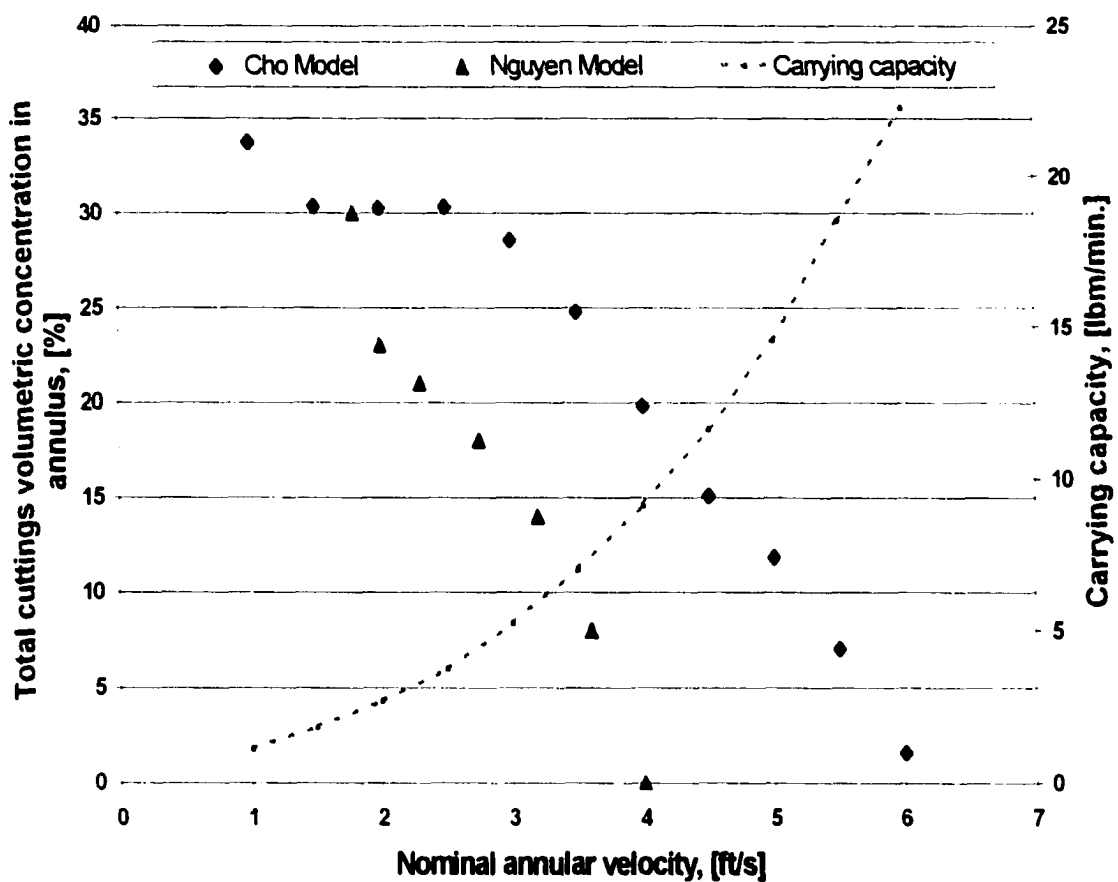
**Fig. 3.10 – Average velocity profile of the suspension layer and the moving bed with the change in nominal annular velocity (base case)**

Figure 3.11 shows the comparison between the total volumetric cuttings concentration in the annulus of the two models and the cuttings transport capacity. Annular volumetric cuttings concentration was calculated by adding cuttings volumetric concentration of each layer. There is no stationary cuttings-bed in the Nguyen and Rahman<sup>5</sup> model before reaching the MTV specified by Ford et al.<sup>10</sup>. Their model may predict faster erosion of a stationary bed in coiled tubing drilling. However, the Cho et al model<sup>25</sup> predicts that the cuttings-bed may erode and disappear when a nominal annular velocity reaches 6 ft/s. This was confirmed by experiments performed by other researchers.<sup>16,29,31</sup> Total cuttings volumetric concentration in an annulus looks stagnant at 2.5 ft/s to 3 ft/s of nominal annular velocity. Carrying capacity ( $G$ ) in Fig. 3.11 was also obtained by the following equation:

$$G = A_{sd} * U_{sd} * C'_{sd} * \rho_s \quad (3.29)$$

where,  $U_{sd}$  is a local velocity of a suspension layer and  $C'_{sd}$  is a cuttings concentration of a suspension layer. Carrying capacity exponentially increases with an increasing nominal annular velocity.

The visual test results for slurry transport<sup>36</sup> showed that the actual volumetric concentration is lower than that of the stationary bed. In this study, the cuttings volumetric concentration of moving bed is assumed to be 75% of the stationary bed. The cuttings carrying capacity increases with an increasing nominal annular velocity.



**Fig. 3.11 – Comparison of total annular cuttings concentration and carrying capacity**

### **3.6 Summary**

The three-layer model properly interrelates nominal annular velocity, cuttings concentration, and fluid rheology to the cuttings transport in horizontal well drilling. The following conclusions were reached from this study:

- (1) A mathematical three-layer model has been formulated to predict and interpret the cuttings transport in a horizontal wellbore while drilling with coiled tubing. The model predictions, based on the series of simulation runs, are in good agreement with the experimental data published by others.<sup>5,26,28,78</sup>
- (2) It is quite clear that the nominal annular velocity of drilling fluid plays a significant role, in both the annular pressure gradient and the cuttings transport. Therefore, the selection of the fluid annulus velocity, the optimum fluid rheology, and a precise prediction of pressure gradient are very important for economical and efficient horizontal drilling using coiled tubing.
- (3) The conventional drilling fluid velocity range of 2 to 3 ft/s should be avoided for coiled tubing horizontal drilling. It is recommended that the nominal annular velocity range of 3.5 to 4.0 ft/s be used. This is because the a lower pressure gradient and a less stationary bed area predicted than those of conventional velocity range.
- (4) A highly viscous fluid increases the pressure gradient under the same nominal annular velocity. For economic drilling, the following factors should be evaluated in the selection of drilling fluid: rheology, fluid velocity, velocity profile, carrying capacity, and the pressure gradient.

## **CHAPTER FOUR**

### **A THREE-SEGMENT HYDRAULIC MODEL**

#### **4.1 Introduction**

An increase in the number of deviated and horizontal wells drilled over the last two decades has focused attention on the problem of cuttings removal. The cuttings transport in deviated wellbores changes markedly as a function of wellbore angle. The dominant factors governing cuttings transport efficiency are changed with the wellbore angles. However, the existing models, which cover cuttings transport in vertical to horizontal wells do not consider that an increase in the wellbore deviation changes both transport pattern and the dominant factors in the transport mechanism.

A new approach to model the three-segment (a horizontal and near horizontal segment, a vertical and near vertical segment, and a transit segment) hydraulic cuttings transport under a two-phase (solid-liquid) fluid in the annulus was developed to predict and interpret the cuttings transport mechanism. This chapter specifically describes the model development for each segment, solution, and the simulation results of the integrated three-segment model. In order to have a comprehensive understanding of the

effects of the parameters affecting cuttings transport efficiency, the simulations were performed under different drilling in-situ conditions. The results can be used to obtain a reasonable pumping velocity and optimize rheology of drilling fluid with the lowest possible pressure gradient, which might serve as an operational guideline while drilling. Moreover, the effects of various parameters that affect the efficiency of cuttings transport were discussed. These results were compared with the published experimental data. The observed agreement and discrepancies are discussed.

## **4.2 Model Description**

### **4.2.1 Basis for Model Development**

A detailed review of the published experimental data reveals that the cuttings transport characteristics are changed with an increase in wellbore angles. The instantaneous bed formation was reported at angles between  $60^\circ$  to  $90^\circ$ . Researchers<sup>4,9,51</sup> reported that the experimental data of wells with angles above  $60^\circ$  were very similar to those for the horizontal. The cuttings-bed tends not to slip downward in wells with angles above  $60^\circ$  when drilling fluid circulation ceases.

Martin et al.<sup>30</sup> showed that the worst situation for hole cleaning appeared between  $30^\circ$  to  $60^\circ$ , while Walker and Li<sup>32,79</sup> noted that the most critical angle range was  $35^\circ$  to  $55^\circ$ . A cuttings-bed slides downward when the wellbore deviation is less than the friction angle between a cuttings-bed and tubing-casing. Leisng and Walton<sup>29</sup> also reported that the wellbore angles between  $30^\circ$  to  $65^\circ$  might be considered dangerous from their

perspective. Other researchers<sup>27-29</sup> also reported that the cuttings-bed heights could not be recorded after the test ended because the cuttings-bed changed immediately and slid down when the flow was stopped.

When the angle changes from  $0^\circ$  to  $30^\circ$ , researchers<sup>10,80</sup> noted that there was no cuttings-bed formed from their experimental investigations. In this region, hole cleaning is largely determined by the slip velocity of the cuttings. Jones and Hughes<sup>80</sup> noted that the cuttings transport mechanism in this range of wellbore angles is not significantly different from vertical wells.

Therefore, a wellbore can be divided into three sections based on wellbore deviation (from the vertical position), cuttings transport characteristics, and existing cuttings stationary bed: a vertical and near vertical section ( $0^\circ$  to  $30^\circ$  deviated from vertical), horizontal to near horizontal section ( $60^\circ$  to  $90^\circ$  deviated), and the transit section ( $30^\circ$  to  $60^\circ$  deviated).<sup>26</sup> A three-layer (stationary bed of drilled cuttings at the bottom, a moving-bed layer above it, and a heterogeneous suspension layer at the top) hydraulic model was used for the horizontal and near the horizontal section (here after called a horizontal segment).<sup>25</sup> An existing two-layer model was modified for the transit section (here after called a transit segment), and a one-layer model was used for the vertical and near vertical section (here after called a vertical segment).

The main parameters in the cuttings transport mechanism of these different segments may be different. These different parameters in each segment are discussed in the following model descriptions and considered in the model development for each categorized segment. The three different mechanistic layer models, representing each



segment, were integrated with different wellbore deviation in order to characterize and predict cuttings transport in any wells between the horizontal and the vertical.

## **4.2.2 Model Descriptions**

### **4.2.2.1 Horizontal Segment**

The drag force, as explained by Luo et al.,<sup>81</sup> tends to drag or slide the cuttings out of a cuttings-bed and thus moves it forward. This is caused by the viscous fluid flow over the upper exposed surface of the cuttings. The drag and the lift forces act against the frictional force and the gravitational force. The increase in available energy accelerates the particle clusters in the moving bed layer to slide over the stationary bed surface as a whole movement.

The other transport mechanism is the dispersed suspension of cuttings in a heterogeneous flow, called the suspension layer. Cuttings can be lifted under strong turbulent eddies when the lift force is strong enough to overcome the gravitational force component in the direction normal to the flow.<sup>82</sup> Therefore, the annular section is composed of three layers: a stationary bed at the bottom, a moving bed above it, and a heterogeneous suspension layer at the top. The role of the carrier fluid in-situ velocity in cuttings suspension and the basic description of a three-layer model are described in Reference 25 .

#### **4.2.2.1 Transit Segment**

There are several forces acting on the particles in cuttings transport. These involve a lift force, a drag force, a gravitational force, and a frictional force. Both the drag and the lift forces are exerted by the flow of drilling fluid around the particle. The lift force tends to lift up the particle to join the main stream of the flow where it moves. This force arises either due to the asymmetric distribution of the fluid viscosity surrounding the cuttings and/or due to the turbulent eddies in the annular flow.<sup>81</sup>

In the transit segment, the coiled tubing is also assumed to lie at the low side of the wellbore as shown in Fig. 4.1. Therefore, a full-eccentric annulus of the wellbore was considered for the transit segment. A cuttings-bed may be formed in the lower side of the annulus in this transit segment. The bed formed may be either stationary, moving upward with a small velocity, or moving downward to the bottom hole. While the bed formed is unstable, the main cuttings transport mechanisms are that the cuttings are dispersed in the heterogeneous suspension layer and are supported by the axial velocity. This annular section is composed of a cuttings-bed and a suspension layer.

A reduction in the wellbore deviation gives an opposite effect on the drag and the lift force on the cuttings' rolling and sliding because of an increase in gravitational force. A decrease in the lift and the drag force, due to the reduction in strength of turbulent eddies (or increase in gravitational force due to the abrupt reduction in the deviated wellbore angle), reduces available energy for particle clusters to move as a whole movement. However, the axial (vertical) velocity of a carrier fluid is gradually increased with a decrease in wellbore angles. The cuttings are more supported by the axial velocity

at reduced wellbore angles than in the horizontal segment, and the cuttings-bed begins to erode.

#### 4.2.2.3 Vertical Segment

A drilled cutting, because of its density difference, tends to settle out of a drilling fluid at a constant rate known as particle settling velocity. When the particle settling velocity is compensated by the axial velocity of the carrier fluid (drilling fluid), the cuttings are strongly supported by the fluid. The cuttings can be transported from the bottom of the hole to the surface by the transport velocity, which is the in-situ axial velocity compensated with the particle settling velocity (Fig 4.2).

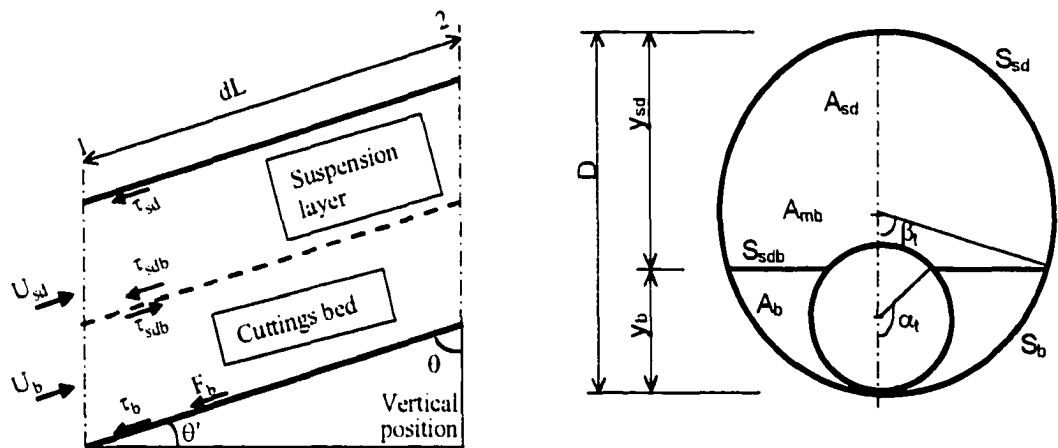


**Fig. 4.1 – Schematic diagram of the two-layer model for transit segment**

As the wellbore deviation is increased, the axial in-situ velocity of drilling fluid decreases. The main domains in cuttings transport efficiency for this vertical segment are axial in-situ velocity of the drilling fluid and the cuttings particle velocity, which is dependent on the particle size, density and shape, the drilling fluid rheology, and

wellbore geometry. There will be no stationary bed in this segment. In order to calculate the settling velocity of a particle in this segment, the correlation for irregularly shaped cuttings recently developed by Chien<sup>55</sup> was used.

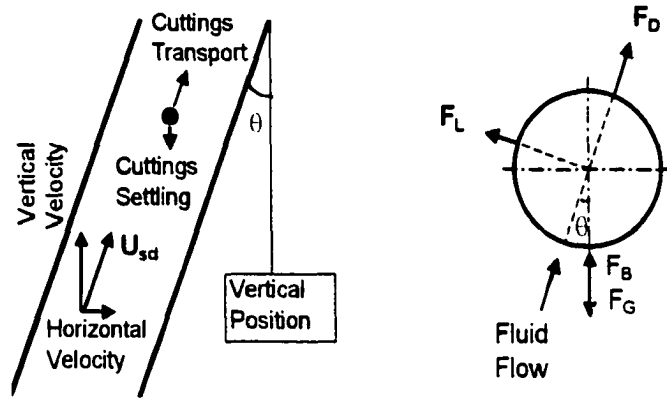


**Fig. 4.2 – Forces acting on particle at the vertical segment**

## **4.3 Model Development**

### **4.3.1 Horizontal Segment**

The mathematical model development for a horizontal segment is based on the fact that the cuttings-drilling fluid flows at flow rates such that there exists three layers in the annulus.

#### **4.3.1.1 Continuity Equations**

Basic continuity equations are the same as the three-layer model for the horizontal wells. Figure 4 3 illustrates the forces and stresses acting on each layer in the horizontal

segment. The velocity of the stationary bed ( $U_{sb}$ ) is almost zero since it is not moving as described by the model.<sup>75</sup> The continuity equations for the fluid and solid particles are summarized as follows:

$$A_{sd}C_{sd}U_{sd} + A_{mb}C_{mb}U_{mb} = A_aC_tU_a \quad (3.5)$$

$$A_{sd}(1 - C_{sd})U_{sd} + A_{mb}(1 - C_{mb})U_{mb} = A_a(1 - C_t)U_a \quad (3.7)$$

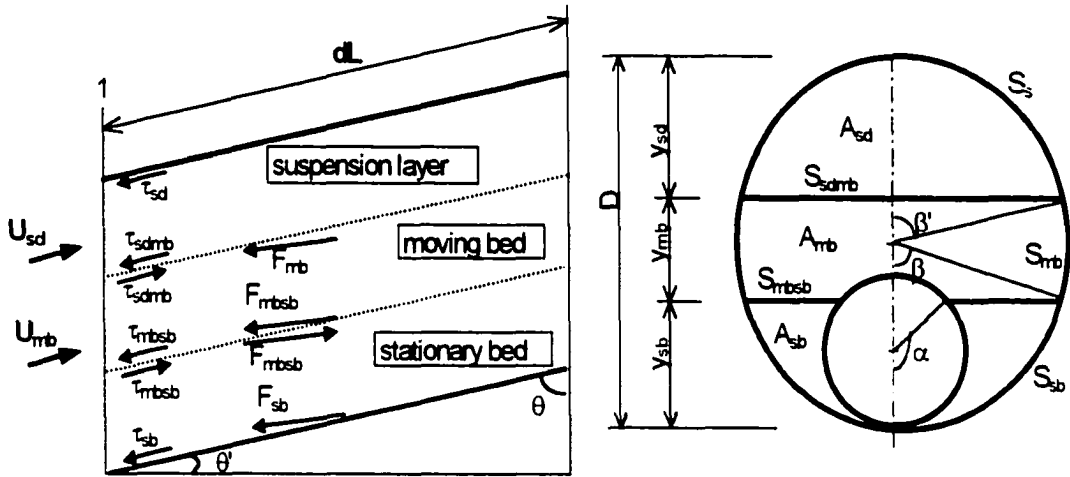


**Fig. 4.3 – Schematic diagram of a three-layer model for the horizontal segment**

Under steady-state flow conditions, the volumetric flow rate of cuttings ( $A_aC_tU_a$ ) is equal to the volume of cuttings generated by the drilling bit per unit of time.

#### 4.3.1.2 Momentum equations

##### Upper dispersed suspension layer

The upper dispersed suspension layer is a relatively clean fluid or a heterogeneous turbulent suspension depending upon the flow conditions. Under a steady-state flow, the sum of the forces acting on the fluid flow zone is given as follows:

$$A_{sd} \left( \frac{\Delta P}{L} \right) = \tau_{sd} S_{sd} + \tau_{sdmb} S_{sdmb} + F_{sd\kappa_i} \quad (4.1)$$

where,  $\tau_{sd}$  is shear stress acting on a relevant wetted-perimeter,  $S$  is the wetted-perimeter.  $F_{sd\kappa_i}$  is the gravitational force acting on the mixture in the dispersed suspension layer, which is the only component affected by the wellbore deviation.

$$F_{sd\kappa_i} = \rho_{sd} g A_{sd} \cos \theta \quad (4.2)$$

where,  $\rho_{sd}$  is the effective density of a dispersed suspension layer.

The shear stresses both at the pipe circumference and the interface between the upper layer and the moving bed are given in Eqs. 3.10 and 3.16. The following correlations for the friction factors of the dispersed layer ( $f_{sd}$ ) and the interface between a suspension layer and moving bed ( $f_{sdmb}$ ) were used in this study:

$$f_{sd} = 0.00454 + 0.645 N_{Re f}^{-1.7} \quad (\text{Doron et al.}^{23}) \quad (3.13)$$

$$f_{sdmb} = h N_{Re f}^p n^q \left( \frac{d_p}{D_{sd}} \right)^t \quad (\text{Martin et al.}^{77}) \quad (3.14)$$

where,  $h = 0.966368$ ,  $p = -1.07116$ ,  $q = 2.360211$ , and  $t = -2.34539$ . For both  $f_{sd}$  and  $f_{sdmb}$ , Reynolds number of the suspension layer was used.

### Moving bed layer

From Fig. 4.3, summing all the forces acting on this region gives:

$$A_{mb} \left( \frac{\Delta P}{L} \right) = \left( \frac{F_{mb}}{L} \right) - \tau_{symb} S_{ymb} + \left( \frac{F_{mbsh}}{L} \right) + \tau_{mbsh} S_{mbsh} + F_{mbG} \quad (4.3)$$

where,  $F_{mbG}$  is the gravitational force acting on the moving bed. The frictional forces ( $F_{mb}$  and  $F_{mbsh}$ ) acting on the associated layers can be found in Reference 23. The gravitational force in the direction parallel to the deviated well is:

$$F_{mbG} = \rho_{mb} g A_{mb} \cos \theta \quad (4.4)$$

The following correlation developed by Doron et al.<sup>23</sup> is used for the calculation of the moving bed friction factor for turbulent flow,  $f_{mbsh}$ :

$$f_{mbsh} = 0.046 N_{Re,f}^{-0.02} \quad (3.18)$$

where, Reynolds number of the moving bed was used.

#### **4.3.1.3 Moving Bed Velocity**

The moment due to forces around the acting point, "A" in Fig. 4.4 is summed up as follows:

$$F_D L_D - (F_G - F_B) L_G + F_L L_L \geq 0 \quad (4.5)$$

where,  $F_D$  is drag force,  $F_L$  is lift force,  $F_G$  is the gravitational force, and  $F_B$  is the buoyancy force.  $L$  with a different subscript is the length of each force acting. The detail derivation procedure is described in Appendix E. The minimum moving bed velocity can then be obtained from equating the driving moment and the opposing moment as shown in Eq. 4.6.

$$U_{mb} = \sqrt{\frac{0.131(\rho_s - \rho_L)g \left[ C_{mb} \frac{y_{mb}}{d_p} \sin \theta \right] [1 + 1.732 \tan \theta'] \sin \theta}{\rho_L (0.1651 C_D + 0.0982 C_L)}} \quad (4.6)$$

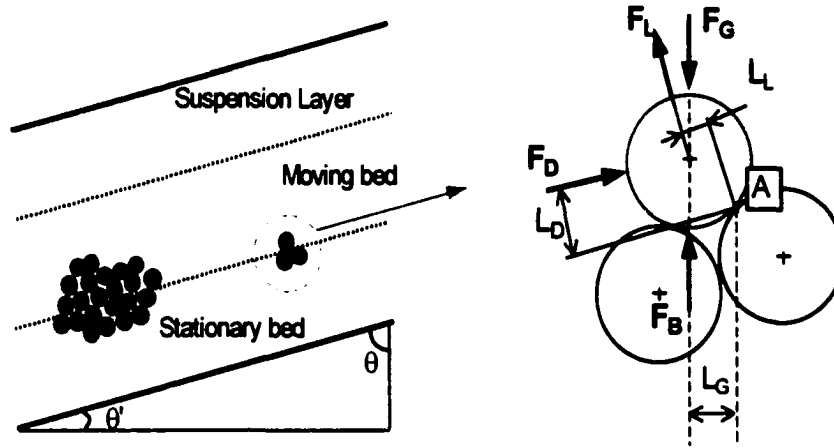


**Fig. 4.4 – Forces acting on a particle at the lower stratum of the moving bed in a deviated wellbore**

### 4.3.2 Transit Segment

The mathematical model is developed based on the steady-state flow condition, neglecting reservoir inflow and outflow, which is the same condition as the horizontal and near horizontal segment.

#### 4.3.2.1 Continuity Equations

The continuity equations for the fluid and solid particles are written as follows:

$$A_{sd} C_{sd} U_{sd} + A_b C_b U_b = A_a C_i U_a \quad (4.7)$$

$$A_{sd} (1 - C_{sd}) U_{sd} + A_b (1 - C_b) U_b = A_a (1 - C_i) U_a \quad (4.8)$$

Equations 4.7 and 4.8 present conservation of mass in the solid and the liquid phase, respectively. The relevant relation can be described as follows:



$$A_{sd} + A_b = A_a \quad (4.9)$$

The cuttings concentration, which is generated at the drilling bit, specified in Eq. 3.8, can also be used for this segment. If the bed is stationary or moving relatively slowly, as explained by Walton,<sup>12</sup> the terms involving  $U_b$  can then be neglected by assuming that the bed formed is stationary. Equations 4.7 and 4.8 can be simplified as:

$$A_{sd} C_{sd} U_{sd} = A_a C_t U_a \quad (4.10)$$

$$A_{sd} (1 - C_{sd}) U_{sd} = A_a (1 - C_t) U_a \quad (4.11)$$

#### 4.3.2.2 Momentum Equations

The equation, which describes the sum of forces acting on the suspension layer, is:

$$A_{sd} \left( \frac{\Delta P}{L} \right) = \tau_{sd} S_{sd} + \tau_{sdb} S_{sdb} + F_{sdG}; \quad (4.12)$$

where,  $F_{sdG}$  is the gravitational force acting on the suspension layer (mixture), which is the only component affected by the wellbore deviation, and can be defined as:

$$F_{sdG} = \rho_{sd} g A_{sd} \cos \theta \quad (4.2)$$

where,  $\rho_{sd}$  is the effective density of the upper dispersed fluid flow layer

From Fig. 4.1, summing up all the forces acting on the cuttings-bed gives:

$$A_b \left( \frac{\Delta P}{L} \right) = \tau_b S_b - \tau_{sdb} S_{sdb} + \left( \frac{F_b}{L} \right) + F_{bG}; \quad (4.13)$$

where,  $F_{bG}$  is the gravitational force acting on the particles, and can be defined as:

$$F_{bG} = \rho_b g A_b \cos \theta \quad (4.14)$$

Equation 4.12 can be written as:

$$\frac{\Delta P}{L} = \frac{1}{A_{sd}} [\tau_{sd} S_{sd} + \tau_{sdb} S_{sdb} + \rho_{sd} g A_{sd} \cos \theta] \quad (4.15)$$

Equation 4.13 can be written as:

$$\frac{F_b}{L} = -\tau_b S_b + \tau_{sdb} S_{sdb} - \rho_b g A_b \cos \theta + A_b \left( \frac{\Delta P}{L} \right) \quad (4.16)$$

By combining Eqs. 4.15 and 4.16 and solving for  $F_b$ , it becomes:

$$F_b = \left[ -\tau_b S_b + \tau_{sdb} S_{sdb} - \rho_b g A_b \cos \theta + \frac{A_b}{A_{sd}} (\tau_{sd} S_{sd} + \tau_{sdb} S_{sdb} + \rho_{sd} g A_{sd} \cos \theta) \right] L \quad (4.17)$$

The force,  $F_b$  can be considered the force acting on the cuttings-bed exerted by gravity, fluid stress, and fluid pressure gradient. Shear stresses in this segment are given as follows:

$$\tau_{sd} = \frac{1}{2} \rho_{sd} U_{sd}^2 f_{sd}(N_{Re_f}) \quad (3.10)$$

$$\tau_b = \frac{1}{2} \rho_b |U_b| U_b f_b \quad (4.18)$$

$$\tau_{sdb} = \frac{1}{2} \rho_{sdb} (U_{sd} - U_b)^2 f_{sdb}(N_{Re_f}) \quad (4.19)$$

where,  $f_{sd}$ , and  $f_{sdb}$  are friction factors as a function of Reynolds number. Dry friction factor,  $f_b$ , can be found from an empirical correlation, which can be calculated based on the hydraulic diameters. Equations 3.13 and 3.14 are used for calculating  $f_{sd}$  and  $f_{sdb}$  respectively. The friction factor  $f_b$  is given as<sup>75</sup>:

$$f_b = 0.046 \left( \frac{\rho_b U_b D_b}{\mu_L} \right)^{-0.2} \quad (4.20)$$

where, hydraulic diameter,  $D_b$ , is given by

$$D_b = \frac{4A_b}{S_b + S_{adb}} \quad (4.21)$$

The solution of the diffusivity equation, Eq. 2.41, for the transit segment is obtained by integrating it twice. The detail solution of the diffusivity equation is described in Appendix B. It gives the following concentration profile for the upper layer of the horizontal annulus:

$$C(y) = C_b \exp \left[ \frac{-V_h}{\varepsilon_p} (y - y_h) \right] \quad (4.22)$$

where,  $C_b$  is cuttings volumetric concentration (0.4805),  $\varepsilon_p$  is particle eddy diffusivity,  $D$  is wellbore diameter, and  $y_h$  is a height of the cuttings stationary bed.

### 4.3.3 Vertical Segment

When cuttings are transported to the surface, there are four different forces acting upon them, i.e., the gravitational force, the upward buoyant force, the drag force, and the lift force (the axial element of the lift force in a vertical well is negligible).

For the lift case (Fig. 4.2), the sum of the forces acting on the particle is given as follows:

$$F_D \cos \theta + F_L \sin \theta - F_G + F_B > 0 \quad (4.23)$$

For terminal settling, the relationship among these forces is:

$$F_D \cos \theta + F_L \sin \theta - (F_G - F_B) = 0 \quad (4.24)$$

The momentum equation, which describes the sum of the forces acting on the suspension layer, is as follows:

$$A_{sd} \left( \frac{\Delta P}{L} \right) = \tau_{sd} S_{sd} + \rho_{sd} g A_{sd} \cos \theta \quad (4.25)$$

Equations 3.10 and 3.13 can be used to define the shear stress and the friction factor, respectively, in this segment.

The net effect of gravity and buoyancy force must be equal to the axial component of both the drag and the lift force when the particle reaches the terminal settling velocity. The related forces acting upon the particle are shown in Fig. 4.2. The cuttings are transported from the bottom at a rate equal to the difference of the axial components between the average annular velocity and the particle settling velocity. This particle velocity (relative to the surface) is called the transport velocity, defined in the following equation:

$$U_t = U_a \cos \theta - V_h \quad (4.26)$$

where,  $U_a$  is the average annular fluid velocity in the vertical segment, which is the only component affected by the wellbore deviation. Since drilled cuttings suspension consists of clusters of many particles, the hindered settling velocity specified by Eq. 2.33 was used in this study.

The transport ratio is defined as the transport velocity divided by the annular velocity.

$$R_t = \frac{U_t}{U_a \cos \theta} = 1 - V_h \left( \frac{1}{U_a \cos \theta} \right) \quad (4.27)$$

As the particle settling velocity increases, the transport ratio decreases and the concentration of cuttings in the annulus increases. Conversely, an increase in the transport ratio indicates that the relative cutting velocity has increased to the nominal annular velocity, and so the cuttings are being transported to the surface more effectively.<sup>7</sup>

#### 4.3.4 Summary of the Model

For the horizontal segment ( $60 - 90^\circ$ ), the model is quite similar to the model for horizontal wellbores ( $90^\circ$ ). The horizontal segment is described by a set of six equations: Eqs. 3.5, 3.7, 4.1, 4.3, 4.6, and 2.43. The six unknowns with the given operational conditions are  $U_{sd}$ ,  $U_{mb}$ ,  $C_{sd}$ ,  $y_{mb}$ ,  $y_{sb}$ , and  $\Delta P dL$ . The auxiliary equations for solving this new model are derived in Appendices or directly imported from other researchers.<sup>23,75,77</sup> For the transit segment, the model is described by a set of five equations: Eqs. 4.1, 4.7, 4.8, 4.12, and 4.22. The five unknowns with the given operational conditions are  $U_{sd}$ ,  $C_{sd}$ ,  $y_{sb}$ ,  $\Delta P dL$ , and  $F_h$ . For the vertical segment, the model is simply described by the pressure gradient (Eq. 4.25) from momentum balance and particle relative velocity (Eq. 4.26).

### 4.4 Solutions

#### 4.4.1 Horizontal Segment

Combining the continuity equation for the solids, Eq. 3.21, to the liquid, Eq. 3.22, and solving for the mean velocity of suspension layer,  $U_{sd}$ , gives the following:

$$A_{sd}U_{sd} + A_{mb}U_{mb} = A_a U_a \quad (3.23)$$

Cuttings volumetric concentration of a dispersed suspension layer,  $C_{sd}$ , is given by:

$$C_{sd} = \frac{A_a C_s U_a - A_{mb} C_{mb} U_{mb}}{A_a U_a - A_{mb} U_{mb}} \quad (3.26)$$

All terms at the right-hand side of Eq. 3.26 are a function of the unknown  $y_{mb}$ ,  $y_{sb}$ , and  $U_{mb}$ , which are dependent on the operational conditions.

The solution to the equations is determined by eliminating the unknown factors.

$$A_{sd} \left( \frac{\Delta P}{L} \right) = \tau_{sd} S_{sd} + \tau_{sdmb} S_{sdmb} + F_{sdG} \quad (4.1)$$

$$A_{mb} \left( \frac{\Delta P}{L} \right) = \left( \frac{F_{mb}}{L} \right) - \tau_{sdmb} S_{sdmb} + \left( \frac{F_{mbsb}}{L} \right) + \tau_{mbsb} S_{mbsb} + F_{mbG} \quad (4.3)$$

$$\rho_{sd} = \rho_s C_{sd} + \rho_L (1 - C_{sd}) \quad (3.12)$$

$$\rho_{mb} = \rho_s C_{mb} + \rho_L (1 - C_{mb}) \quad (3.17)$$

Eliminating the pressure gradient terms from Eqs. 4.1 and 4.3, Equation 4.28 is obtained:

$$\begin{aligned} \frac{A_{mb}}{A_{sd}} (\tau_{sd} S_{sd} + \tau_{sdmb} S_{sdmb} + \rho_{sd} g A_{sd} \cos \theta) = \\ \frac{F_{mb}}{L} - \tau_{sdmb} S_{sdmb} + \frac{F_{mbsb}}{L} + \tau_{mbsb} S_{mbsb} + \rho_{mb} g A_{mb} \cos \theta \end{aligned} \quad (4.28)$$

Equation 4.27 can be rearranged as:

$$\begin{aligned} \frac{\tau_{sd} S_{sd} + \tau_{sdmb} S_{sdmb} + \rho_{sd} g A_{sd} \cos \theta}{A_{sd}} = \\ \frac{\left( \frac{F_{mb}}{L} \right) + \left( \frac{F_{mbsb}}{L} \right) + \tau_{mbsb} S_{mbsb} - \tau_{sdmb} S_{sdmb} + \rho_{mb} g A_{mb} \cos \theta}{A_{mb}} \end{aligned} \quad (4.29)$$

Solving these equations simultaneously is quite complicated, hence an iterative technique is used. The hierarchy flow chart for a step-by-step procedure is given in Appendix E.

#### 4.4.2 Transit Segment

A solution of the two-layer model for the transit segment is somewhat easier than the three-layer model. By adding Eqs. 4.7 and 4.8 and solving for the average velocity of the dispersed suspension layer, it becomes:

$$U_{sd} = \left( \frac{A_a}{A_{sd}} \right) U_a - \left( \frac{A_b}{A_{sb}} \right) U_b \quad (4.30)$$

When the bed is stationary or its velocity is relatively slower than the suspension layer, the velocity of a cuttings-bed can be negligible, that is to say,  $U_b \approx 0$ . Then, Eqs. 4.7 and 4.8 can be simplified as:

$$A_{sd} C'_{sd} U_{sd} = A_a C'_t U_a \quad (4.31)$$

Equation 4.29 can also be simplified as:

$$U_{sd} = \left( \frac{A_a}{A_{sd}} \right) U_a \quad (4.32)$$

From Eqs. 4.31 and 4.32, it clearly shows that:

$$C'_{sd} = C'_t \quad (4.33)$$

Equation 4.33 is satisfied under steady-state flow conditions. Equation 4.31 can then be rewritten as:

$$A_{sd} = \left( \frac{U_a}{U_{sd}} \right) A_a \quad (4.34)$$

Equation 4.34 is a function of  $y_{sd}$  (or  $y_b$ ) and nominal annular velocity,  $U_a$ . The stationary bed height,  $y_b$ , directly affects a local velocity of a suspension layer and its cuttings volumetric concentration. A change in these parameters changes the force and momentum balances. Hindered settling velocity ( $V_h$ ) and diffusivity ( $\varepsilon_p$ ) are also

functions of a cuttings volumetric concentration on the dispersed suspension layer ( $C_{sd}$ ). Therefore, the stationary bed height can be obtained by iterative calculation of all the related equations. The details of the calculation procedure are described in Appendix E. Once the cuttings-bed height ( $y_b$ ) is obtained, the average velocity of the dispersed suspension layer,  $U_{sd}$ , can be obtained from the wellbore geometry.

By combining Eqs. 4.15 and 4.16 and solving for  $F_b$ , the force acting on the cuttings-bed, it becomes:

$$F_b = \left[ \begin{aligned} & -\tau_b S_b + \tau_{sdb} S_{sdb} - \rho_b g A_b \cos \theta + \\ & \frac{A_b}{A_{sd}} (\tau_{sd} S_{sd} + \tau_{sdb} S_{sdb} + \rho_{sd} g A_{sd} \cos \theta) \end{aligned} \right] L \quad (4.17)$$

The fluid pressure gradient can be obtained from Eq. 4.1, which describes the sum of the forces acting on the suspension layer.

$$A_{sd} \left( \frac{\Delta P}{L} \right) = \tau_{sd} S_{sd} + \tau_{sdb} S_{sdb} + F_{sd\zeta}; \quad (4.12)$$

where,  $F_{sd\zeta}$  is the gravitational force acting on the suspension layer, which is the only component affected by the deviated wellbore angles. It is defined in Eq. 4.2.

## 4.5 Model Simulation Results and Discussion

The simulation was performed for the base case described in Table 3.1. The effect of various parameters such as nominal annular velocity ( $U_a$ ), wellbore deviation, carrier fluid rheology, and the cuttings concentration on the cuttings transport efficiency were simulated and investigated with the base case. Three different fluids (fluid A, fluid B, and the base case) were simulated to investigate the effect of fluid rheology on the cuttings



transport. Three different mathematical models, representing each segment, produced slightly different values at each segment boundary. In order to reduce the discontinuity of the combined results from the three segment models, the average simulation results at each segment boundary were used. The following simulation results show the effects of the various parameters.

#### **4.5.1 Effects of Nominal Annular Velocity in the Annulus**

The simulation results for the base case are presented in Figs. 4.5 to 4.7. Figure 4.5 shows the area distribution of each layer in the annulus with a change in the wellbore deviation at the nominal annular velocity of 3 ft/s. The three layers are distinct, i.e., a stationary bed of drilled cuttings at the bottom, a moving bed layer above it, and a heterogeneous suspension layer at the top. The stationary bed and the moving bed layer are somewhat stable under the horizontal segment. Below the wellbore deviation of 60°, the moving bed abruptly diminishes. The results shown in Fig. 4.5 confirm the findings published by other researchers.<sup>21,30,51</sup> The results indicate that it is more difficult to clean deviated wellbores than those close to vertical wellbores. Moreover, the axial velocity (vertical velocity) of the fluid increases with a decrease in the wellbore deviation. An increase in a vertical velocity can support the particles longer in the suspension layer. The highest vertical velocity is shown around 55° (Fig. 4.6) and the cuttings-bed begins to erode in this region. The cuttings-bed continuously erodes and will disappear at the end of the transit segment.

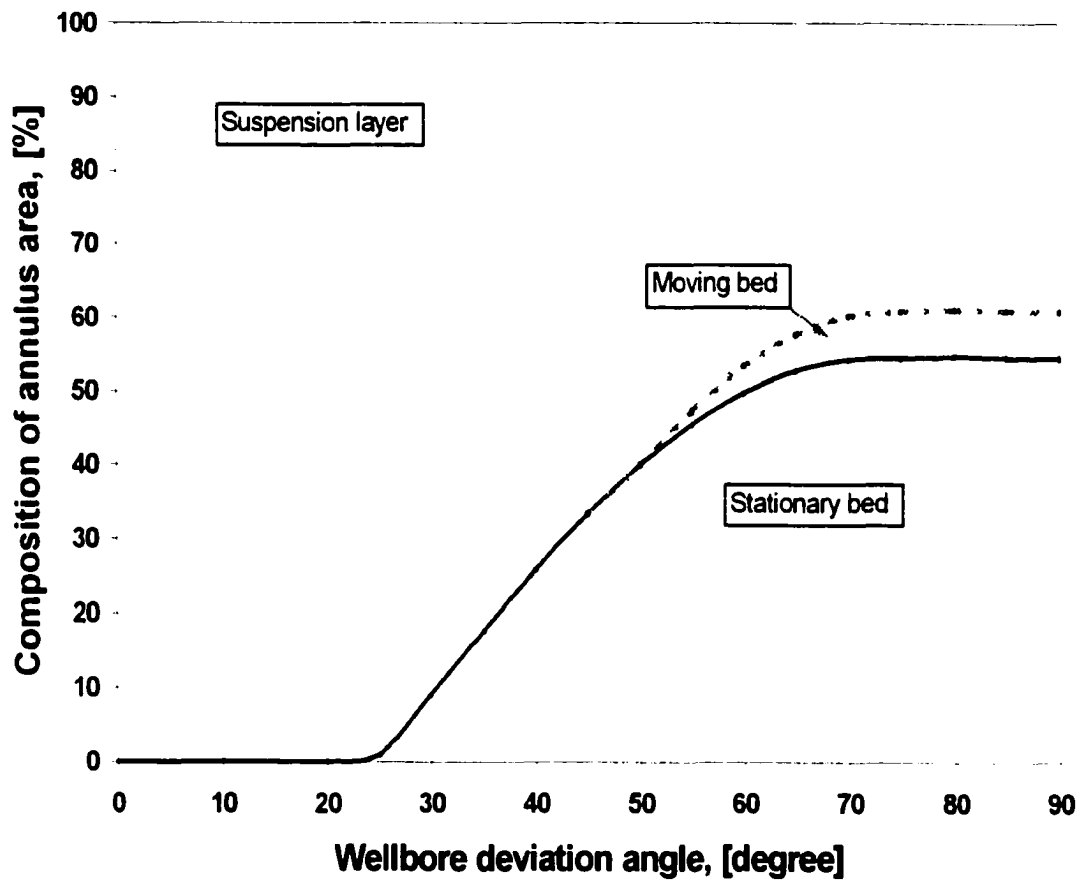


**Fig. 4.5 – Cuttings-bed distribution with the wellbore deviation from the vertical position (base case,  $U_a = 3$  ft/s)**

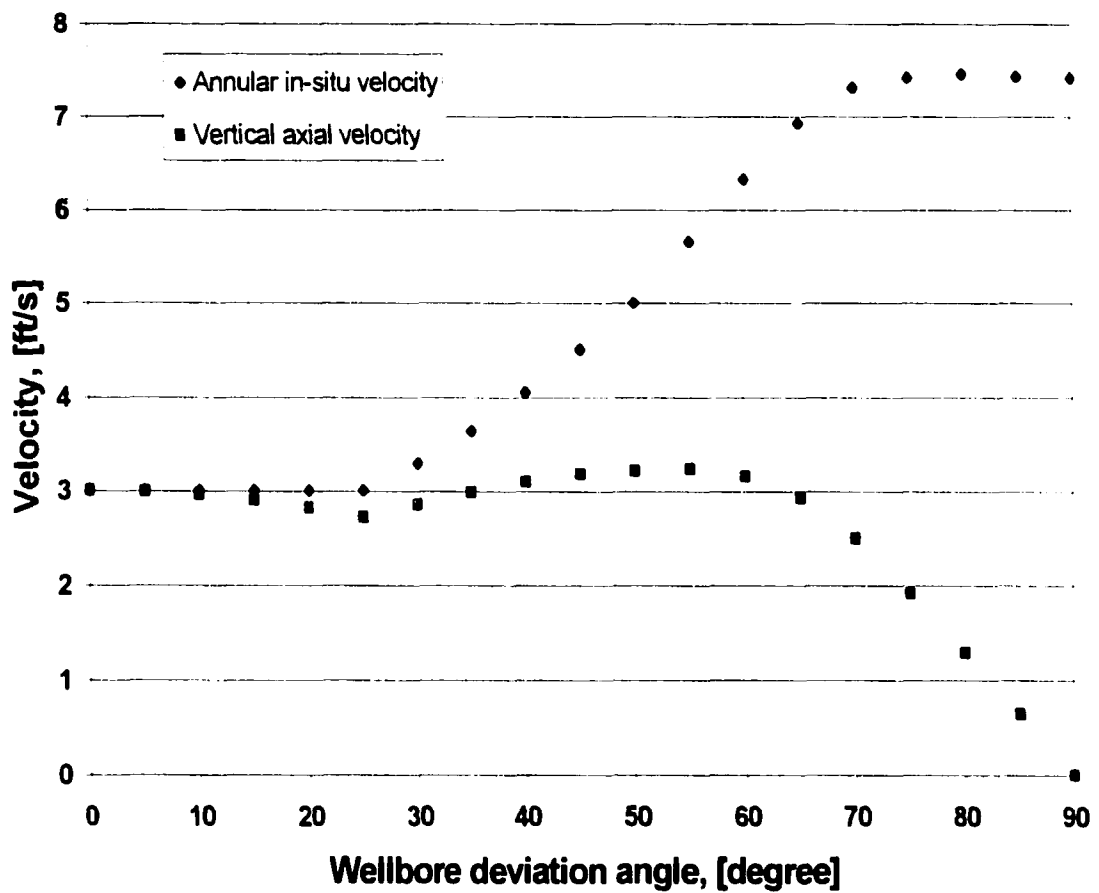


**Fig 4.6 – Velocity of the dispersed suspension layer at nominal annular velocity of 3 ft/s (base case)**

The cuttings-bed is almost non-existent in the vertical segment. The cuttings transport velocity is the dominant factor for hole cleaning in the vertical segment.

Comparison of the cuttings-bed area with the experimental data is shown in Fig. 4.7. The simulated cuttings stationary bed is stable in the horizontal segment. This pattern matches well with the experimental data taken from Tomren.<sup>9</sup> Simulation results shows 54 % of the stationary bed with a nominal annular velocity of 3 ft/s in the horizontal segment. The cuttings-bed diminishes around the wellbore angle of 30°. Meanwhile, the experimental data shows that the cuttings-bed areas are 30 % and 20 % with the nominal annular velocity of 2.86 ft/s and 3.34 ft/s, respectively. A 50 % eccentricity and drillpipe rotation at 50 rpm were considered in the experiment. Sanchez et al.<sup>79</sup> noted that the effect of drill pipe rotation on cuttings transport is about 32 %.

Peden et al.<sup>38</sup> noted that the effect of pipe eccentricity on the required transport velocity is 26%. The full eccentricity of coiled tubing drilling is intuitively considered for both horizontal and transit segments. This may lead to a large difference between the simulation and the experimental data because of the different conditions used in the simulation and the experiments. After consideration of differences between experimental conditions and simulation conditions, the simulation results for cuttings-bed area are in good agreement with these experiments.

Figure 4.8 shows the effect of nominal annular velocity on the cuttings-bed. From this figure the cuttings-bed with the nominal annular velocity of 3.0 ft/s shows the higher cuttings-bed area rather than those of the nominal annular velocity of 2.0 and 4.0 ft/s. The velocity profiles of the eccentric annulus presented by the researchers<sup>9, 20</sup> show that the velocities are very low in the bottom area where the coiled tubing is located.

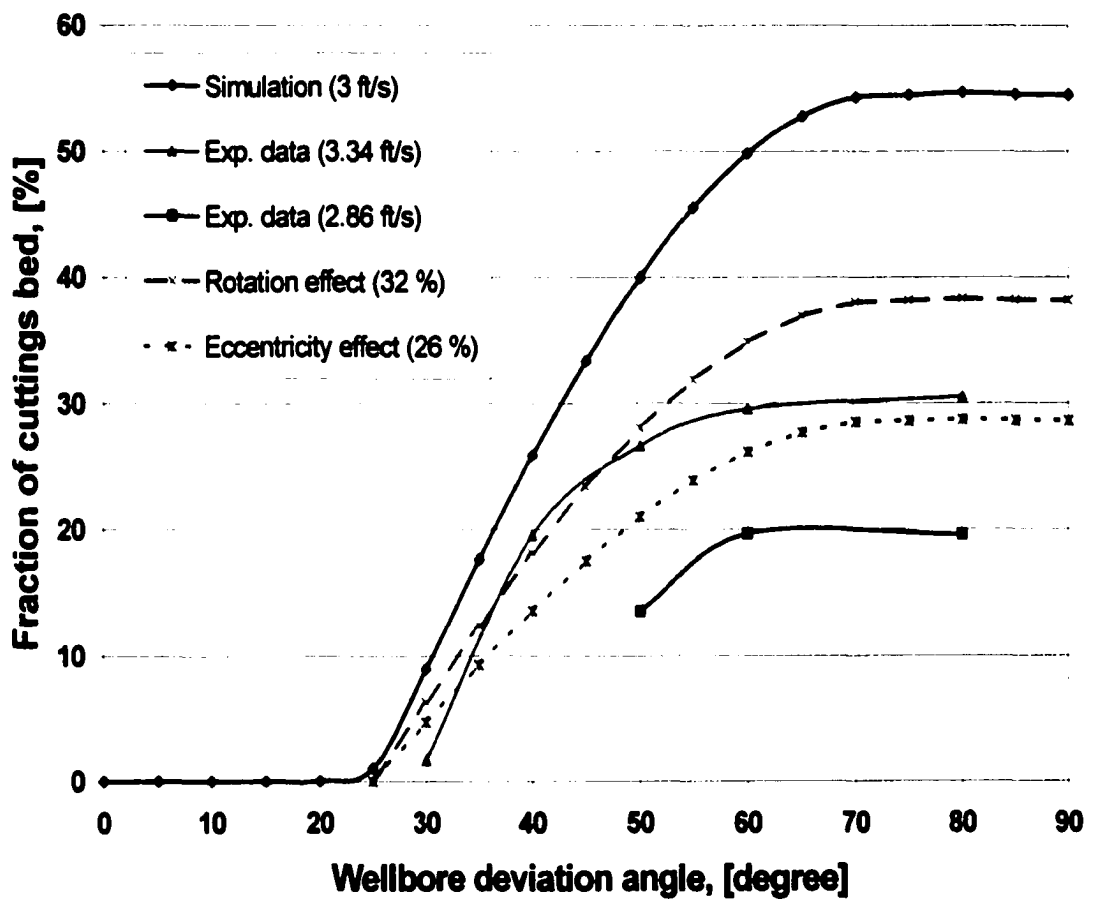


**Fig.4.7 – Comparison of cuttings stationary bed area with experimental data (taken from Tomren<sup>9</sup>)**

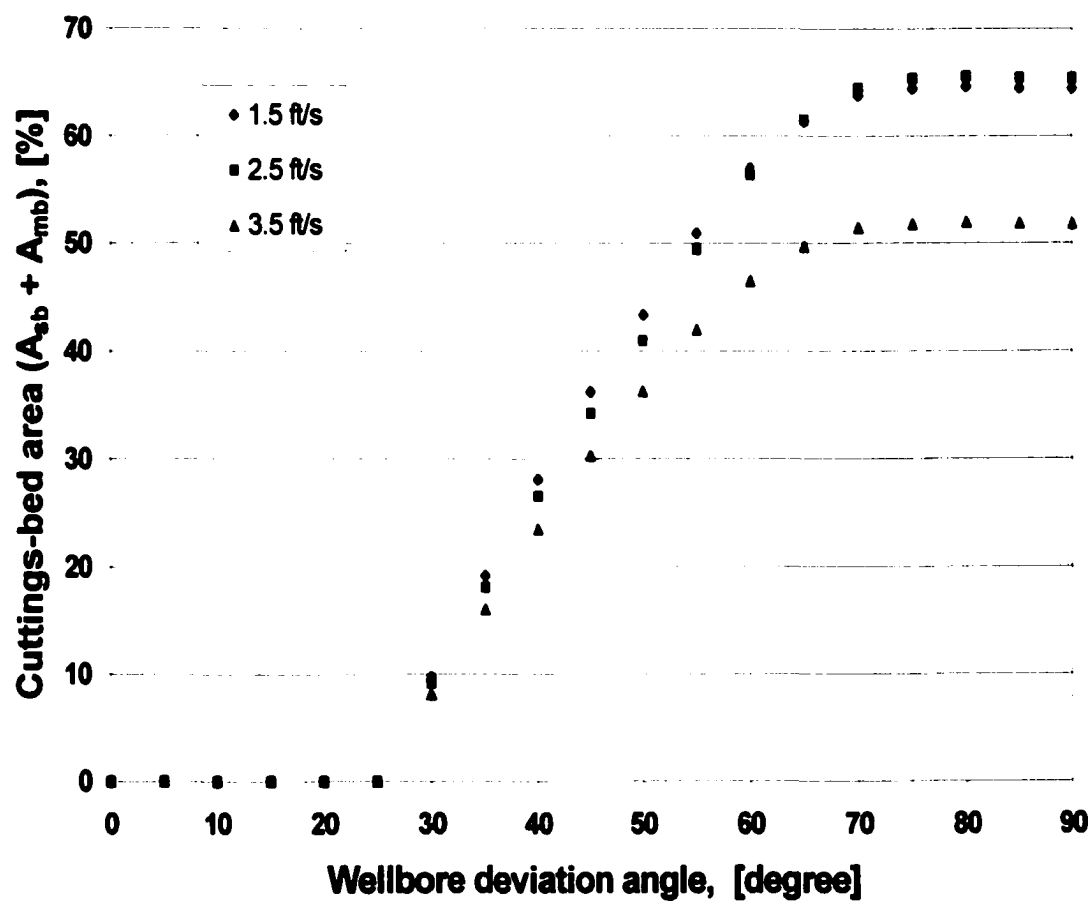


Fig. 4.8 – Effect of nominal annular velocities on the cuttings-bed

Therefore, cuttings settlement around the bottom area is inevitable in coiled tubing drilling with a normal pumping velocity (2 – 3 ft/s). The cuttings-bed diminishes with the nominal annular velocity of 5 to 6 ft/s.<sup>10,25,78</sup>

The particle concentration in an annulus is a strong function of the nominal annular velocity. Simulations of the particle concentration for the base case are compared with the experimental results, as shown in Fig. 4.9. The patterns of particle concentration in the annulus between the simulations and the experimental data are well matched through the entire wellbore deviation. As stated earlier, the effects of drillpipe rotation and eccentricity on cuttings transport efficiency are 32% and 26%, respectively. The different conditions between the experiment and the simulation were considered to correct the simulation data. The simulation result (28% of the cuttings volumetric concentration) was then converted into 14% after correction of effects of drillstring rotation and eccentricity. The drilling string rotation effect diminishes in the vertical segment, for which the cuttings transport velocity is a dominant factor in cuttings transport

#### **4.5.2 Analysis of Pressure Gradient**

The pressure drop profile of the horizontal section with the different nominal annular velocities is shown in Fig. 4.10. The pressure drop can be defined as a function of the stationary bed area (which affects the in-situ velocity of suspension layer), nominal annular velocity, and cuttings concentration in the suspension layer. The Nguyen and Rahman<sup>5</sup> model shows similar pattern as the Cho et al. model,<sup>25</sup> but the peak point of the pressure gradient and its relevant velocity point are different.

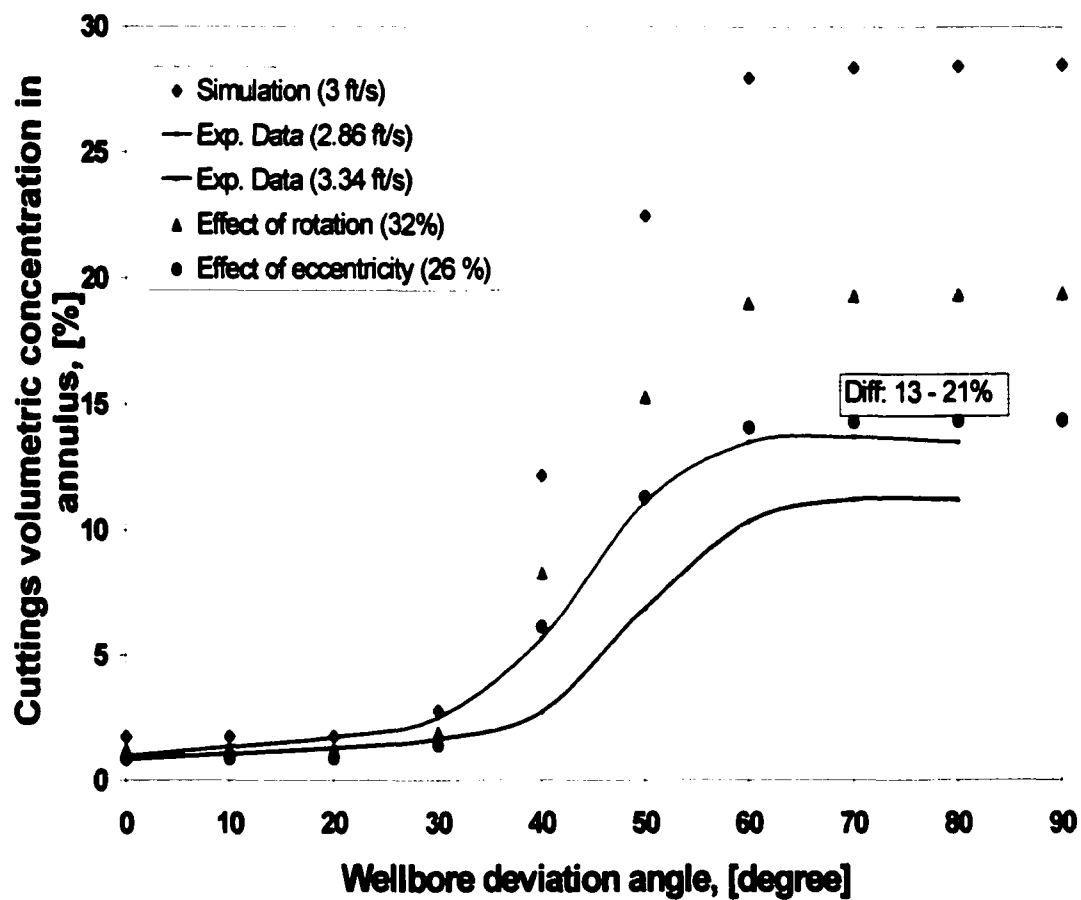


**Fig. 4.9 – Effect of the wellbore deviation on particle concentration (experimental data taken from Tomren<sup>9</sup>)**



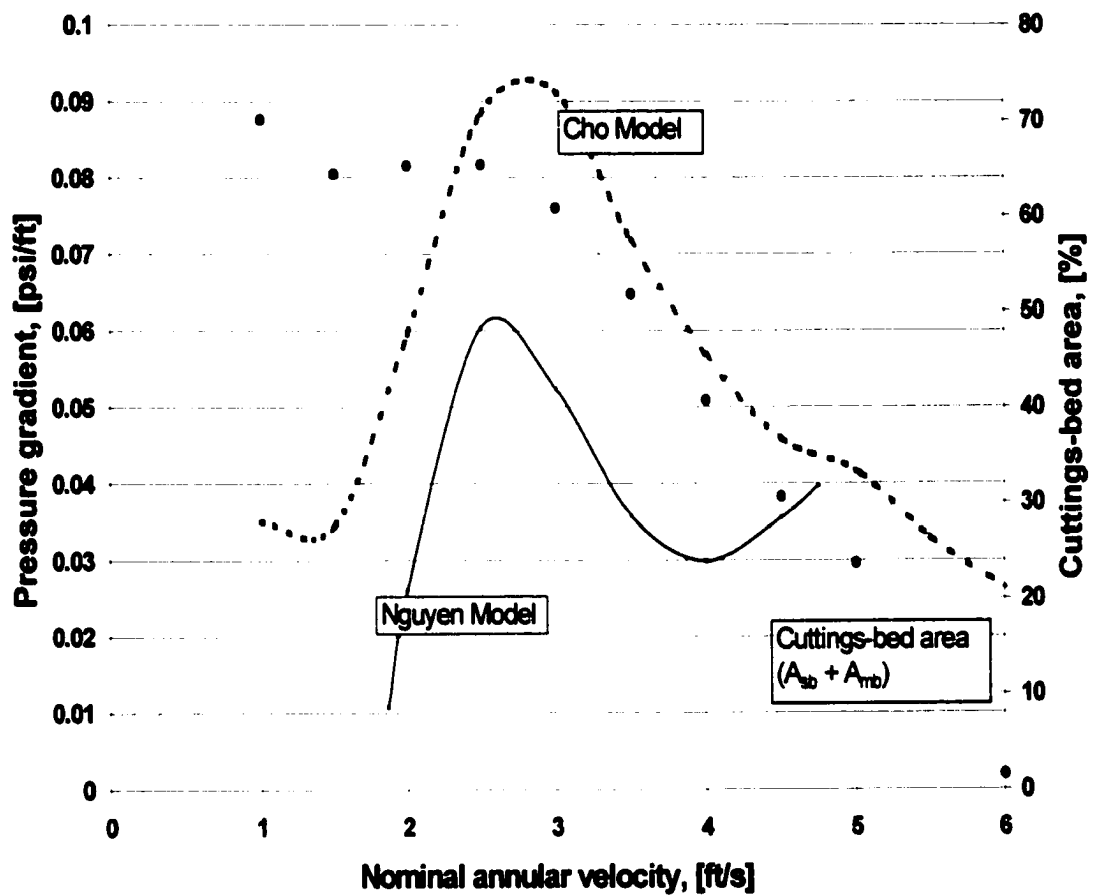


**Fig. 4.10 – Pressure drop for horizontal section with different three-layer models (base case)**

The simulation results show that the pressure gradient increases with an increase in the nominal annular velocity up to 2.8 ft/s, and then it decreases. Pressure gradient is a strong function of cuttings-bed area as shown in this figure. The cuttings-bed area increases slightly with an increase in nominal velocity from 1.5 ft/s until it reaches 2.5 ft/s.

Effects of wellbore deviation on the pressure gradient are shown in Fig. 4.11. The gravitational effect on pressure gradient is about 0.433 psi/ft physically for vertical wells. The magnitude of frictional pressure loss is relatively smaller than the gravitational effect. This magnitude of gravitational effect decreases as a wellbore deviation increases. This is because the pressure gradient gradually decreases with an increase in wellbore deviation. The pressure gradient in the vertical segment increases with the increase in nominal annular velocity. Each layer with its relevant velocity also affects the pressure gradient. Table 4.1 presents the effects of the wellbore deviation and the nominal annular velocity on the area of each cuttings-bed layer. Since there is no cuttings-bed in the vertical segment, the pressure gradient is only a function of cuttings concentration (which is also function of the rate of penetration) and nominal annular velocity.

Figure 4.12 presents the pressure gradient without gravitational effect under the different pumping velocities. The pressure gradient at the nominal velocity of 3 ft/s shows up high in the horizontal segment. This is because both cuttings-bed and cuttings volumetric concentration in the suspension layer are high at that velocity. However, the nominal velocity of 4 ft/s shows high pressure gradient (0.017 psi/ft) for the vertical segment. The pressure gradient in the vertical segment increases with the increase in nominal annular velocity

**Table 4.1 – Area fraction of each cuttings-bed layer (base case)**

Deviation angle	$U_a = 2.0$ ft/s			$U_a = 3.0$ ft/s			$U_a = 4.0$ ft/s		
	$A_{sd}$	$A_{mb}$	$A_{sb}$	$A_{sd}$	$A_{mb}$	$A_{sb}$	$A_{sd}$	$A_{mb}$	$A_{sb}$
0	100.0	0.0	0.0	100.0	0.0	0.0	100.0	0.0	0.0
10	100.0	0.0	0.0	100.0	0.0	0.0	100.0	0.0	0.0
20	100.0	0.0	0.0	100.0	0.0	0.0	100.0	0.0	0.0
30	90.3	0.0	9.7	90.8	0.0	9.2	91.9	0.0	8.1
40	72.0	0.0	28.0	73.5	0.0	26.5	76.5	0.0	23.5
50	56.6	0.0	43.4	59.0	0.0	41.0	63.7	0.0	36.3
60	43.0	3.0	54.0	43.6	5.3	51.0	53.5	1.3	45.2
70	36.2	4.9	58.9	35.5	8.8	55.6	48.6	2.2	49.3
80	35.4	5.3	59.3	34.4	9.5	56.0	48.0	2.3	49.7
90	35.6	5.3	59.1	34.6	9.5	55.8	48.2	2.3	49.5

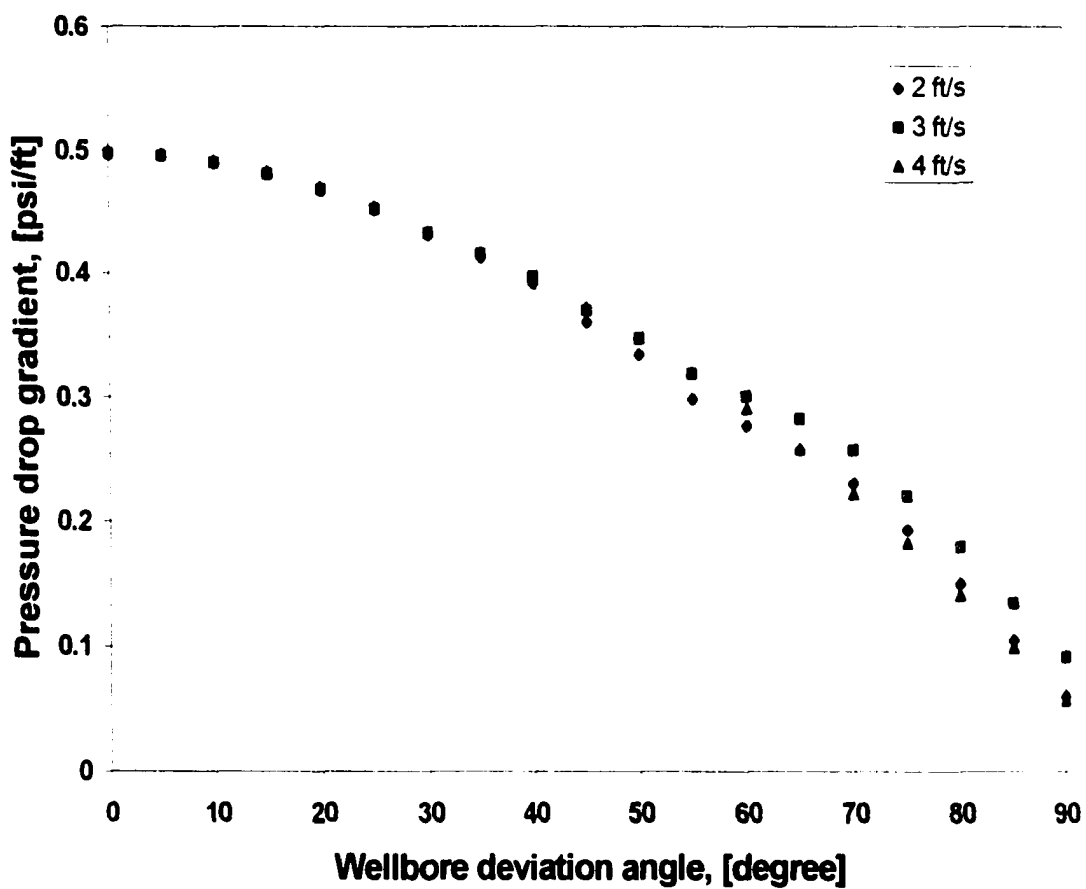


**Fig. 4.11 – Effect of wellbore deviation on pressure gradient**

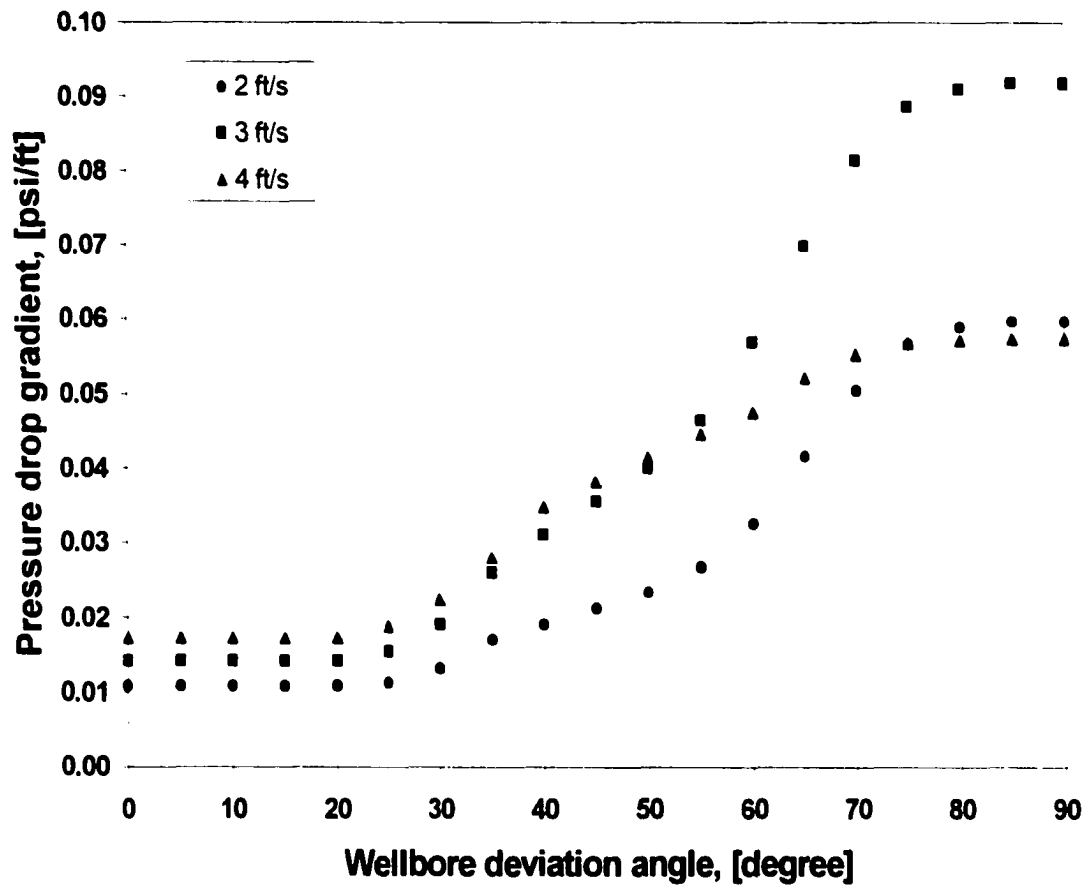


**Fig. 4.12 – Pressure gradient without gravitational effect of different nominal annular velocities (base case)**

### 4.5.3 Effects of Fluid Rheology

The effect of drilling fluid rheology with a change in the angles of deviation is simulated by the different fluid systems (fluid A, fluid B, and base case). The details of the fluid systems used in the simulation are presented in Table 4.2. The effects of the wellbore deviation and rheological properties of the fluids on cuttings-bed are presented in Fig. 4.13.

**Table 4.2 – Fluid systems used in comparison**

Description	Base case	Fluid A	Fluid B
Fluid type	Low-Vis Bentonite	HEC based Drilling fluid	HEC based Drilling fluid
$n$	0.68	0.76	0.50
$K$ ( $\text{lb}_f \text{s}^n / \text{ft}^2$ )	0.006	0.001	0.028
Density (ppg)	9.2	9.2	9.2
$\mu_a$ (cp) @ $511 \text{ s}^{-1}$	39.0	10.9	60.0

The simulation results show that a decrease in fluid behavior index slightly decreases the area of the stationary bed but, keeps the moving bed layer almost constant. An increase in the viscosity of the carrier fluid increases cuttings transport efficiency for both the cuttings rolling/sliding and suspension mechanism. The stationary cuttings-bed is easily eroded by the viscous fluid at the transit segment. The more viscous fluid (fluid B) may support particles in the suspension layer longer than the less viscous fluid (fluid A). However, the pressure gradient of the more viscous fluid is greater than the less viscous fluid for both the vertical and horizontal segments (Fig. 4.14).

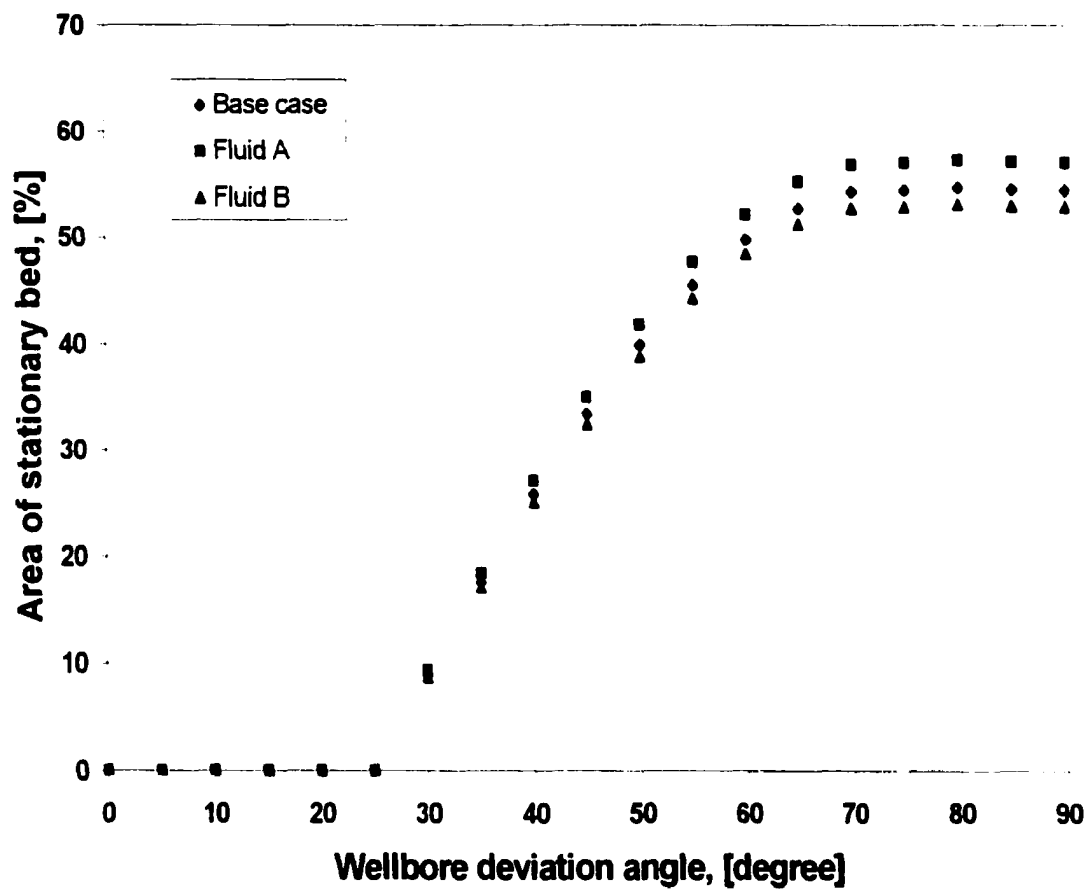


Fig. 4.13 – Effect of fluid rheology on the cuttings stationary bed area ( $U_a = 3$  ft/s)

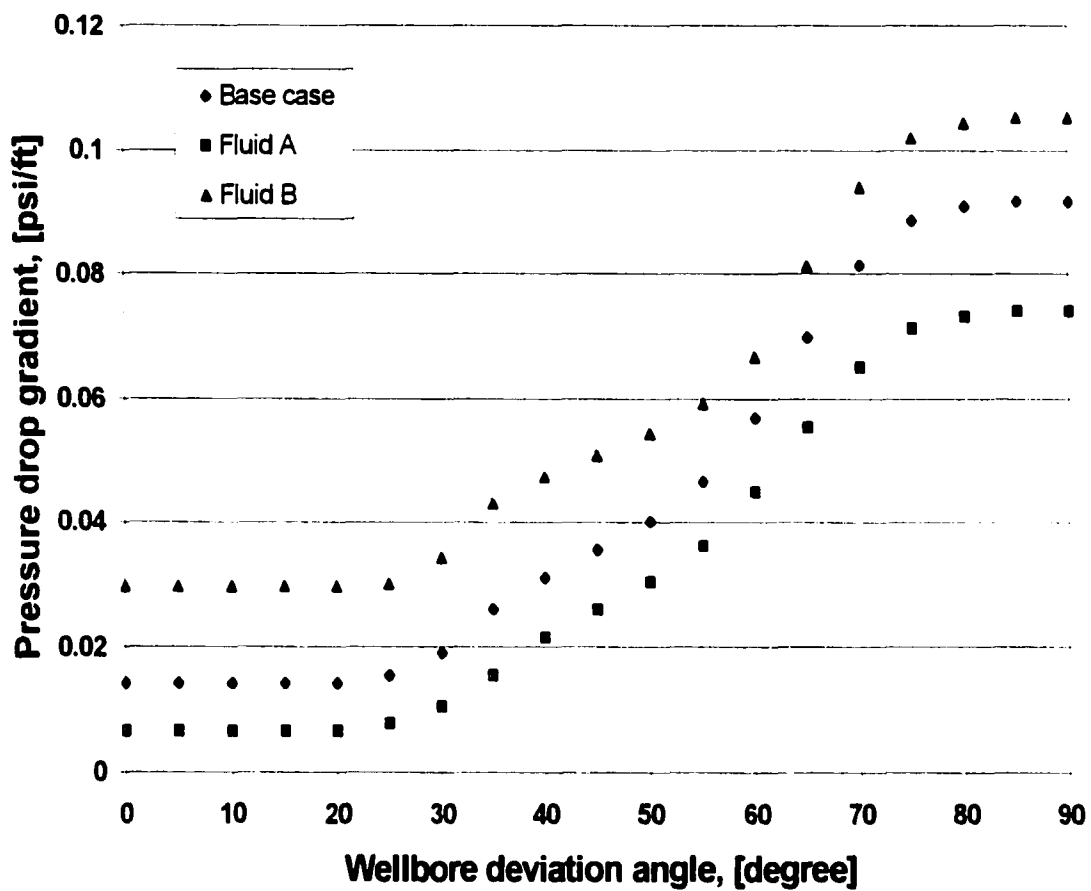


Fig. 4.14 – Effect of fluid rheology on pressure gradient ( $U_a \approx 3$  ft/s)



These results indicate that the effectiveness of a carrier fluid in cuttings transport is not only dependent on the rheology of the fluid, but also on the fluid flow regimes. These simulation results also show that the viscous drilling fluid with a high in-situ velocity brings good results in the long transit segment, and the viscous drilling fluid with a low velocity (laminar flow regime) gives good results in the long vertical segment, in view of the cuttings transport. The simulation results are within the industry's accepted rules of thumb.<sup>5,6,10,12,32,84</sup>

#### **4.5.4 Effects of Fluid Density**

Some researchers have emphasized that the fluid density plays an important role in hole cleaning in deviated wellbores.<sup>27</sup> In vertical and deviated wellbores, the increased fluid density can serve to reduce particle settling velocities caused by increased buoyancy effects. Whether the reduced particle settling velocities promote better cleaning is dependent upon other factors as well.<sup>83</sup> Figure 4.15 presents the effects of fluid density on cuttings bed area distribution with base case. Three base fluids with different densities (8, 12, and 18 ppg) were used for simulation with pump rate 3.7 bbl/min. that corresponds to nominal annular velocity of 3 ft/s. Higher density fluid shows less cuttings-bed remained under the same nominal annular velocity. An increase of 50% in fluid density (from 8 ppg to 12 ppg) decreases the cuttings stationary bed area in horizontal segment by 8.5%. From this figure, the heavier mud outperformed the lighter fluid, indicating that increased mud density can improve cuttings transport somewhat in horizontal and transit segments. However, the other points such as static pressure and pressure gradient must be considered in the design of an optimum drilling program.

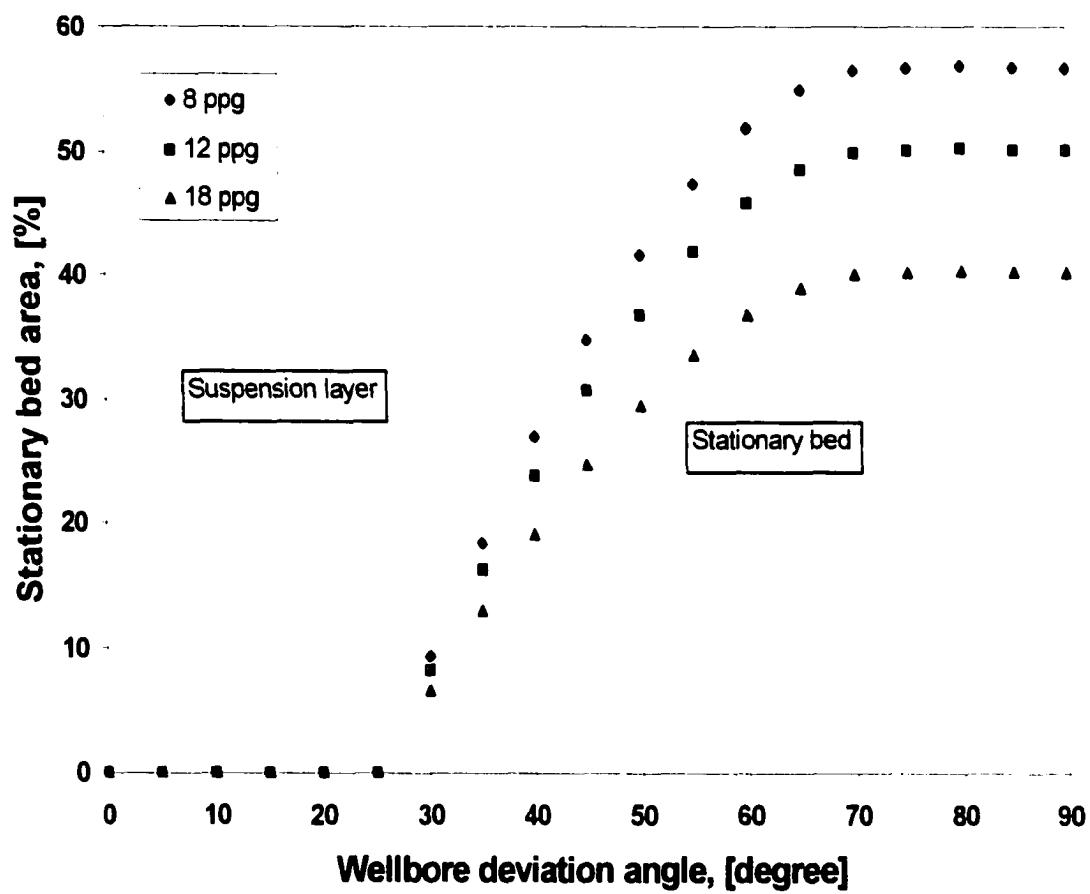


Fig. 4.15 – Effects of fluid density on cuttings-bed distribution (base case,  $U_a = 3$  ft/s)

Hemphill and Larsen<sup>83</sup> performed experimental works to investigate the effects of circulating fluid density on the required critical velocity. They performed experiments on a 5-in. flow loop with 2-5/8-in. diameter inner pipe, which simulated drillpipe rotating at 50 rev/min. Limestone cuttings having 0.25-in. average diameter were used with an injection rate maintained at 20 – 21 lb<sub>m</sub>/min. that corresponds to a penetration rate of 54 – 56 ft/hr. Two different fluid systems, presented in Table 4.3, were used.

In their experiments,<sup>83</sup> the effects of fluid density were studied in terms of the critical fluid velocity for the 10.1-lbm/gal (fluid #1) and 15-lbm/gal (fluid #2). Figure 4.16 illustrates that at the higher deviation angles (horizontal segment), higher fluid density requires less critical fluid velocity. It can be interpreted that a higher density fluid erodes the cuttings-bed more easily than a fluid with less density. These experimental results are in good agreement with the cuttings-bed distribution for the different fluid density.<sup>83</sup>

**Table 4.3 – Fluid systems used in the comparison of fluid density effects**

Fluid Property	Fluid #1	Fluid #2
Density (lb <sub>m</sub> /gal)	10.1	15
Plastic viscosity (cp)	16	28
Yield point (lb <sub>f</sub> /100 ft <sup>2</sup> )	11	15
Flow behavior index, <i>n</i>	0.67	0.73
Flow consistency index, <i>K</i> (lb <sub>f</sub> s <sup><i>n</i></sup> /ft <sup>2</sup> )	0.0044	0.0048

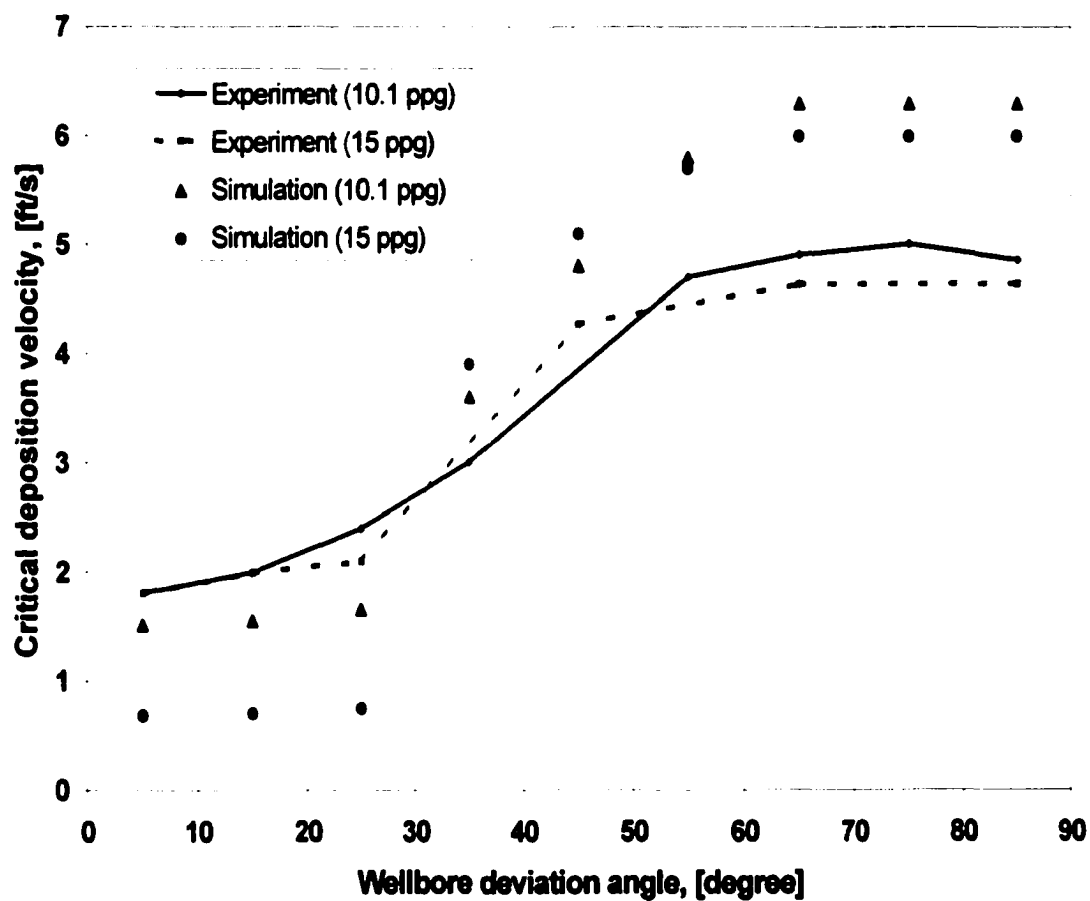


**Fig. 4.16 – Fluid density effects on critical fluid velocity vs. wellbore deviation (borehole: 5", drillpipe: 2-5/8", cuttings size: 0.25", ROP: 55 ft/hr, experimental data taken from Hemphill and Larsen<sup>83</sup>)**

The required critical fluid velocity in transit segment has no consistency. Fluid #2 shows higher critical fluid velocity in deviation angle range 35 – 50°. However, fluid #1 shows higher fluid velocity in deviation angle range 20 – 35°. In this segment, the cuttings-bed has been observed to slide down frequently.<sup>78</sup> The cuttings-bed is not stable in this segment. Hemphill and Larsen<sup>83</sup> noted that increasing mud density and mud viscosity could improve cuttings transport somewhat in the transit segment.

The simulation results, illustrated in Fig. 4.16, show that higher-density fluid requires lower critical velocity in a horizontal segment. The difference in simulation results for the horizontal segment is 5% (18 – 23%) for both fluids. This can be explained from the different conditions: drillpipe was rotated at 50 rpm in experimental conditions, but the simulation program(CT-WellClean<sup>®</sup>) is based on coiled tubing drilling without the effects of drillstring rotation. The effect of drillstring rotation in this case was 19.1 % obtained from the University of Tulsa Drilling Research Project (UTDRP) study.<sup>21</sup> Considering the effects of drillstring rotation on the simulation, the results of both simulation and experiments are in good agreement for horizontal segment.

For the vertical segment, the required critical fluid velocities for the simulation runs were obtained by doubling the particle settling velocities as recommended by Wlaton.<sup>12</sup> However, it is not clear, which experimental conditions were applied to measure critical fluid velocities in the vertical segment. Generally, the dominant factors in cuttings transport in a vertical segment are cuttings settling velocity and buoyancy corrected gravity force. The differences between experiment and simulation for fluid #1 are about 17 – 45%; on the other hand, the differences for fluid #2 are about 165 – 180 %. Even

though, different conditions (drillstring rotation) were considered in these results, the simulation results show much lower critical fluid velocities. The drilling fluid velocity 1 – 2 ft/s, shown in the experimental result as critical fluid velocities, are generally accepted in conventional vertical drilling.

#### **4.5.5 Effects of Borehole Size**

Because of economical advantages, the applications of coiled tubing technique have been developed in many areas. Coiled tubing drilling was initiated with the application of sidetracking. The development of coiled tubing drilling technology allows drilling larger wellbores and long horizontal wells as well as extended reach wells. The location of coiled tubing in horizontal and transit segments intuitively is at the lower part of wellbore, which makes the annulus area fully eccentric.

It is evident that significant variations in flow occur in the narrow regions in the annulus. Zamora et al.<sup>84</sup> showed from their experimental results that flow in the fully eccentric annulus was highly skewed, as seen in Fig. 4.17. The details of fluid system used in their experiment are well described in Reference 84. Vinod and McIntire<sup>20</sup> argued that narrow regions of the annulus always show low velocity profile resulting in laminar flow regime, while the wider regions easily reach flow development resulting in a turbulent flow regime. This is one of the reasons for cuttings accumulation around coiled tubing in the annulus under the normal range of drilling fluid circulation.

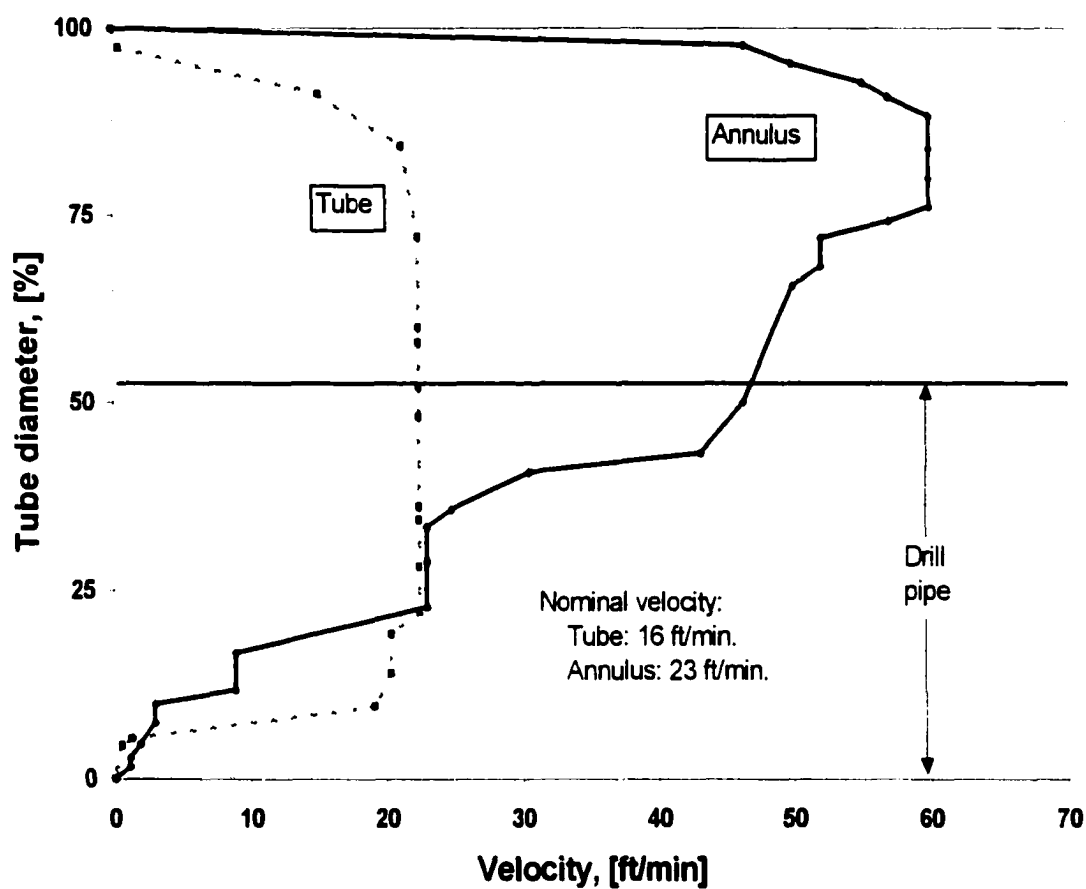


Fig. 4.17 – Comparison of tube and annulus velocity profile of 4 lb<sub>m</sub>/Mgal HEC in 0.692-in. \* 0.375-in. annulus (experimental data taken from Zamora et al.<sup>84</sup>)

The change of wide region (due to change in borehole size) may affect the flow development resulting in the cuttings transport efficiency. Simulations were performed with the base case changing pump rates. Figure 4.18 shows the effects of the ratio of the wellbore diameter ( $D$ ) to the coiled tubing diameter ( $d$ ) in horizontal well. The high ratio of  $D/d$  (4) reaches low cuttings-bed area as well as critical fluid velocity (5.4 ft/s). However, the low ratio of  $D/d$  (2) shows high critical fluid velocity (6.5 ft/s).

Effects of borehole size on cuttings transport efficiency with the different ratio ( $D/d$ ) are shown in Fig. 4.19. The stationary bed decreases with an increasing the diameter ratio. The moving bed gradually decreases as the ratio of borehole diameter to the coiled tubing diameter increases under the same nominal annular velocity ( $U_a = 3$  ft/s). In addition, the pressure gradient in horizontal well also decreases exponentially with an increasing the diameter ratio.

#### **4.5.6 Effects of Cuttings Specific Gravity**

The specific gravity of various formations depends upon the rock types; the range of specific gravity of sedimentary rock<sup>85</sup> is 2.20 to 2.88. Generally, the range of specific gravity for shale and sand formation<sup>85</sup> is 2.5 - 2.75. The range of specific gravity of the formation being drilled in the drilling industry is somewhat limited. Therefore, the experimental studies for the effects of particlespecific gravity on cuttings transport efficiency have not been studied much yet.



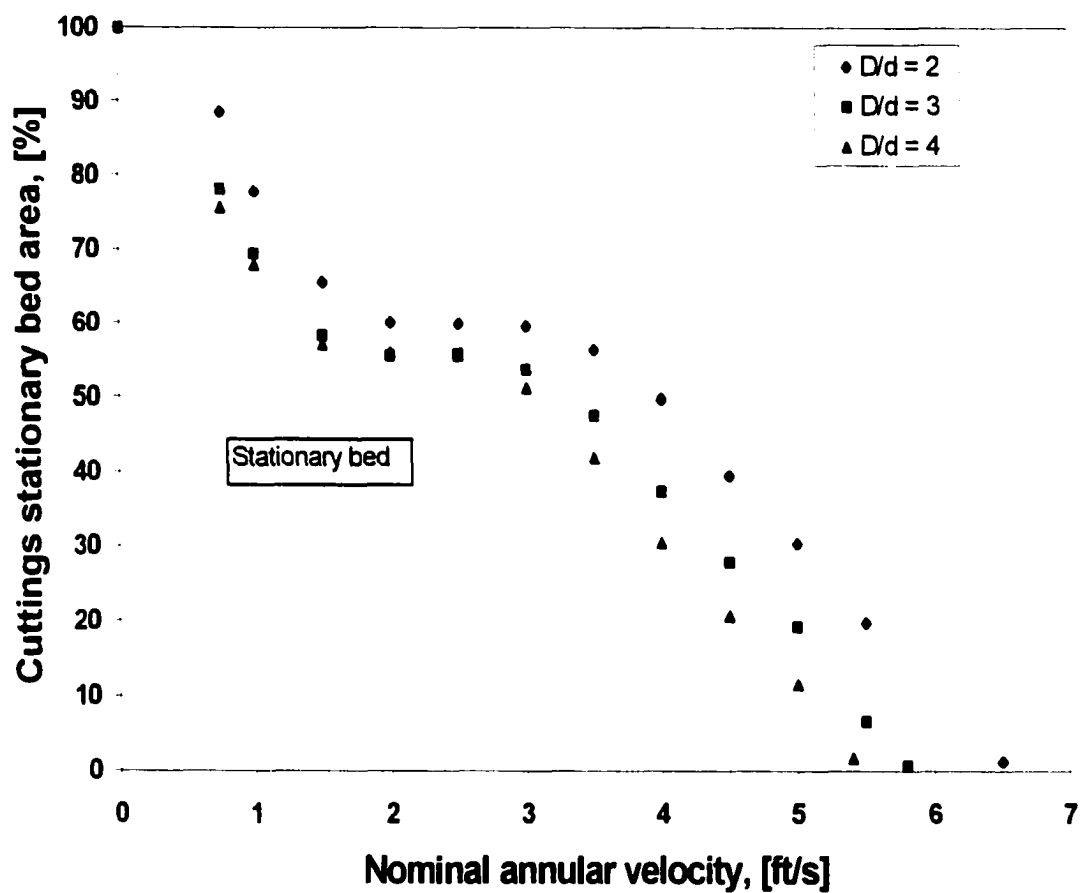


**Fig. 4.18 – Effects of the ratio of a wellbore diameter to a coiled tubing diameter (base case)**

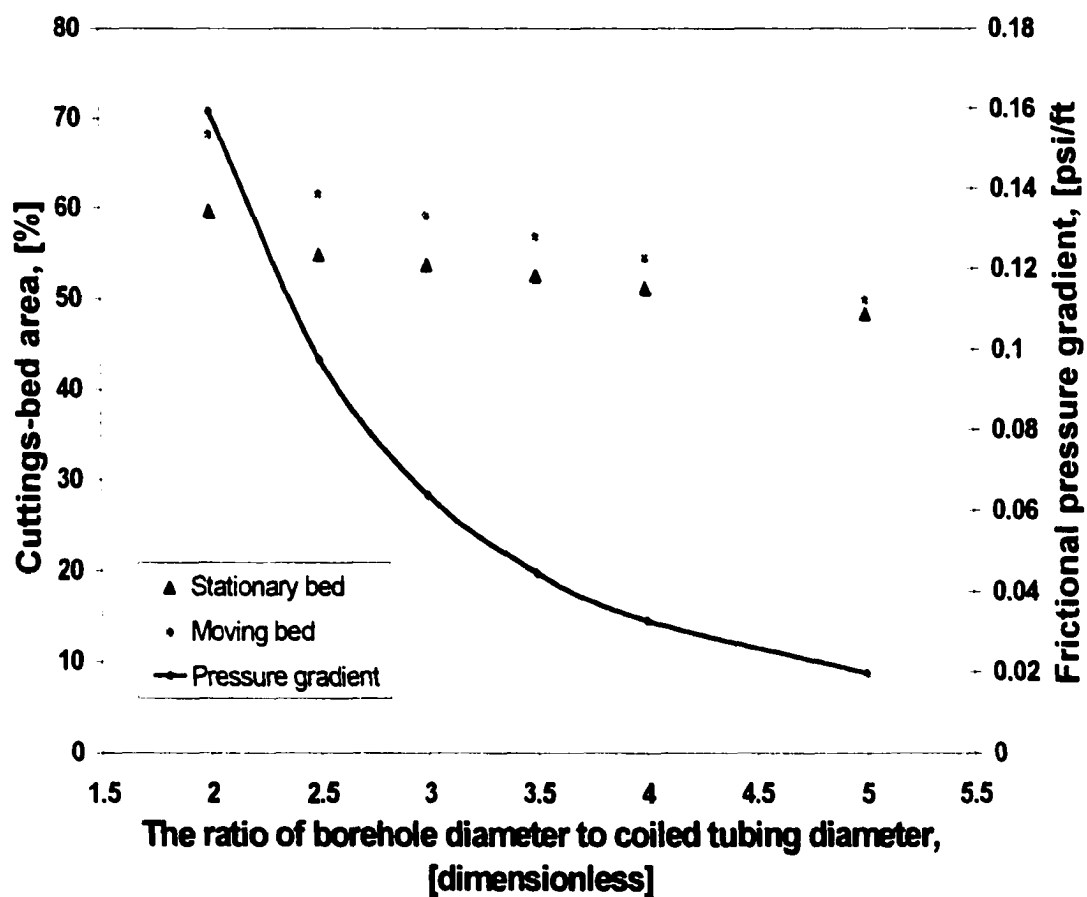


**Fig. 4.19 – Effects of borehole size on cuttings transport efficiency of horizontal well (base case,  $U_a = 3$  ft/s)**

Computer simulations were performed to investigate the effects of specific gravity in horizontal well. Figure 4.20 presents the relationship between cuttings bed distribution and pressure gradient. The stationary bed increases with an increasing particle specific gravity. The moving bed shows gradually decreasing its bed area with an increase in particle specific gravity. This may be due to the fact that cuttings with heavier specific gravity are more difficult to transport than lighter one under the same fluid density. An increase in the cuttings-bed area decreases fluid path area in annulus resulting in increased local velocities. These increased local velocities and relatively higher density (due to high particle specific gravity) result in pressure gradient increase.

#### **4.5.7 Effects of Penetration Rate**

Li and Walker<sup>14</sup> performed over 600 tests using 20/40 (USA mesh) Carbolite and 20/40 Frac Sand at various concentrations. In their experiments, the drillpipe was not rotated and positioned at the bottom of the openhole (100 % eccentricity). The test loop used consists of a 20 ft long transparent Lexan pipe with a 5-in. (internal diameter) simulating openhole and a 2-3/8-in. steel inner pipe to simulate a drillpipe. They confirmed that there was always a cuttings-bed covering drillpipe in the annulus of a horizontal wellbore under the practical value of fluid rates (  $< 0.6 \text{ m}^3/\text{min.}$ ;  $U_a < 3.34 \text{ ft/s}$ ), which is also consistent with this simulation result.

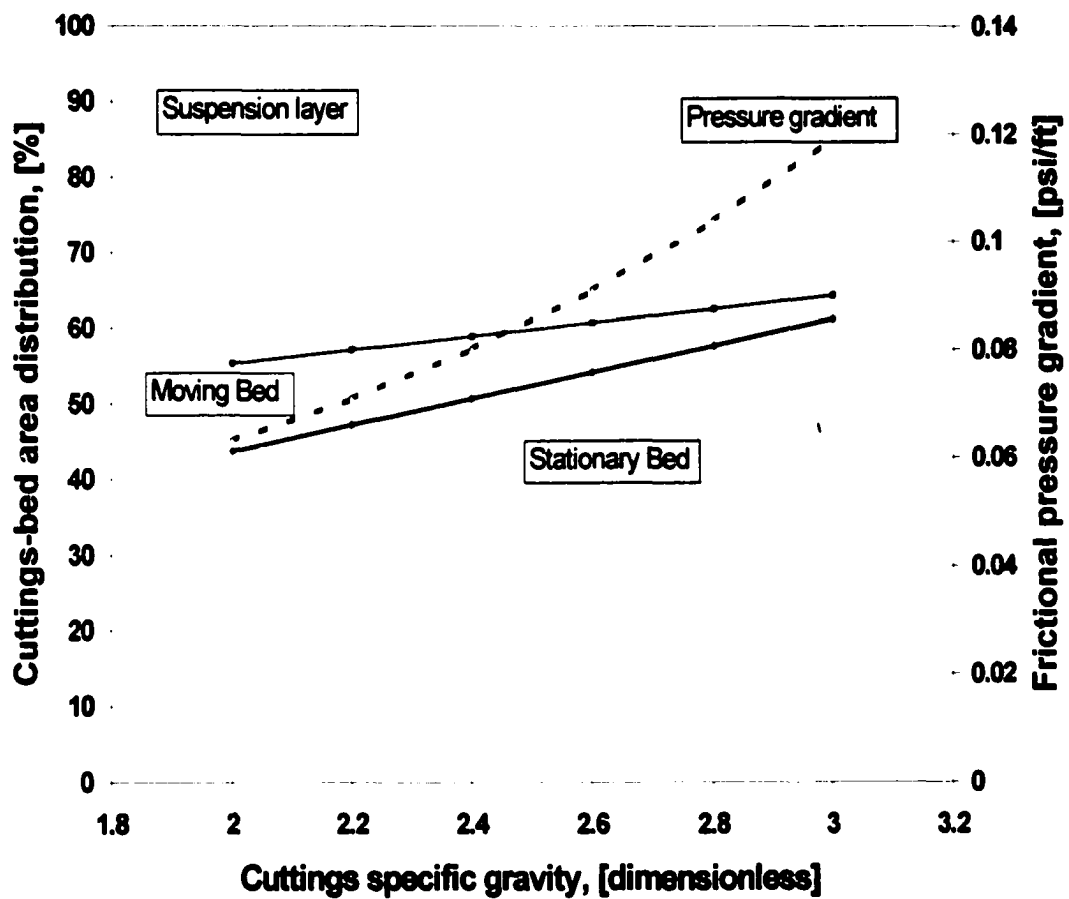


**Fig. 4.20 – Effects of cuttings specific gravity on cuttings-bed distribution and pressure gradient of horizontal well (base case,  $U_a = 3$  ft/s)**

Simulations were performed with the same conditions. Figure 4.21 illustrates the comparison of bed height for the horizontal wellbore between experimental data, taken from Li and Walker,<sup>32</sup> and the simulation results using CT-WellClean<sup>®</sup>. Both results show that an increase in nominal annular velocity decreases cuttings-bed height in horizontal wellbore. However, the simulation results have a flattening in the curve at 2.0 – 2.5 ft/s of nominal annular velocity. The differences in bed height between experimental data and those predicted by simulations are about 1 – 13.5%. For the simulation, the data for Fluid A and 0.025-in. average particle size sands were used.

Figure 4.22 shows the effects of ROP on cuttings transport efficiency with the base case of which pump rate was 3.7 bbl/min. corresponding to a 3 ft/s of nominal annular velocity. The stationary bed area with 50 ft/hr ROP shows 51% of cuttings bed in horizontal segment. This stationary bed area is increased 8.2 % with 150 ft/hr ROP. The cuttings bed accumulation is not sensitive to ROP as compared to pressure gradient. However, pressure gradient abruptly increases with an increasing ROP in the horizontal segment: pressure gradient increases 2-times with an increase of 3-times in ROP in horizontal segment.

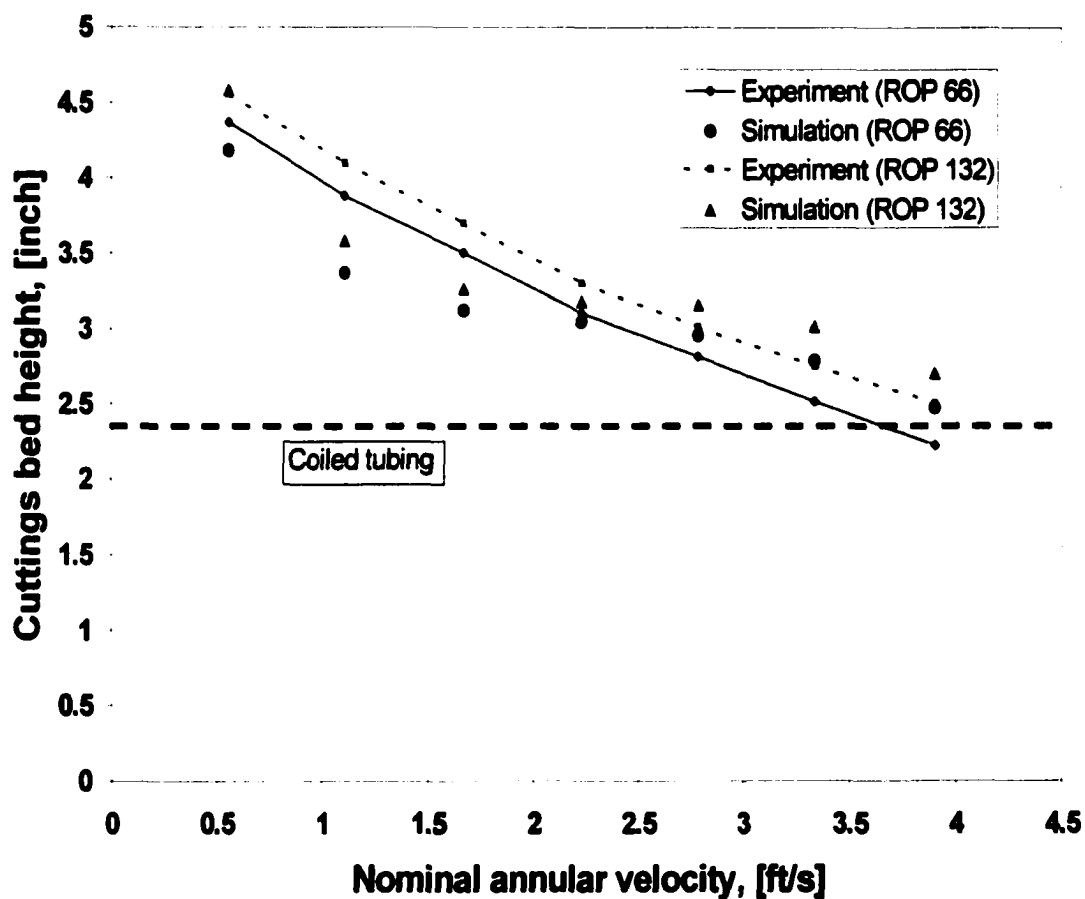


**Fig. 4.21 – Comparison of ROP effects on cuttings-bed height for the horizontal wellbore (Fluid A, Wellbore: 5", coiled tubing: 2-3/8", particle size: 0.025" – experimental data taken from Li and Walker<sup>32</sup>)**

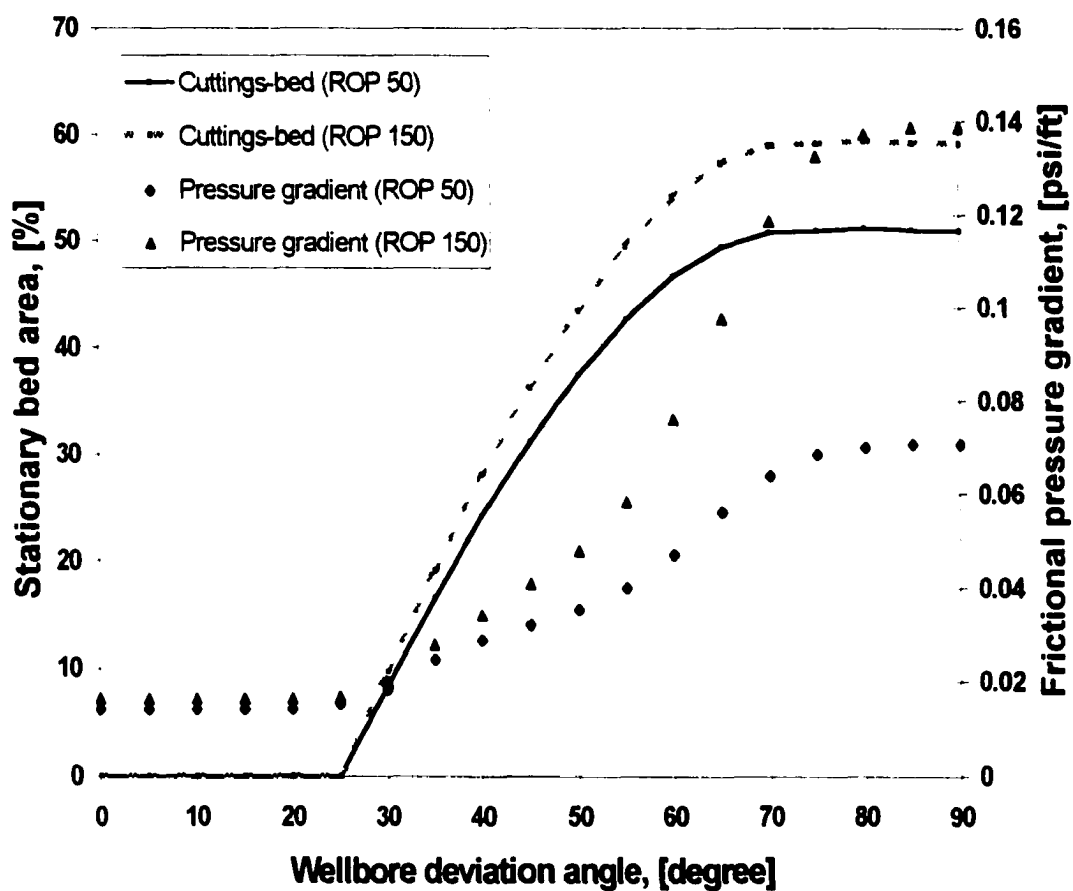


Fig. 4.22 – Effects of ROP on cuttings transport efficiency with wellbore deviation (base case,  $U_a = 3$  ft/s)

#### 4.5.8 Effects of Cuttings Size

The characteristics of cuttings (such as size, shape, and density) are related to their dynamic behavior in a flowing media. The terminal velocity, drag force, buoyancy corrected gravity force, and shear forces between cuttings are affected by both the characteristics of the cuttings and the properties of the circulated fluids.<sup>79</sup> There are no consistent conclusions related to the effect of particle size on cuttings transport that can be drawn on previous study.<sup>6,21,79,86</sup>

Figure 4.23 illustrates the effects of particle size on the cuttings bed and frictional pressure gradient based on the simulation results. Parameters specified in the base case were used while varying only the particle size. These simulation results are for the horizontal well with nominal annular velocity of 3 ft/s (equivalent flow rate: 157 gpm). This figure indicates that an increase in particle size increases cuttings-bed and pressure gradient abruptly at particle size greater than 0.2-in. (5 mm). For the same fluid pump rate, larger particle size results in a higher bed height than smaller ones.

Figure 4.24 presents the effects of particle size on cuttings-bed distribution and pressure gradient with the base case ( $U_a = 3$  ft/s). The cuttings stationary bed with fine particle size (0.06-in.) is lower than coarse particle (0.25-in.) case. The difference in the cuttings-bed area is about 6.5 % only. However, pressure gradient in horizontal segment increases 25 % (from 0.069 psi/ft to 0.092 psi/ft). In the vertical segment, the differences in the pressure gradient are not significant.



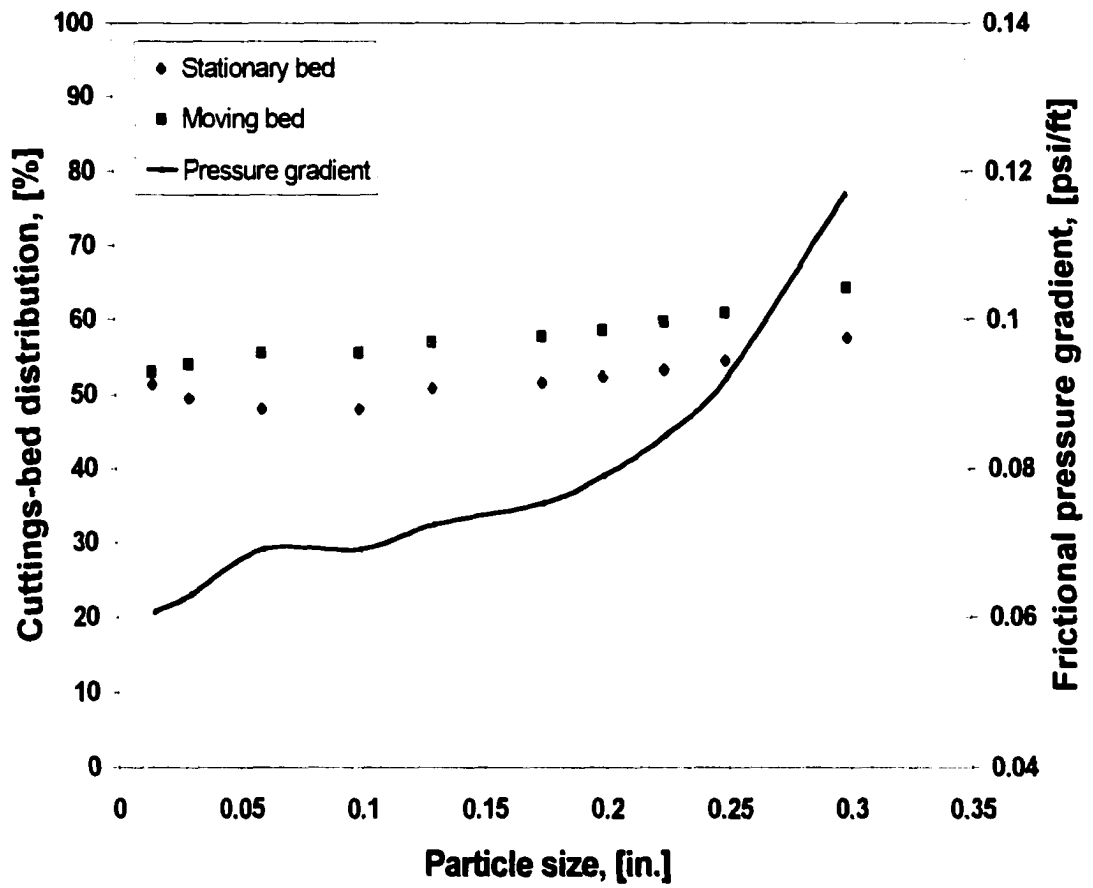


Fig. 4.23 – Effects of particle size on cuttings transport efficiency in horizontal well (base case,  $U_a = 3$  ft/s)

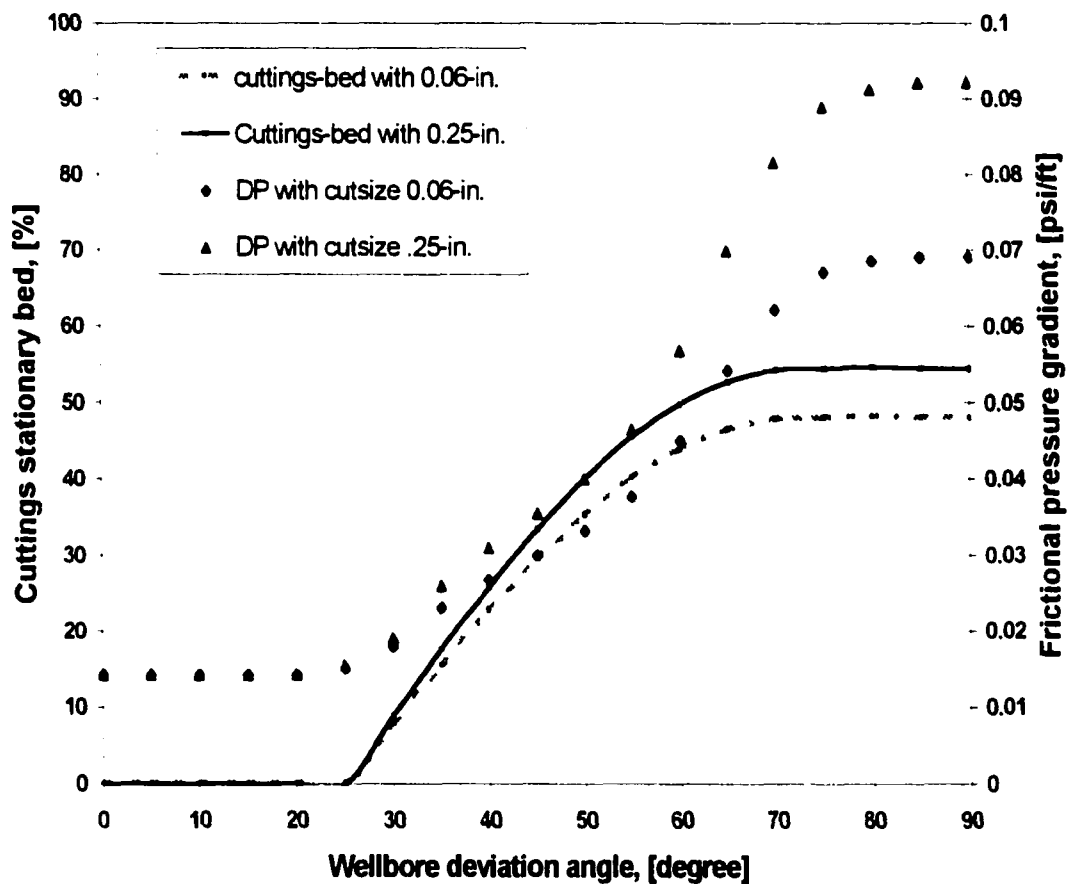


Fig. 4.24 – Effects of particle size on cuttings-bed distribution and pressure gradient (base case,  $U_a = 3$  ft/s)

Walker and Li<sup>79</sup> experimental study showed a similar trend concerning the particle size (0.006 – 0.276-in.: 0.15 – 7 mm) effect on cuttings transport. This experiment result showed that larger particle requires high fluid velocity (5 – 5.5 ft/s) to avoid cuttings (0.04 – 0.276-in.) accumulation in annulus with a viscous fluid (20lb<sub>m</sub>/Mgal Xanthan fluid). However, UTDRP<sup>6,21</sup> reached a different conclusion from that of Walker and Li.<sup>79</sup> UTDRP observed that smaller cuttings are slightly harder to transport. Particles with average diameter from 0.08-in. to 0.28-in. (2 – 7 mm) were used for their study.

## 4.6 Summary

The developed three-segment hydraulic model properly interrelates nominal annular velocity, wellbore deviation, cuttings concentration, and fluid rheology for cuttings transport in wellbore during while coiled tubing drilling. The following conclusions were reached directly from the various simulations and the comparison of the results with the published experimental data:

- (1) A mathematical three-segment model has been formulated to predict and interpret cuttings transport in a deviated wellbore from the horizontal section to the vertical section during coiled tubing drilling. These model predictions, based on the simulation, are in good agreement with the experimental data published by others.
- (2) There are significant effects on cuttings transport when the wellbore is at various deviated angles. The height of a stationary bed in a horizontal segment is almost constant or slightly increases with a decreasing wellbore deviation within this

segment. The cuttings bed abruptly decreases with a decrease in wellbore deviation angle in a transit segment. This cuttings bed is almost non-existent at the wellbore deviation around 25 – 30°. No cuttings-bed is found at the wellbore deviation between 0° and 25°.

- (3) There is a need for optimization between prevention of cuttings-bed accumulation, pressure gradient, and rheology of the fluid to obtain an optimum hole cleaning in the transit segment. Adjustment of one parameter affecting the cuttings transport will not promote an efficient cuttings transport. The simulation results are useful for estimating the total pressure gradient during a coiled tubing drilling job because the coiled tubing consists of a vertical section, a deviated section, and a horizontal section.
- (4) The most dominant parameters affecting cuttings transport while drilling a deviated well with coiled tubing drilling are nominal annular velocity and the carrier fluid's rheology. However, cuttings transport efficiency is also affected by in-situ drilling variables, which may be difficult to control by drilling engineers. These involve coiled tubing location in annulus, cuttings density, and cuttings size. Therefore, the effects of in-situ drilling conditions on cuttings transport should be carefully evaluated before designing a drilling program. The simulation program developed in this study allows drilling engineers to simulate all possible in-situ drilling variables, resulting in the proper design of drilling programs and selection of fluid systems.
- (5) Effects of fluid density have a significant role in cuttings transport. On the other hand, the cuttings size is less significant within the range of general cuttings size

distribution (0.09 – 0.19-in.). An increase in cuttings size up to 0.30-in. in diameter significantly decreases cuttings transport efficiency.

- (6) A highly viscous fluid slightly increases cuttings carrying capacity in horizontal and transit segments under a turbulent flow regime, as well as the pressure gradient, under the same nominal annular velocity. Again, there is a need for optimization between prevention of cuttings-bed accumulation, allowable pressure gradient, cost, and readily available drilling fluids in order to achieve optimum hole cleaning.

## CHAPTER FIVE

### CUTTINGS-BED CHARACTERIZATION

#### 5.1 Introduction

In an attempt to avoid problems of cuttings accumulation in the annulus, drilling operations often include such practices as *washing and reaming*.<sup>1</sup> Other operations, such as *wiper trips*, are often performed to attempt to control the amount of cuttings accumulated in the wellbore.

A detailed review of the published experimental data reveals that the cuttings transport characteristics are changed with a change in the wellbore deviation. Researchers<sup>27-29</sup> noted that the cuttings-bed in annuli is unstable under a certain range of wellbore deviation. The most unstable and difficult region for cuttings transport in a deviated well is reported as 30 to 60° from a vertical position.<sup>30-32</sup> In addition, the cuttings-bed is unstable and sometimes it slides down toward the bottom hole or moves up in the same direction as the drilling fluid flow.<sup>10-12</sup>

The objective of this chapter was to develop a mathematical model to predict and interpret a cuttings-bed movement, and to examine the effect of fluid flow through the

cuttings-bed. In order to examine the effect of fluid flow through the cuttings porous matrix, the bed layer was considered in the present work as a modified porous medium, where the velocities of the cuttings and the fluid in the bed are no longer identical. The concept of minimum anti-sliding velocity of cuttings-bed (MASV) was developed based on the inter-relationship between the parameters, which involve fluid rheology, wellbore deviation, interfacial friction between the suspension layer and the cuttings-bed, and in-situ fluid velocity in the suspension layer.<sup>87</sup>

This chapter presents the development process of a mathematical model to predict a cuttings-bed movement and estimate the frictional pressure drop, due to drilling fluid flow through a cuttings-bed in a transit segment. The effects of the related drilling parameters, which affect a cuttings-bed characterization: cuttings bed distribution, movement with its direction, transport efficiency, and pressure gradient are also described.

## **5.2 Model Description**

There are several forces acting on particles in cuttings transport. These involve the lift force, drag force, gravitational force, and the frictional force. Both the drag and the lift forces are exerted by the flow of drilling fluid around the particle. The lift force tends to lift up the cuttings to join the main stream of the flow where they move. This force arises either due to the asymmetric distribution of the fluid viscosity surrounding the cuttings and/or to the turbulent eddies in the annular flow<sup>81</sup>.

In a transit segment, the coiled tubing is assumed to lie at the bottom of the

wellbore, as shown in Fig. 4.1. Therefore, a full-eccentric annulus of the wellbore was considered intuitively for the transit segment. A cuttings-bed may be formed in the lower side of the annulus in this segment. The tendency to form a bed is reduced as the angle to the vertical is reduced, but there is a possibility that the bed will slide downward against the direction of the fluid flow<sup>12</sup>. There are many reported observations of the bed sliding downward at 45 to 60° from the vertical position.<sup>9,10,16</sup>

The cuttings-bed itself is a porous matrix, which allows drilling fluid to flow through the pores. Effects of drilling fluid flow in cuttings-bed must be evaluated in order to analyze the cuttings transport efficiency and fluid hydraulic associated with the cuttings-bed movement. The main assumption underlying the existing analysis is that there is no slip between the cuttings and the drilling fluid. This assumption may seem quite unrealistic, especially regarding the bed layer. The cuttings-bed is a porous medium, where the velocities of the solids are no longer identical with the fluid. However, the existing models, which can handle cuttings transport in a highly deviated to a horizontal well, do not consider these characteristics for this region of intermediate wellbore deviation.

Therefore, a mathematical model was developed to characterize a cuttings-bed in this region (transit segment) based on analysis of stress and forces involved in cuttings transport with the use of applicable basic physical principles. This mathematical model specifically covers a cuttings-bed velocity with its direction and MASV. Effect of drilling fluid flow in a cuttings-bed on frictional loss is also included in this model.



## 5.3 Model Development

A mathematical model was developed based on the fact that the cuttings-drilling fluid suspension flows at flow rates such that there exists a cuttings-bed and a dispersed suspension layer in the annulus.

### 5.3.1 Continuity Equations

#### 5.3.1.1 For Solid phase

By assuming there is no slip between the solid and fluid phase in the cuttings-bed, the steady-state continuity equation for the solid particles can be written as:

$$\frac{\partial}{\partial Y} (\rho_{sd} A_{sd} C_{sd} U_{sd} + \rho_b A_b C_b U_b) = 0 \quad (5.1)$$

Here, the subscripts "sd", and "b" refer to the dispersed suspension layer and the cuttings-bed, respectively. The density of each layer at a certain point between 1 and 2 in the flow system in Fig. 4.1 can be considered constant. As shown in Chapter 4, Eq. 5.1 can be integrated to obtain:

$$A_{sd} C_{sd} U_{sd} + A_b C_b U_b = A_a C_i U_a \quad (4.7)$$

The relevant relation of each area is described as:

$$A_{sd} + A_b = A_a \quad (4.9)$$

#### 5.3.1.2 For liquid phase

The material balance for the liquid phase is written as:

$$A_{sd} (1 - C_{sd}) U_{sd} + A_b (1 - C_b) U_b = A_a (1 - C_i) U_a \quad (4.8)$$

If the bed is stationary or moving relatively slowly, as explained by Walton,<sup>12</sup> the terms involving  $U_b$  can then be assumed as relatively small or negligible. Equations 4.7 and 4.8 can be simplified as:

$$A_{sd}C_{sd}U_{sp} = A_aC_tU_a \quad (5.2)$$

$$A_{sd}(1 - C_{sd})U_{sl} = A_a(1 - C_t)U_a \quad (5.3)$$

The mean velocity of a suspension layer,  $U_{sm}$ , is then calculated:

$$U_{sm} = C_{sd}U_{sp} + (1 - C_{sd})U_{sl} \quad (5.4)$$

where,  $U_{sp}$  and  $U_{sl}$  are velocities of the particle and liquid in the suspension layer, respectively. Multiplying both sides by  $A_{sd}$  and combining Eqs. 5.2 and 5.3, Eq. 5.4 becomes:

$$A_{sd}U_{sm} = A_aC_tU_a + A_a(1 - C_t)U_a = A_aU_a \quad (5.5)$$

Rearranging Eq. 5.5 gives:

$$A_{sd} = \frac{U_a}{U_{sm}} A_a \quad (5.6)$$

By combining Eqs. 5.2 and 5.6 gives:

$$U_{sm} = \frac{C_{sd}}{C_t} U_{sp} \quad (5.7)$$

If there is no slip between the suspended cuttings particles and the fluid in the suspension layer, the mean velocity of the suspension layer is the same as the in-situ fluid velocity under steady-state flow condition. Thus  $U_{sm} = U_{sp}$  or  $U_{sm} = U_{sl}$ .

### 5.3.2 Momentum Equations

The upper dispersed suspension layer consists of a relatively clean carrier fluid and heterogeneously suspended solids depending on the flow conditions. Under the steady-state flow condition, the sum of the stresses and the forces acting on the fluid flow zone should be:

$$A_{sd} \left( \frac{\Delta P}{L} \right) = \tau_{sd} S_{sd} + \tau_{sdb} S_{sdb} + F_{sdG}; \quad (4.1)$$

where,  $F_{sdG}$  is the gravitational force acting on the mixture in the dispersed suspension layer, which is the only component affected by the wellbore deviation angle.

$$F_{sdG} = \rho_{sd} g A_{sd} \cos \theta \quad (4.2)$$

where,  $\rho_{sd}$  is the effective density of the dispersed suspension layer.

Summing up all of the forces acting on the cuttings-bed gives (Fig. 4.1):

$$A_b \frac{\Delta P}{L} = \tau_b S_b - \tau_{sdb} S_{sdb} + \frac{F_b}{L} + F_{bG}; \quad (4.13)$$

where,  $F_{bG}$  is the gravitational force acting on the particles and was defined as:

$$F_{bG} = \rho_b g A_b \cos \theta \quad (4.14)$$

The shear stresses both at the pipe circumference and the interface between the upper layer and the cuttings-bed are given by:

$$\tau_{sd} = \frac{1}{2} \rho_{sd} U_{sm}^2 f_{sd(N_{Re f})} \quad (3.10)$$

$$\tau_b = \frac{1}{2} \rho_b |U_b| |U_b| f_b \quad (4.18)$$

$$\tau_{sdb} = \frac{1}{2} \rho_{sdb} (U_{sm} - U_b)^2 f_{sdb(N_{Re f})} \quad (4.19)$$

where,  $f_{sd}$  and  $f_{sdb}$  are the friction factors that can be estimated based on the hydraulic diameters. The average friction coefficient ( $f_b$ ) for steel on rock cuttings in water base muds were measured by Quigley.<sup>88</sup> He suggested that the friction factor between the borehole and the cuttings be less than 0.2. Martins et al.<sup>22</sup> also suggested that the friction factor,  $f_b$ , be 0.15, which is used in this study. The following correlations for the friction factors of the dispersed layer and the interface are used in this study:

$$f_{sd} = 0.00454 + 0.645 N_{Re'f}^{-0.7} \quad (\text{Doron et al.}^{23}) \quad (3.13)$$

$$\frac{1}{\sqrt{2f_{sdb}}} = -0.86 \ln \left[ \frac{\frac{d_p}{D_{sd}} + 2.51}{3.7 N_{Re'f} \sqrt{2f_{sdb}}} \right] \quad (\text{Televantos et al.}^{89}) \quad (5.8)$$

For both  $f_{sd}$  and  $f_{sdb}$ , Reynolds number of the suspension layer was used. The hydraulic diameter, given by the following equation, was used in the calculation of Reynolds number.

$$D_{sd} = \frac{4A_{sd}}{S_{sd} + S_{sdb}} \quad (5.9)$$

### 5.3.3 Suspension of Drilled Cuttings

The mechanism, which governs the dispersed suspension of the solid particles in the upper layer, is represented by the diffusion equation specified in Eq. 2.40:

$$\varepsilon_p \frac{d^2C}{dy^2} + V_h \frac{dC}{dy} = 0 \quad (2.40)$$

where,  $C$  is the local volume concentration (fraction) of the particle,  $y$  is the vertical

coordinate (perpendicular to the pipe axis),  $\varepsilon_p$  is the diffusion coefficient, and  $V_h$  is the hindered settling velocity.

The boundary condition,  $C_{sd} = C_b$  at the interface between the cuttings-bed and the flowing suspension layer is utilized in the solution of Eq. 2.40. Integration of the diffusion equation gives the following concentration profile in the upper layer,<sup>25</sup> which is the same for the transit segment:

$$C(y) = C_b \exp \left[ \frac{-V_h}{\varepsilon_p} (y - y_b) \right] \quad (4.22)$$

The particle diffusivity,  $\varepsilon_p$ , depends on the physical properties of the particle and the fluid, concentration of particles in the suspension, and the in-situ velocity of the suspension,  $U_{sd}$ .

### 5.3.4 Minimum Anti-Sliding Velocity

By combining Eqs. 4.15 and 4.16,  $F_b$  can be obtained as:

$$F_b = \left[ \frac{-\tau_b S_b + \tau_{sdb} S_{sdb} - \rho_b g A_b \cos \theta - \frac{A_b}{A_{sd}} (\tau_{sd} S_{sd} + \tau_{sdb} S_{sdb} + \rho_{sd} g A_{sd} \cos \theta)}{A_{sd}} \right] L \quad (4.17)$$

The force,  $F_b$ , can be considered as the force acting on the cuttings-bed, exerted by the gravity, fluid stress, and the fluid pressure gradient.

The hydrodynamic friction force,  $F_{hf}$ , acting between a cuttings-bed and borehole wall, is composed of two components: a dry friction force,  $F_{df}$ , which is exerted by bed particles on the contact surface between a cuttings-bed and a borehole wall, and a interfacial friction force,  $F_{\phi}$ , which stems from the bed movement.<sup>12</sup>

$$F_{hf} = F_{df} + F_{\phi} \quad (5.10)$$

The dry friction force is determined by multiplying the dry friction coefficient and the sum of the normal force exerted by the bed particles,<sup>75</sup> as shown in Eq. 5.11.

$$F_{df} = \eta(\rho_s - \rho_L)g \cos\theta C_b A_b L \quad (5.11)$$

An interfacial friction force,  $F_{\phi}$ , is due to a transmission of stress from the interface through the bed particles. Bagnold<sup>90</sup> showed that when a fluid flows over a deposit of solid particles, there exists a normal stress at the interface, which is associated with the shear stress exerted by the fluid on the bed.<sup>75</sup> The relationship is as follows:

$$F_{\phi} = \eta \frac{\tau_{sib} S_{sib}}{\tan \phi} L \quad (5.12)$$

where,  $\eta$  is the slip coefficient for given solids, and  $\phi$  is the angle of internal friction. The value of  $\tan\phi$ , which is between 0.35 and 0.75, depending on the type of flow and particle characteristics.<sup>75</sup> The values of  $\eta = 0.15$  and  $\tan\phi = 0.6$  were used in this study as recommended by Martins et al.<sup>22</sup>. These experimental coefficients are based on the interaction between cuttings-bed and casing. The effects of wellbore roughness and resulting slip coefficient, as the applicable conditions, are required in the estimation of MASV for each case.

A cuttings-bed frequently slides down in the transit segment. The movement of a cuttings-bed movement toward the bottomhole increases cuttings accumulation in the borehole. In addition, a cuttings-bed will abruptly slide down when carrier fluid is ceased in this segment resulting in a wellbore pack off and a stuck pipe.

Minimum anti-sliding velocity (MASV) is the fluid velocity to keep a cuttings-bed stationary. MASV can serve as an operational guideline to avoid the sliding down of a cuttings-bed. When  $F_b$  is exactly equal in magnitude to the hydrodynamic friction force,

$F_{hf}$ , the cuttings-bed is stationary. The suspension fluid velocity is MASV, which occurs when forces are equal ( $F_b = F_{hf}$ ) and cuttings-bed is stationary according to the definition of MASV. The MASV is determined by solving Eqs. 4.17, 4.18, 4.19, 5.10. If  $F_{hf}$  is larger than  $F_b$ , the cuttings-bed will slide down. The cuttings-bed slides upward in the reverse case.

### 5.3.5 Cuttings-Bed Movement

The force ( $F_b$ ), defined in Eq. 4.17, acting on a cuttings-bed is a function of shear stress between the borehole wall and the cuttings-bed. The shear stress defined in Eq. 4.17 is also a function of a cuttings-bed velocity. The iteration method was used to solve Eqs. 4.17, 4.18, 4.19, and 5.10 for the cuttings-bed velocity. The calculation procedures are shown in Appendix F.

The net force,  $F$ , acting on a cuttings-bed is defined as:

$$F = F_b - F_{hf} \quad (5.13)$$

The magnitude of the force  $F$  may be arbitrarily expressed as the product of a characteristic area  $A$ , a characteristic kinetic energy per unit area  $k_t$ , and a dimensionless quantify  $f$  known as the friction factor<sup>91</sup>:

$$F = Ak_t f \quad (5.14)$$

For flow around submerged objects, the characteristic area,  $A$ , is usually taken to be the area obtained by projecting the solid onto a plane perpendicular to the velocity of approach of the fluid, and  $k_t$  is taken to be  $\frac{1}{2} \rho_s v_t^2$ . For example, force  $F$  can be defined for flow around spheres of radius  $r$  as:

$$F = (2\pi r L) \left( \frac{1}{2} \rho_s v_t^2 \right) f \quad (5.15)$$

In deriving the cuttings-bed movement, the area  $A$  and kinetic energy  $k_t$  can be defined as:

$$A = S_b \times L \quad (5.16)$$

$$k_t = \frac{1}{2} [C_b \rho_s + (1 - C_b) \rho_L] v_t^2 \quad (5.17)$$

Friction coefficient is defined based on flow regime.<sup>91</sup> For the Stoke's region:

$$f = \frac{24}{N_{Re\ p}} \quad (5.18)$$

For intermediate region:

$$f = \frac{18.5}{N_{Re\ p}^{3/5}} \quad (5.19)$$

Since the components of the net force ( $F$ ) vary as the wellbore deviation and cuttings-bed distribution are changing, the net force is a function of wellbore deviation. If  $F$  is positive, the cuttings-bed slowly moves up. The gravity acceleration is acting on the cuttings weight with the wellbore deviation angle. Re-arranging Eqs. 5.15 to 5.19 and solving for terminal velocity is:

$$v_t = \left[ \frac{2F}{S_b L \{C_b \rho_b + (1 - C_b) \rho_L\} f} \right] \quad (5.20)$$

The velocity obtained from Eq. 5.20 was used in the calculation of  $F_b$  in Eq. 4.17. Iteration calculations were performed until the value of previous and present iteration ( $F_{bi} - F_{bi-1}$ ) reaches less than 0.0001, as shown in the flow chart (Appendix F). The cuttings-bed velocity  $v_t$  can be estimated by the value of  $F_{bi} - F_{hfi}$  based on  $v_{t,i}$ , where,  $i$  is



the iteration integer. If the absolute value of  $|F_{b_i} - F_{b_{i-1}}|$  is less than a specific value (0.0001), the calculated value can be regarded as the final cuttings-bed velocity.

### 5.3.6 Fluid Flow Through Cuttings-bed

The existence of relative velocity between a cuttings particle and the drilling fluid in the cuttings-bed generates additional frictional pressure loss. It is assumed that the commonly used expressions for the flow through porous media can be applied inside the bed layer. The porous matrix itself may be moving (moves slightly up or slides down) in this case. It is further assumed that the diameter of the packing is small compared to the area of a cuttings-bed.

The pressure drop for fluid flow through a porous media is commonly based on Darcy's law. In the case of packed beds of large spheres, the pressure drop is given by the Blake-Kozeny equation. It is defined as:

$$\frac{\Delta P}{L} = 150 \frac{\mu V_o}{d_p^2} \frac{C_b^2}{(1-C_b)^3} \quad (5.21)$$

This result is generally good for a void fraction less than 0.5, and is valid only in the laminar region.<sup>91</sup>

Burke-Plummer<sup>91</sup> proposed a pressure drop equation for the turbulent region. It is defined as:

$$\frac{\Delta P}{L} = 1.75 \frac{\rho_L V_o^2}{d_p} \frac{C_b}{(1-C_b)^3} \quad (5.22)$$

When the Blake-Kozeny equation and the Burke-Plummer equation are simply added together, the result is the Ergun equation.<sup>91</sup>

$$\frac{\Delta P}{L} = \frac{150\mu C_b^2 V_o}{d_p^2 (1-C_b)^3} + \frac{1.75\rho_L C_b V_o^2}{d_p (1-C_b)^3} \quad (5.23)$$

These equations consider Newtonian fluid only. However, the fluids generally used in the drilling industry are non-Newtonian.

Recently, Gibilaro et al.<sup>92</sup> proposed the following pressure drop correlation for high voids of fixed beds of spheres.

$$\frac{\Delta P}{L} = \left( \frac{17.3}{N_{Re f}} + 0.335 \right) \frac{\rho_L C_b V_o^2}{d_p (1-C_b)^{4.8}} \quad (5.24)$$

where,  $V_o$  is a relative fluid velocity in the cuttings-bed layer. Equation 5.24 was originally developed for a Newtonian fluid as a function of Reynolds number. Cho et al.<sup>93</sup> extended Eq. 5.24 to non-Newtonian fluid (Power-law model) with the generalized Reynolds numbers. The effects of slip between cuttings and fluid in the bed layer on relative velocity was proposed as a function of volumetric concentration of a cuttings-bed by Doron et al<sup>94</sup>:

$$V_o = (1 - C_b)(U_{mb} - U_b) \quad (5.25)$$

This relative velocity term was used in this study.

## 5.4 Model Simulation Results and Discussion

The simulations were performed for the various conditions including the base case described in Table 3.1. The effects of various parameters, such as the nominal annular velocity,  $U_a$ , wellbore deviation, and the cuttings-bed area on the cuttings-bed characterization, were simulated and investigated with the base case. Three different

fluids (base case, fluid A, and fluid B; shown in Table 4.2) were used to investigate the effect of fluid rheology on MASV. The following simulation results show the effects of the various parameters.

#### 5.4.1 Local Velocity Distribution

Local velocity is defined as the velocity of a heterogeneous suspension layer at the top of the annulus, which is affected by a cuttings-bed accumulation. On the other hand, the nominal annular velocity is the pumping velocity without the presence of a cuttings-bed. Cho et al.<sup>26</sup> demonstrated the effects of nominal annular velocity on a cuttings-bed distribution with different wellbore deviations. Figure 5.1 illustrates the local velocities with the different fraction of the cuttings-bed. A high cuttings-bed leads to a small flow path area. A high cuttings-bed shows a high local velocity.

#### 5.4.2 Forces Acting on a Cuttings-bed

Forces acting on a cuttings-bed as a function of local velocity are illustrated in Figs. 5.2 and 5.3. The hydrodynamic friction force acting on a cuttings-bed increases exponentially with an increase in local velocity. When the wellbore deviation is increased, the hydrodynamic force,  $F_{hf}$ , is also increased. Forces acting on the cuttings-bed, which are exerted by gravity, fluid velocity, fluid shear stress, and fluid pressure gradient, increases exponentially with an increase in local velocity. The force,  $F_h$ , is negative until the local velocity reaches about 6.5 ft/s, except when the wellbore deviation is 60°. This wellbore deviation, defined as near horizontal,<sup>26</sup> shows positive force at a low velocity profile. This feature may have some relationship with the MASV.

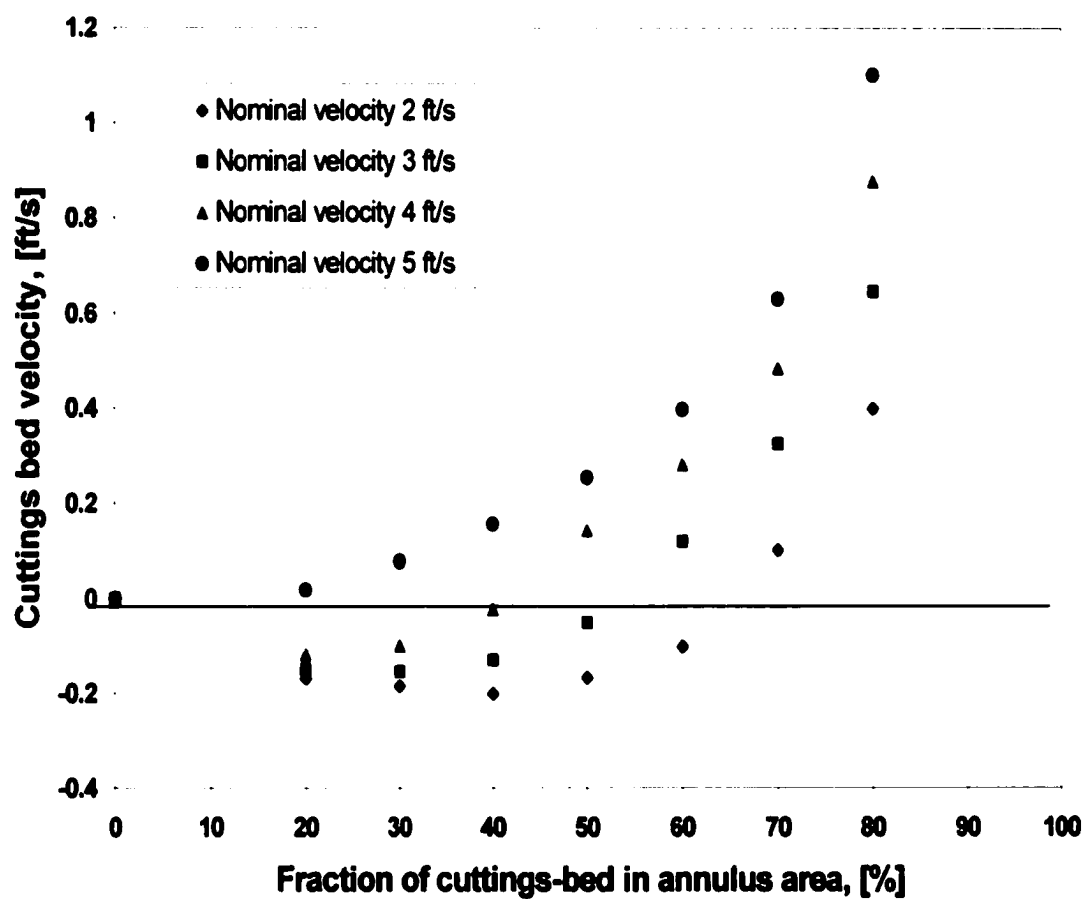


**Fig. 5.1 – Cuttings-bed velocity profile with its area fraction (base case)**

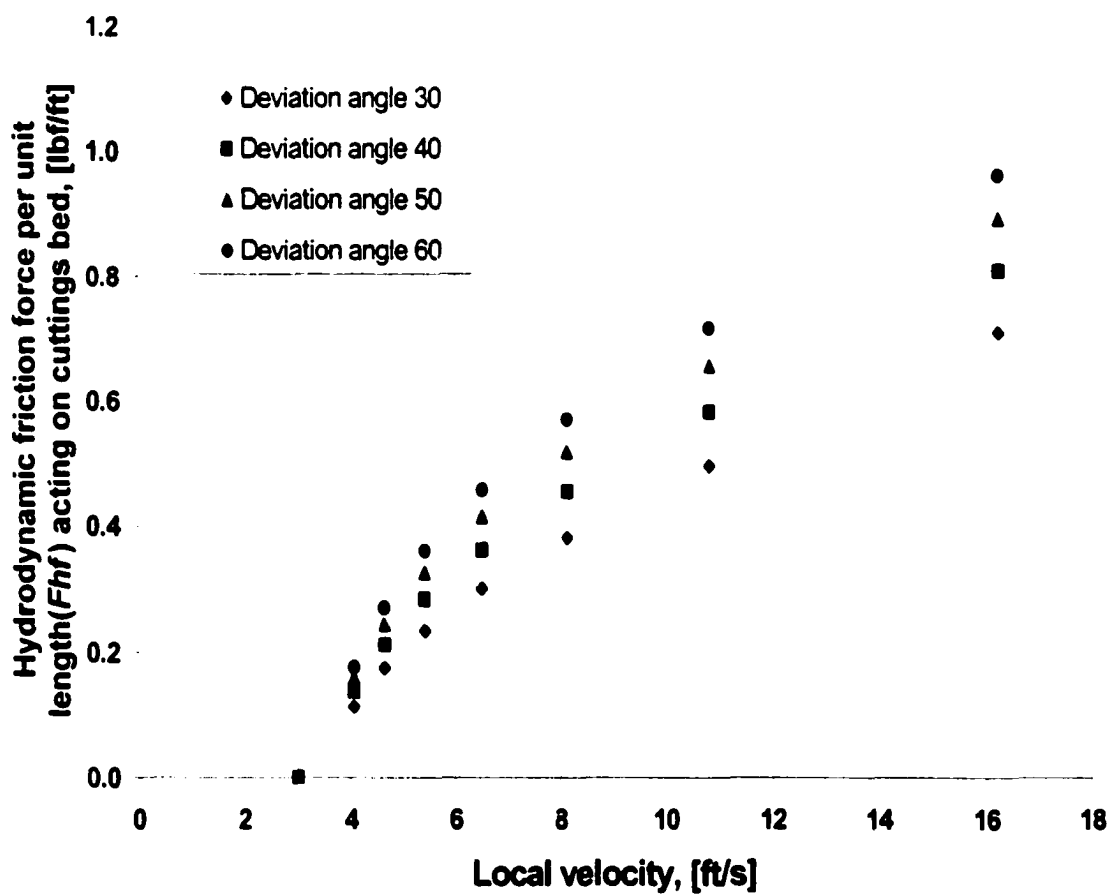
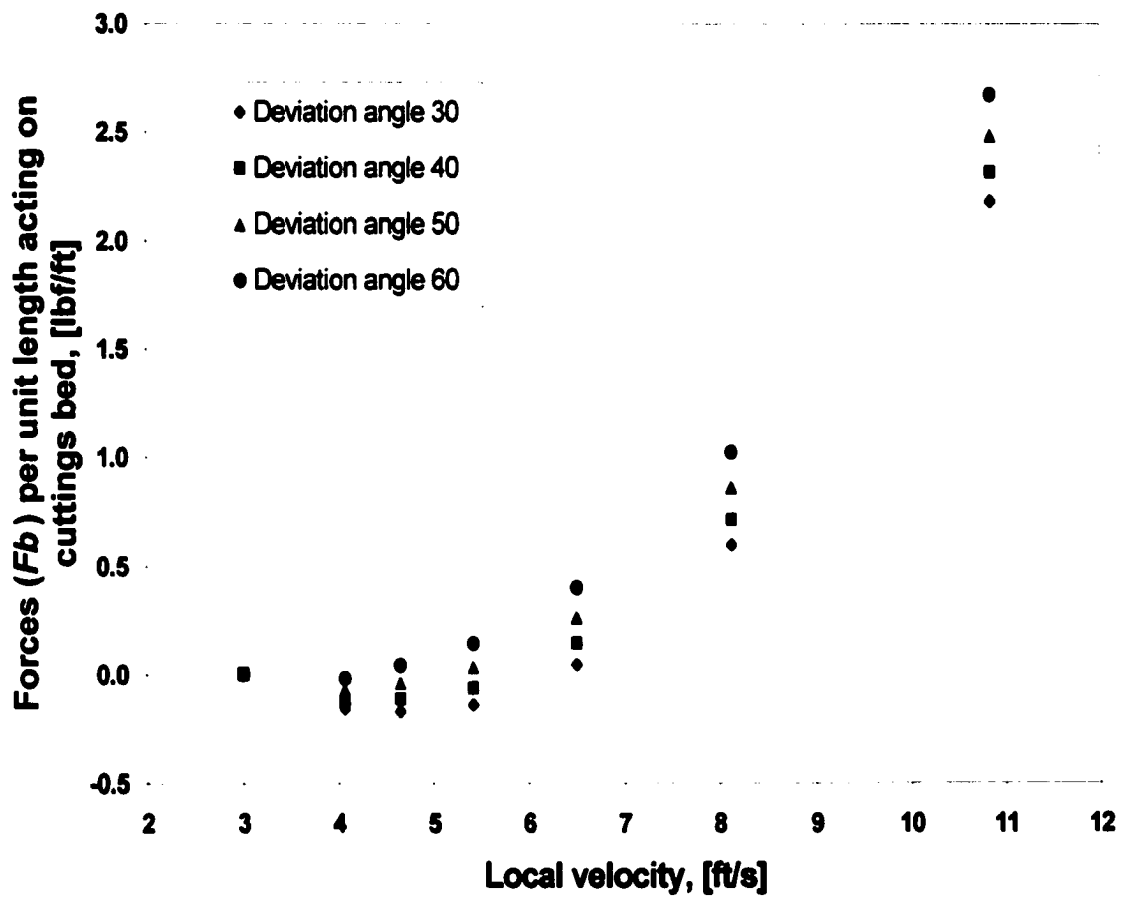


Fig. 5.2 – Hydrodynamic friction force per unit length acting on cuttings-bed (base case,  $U_a = 3$  ft/s)



**Fig 5.3 – Forces acting on cuttings-bed (base case,  $U_a = 3$  ft/s)**

Velocities below MASV show negative forces. This means that the gravity force, which tends to slide a bed downward, is bigger than the shearing force.

Figures 5.4 and 5.5 present two different forces discussed in the previous section of minimum anti-sliding velocity. The forces,  $F_b$ , acting on the cuttings-bed are higher than the hydrodynamic forces,  $F_{hj}$ , which are above 55 % of the cuttings-bed portion for a 3 ft/s the nominal annular velocity. This trend decreases up to 40 % of the cuttings-bed fraction, which is defined as the area occupied by a cuttings-bed divided by the annular section area, with an increase in nominal annular velocity of 4 ft/s

For nominal annular velocity of 3 ft/s, a cuttings-bed slowly slides down until it cuttings-bed reaches 55%, which may increase the local velocity. The increase in local velocity also increases the force ( $F_b$ ), acting on the cuttings-bed. The cuttings-bed will be stationary at the 55% cuttings-bed fraction. The local velocity of the suspension layer is MASV at this condition. For the nominal annular velocity of 4 ft/s, a cuttings-bed slowly slides down until it reaches 40 %. The cuttings-bed will then move up after 40% cuttings-bed fraction.

The MASV, as a function of the wellbore deviation with the different nominal annular velocity, is shown in Fig. 5.6. The MASV increases with an increase in the wellbore deviation until it reaches about 50°, then it decreases again. Generally, it can be said that a cuttings-bed in a horizontal segment is stable. Since sliding force in a horizontal segment is less than in a transit segment, the MASV in a horizontal segment is less than in a transit segment. The MASV decreases with a decrease in wellbore deviation angles because a cuttings-bed area also is decreasing as a wellbore deviation decreases.

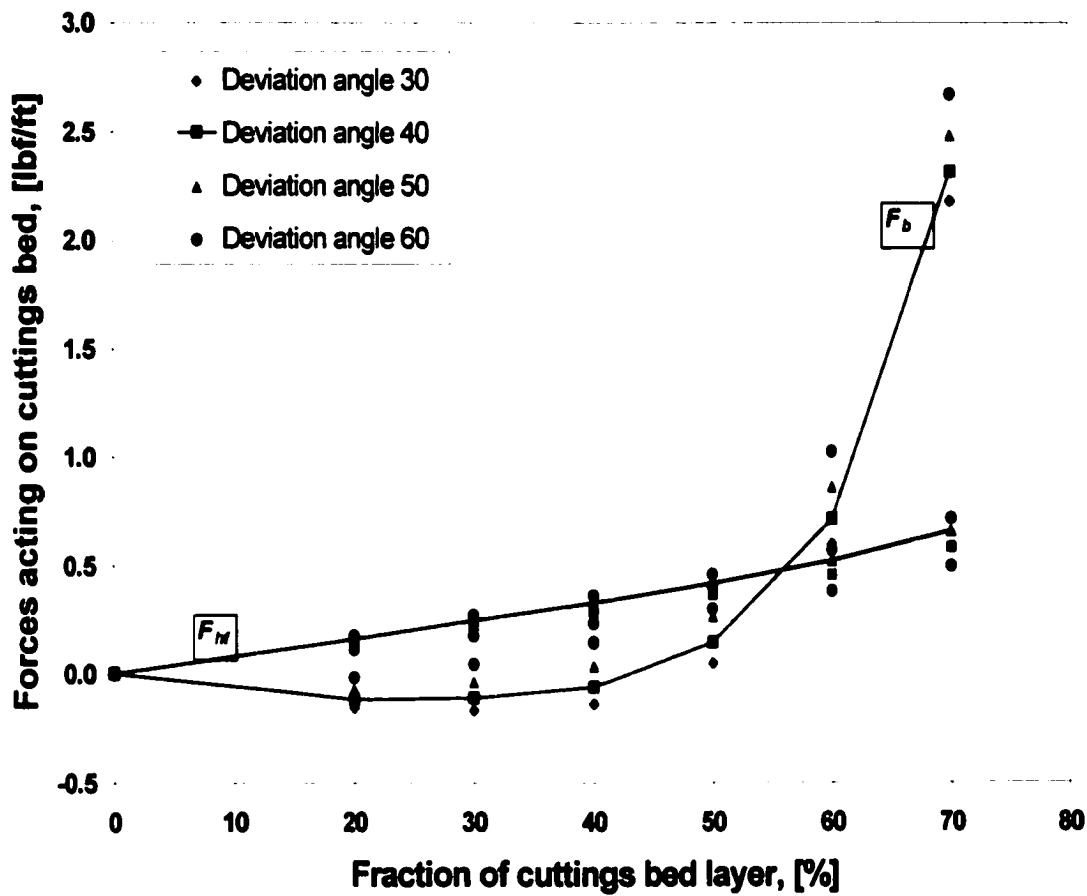


Fig. 5.4 – Comparison of  $F_b$  and  $F_M$  with nominal annular velocity of 3 ft/s (base case)



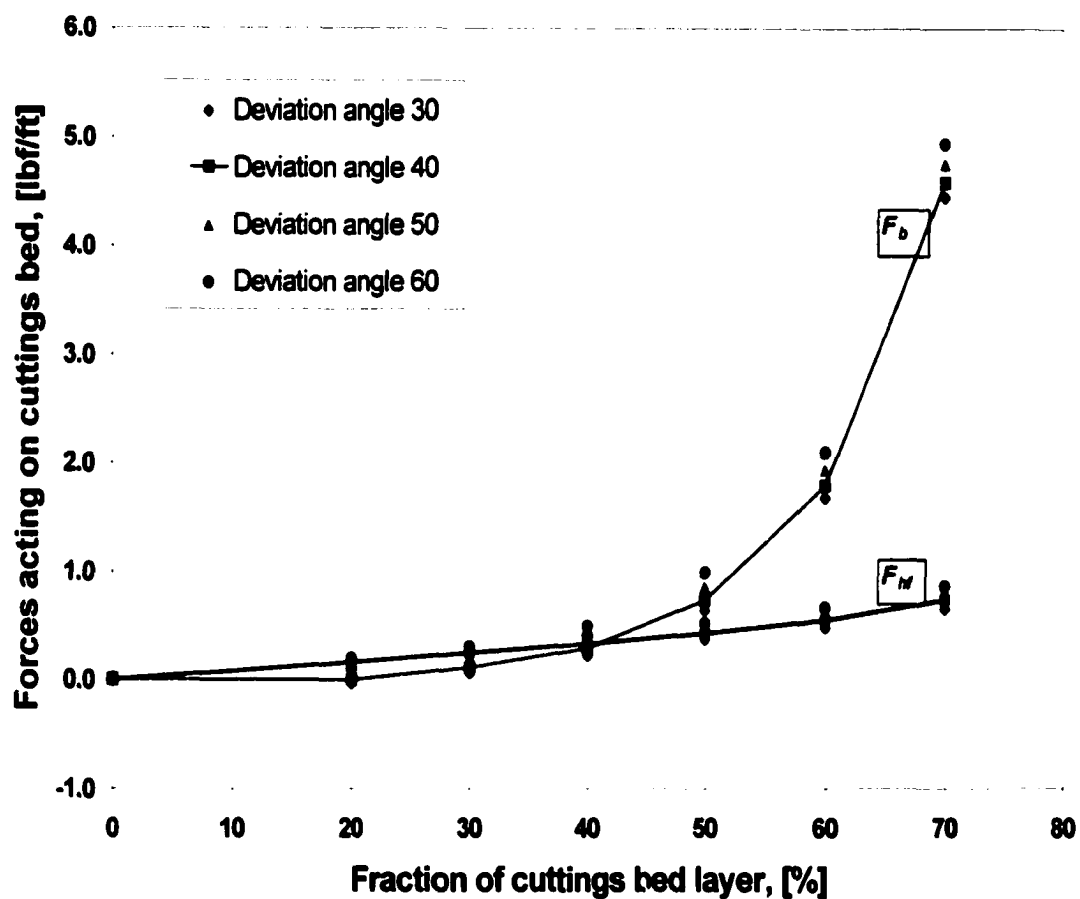
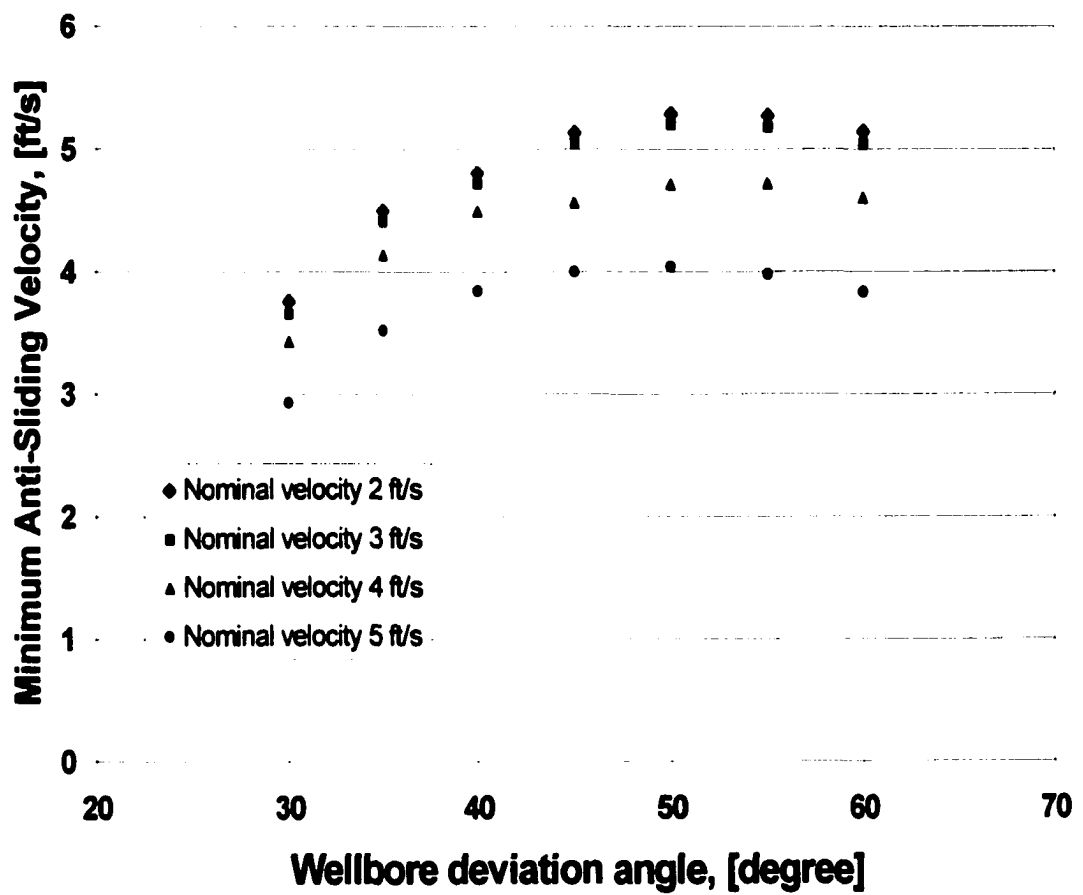


Fig. 5.5 – Comparison of  $F_b$  and  $F_M$  with nominal annular velocity of 4 ft/s (base case)



**Fig 5.6 – Minimum anti-sliding velocity with different nominal annular velocity (base case)**

The range of the MASV for the base case specified in Table 3.1 is 3 ft/s to 5.3 ft/s. It varies with the nominal annular velocities and the wellbore deviation angle. The MASV obtained by nominal annular velocity of both 2 ft/s and 3 ft/s are almost the same. This result may be related to the cuttings-bed area.

### 5.4.3 Rheology Effects

The effect of drilling fluid rheology with a changing wellbore deviation is simulated for different fluid systems (fluid A, fluid B, and base case). The details of the fluid systems used in the simulation were presented in Table 4.2. Figure 5.7 illustrates the effects of rheological characteristics of drilling fluid on MASV under the nominal annular velocity of 3 ft/s. Simulation results show that a decrease in the fluid behavior index slightly decreases MASV.

Figure 5.8 presents the effects of rheology characteristics on forces acting on the cuttings-bed with a different fraction of the cuttings-bed. The balance point between  $F_b$  and  $F_{hf}$  is slightly less than the case shown in Fig 5.4. The problem of a cuttings-bed sliding down is more severe in less viscous fluid. However, the other parameters such as pressure gradient and cuttings-bed distribution have to be considered for optimum combination of the parameters.<sup>12</sup>

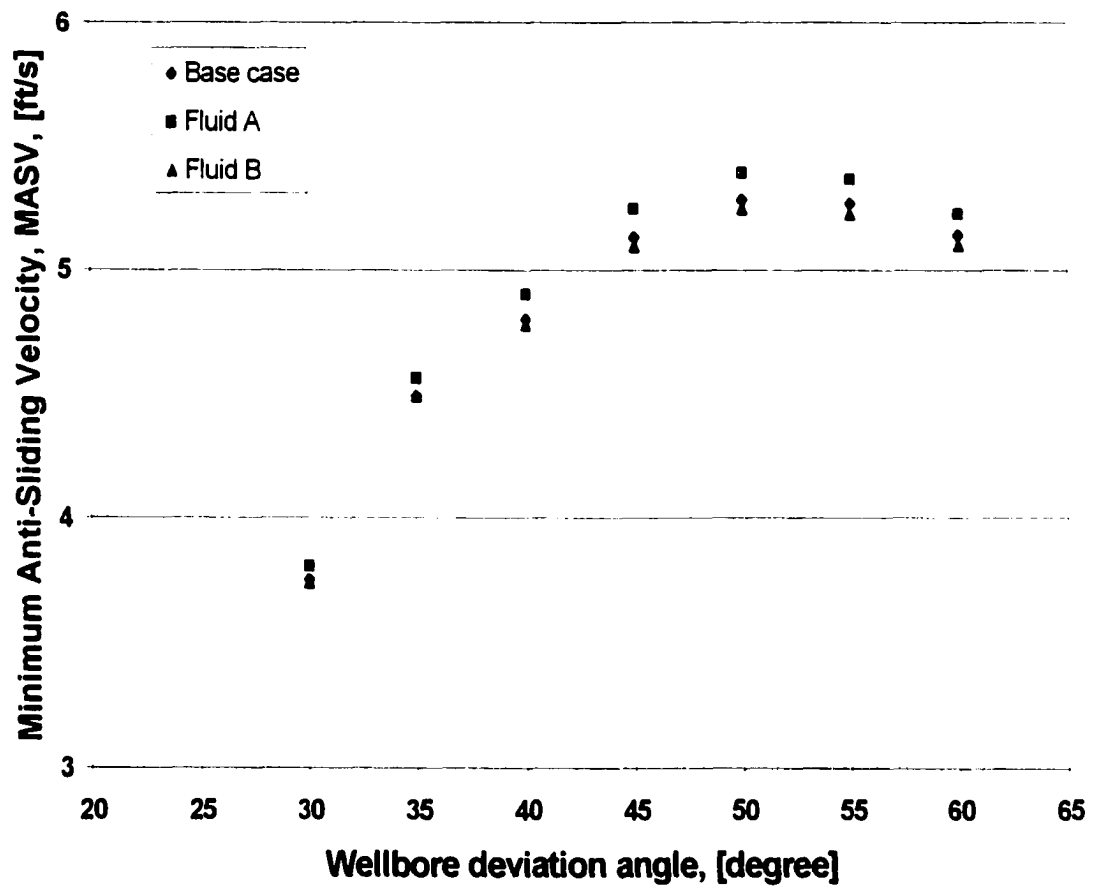


Fig 5.7 – Effect of rheology on minimum anti-sliding velocity ( $U_a = 3$  ft/s)

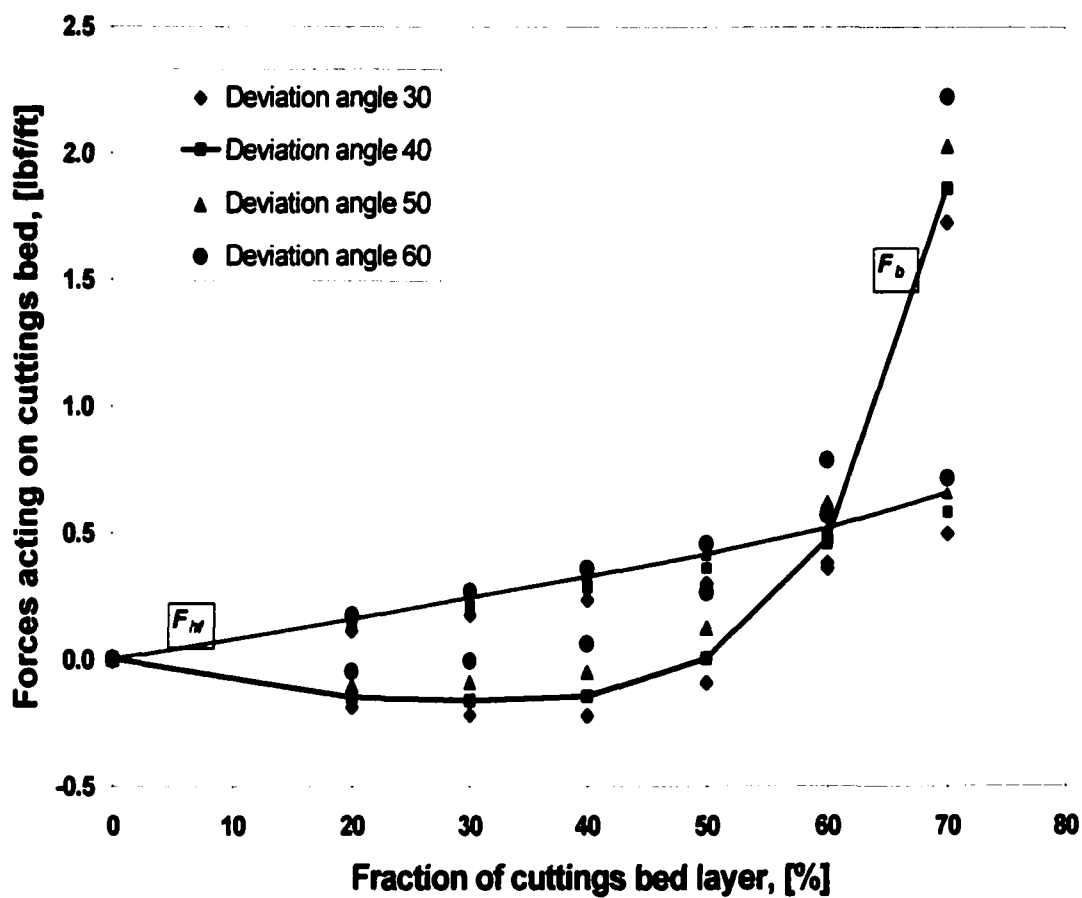
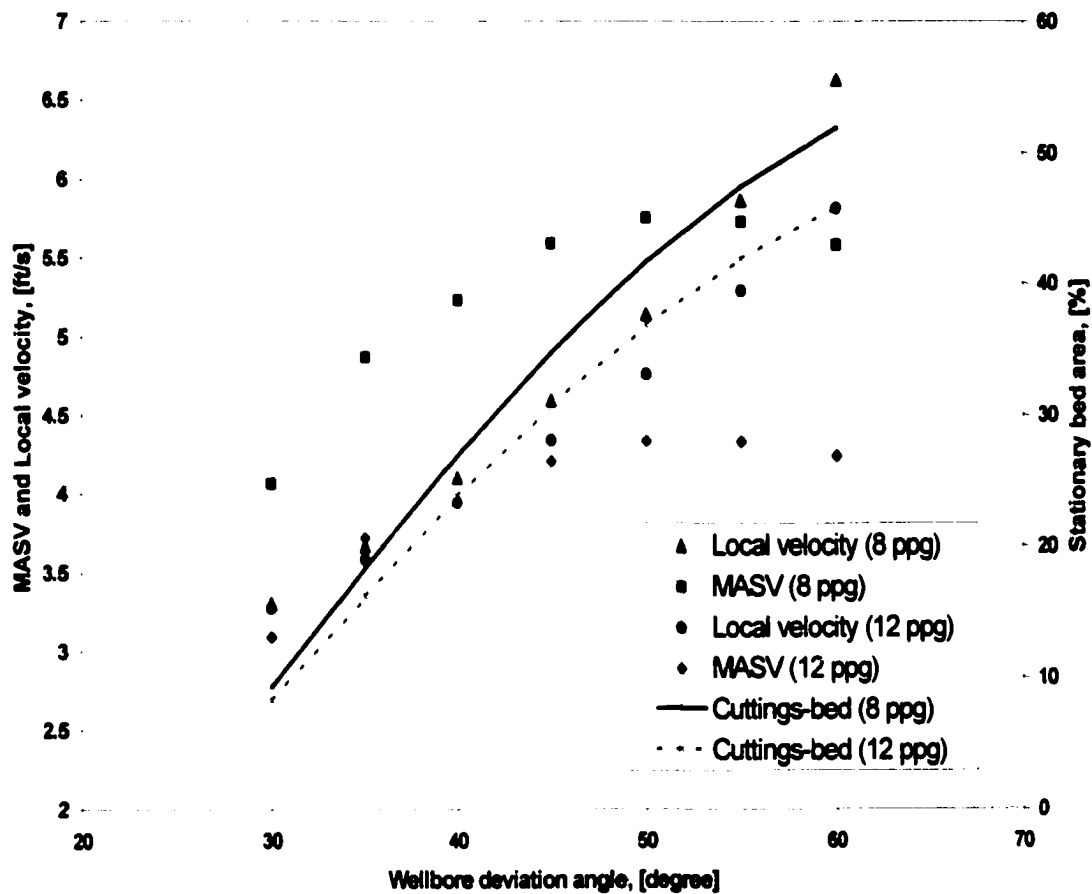


Fig. 5.8 – Comparison of  $F_b$  and  $F_{hf}$  with fluid A ( $U_a = 3$  ft/s)

Figure 5.9 illustrates the relationship between MASV and fluid density. The simulations were performed with the base case and nominal annular velocity of 3 ft/s. Local in-situ velocity in suspension layer increases with an increasing the cuttings stationary bed height. In addition, the higher-density fluid reduces particle settling velocity as well as gravity force (corrected by buoyancy force). From these simulation results, cuttings-bed with low fluid density (8 ppg) in deviated wellbore range between 30° and 55° may slide downward because the local fluid velocities in suspension layer are less than the MASV. However, increase in fluid density (12 ppg) decreases MASV as shown in Fig. 5.9. The cuttings-bed at the deviated wellbore 35 – 60° will slightly moves up at the same pump rate (157 gpm: corresponding to nominal annular velocity of 3 ft/s).

#### **5.4.4 Cuttings-Bed Movement**

The cuttings-bed velocities with different nominal annular velocities are illustrated in Fig. 5.10. A negative cuttings-bed velocity means the bed slides downward. A positive cuttings-bed velocity means the bed is slowly moving up. An increase in the cuttings-bed accumulation increases the local velocity. In addition, increased local velocity increases energy available for the cuttings-bed to move up. High nominal annular velocities show that a cuttings-bed moves up with the lower fraction of the cuttings-bed.



**Fig. 5.9 – Effects of fluid density on MASV (base case,  $U_a = 3$  ft/s)**

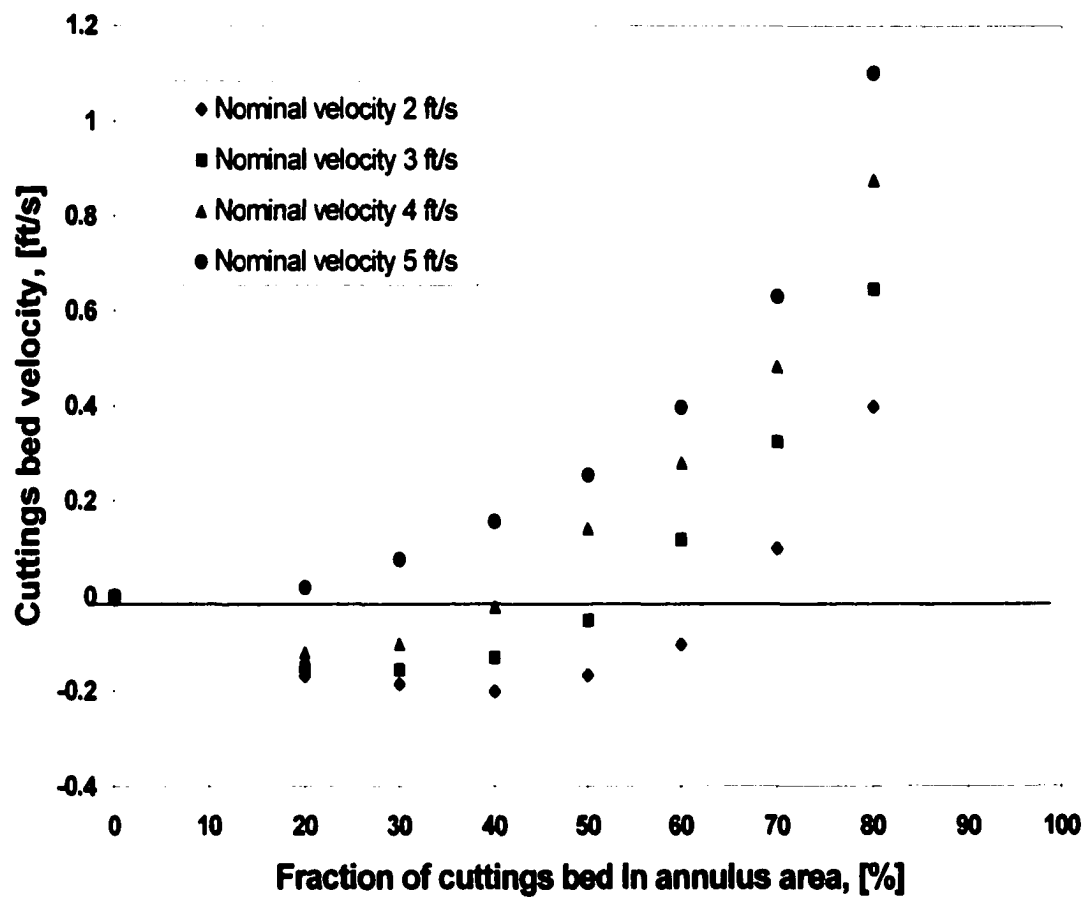


**Fig. 5.10 – Cuttings-bed velocity with different nominal annular velocity (base case)**



For a nominal annular velocity of 5 ft/s, the cuttings-bed reaches a stationary condition at 20% cuttings-bed fraction. The cuttings-bed begins to move up when MASV is increased with an increase in the cuttings-bed (reduction in the flow path area and increase in the local velocity). In contrast, a cuttings-bed reaches a stationary condition with a nominal annular velocity of 2 ft/s at 65% cuttings-bed fraction. The effects of a cuttings-bed movement on the pressure gradient with the base case are presented in Table 5.1. This effect is approximately a 0.5 % increase in the pressure gradient of the conventional method (without the effect of a cuttings-bed movement). A possible reason for this is that the cuttings-bed velocity is relatively small compared to the fluid velocity of a suspension layer.

**Table 5.1 – Effects of cuttings-bed movement on pressure gradient (base case)**

Angle (from vertical)	$U_t = 2$ ft/s		$U_t = 3$ ft/s		$U_t = 4$ ft/s	
	Convent	Bed Move	Convent	Bed Move	Convent	Bed Move
60	0.277	0.277	0.300	0.300	0.291	0.292
50	0.334	0.335	0.347	0.348	0.347	0.348
40	0.392	0.393	0.397	0.398	0.400	0.401
30	0.431	0.431	0.432	0.432	0.434	0.435

- Note: 1. Convent means conventional method without the effect of bed movement  
2. Bed move means new method with the effect of bed movement  
3. Gravity force effect is included in the pressure gradient (unit is psi/ft)

#### **5.4.5 Fluid Flow Through a Porous Cuttings Bed**

The effects of fluid flow in a porous cuttings-bed on frictional pressure drops with base case fluid are shown in Fig. 5.11. The pressure drops are calculated purely for the fluid flow in the porous cuttings-bed. Frictional pressure drop increases logarithmically with an increasing wellbore deviation. The cuttings-bed area also increases with an increase in wellbore deviation. An increased cuttings-bed area increases a fluid flow sectional area, which leads to increased frictional pressure drop. The increased nominal velocity increases local velocity as well as relative velocity in porous cuttings-bed, as defined by Eq. 5.31. A high nominal velocity increases the frictional pressure drop. This trend increases with an increasing wellbore deviation.

Figure 5.12 presents the comparison of frictional pressure drops, which are representing the sum of the conventional frictional drop (fluid flow through suspension layer, i.e. open flow path) and the frictional drop, due to fluid flow in the porous cuttings-bed. Table 5.2 shows the comparison of these frictional pressure losses. The frictional pressure drop increases 1 to 20%, due to the fluid flow in a porous cuttings-bed. Therefore, it is important to consider the effects of fluid flow in a porous cuttings-bed in drilling hydraulics.

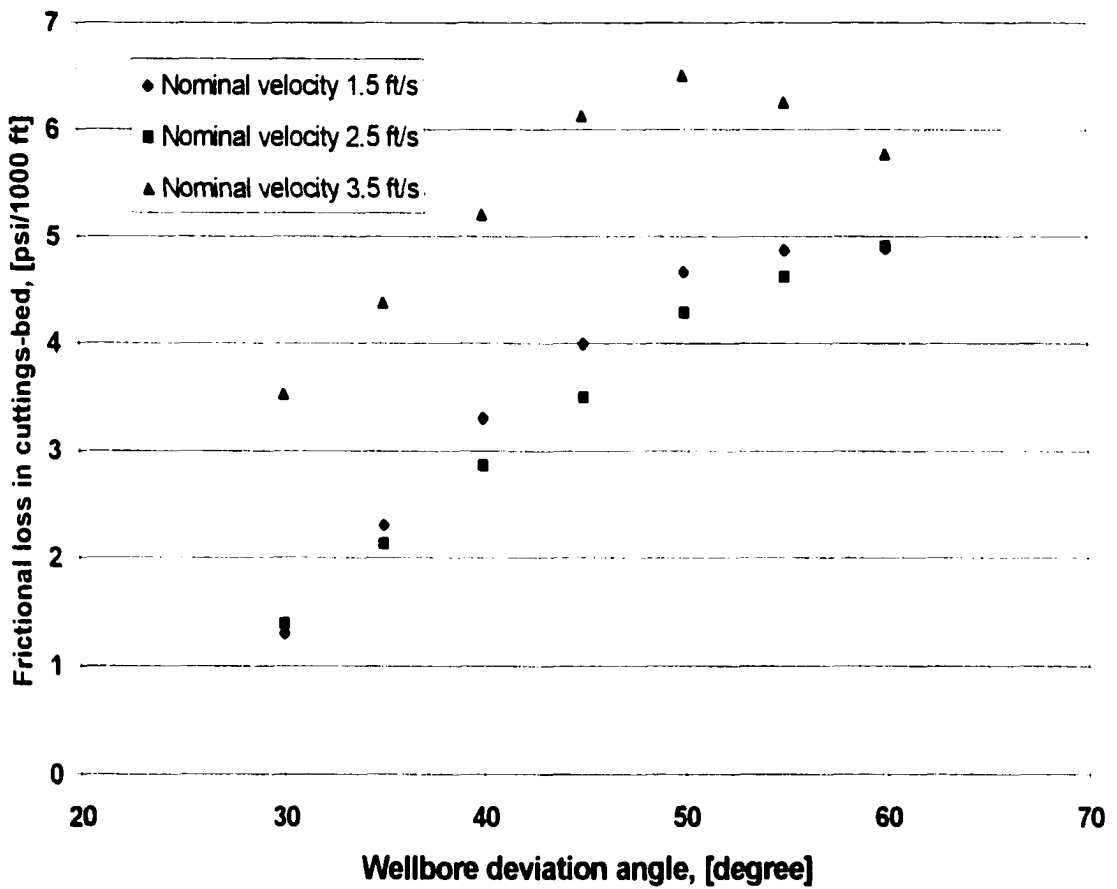


**Fig. 5.11 – Effects of fluid flow in a porous cuttings-bed on pressure loss (base case)**

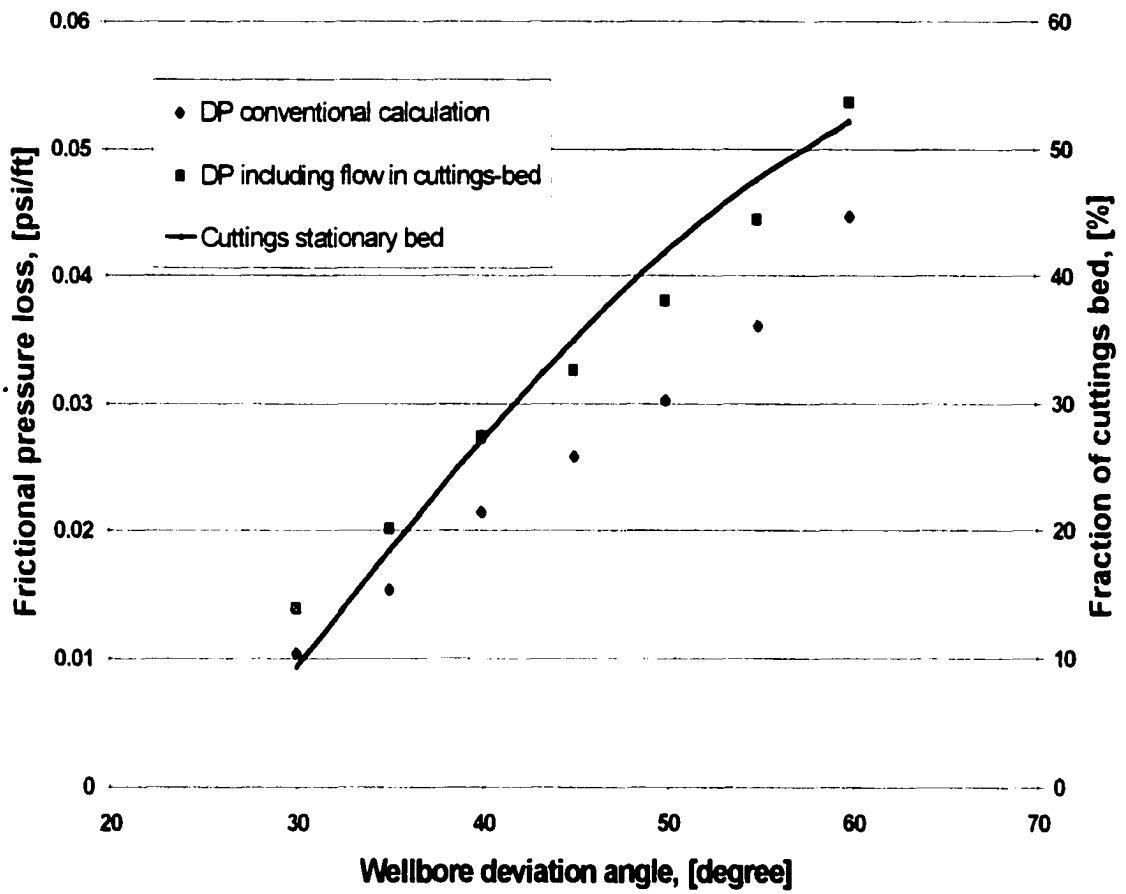


**Fig. 5.12 – Comparison of frictional pressure drop with and without the effects of fluid flow in a porous cuttings-bed (base case,  $U_a = 2.5$  ft/s)**

**Table 5.2 – Effects of fluid flow in the porous cuttings-bed on frictional pressure gradient (base case, without gravitational effect)**

Wellbore Deviation (angle)	$U_a = 2 \text{ ft/s}$			$U_a = 3 \text{ ft/s}$			$U_a = 4 \text{ ft/s}$		
	Conv	Bed flow	Diff (%)	Conv	Bed flow	Diff (%)	Conv	Bed flow	Diff (%)
30	0.013	0.015	9.8	0.019	0.021	7.3	0.022	0.026	15.7
35	0.017	0.019	13.5	0.025	0.027	8.5	0.028	0.032	15.6
40	0.019	0.022	17.3	0.031	0.034	9.2	0.035	0.040	15.0
45	0.021	0.025	18.7	0.036	0.039	9.9	0.038	0.044	16.1
50	0.023	0.028	20.0	0.041	0.045	10.5	0.041	0.048	15.7
55	0.027	0.032	18.2	0.047	0.051	9.9	0.045	0.051	14.0
60	0.033	0.037	15.1	0.057	0.062	8.6	0.048	0.053	12.2

Note: 1. Conv means conventional method without the effect of fluid flow in cuttings-bed  
2. Bed flow means new method with the effect of fluid flow in cuttings-bed  
3. Gravity force effect is excluded in the pressure gradient (unit is psi/ft)

Figure 5.13 shows the comparison of the frictional pressure loss of fluid flow in a porous cuttings-bed with different fluid systems specified in Table 4.2 under 3 ft/s nominal annular velocity. The pressure drop of the less viscous fluid (Fluid A) in a porous cuttings-bed shows almost the same pressure drop as the base case. A highly viscous fluid (Fluid B) shows a lower cuttings-bed area. However, the pressure drop increases abruptly with an increase in wellbore deviation. From a drilling hydraulics point of view, the more viscous fluid is not recommended as a drilling fluid media in a highly deviated wellbore. However, the selection of drilling fluid is a somewhat complicated matter, and involves optimization and economics.

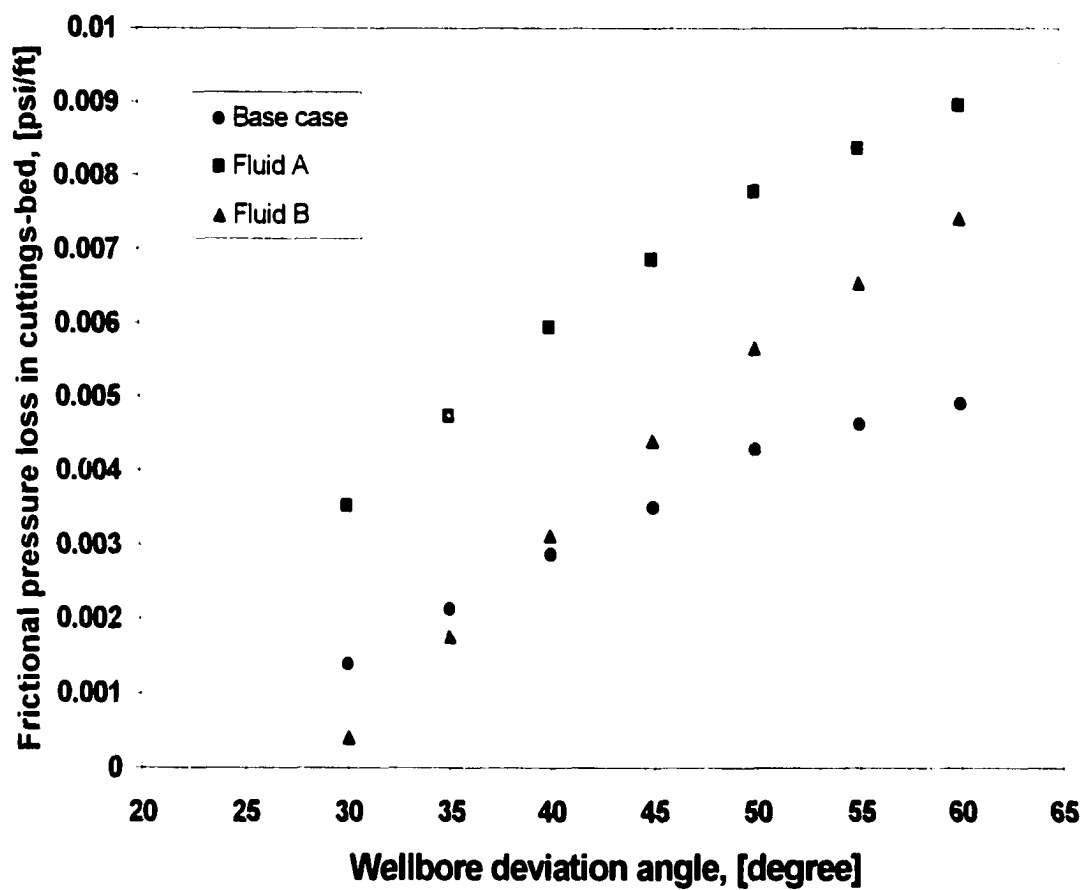


**Fig. 5.13 – Comparison of frictional pressure drop of fluids flow in a porous cuttings-bed with the nominal annular velocity of 3 ft/s (base case)**

## 5.5 Summary

The newly developed minimum anti-sliding velocity model properly interrelates nominal annular velocity, wellbore deviation, in-situ velocity, fluid rheology, and the cuttings-bed area for the cuttings-bed characterization. The following conclusions were obtained from this study:

- (1) A mathematical model for minimum anti-sliding velocity to predict and interpret a cuttings-bed movement around intermediate wellbore deviation ( $30^\circ$  to  $60^\circ$ ) based on computer simulation has been formulated.
- (2) It is quite clear that nominal annular velocity and the fraction of the accumulated cuttings-bed play a significant role in a cuttings-bed movement. Therefore, the selection of a fluid, the nominal annular velocity, and its operational conditions are important for avoiding the cuttings sliding down in this region of the wellbores.
- (3) A highly viscous fluid slightly reduces MASV and increases the pressure gradient under the same nominal annular velocity. It is recommended that an optimum combination of the cuttings-bed area, pressure gradient, rheology of the fluid, and the nominal annular velocity should be considered. An adjustment in one parameter that affects cuttings transport will not necessarily promote efficient cuttings transport as a whole.
- (4) The effect of a cuttings-bed movement on the pressure gradient is negligible because a cuttings-bed velocity is relatively small compared to the fluid velocity of a heterogeneous suspension layer.

- (5) The effect of drilling fluid flow in a porous cuttings-bed on pressure drop is significant. This effect considerably increases frictional pressure drop (up to 20%). It is highly recommended that this effect be considered in drilling hydraulics of a deviated wellbore with a high cuttings-bed area.



## **CHAPTER SIX**

# **DEVELOPMENT PROCESS OF THE SIMULATION PROGRAM**

### **6.1 Introduction**

The preceding chapters enumerated two things: (1) that a proper design of drilling fluid rheology and pumping rate are very important parameters for a successful drilling operation, and (2) how the drilling parameters affect cuttings transport and the drilling hydraulic design. Specifically, the selection of optimum drilling parameters requires a compromised process between the following factors. These factors involve the cuttings-bed thickness, the frictional pressure gradient, fluid rheology, wellbore geometry, and wellbore deviation.

The role of drilling engineers is to design an optimum drilling program, based on the estimation and prediction of effects of each drilling parameter, under in-situ conditions. This can be achieved by simulations of various drilling conditions. A simulator was developed based on the mathematical models described in the previous

chapters. This simulator allows drilling engineers to predict and estimate the effects of drilling parameters on cuttings transport. Minimum anti-sliding velocity (MASV), which prevents a cuttings-bed from sliding downward in a transit segment, can be calculated by this program based on the forces acting on a cuttings-bed.

This chapter provides detailed descriptions of the development process of the simulator. The details of the step-by-step procedures used to develop the mathematical algorithms are also described in this chapter.

## **6.2 Development of Simulation Program, CT-WellClean<sup>®</sup>**

A computer simulator program, called CT-WellClean<sup>®</sup>, was developed to predict and interpret the cuttings transport efficiency in horizontal, vertical, and deviated wellbores. The development process was divided into principal steps, and each step was further divided into sub-steps to accomplish this task.

### **6.2.1 Selection of user input parameters**

There are numerous drilling parameters that affect cuttings transport and drilling hydraulics. In this chapter, the selection of input parameters in the simulation program is discussed.

#### **6.2.1.1 Pump Rate**

One of the most important parameters that affect cuttings transport and wellbore cleanout is the carrier fluid velocity. High fluid velocity generates high turbulent eddies,

which allow cuttings to be easily suspended in a dispersed suspension layer. At the same time, high velocity in the annular section requires a large volume of fluid to be transported through coiled tubing, resulting in a high frictional loss in the coiled tubing. One of the main differences between coiled tubing drilling and a wellbore cleanout is the fluid flow rate required. For wellbore cleanout, in order to generate a high turbulence, large capacity pumps are operated. Since fluid velocity at the low side of a wellbore is quite low, some cuttings-bed accumulations at the low side of the wellbore are inevitable under the normal fluid velocity.

Regardless, some ranges of nominal annular velocities exist which satisfy the three-layer model concept. From the numerous simulations, the range of 0.75 to 5 ft/s nominal annular velocity has a general solution (satisfaction in view of obtaining the positive moving bed area). This range is also affected by fluid rheological properties. If this velocity is greater than 5 ft/s, a moving bed does not exist, resulting in no solution of the model. Similarly, there is no solution of the model under the low annular velocity, because it is difficult to distinguish the two beds (a suspension layer and a moving bed) due to the high stationary bed.

In order to extend the simulation limitation, the range of the nominal annular velocity between 0.5 ft/s and 6 ft/s was selected as the fluid velocity limitation. Outside the specified range (less or beyond of 0.75 – 5 ft/s), this program was designed to use a two-layer model automatically in order to extend its operation limit. The extension of simulation limit allows this program can be used for the simulation of a wellbore cleanout. This program is designed for a user to input various pump rates (gal/ min) to simulate its effect. By changing a pump rate under the given conditions, the cuttings

transport efficiency (cuttings-bed distribution) and frictional pressure gradient can be simulated.

#### 6.2.1.2 Fluid Rheology

There are several rheological fluid models used in the drilling industry, but the Bingham plastic model and the Power-law model are the most common. The Bingham plastic model is widely used in the drilling industry to define rheological characteristics of the drilling fluid, since it is simpler than any other model. The Bingham-plastic model is defined as:

$$\tau = \tau_y + \mu_p \dot{\gamma} \quad (6.1)$$

A Bingham plastic model will not flow until the applied shear stress exceeds a certain minimum value  $\tau_y$ , known as the yield point. After the yield point has been exceeded, changes in shear stress are proportional to changes in shear rate and the constant of proportionality is called the plastic viscosity,  $\mu_p$ . However, published data for the effects of rheological characteristics of the Bingham plastic models are quite rare.

The other model is the Power-law model, which is defined as:

$$\tau = k \left( \dot{\gamma} \right)^n \quad (6.2)$$

Like the Bingham plastic model, it requires two parameters for fluid characterization. The Power-law model can be used to represent a pseudoplastic fluid ( $n < 1$ ), a Newtonian fluid ( $n = 1$ ), or a dilatant fluid ( $n > 1$ ). The parameter  $k$  is called the consistency index of the fluid, and the parameter  $n$  is usually called either the Power-law exponent or the flow

behavior index. The deviation of the dimensionless flow behavior index from 1.0 characterizes the degree to which the fluid behavior is non-Newtonian.<sup>43</sup>

Several studies for the effects of the Power-law models' rheological characteristics on cuttings transport are available. This is because this model effectively represents the fluid characteristics of a variety of fluid types (including fracturing fluids and drilling fluids). This study uses the Power-law model. The Bingham plastic model was reserved for future development of this program. Oil field units of rheology were also used. This program was designed to automatically convert the unit for applications in different calculations.

From numerous simulation operations, there may be no solutions (positive moving bed area) with certain drilling conditions. When this program has no positive moving bed in three-layer model, a two-layer model is used automatically in horizontal segment. This change up extends the program capability and reduces its limitation of simulation. This design concept of the program may bring a quite large flexibility in prediction of cuttings transport efficiency with a broad range of drilling situations.

#### **6.2.1.3 Density of the Fluid**

The density of the fluid directly affects a particle settling velocity. This settling velocity influences the cuttings transport efficiency. This program is developed for the water-based mud as a carrier fluid. However, this program can be extended to oil-based mud, based on the fluid rheological characteristics. In order to cover the density of oil-based muds, which are frequently used for drilling sensitive shale formations, the range of the fluids specific gravity available for a simulation is 0.8 to 2.3 times of water. These

are equivalent to 6.6 to 19.2 lb/gal (ppg). The fluid density used in the simulation is corrected temperature effect by using the average temperatures between surface and bottomhole. Both viscosity and density of water are correlated for temperature in this program.<sup>97</sup> The default temperature is 75 °F.

#### **6.2.1.4 Wellbore Configuration**

Well length, wellbore deviation, wellbore diameter, and coiled tubing diameter used in drilling or wellbore cleanout are important in predicting the cuttings transport efficiency and frictional pressure loss. This program allows a user to input in each wellbore length corresponding to the wellbore deviation angle of 5°. Figure 6.1 shows a typical wellbore trajectory for angle build and hold. For example, 12 sections of wellbore length with its angle increment (5°) can be entered in the program if the wellbore deviation is 60°. Though the wellbore curvature between each point ( $A_0$  to  $A_n$ ) is not straight, it can be assumed as straight between the sections as shown in Fig. 6.1.

Frictional pressure gradient per unit length of each section is calculated, based on the cuttings-bed distribution, the cuttings volumetric concentrations, and wellbore deviation corresponding to each section. The frictional pressure gradient of each section is computed with its length, and the sum of each section's frictional loss is displayed. The pressure gradient of each section is shown in the table of the Form Field (Fig 6.2). Total frictional pressure losses in the entire wellbore length can be obtained by summing up the frictional pressure losses.

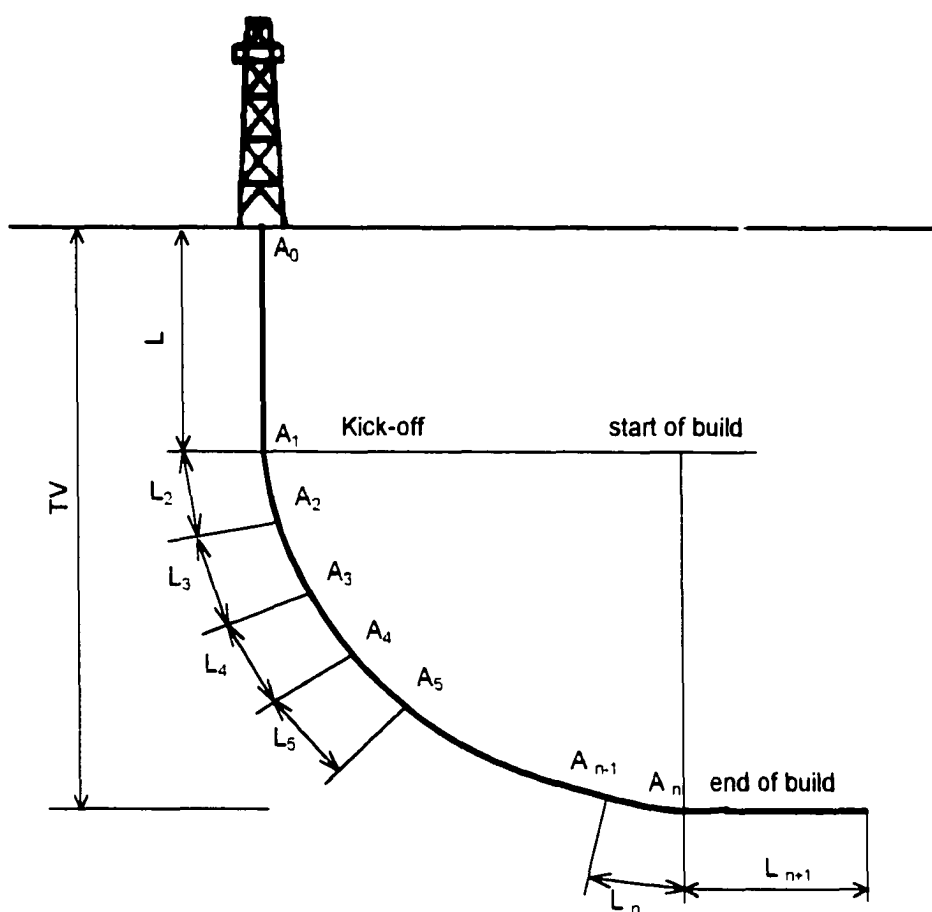


**Fig. 6.1 – Wellbore geometry for the angle build and hold**

Coiled tubing is intuitively located at the lower part of the wellbore in both the horizontal and the transit segment. The wellbore configuration is fully eccentric in those segments. The wellbore configuration in the vertical segment is quite unpredictable. Clearly, it is not to be concentric or fully eccentric. The most critical case in frictional pressure loss is the concentric annulus. Therefore, the concentric case is considered an estimation of the frictional loss.

Back to plots      Back to tables

	A	B	C	D
1	ANNUITY	DISPERSED	CONCENTRIC	CONCENTRIC
2	0	1.500973		
3	5	1.498514		
4	10	1.482177		
5	15	1.495088		
6	20	1.417452		
7	25	1.363556		
8	30	0.9979028		
9	35	0.6586093		
10	40	0.6195906		
11	45	0.575268		
12	50	0.5273863		
13	55	0.4817361		
14	60	0.4041719		
15	65	0.3084678		
16	70	0.3187439		
17	75	0.2980236		
18	80	0.2543014		
19	85	0.2048154		
20	90	0.1740931		
21			TOTAL	
22				

New      Save

Finish

Please define the different eight sections of the wellbore that you want to analyze. Each one of this sections will be treated as a straight segment.

**Fig. 6.2 – The user interface for the calculation of frictional pressure gradient between each section of the wellbore trajectory**



#### **6.2.1.5 The Other Parameters**

The following parameters are also required in the simulation of this program.

- Rate of penetration
- Cuttings specific gravity
- Cuttings size

The input data for the rate of penetration (ROP) is used to calculate the cuttings volume generated by a drilling bit during a drilling. This cuttings volume directly affects the time that the system reaches steady-state conditions and diffusivity. A cuttings volumetric concentration in a dispersed suspension layer is calculated by this cuttings volume under a steady-state flow condition. Researchers<sup>73,74</sup> found from their experiments that over 5% of cuttings volumetric concentration frequently causes pack-off and stuck pipe problems. In this program if the ROP value, input by a user, leads to over 5 % cuttings volumetric concentration, an alert message is displayed. The user may increase the flow rate or reduce ROP. In order to simulate over 5 % cuttings volumetric concentration, the user ignores the alert message. However, the upper limit is set at 12 % of volumetric concentration in a suspension layer because of the limitation of the particle diffusivity coefficient (Eq. 2.47). This coefficient, proposed by Walton,<sup>12</sup> was obtained from sand transport experiments in horizontal pipe at 12% of volumetric concentration.

The specific gravity of formations varies depending upon the rock types. The specific gravity of sedimentary rock<sup>85</sup> varies between 2.20 and 2.88. In order to provide a wide availability in the simulation, the cuttings specific gravity range was decided as 0.9 to 1.1 times of the specific gravity of sedimentary rocks, which is equivalent to 1.98 to 3.17. This range of specific gravity can cover most oil formations.

The mathematical model developed in this study only considers diffusivity. Brownian motion and shear-induced random motion of the particles, which may affect suspensions for light and fine particles are not included. The general drilled cuttings size distribution is US mesh 4 to 8 (0.094 – 0.187-in.).<sup>67</sup> Durand<sup>82</sup> noted that particles less than 0.006-in. (0.15 mm) were enveloped in an accompanying film of carrying fluid, which had the effect of reducing the relative density of the falling mass with a consequent low settling velocity. In addition, the experimental study, performed by Walker et al.<sup>79</sup>, showed that larger particles were always harder to clean out than smaller ones. Therefore, the cuttings size range of 0.012 to 0.315-in. (0.3 - 8 mm) was selected for this simulator. This range includes the sand size (US mesh 20 - 40) generally used in fracturing jobs. The size of this sand is equivalent to 0.017 to 0.033-in. (0.43 – 0.84 mm). If the input data are out of range for a simulation, an alert message is displayed and the input data are cleaned automatically. The cursor is then moved to the empty data box for a new data input. A summary of the simulation ranges is presented in Table 6.1.

### **6.2.2 Development of Algorithm**

Algorithm is a word used by the computing community to mean a rule, procedure, or sequence of instructions. An algorithm is a description of how to do tasks. Each step of the description is understood by the person or machine that is to perform the task.<sup>95</sup> Algorithms developed for solving the models developed in this study and calculations are described in this section.

**Table 6.1 – Summary of simulation ranges of each parameter**

Parameters	Ranges	Remarks
Fluid velocity (nominal annular velocity)	1 – 6 (ft/s)	Note 1
Fluid rheology	Power-law	Note 2
Density of fluid	6.6 – 19.2 (ppg)	
Specific gravity of formation	1.98 – 3.17	
Cuttings volumetric concentration	0 – 12 (%)	Note 3
Cuttings size	0.012 – 0.315 (in.)	

Note 1: When over the range, need to adjust pump rate or increase a wellbore size

Note 2: The Bingham plastic model is reserved for future development

Note 3: There is no limitation directly to ROP. Cuttings volumetric concentration is calculated based on the input data. If this concentration is over the range, need to decrease ROP, or increase pump rate and/or wellbore size.

#### 6.2.2.1 Horizontal and Transit Segment

The following step-by-step procedure was developed for solving cuttings-bed distribution of the horizontal segment.

Step 1) Calculate particle settling velocity using Eq. 2.28.

Step 2) Calculate total cuttings concentration using Eq. 3.8.

Step 3) Calculate the hindered settling velocity using Eq. 2.33.

Step 4) Assume area distribution

$$F_l = \frac{A_{mb} + A_{sd}}{A_u} \quad (6.3)$$

$$F_2 = \frac{A_{sd}}{A_{mb}} \quad (6.4)$$

Step 5) Calculate the cuttings-bed heights and wet perimeters using Appendix C.

Step 6) Calculate the fluid Reynolds number using Eq. 2.17.

Step 7) Calculate diffusivity using Eq. 2.45.

Step 8) Solve Eq. 2.44 to get the cuttings concentration in the suspension layer.

Step 9) Calculate the particle Reynolds number using Eq. 2.26.

Step 10) Calculate drag coefficient and lift coefficient using Eqs. 2.25 and 2.34.

Step 11) Calculate a moving bed velocity using Eq. 4.6.

Step 12) Calculate local velocity in a suspension layer using Eq. 3.24.

Step 13) Calculate the areas of a suspension layer and a moving bed using Eqs. 4.34 and 3.23, respectively.

Step 14) Calculate new  $F_1$  and  $F_2$  value using Eqs. 6.3 and 6.4.

Step 15) Iterate step 5 to step 14 until the differences of  $F_1$  and  $F_2$  between previous and present values reaches 0.0001. If this condition is satisfied, the values are final. The flow chart for the calculation of a cuttings-bed distribution is shown in Appendix E.

### 6.2.2.2 Frictional Pressure Gradient

This calculation module shares the data calculated from the flow layer calculations.

The following is a brief algorithm used to solve the frictional pressure gradient.

Step 1) Import the following data from the flow layer calculation module ( $C_{sd}$ ,  $U_{sd}$ ,  $S_{sd}$ ,  $S_{smb}$ ,  $S_{sb}$ ,  $D_{sd}$ ,  $N_{Ref}$ ).

Step 2) Calculate the fluid density in a suspension layer using Eq. 3.12.

Step 3) Calculate the Fanning friction factor using Eqs. 3.13, 3.14, and 4.20.

Step 4) Calculate shear stress using Eqs. 3.10, 4.18, and 4.19.

Step 5) Calculate frictional pressure losses

For the horizontal section: Eq. 3.9;

For the horizontal segment: Eq. 4.1;

For the transit segment: Eq. 4.12;

For the vertical segment: Eq. 4.25.

The effect of the cuttings-bed sliding on frictional pressure loss is excluded because this effect is insignificant, as discussed in Chapter 5. However, the recommended MASV is calculated in this program. The detail flow chart is shown in Appendix G.

### **6.2.3 Graphical Data Processing**

The operation of this program generates simulation results in either tabulated forms or graphic forms. To enhance the visual presentation, this program provides the data plotted by the graphic engine. This graphic data can be directly exported to a Microsoft<sup>®</sup> Office program for a user to compare the simulation data with the experimental data. After a user confirms the simulation results by graphical presentation form, then the tabulated form is simply obtained by using the back button. The tabulated data, which are in rich text form, can be saved directly on a file form and plotted by a different graphic program, such as Microsoft<sup>®</sup> Excel or a user customized graphic engine.

The user interface is created by using the Visual Graphic Array (VGA), which allows  $800 \times 600$  pixels, or Super Visual Graphic Array (SVGA), which allows  $1020 \times 780$  pixels. These graphic modes permit 58 rows in all, in which programming features

like “Form Fields” can be written from rows 1 to 48 at the top of the screen. With this allowable resolution, it is possible to create “Form Field” in the monitor.

The program is designed to plot the processed graphic data on the Visual Basic® basis. The user can select the graphical presentation forms. All graphical presentation forms are booted at the same time, and each presentation is displayed by activation of the plot commander. When the next graphical presentation is displayed, the previous plot is in a standby position. This presentation can be redisplayed simply by activation of the display commander.

## **6.3 Description of the Simulation Program**

The development of a simulator involves writing the program in a special language. CT-WellClean® is a Window® based application program. It allows the user to enter the simulation data by moving from point to point using a mouse. The user interfaces, briefly explained in the following sections, are provided to make the program user-friendly.

### **6.3.1 Program Description**

This CT-WellClean® simulation program uses the Microsoft® Visual Basic® version 6.0 for the user interface. This program communicates with the user who selects a simulation method, range of simulation, input simulation parameters, and output methods of the simulation results. Many unknown parameters are involved and combined together in the model. The analytical solution is obtained by several iterations. The algorithm for calculations of cuttings-bed distribution requires vast amounts of iteration. Input and

output (I/O) devices provide means of communication between the user and the machine. The Visual Basic<sup>®</sup> system has a standard input device and a standard output device for the user/machine communication. The standard I/O device is a keyboard, a video display monitor, and a cursor mover (mouse). This Visual Basic<sup>®</sup> is the powerful tool used for the user interface.

A layout form window allows a user to design the visualized application forms in a screen display. One of the features of Visual Basic<sup>®</sup> used in this program is that the different projects can be included in a single application by using custom controls and programs. This allows a user to work with multiple projects within a single instance of Visual Basic<sup>®</sup>, as well as allows a user to carry out multiple simulations at one time. When a user presses a commander button in each form, select a menu item, or select a value of a scroll bar, the program performs the task designated and then laps back into hibernation to await the user's next command. Another feature of the Visual Basic<sup>®</sup> is that the compiling and debugging of the program are quite easier than other programming languages.

## **6.3.2 Iteration Calculations**

### **6.3.2.1 Introduction**

To simultaneously solve the models described in the previous chapters is quite complicated. Some unknown parameters are also involved or included in other parameters. Examples are the determination of the drag coefficient and the particle Reynolds number. To define the drag coefficient, the particle Reynolds number is needed. To solve both simultaneously, it requires iterations.<sup>57</sup> The other example in this

study is the prediction of cuttings concentration in a dispersed suspension layer, which is required to estimate the density of the fluid in the suspension layer. The cuttings concentration in a dispersed suspension can be obtained from a diffusivity calculation. To calculate this diffusivity, Reynolds number has to be defined, which requires the fluid flow path area, which is a function of diffusivity coefficient. Therefore, almost all calculations used in solving these mathematical models require a different iteration. The following sub-chapters describe the iteration procedures used in this study.

### 6.3.2.1 Wellbore Geometry Calculations

The areas occupied by each layer are obtained from the initially assumed fractions of each layer. Two layers (the dispersed suspension layer and the stationary layer) are used to define wellbore geometry (Appendix C) because a moving bed can be easily obtained by deducting areas of these two layers from the annular section area. For a three-layer model, the area and the height of the moving bed can be obtained from the following equations, respectively.

$$A_{mb} = A_a - A_{sd} - A_{sh} \quad (6.5)$$

$$y_{mb} = D - y_{sd} - y_{sh} \quad (6.6)$$

For the two-layer model (transit segment), the height and area of the moving bed should be zero.

The next step is to calculate the bed height and the wet perimeters. In order to define each area as a function of contact angles ( $\alpha, \beta, \alpha', \beta'$ ), the wellbore geometry is divided into four cases (Appendix C). The assumed area is allocated to the geometry case, which satisfies the area conditions. The calculation of the bed height begins with the



minimum bed height of the case. The calculated area with the minimum bed height will then be compared with the area. If the absolute value difference between the area and the calculated area with minimum bed height exceeds 0.0001 square inches (in.<sup>2</sup>), iteration will be done with the new bed height (small increment of bed height) until the absolute value difference falls within the design criteria (0.0001 in.<sup>2</sup>). The wet perimeter can be obtained from the contact angles specified with bed heights. The details are described in the Appendix C.

### 6.3.2.2 Cuttings-Bed Distribution

The basic idea to solve this model is the iterative calculation of the mathematical equations simultaneously until the conditions are satisfied. For this, the area of each layer was assumed initially. Fractions of these areas,  $F_1$  and  $F_2$  are defined as:

$$F_1 = \frac{A_{mb} + A_{sd}}{A_a} \quad (6.3)$$

$$F_2 = \frac{A_{sd}}{A_{mb}} \quad (6.4)$$

These areas are readjusted after each iteration. If the area of a suspension layer,  $A_{sd}$ , is small, the local velocity will increase. The available energy increases for particles to be lifted up into the suspension layer. The area of a suspension layer then increases in the next iteration because of cuttings suspension. The increased fluid flow path area (the area of a suspension layer) reduces turbulent eddies and also its strength to hold particles. Therefore, the area should be reduced again. This iteration is done until the differences between two consecutive calculated areas are within the specified values (0.0001- in.<sup>2</sup>).

Each area will be converged into one value during the iteration process. In some cases, negative area was found in the calculation process of diffusivity compensation. This may lead to an error message during calculation. In order to avoid this large fluctuation in the convergence process, one of the guideline for the assumption of  $F_1$  and  $F_2$  is necessary. The guidelines for  $F_1$  and  $F_2$  were developed from the numerous simulation results. This increases system reliability in finding the convergence value resulting in avoiding any negative area during iterations. This is one of the highlights for solving the model developed in this study. The stationary bed area,  $A_{sb}$ , is also estimated by the iteration process until all the conditions specified in the previous chapter are satisfied.

#### **6.3.2.4 Cuttings-Bed Velocity**

At the initial stage, it is assumed that a cuttings-bed is stationary. After calculation of the hydrodynamic friction force,  $F_{hf}$ , and the force acting on a cuttings-bed,  $F_h$ , the cuttings-bed velocity is estimated. This estimated cuttings-bed velocity is iterated to calculate both forces ( $F_{hf}$  and  $F_h$ ) until the absolute differences of the cuttings velocity before and after the iteration reaches the value specified in the hierarchy chart (0.0001 ft/s).

### **6.3.3 Integration of Simulation Results**

The simulations are performed by the different layer models developed for each segment. The results from each segment model are integrated into one as a function of wellbore deviation. There are two boundaries in layer models between the two segments:

30° of wellbore deviation (vertical and transit segment) and 60° of wellbore deviation (transit and horizontal segment). However, this integrated result may have a small discrepancy within the value of the neighbor's segment. Additionally, the magnitude of this discrepancy, which seems to be a discontinuity of the result, may be high at the boundaries between each segment.

In order to reduce this discontinuity in the simulation result at the boundaries, the simulations were performed by overlapping 5° degrees. For example, the wellbore deviation angle is 0° to 80°. A simulation is performed for wellbore deviation from 55° to 80° based on a horizontal segment (using a three-layer model). A different simulation is performed for wellbore deviation from 25° to 65°, based on a transit segment (using a two-layer model). Another simulation is performed simultaneously for wellbore deviation from 0° to 35°, based on a vertical segment (using a one-layer model).

The overlapped simulation results from the different segments are used to obtain the average value around the boundaries. The simulation results for 55° to 65°, obtained from both the horizontal segment and the transit segment, are averaged. In the same manner, the simulation results for 25° to 35°, obtained from both the vertical segment and the transit segment, are averaged. This procedure reduces the discrepancy between the boundaries.

#### **6.3.4 Hydraulic Reference Module**

A precise estimation of the hydraulics inside coiled tubing is essential to accurately estimate the hydraulic power available with the hydraulic motor at the bottomhole. An estimation of frictional pressure loss is also important in order to control and maintain the

wellbore pressure. This data is useful in the design and selection of coiled tubing system. Calculation of the hydraulic friction pressure losses inside both the coiled tubing and the annulus is included in the hydraulic reference module.

The Fanning friction factor for fluid flow in coiled tubing is correlated with the generalized Reynolds numbers. The Shah correlation for pipe flow, proposed in Reference 39, was used in the estimation of frictional pressure loss inside the coiled tubing. This frictional pressure loss was corrected by the correlation related to the pipe wall roughness as a function of apparent viscosity.<sup>41</sup>

The frictional pressure loss due to annulus fluid flow is a function of in-situ fluid velocity, effective density, and fluid rheological properties. Three different fluid models: Newtonian, Bingham plastic, and Power-law model, are available for the hydraulic calculations. The effective density of a fluid, flowing in the annulus (or a dispersed layer), is affected by a cuttings concentration. Moreover, a cuttings-bed also affects the in-situ velocity in the annulus. An estimated frictional pressure loss with the cuttings accumulation inside the annulus is a valuable guideline for the design of a drilling program. Therefore, this hydraulic reference module allows a user to calculate the frictional pressure loss with the fraction of a cuttings-bed in the annulus. The fraction of a cuttings-bed is defined as the ratio of the cuttings-bed area to the annular section area. This fraction of a cuttings-bed can be entered freely by a user.

In this reference module, the allowable range of a fluid density is 6.6 to 19.2 lb<sub>m</sub>/gal. If the value entered by a user is out of this range, this program will notify the user to re-enter the realistic data. In order to avoid any illogical data input, this program also warns of unrealistic data when a user enters the data for a wellbore size less than

1.25 times of a coiled tubing's outer diameter. When a coiled tubing's inner diameter is larger than the outer diameter, this program will also notify the user to re-enter the realistic data. If the drilling bit size is smaller than the wellbore size in input data, an error message is displayed.

If a user knows the exact rheometer data for the ratio of bob to sleeve radius, the input values will be used for the conversion of fluid consistency index. Otherwise, this program is designed to use the default data: the rheometer constant ( $\Omega$ ) is 1.1835166, used in Eq. 2.21, based on the standard radius of sleeve,  $R_c$ , is 1.8415-in. and the radius of bob,  $R_b$ , is 1.7245-in. A user's input data have higher priority than the default data. If a user knows either the flow consistency index among the pipe flow consistency index,  $K_p$ , annulus flow consistency index,  $K_a$ , or viscometer consistency index,  $K_v$ , this program automatically calculates the consistency index, which is unknown.

Annulus eccentricity can be selected by a user during a simulation stage. However, full eccentricity is a default with the cuttings fraction because coiled tubing is intuitively located at the bottom. If a user enters any fraction of the cutting-bed, the hydraulic wet diameter of the fluid flow path area is calculated. These wet perimeters and fluid flow path area (deducted the cuttings-bed area from the annular section area) are used for the calculation of Reynolds number. Once the value of a cuttings fraction is plugged in, the selection of concentric case is then invalid (the concentric selection button is deactivated to avoid any mis-operation of this program). The calculation results show two different cases for frictional pressure loss in an annulus: with a fraction of a cuttings-bed and without a cuttings-bed fraction.

A horizontal well case is only considered in the calculation of frictional pressure loss, since the objective of this module is to provide the user with a guideline for the frictional pressure loss in both coiled tubing and annulus. The pressure gradient with the effects of the cuttings distribution for deviated wellbores can be simulated by the main program. A user can select to repeat this calculation by resetting the data or returning to the main simulation program. Figure 6.3 illustrates the Form Field for the hydraulic reference module.

**Hydraulic calculation module**

**Fluid Data Input**

Fluid Model: Power Law

Flow rate: 157 (gpm)

Fluid density: 8.5 (lpm)

CT ID: 1.7 (in.)

CT OD: 2 (in.)

Wellbore size: 5 (in.)

Eccentricity: Eccentric

Cuttings Specific Grav.: 2.62

Fraction of cuttings bed: 35 (percent)

Rheometer data: Rc 1.8415 Rb 1.7245

**Fluid Model Data**

Bingham Plastic: Yp, PV

Power-Law: n, Kv, Kp, Ks, Temperature

Reynolds Number: Coiled Tubing 9,607.32, Annulus 1,740.652

**Frictional Losses**

Coiled Tubing: 0.277698 (psi/ft)

Annulus with cuttings bed: 0.009005 (psi/ft)

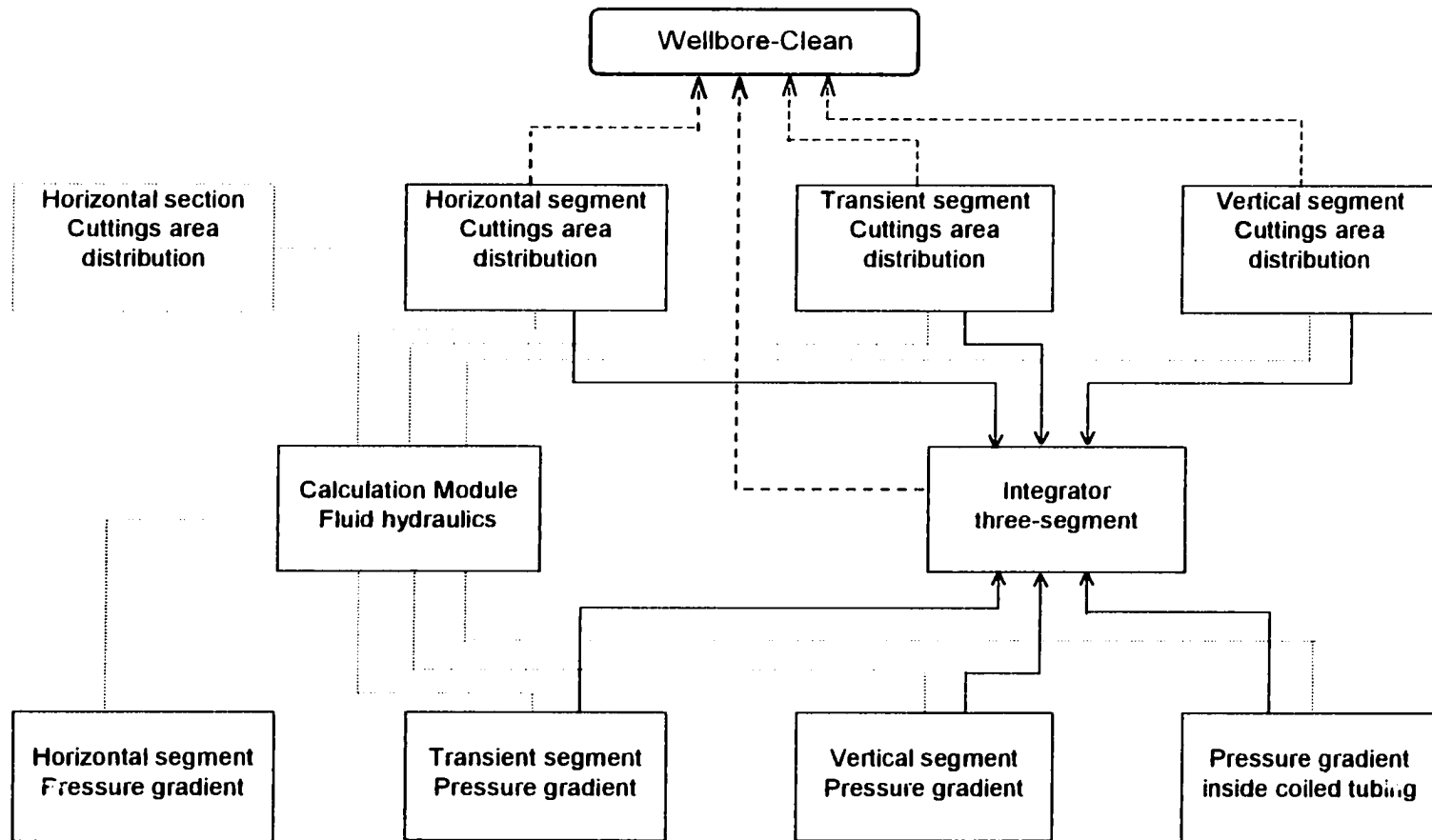
Annulus without cuttings bed: 0.007120 (psi/ft)

Calculate values  
Reset All Values  
Return to Main Menu  
End Program  
**Execute**

**Fig. 6.3 – The user interface for hydraulic reference module**

## **6.4 Program Layout**

A total of nine main modules are incorporated in CT-WellClean®. All of the main modules are linked to the main program, and in some cases the modules are interconnected. Although it is possible to link each of the modules and forms together, this was not done deliberately to avoid any confusion or possible mis-operation. In the present set-up, a user can go from one form to the other by clicking the 'Back' or 'Next' button to the previous or next form. Modules are automatically connected, if necessary. At all times, however, the program interface will inform the user of the operating form currently being used. Figure 6.4 shows the program layout.



Legend:   
 -.- Interlink for calculation,   
 - - - Output Data   
 — Internal data transfer

**Fig. 6.4 – Program layout of CT-WellClean®**



## 6.5 User Interface

Only authorized user is allowed to use this simulation program. The user can proceed or go back by using the control keys: 'Next' and 'Back', respectively. The first user interface Form Field is 'Selection of Simulation'. This form allows a user to select four different cases as shown in Fig. 6.5.

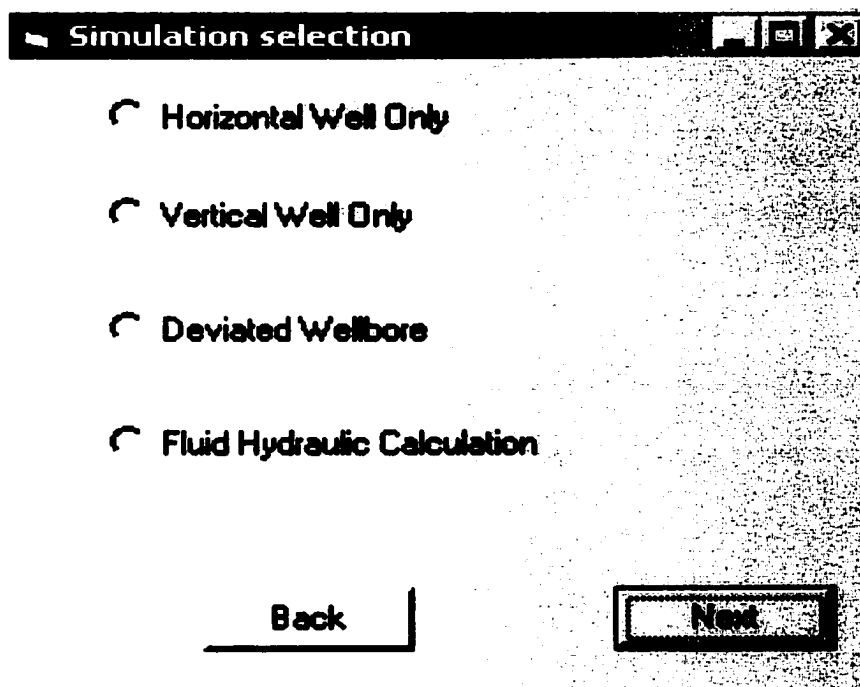


**Fig. 6.5 – The user interface for the selection of simulation methods**

If the user selects the vertical well only option or the horizontal well only option, this user interface will then be skipped. Once the user selects any one of the simulation methods, the user interface for input angles is displayed (See Fig. 6.6). A user may select the range of wellbore angles for simulation from list buttons. When a user selects the

initial wellbore angle (Theta 1), and final wellbore angle (Theta 2), the selected wellbore angles are shown in a dialog box. A user may confirm the selected angle values. If a user wants to change the simulation angle value selected, a new value is simply re-selected from the list buttons. The latest value selected will be used for the simulation. This was designed to enhance user's operation reliability.

Angle Input

Wellbore Deviation 0 to 65

[ Angles from vertical position , Theta 2 should be bigger than Theta 1]

Theta 1= 0  
Theta 2= 65

Back Next

**Fig. 6.6 – The user interface for input angles**

The next user interface inputs fluid rheological data with the expected temperature. Figure 6.7 shows the user interface for fluid rheology input. The input data in the Form Field is also transferred to the public module for fluid hydraulic calculation. Based on the input provided by the user, this program first calculates the designated algorithm. The

calculation result from this module is interfaced with the Form Field, which the user is using. Three different fluid models: Newtonian, Bingham plastic, or Power-law model, are available to calculate hydraulics in both coiled tubing and annulus with the hydraulic reference module (Fig. 6.2). However, the Power-law model is only used in the simulation process. Fluid rheology changes as temperature varies between a surface temperature and bottomhole temperature.

The screenshot shows a window titled "Fluid type data". It contains the following fields and controls:

- Fluid Type:** A dropdown menu currently set to "Power-Law".
- Fluid Density:** A text input field containing "8.5" with a unit label "(ppg)" to its right.
- n value:** A text input field containing ".68".
- k value:** A text input field containing ".006" with a unit label "lbm/ft-sec" to its right.
- Temperature at surface:** A text input field containing "75" with a unit label "(F)" to its right.
- Temperature at bottomhole:** A text input field containing "125" with a unit label "(F)" to its right.
- Navigation:** Two buttons at the bottom, "Back" and "Next", each with a rectangular border.

**Fig 6.7 – The user interface for fluid data**

Development of a specific correlation to correct temperature effect on rheology has been attempted. However, it is known that a universal correlation for correction of temperature effects is yet to be developed. Therefore, this program reserved the temperature effects on rheology for future development. The input temperature data are used only for correction

of fluid density and calculation of water (as one of Newtonian fluids) viscosity proposed by Dodson and Standing.<sup>96</sup> The following Colebrook correlations<sup>97</sup> for the calculation of water density and viscosity were used in this program.

$$\rho_w = \frac{1}{0.01600199 + 2.8404282 * 10^{-9} * (T)^2 * \ln(T)} \quad \left[ \text{lb}_m / \text{ft}^3 \right] \quad (6.7)$$

$$\mu_w = \exp \left[ -5.4381328 - 0.10613679 * (\ln T)^2 \right] \quad \left[ \text{lb}_m / \text{ft} - \text{s} \right] \quad (6.8)$$

The user interface is a path to input data representing in-situ conditions, including wellbore geometry. These conditions consist of a wellbore diameter (or casing), inner and outer diameters of coiled tubing, drilling bit diameter, rate of penetration (ROP), and cuttings specific gravity data. Figure 6.8 shows the user interface for general input. The simulation is performed with this set-up. The next user interface is an output selection.

Parameter	Value	Unit
Borehole size (ID)	5	(in)
Coiled tubing (OD)	2	(in)
Estimated cuttings size	.25	(in)
Rate of Penetration	75	(ft/h)
Cuttings specific gravity	2.65	
Coiled Tubing (ID)	1.7	(in)
Drill Bit Size	5	(in)

Back Next

**Fig. 6.8 – The user interface for general input data**

Wellbore Layers Profile (in<sup>2</sup>) vs. Angle (degrees)

(Function)

1.00  
0.90  
0.80  
0.70  
0.60  
0.50  
0.40  
0.30  
0.20  
0.10  
0.00

0 5 10 15 20 25 30 35 40 45 50 55 60 65 70 75 80 85 90

Ash - Ashy sand  
Ash - Ash

0.09 0.18 0.27 0.34 0.41 0.47 0.51 0.55 0.59 0.62 0.63 0.63 0.63 0.63

0.05 0.10 0.15 0.20 0.25 0.30 0.35 0.40 0.45 0.50 0.55 0.58 0.60 0.61 0.62 0.62

Results for Deviated Well - Plot Format

Pressure Losses	Pressure Losses Ashy sand effect	M.A.S.V.	Up (vertical) transport rate
0.00	0.00	0.00	0.00
0.00	0.00	0.00	0.00

Back Save into a file Print

207

This graphical output provides various simulation results: minimum anti-sliding velocity (MASV), area distribution of each layer as well as combined distribution, cuttings concentration in a suspension layer, moving bed velocity, and bed heights of each layer. The combined cuttings-bed distribution is plotted in order to demonstrate visually the actual position of each layer: a stationary bed is plotted at the bottom, a moving bed is plotted above the stationary bed, and rest of them represents a suspension layer. All these data are plotted as a function of wellbore deviation. These graphical outputs can be saved in tabulated form (rich text file), which also can be plotted by a different graphic program, such as Microsoft<sup>®</sup> Excel or a user customized graphical engine.

## 6.5 Summary

A typical simulator program is composed of a user interface for data input, data processing calculation module, and an output of the simulator results. The development of any simulation program requires working in a direction that links these three components together. Organizing the structure of a simulator, developing algorithms, and finally, writing the program, are three distinctive steps that help achieve this goal.

A simulation program called CT-WellClean<sup>®</sup> has been developed, using interface Form Fields based on the Microsoft<sup>®</sup> Visual Basic<sup>®</sup> version 6.0. This user interface increases the communication between a computer and its user. This simulation program, CT-WellClean<sup>®</sup>, is capable of carrying out several important simulations, including estimation of cuttings-bed distribution, and frictional pressure gradient in each segment under in-situ drilling conditions. This simulator also allows a user to change in-situ conditions and to predict the cuttings transport, drilling hydraulics, and the effects of change in other drilling parameters. The user can use this simulator to determine or select the optimum drilling parameters as well as selecting the best economical fluid system.

## **CHAPTER SEVEN**

### **SUMMARY, CONCLUSIONS, AND RECOMMENDATIONS**

#### **7.1 Summary and Conclusions**

A computer simulation program, CT-WellClean<sup>®</sup>, for analyzing cuttings transport in deviated wellbores was developed based on a three-segment hydraulic model. Different layer models were used for each segment, which effectively represents the dominant parameters affecting cuttings transport. The simulation results were compared with the published experimental data for validation of the model. Based on the results of this study, the following conclusions were reached:

1. A mathematical three-layer model has been formulated to predict and interpret cuttings transport in a deviated wellbore from horizontal to vertical during coiled tubing drilling. The model predictions, based on the simulation results, are in good agreement with the published experimental data.



2. The wellbore deviation has significant effects on cuttings transport. The height of a stationary bed in a horizontal segment is almost constant or slightly increases with a decreasing wellbore deviation. The cuttings bed abruptly decreases with a decrease in wellbore deviation angle in a transit segment. This cuttings bed is almost vanished ( $25 - 30^\circ$ ) or there is no bed ( $0 - 25^\circ$ ).
3. The most dominant parameters affecting cuttings transport while drilling a deviated well with coiled tubing are the nominal annular velocity and the carrier fluid rheology. However, cuttings transport efficiency is also affected by in-situ drilling variables, which cannot be controlled by drilling engineers. These involve coiled tubing location in the annulus, cuttings density, and cuttings size. The effects of in-situ drilling conditions on cuttings transport should be carefully evaluated before designing a drilling program. The simulation program developed in this study allows drilling engineers to simulate all possible in-situ drilling conditions, resulting in the proper design of optimum drilling programs and selection of appropriate fluid systems.
4. The conventional drilling fluid velocity range of 2 to 3 ft/s should be avoided while drilling horizontal wells with coiled tubing. It is recommended that the nominal annular velocity range of 3.5 to 4.0 ft/s be used for a well having a long horizontal section, because a lower pressure gradient and a less stationary bed area are predicted than those of conventional velocity range.

5. Effects of fluid density have a significant role in cuttings transport; however, it is less significant than that of fluid rheology. The cuttings size is insignificant within the range of general cuttings size distribution (0.09 – 0.19-in.). However, an increase in cuttings size up to 0.30-in. in diameter significantly decreases cuttings transport efficiency.
6. A highly viscous fluid slightly increases cuttings carrying capacity in horizontal and transit segments under a turbulent flow regime, as well as the pressure gradient, under the same nominal annular velocity. Thus, there is need for optimization between the various parameters.
7. It is quite clear that nominal annular velocity and the fraction of the accumulated cuttings-bed play a significant role in a cuttings-bed movement. A heavier drilling fluid requires a low minimum anti-sliding velocity (MASV) than lighter fluid under the same wellbore deviation and nominal annular velocity. A highly viscous fluid reduces the MASV to prevent a cuttings-bed from sliding downward toward the bottomhole.
8. Even though the effect of a cuttings-bed movement on the pressure gradient is negligible because the cuttings-bed velocity is relatively small compared to the fluid velocity of a heterogeneous suspension layer, the effect of drilling fluid flow in a porous cuttings-bed on pressure drop is significant. This effect considerably increases pressure drop (up to 20%). It is recommended that this effect be considered in drilling hydraulics of a deviated wellbore with a high cuttings-bed area.

9. A high velocity with a less viscous fluid, resulting in high turbulence compared to a highly viscous fluid, is effective in cuttings transport in a horizontal segment. In a vertical segment, high fluid density under laminar flow regime is effective in obtaining a good cuttings transport. While, the highly viscous fluid under a turbulent flow regime easily prevents a cuttings-bed from sliding downward, it can lead to pack-off or cause the coiled tubing to become stuck in the hole during drilling in a transit segment. The required drilling conditions for the best cuttings transport is different for each segment. Simulations with the program CT-WellClean<sup>®</sup> can be used for optimization of all parameters that affect cuttings transport.

## **7.2 Recommendations**

Although, the hydraulic layer model and simulation program developed in this study are very useful for predicting cuttings-bed distribution and estimating the pressure gradient under the given in-situ conditions, the following recommendations seem appropriate:

1. A development of the model covering three-phase (solid, liquid, and gas) fluid conditions is recommended in order to strengthen the applications of the program (CT-WellClean<sup>®</sup>) for a foam fluid, which is frequently used in underbalanced drilling.
2. The three-segment hydraulic model can be improved by considering other parameters such as the effect of temperature on fluid rheology, coiled tubing vibration/movement on cuttings rebound, and wellbore straightness.

3. In order to improve the accuracy of simulation results, it is recommended that experimental coefficients, which are directly imported from other studies, be re-established with new experiments. These coefficients, directly affecting cuttings transport efficiency, involve diffusivity, friction factor with drilled cuttings, friction coefficient between cuttings-bed and borehole well, and interfacial friction coefficients: a) between a suspension layer and a moving bed, and b) between a moving bed and a stationary bed.

## **NOMENCLATURE**

- $A$  = cross-sectional flow area of each layer, (sq. in.)
- $a, b$  = constants for the Fanning friction factor (Eq. 2.9) , (dimensionless)
- $a_1, b_1$  = constants for settling velocity (Eq. 2.31) , (dimensionless)
- $A(n)$  = an empirical fluid parameter, (dimensionless)
- $B(n)$  = an empirical fluid parameter, (dimensionless)
- $B$  = an experimental constant for friction factor (Eq. 2.23) , (dimensionless)
- $C$  = cuttings volumetric concentration of each layer, (fraction)
- $C_1, C_2$  = integration constants, (dimensionless)
- $C_D$  = drag coefficient, (dimensionless)
- $C_L$  = lift coefficient, (dimensionless)
- $C_t$  = delivered cuttings volumetric concentration, (fraction)
- $C_\phi$  = shape factor of a particle, (Eq. 2.31), (dimensionless)
- $D$  = internal diameter of casing, (in.)
- $D_h$  = hydraulic diameter of cuttings bed in transit segment, (in.)
- $D_{eff}$  = effective diameter of annulus, (in.)
- $D_{mb}$  = hydraulic diameter of moving bed layer, (in.)
- $D_{vd}$  = hydraulic diameter of suspension layer, (in.)
- $D_t$  = nominal diameter of drill bit, (in.)
- $d$  = outer diameter of coiled tubing, (in.)
- $d_i$  = inner diameter of coiled tubing, (in.)
- $d_p$  = cuttings diameter, (in.)

$\Delta p$	= frictional pressure drop, (psi)
$\Delta p/dL$	= Pressure gradient, (psi/ft)
$e$	= eccentricity, (dimensionless)
$F$	= net force acting on the cuttings-bed, (lb <sub>f</sub> )
$F_1$	= ratio of the assumed area distribution, (Eq. 6.3)
$F_2$	= ratio of the assumed area distribution, (Eq. 6.4)
$F_B$	= buoyancy force, (lb <sub>f</sub> )
$F_h$	= a force acting on cuttings bed exerted by gravity, fluid stress, and fluid pressure gradient, (lb <sub>f</sub> )
$F_{hG}$	= gravitational force acting on particles in cuttings bed, (lb <sub>f</sub> )
$F_D$	= drag force, (lb <sub>f</sub> )
$F_{df}$	= dry frictional force acting on cuttings bed, (lb <sub>f</sub> )
$F_{G_i}$	= gravitational force, (lb <sub>f</sub> )
$F_{hf}$	= hydrodynamic friction force, (lb <sub>f</sub> )
$F_L$	= lifting force, (lb <sub>f</sub> )
$F_{mbG}$	= gravitational force acting on the moving bed layer, (lb <sub>f</sub> )
$F_{sdG}$	= gravitational force acting on the mixture in suspension layer, (lb <sub>f</sub> )
$F_{\phi}$	= interfacial friction force, (lb <sub>f</sub> )
$F_1$	= ratio of the assumed cuttings bed distribution (Eq. 6.3)
$F_2$	= ratio of the assumed cuttings bed distribution (Eq. 6.4)
$f$	= friction coefficient, (dimensionless)
$f_{sd}$	= Fanning friction factor for a dispersed suspension layer, (dimensionless)
$f_{sdmb}$	= friction coefficient between a dispersed suspension layer and moving bed, (dimensionless)

$f_x$	= infinite friction factor (Eq. 2.23) , (dimensionless)
$f_x(n)$	= an empirical fluid parameter (Eq. 2.7), (dimensionless)
$G$	= carrying capacity, (lb <sub>m</sub> /min.)
$g$	= gravitational acceleration, (ft/s <sup>2</sup> )
$k_a$	= power-law consistency index for annulus flow, (lb <sub>f</sub> s <sup>n</sup> /ft <sup>2</sup> )
$k_p$	= power-law consistency index for pipe flow, (lb <sub>f</sub> s <sup>n</sup> /ft <sup>2</sup> )
$k_v$	= rheometric power-law consistency index, (lb <sub>f</sub> s <sup>n</sup> /ft <sup>2</sup> )
$k_l$	= proportionality constant (Eq. 5.13), (lb <sub>f</sub> s/ft)
$L$	= wellbore length, (ft)
$L_D$	= acting distance on drag force, (in.)
$L_G$	= acting distance on lift, buoyancy and gravitational force, (in.)
$L_L$	= acting distance on lifting force, (in.)
$m$	= solid particle density (g <sub>m</sub> /cm <sup>3</sup> )
$h,p,q,t$	= constants for interfacial friction factor (Eq. 3.14) , (dimensionless)
$N_{He}$	= Hedstrom number (Eq. 2.13)
$N_{Ref}$	= fluids Reynolds number, (dimensionless)
$N_{Reg}$	= generalized Reynolds number, (dimensionless)
$N_{Rep}$	= particle Reynolds number, (dimensionless)
$n$	= flow behavior index (Power-law model: Eq. 6.2), (dimensionless)
$PV'$	= plastic viscosity of Bingham Plastic mode (cp)
$R$	= coiled tubing curvature, (dimensionless)
$R_t$	= cuttings transport ratio in vertical segment, (dimensionless)
$r$	= radius of cutting particles, (in.)

$S$	= wetted perimeter, (in.)
$U$	= local velocity in each layer (the average velocity when a cuttings bed is present in the annulus), (ft/s)
$U_a$	= nominal annular velocity (the average velocity when a cuttings bed is not present in the annulus), (ft/s)
$U_l$	= local annular velocity (the average velocity when a cuttings bed is present in the annulus), (ft/s)
$U_t$	= particle transport velocity in vertical segment, (ft/s)
$U_{sl}$	= liquid velocity in suspension layer, (ft/s)
$U_{sm}$	= mean fluid velocity in suspension layer, (ft/s)
$U_{sp}$	= particle velocity in suspension layer, (ft/s)
$V_D$	= typical deposition velocity, (Fig. 2.10)
$V_S$	= critical re-suspension velocity in slurry flow, (Fig. 2.11)
$V_T$	= typical viscous viscous transition critical velocity, (Fig. 2.10)
$v$	= cuttings-bed velocity, (ft/s)
$v_t$	= cuttings-bed terminal velocity, (ft/s)
$V_h$	= hindered particle settling velocity, (ft/s)
$V_p$	= terminal particle settling velocity, (ft/s)
$y$	= bed thickness, (in.)
$X$	= horizontal coordinate
$Y$	= vertical coordinate

### **Subscript**

$a$	= annulus
$b$	= cuttings bed
$c$	= casing in cartesian coordinate



d = tubing in cartesian coordinate  
i = any one layer  
L = liquid  
mb = moving bed layer  
mbsb = interface between a moving bed and a stationary bed  
s = solid particle (cuttings)  
sb = stationary bed layer  
sd = solid dispersed suspension layer  
sdb = interface between a suspension layer and a cuttings-bed  
sdmb = interface between a suspension layer and a moving bed  
w = wall

## **GREEK SYMBOLS**

$\alpha$	= angle between center point of casing and upper contact point of a stationary bed, (radian)
$\alpha'$	= angle between center point of casing and upper contact point of a moving bed layer at the inner casing well, (radian)
$\alpha_t$	= angle between center point of casing and upper contact point of a stationary bed in transit segment, (radian)
$\beta$	= angle between center point of coiled tubing and upper contact point of a stationary bed, (radian)
$\beta'$	= angle between center point of coiled tubing and upper contact point of a moving bed layer at the outer coiled tubing surface, (radian)
$\beta_t$	= angle between center point of coiled tubing and upper contact point of stationary bed in transit segment, (radian)
$\delta$	= distance between center points of wellbore and coiled tubing, (in.)
$\varepsilon_o$	= cuttings particle diffusion coefficient, (dimensionless)
$\varepsilon_p$	= cuttings particle diffusivity coefficient, (dimensionless)
$\phi$	= angle of internal friction, (degree)
$\dot{\gamma}$	= shear rate, (sec <sup>-1</sup> )
$\eta$	= slip coefficient, (dimensionless)
$\varphi$	= sphericity of cuttings, (dimensionless)
$\lambda$	= rheometry constant (Eq. 2.21), (dimensionless)
$\mu_e$	= effective viscosity (Eq. 2.30), (lb <sub>r</sub> s/ft <sup>2</sup> )
$\mu_a$	= apparent viscosity, (cp)
$\mu_p$	= plastic viscosity for Bingham-plastic model, (cp)
$\theta$	= deviated wellbore angles from vertical (0 – 90°)

- $\theta'$  = wellbore inclination angle ( $90^\circ - \theta$ )
- $\rho$  = density, (ppg)
- $\Omega$  = a ratio of the bob to sleeve radius, (dimensionless)
- $\tau$  = shear stress acting on each relevant wetted perimeter, (lb<sub>f</sub>/in<sup>2</sup>)
- $\tau_y$  = yield stress of Bingham Plastic model, (lb<sub>f</sub>/100 ft<sup>2</sup>)
- $\omega$  = a constant for Fanning friction factor for annulus pipe (Eq. 2.22), (dimensionless)
- $\varpi$  = absolute roughness of coiled tubing, (in.)
- $\psi$  = cuttings-bed porosity, (fraction)

## **References**

1. Adari, R.B., Miska, S., Kuru, E., Bern, P. and Saasen, A.: "Selecting Drilling Fluid Properties and Flow Rates for Effective Hole Cleaning in High Angle and Horizontal Wells," SPE Paper 63050 presented at the 2000 SPE Annual Technical Conference and Exhibition held in Dallas, Texas, 1-4 October 2000.
2. Massie, G.W., Castle-Smith, J., Lee, J.W., and Ramsey, M.S.: "Amoco's Training Initiative Reduces Wellsite Drilling Problems," Petroleum Engineer International, March 1995.
3. Hopkins, C.J. and Leicksenring, R.A.: "Reducing the Risk of Stuck Pipe in the Netherlands," paper IADC/SPE 29422 presented at the 1995 IADC/SPE Drilling Conference, Amsterdam, February 28 - March 2.
4. Bradley, W.B. et al.: "Task Force Approach to Reducing Stuck Pipe Costs," SPE Paper 21999 presented at the 1991 SPE/IADC Drilling Conference held in Amsterdam, Netherlands, 11-14 March 1991.
5. Nguyen, D. and Rahman, S.S.: "A Three-Layer Hydraulic Program for Effective Cuttings Transport and Hole Cleaning in Highly Deviated and Horizontal Wells," SPE Paper 51186, revised from the paper 36383, first presented at the 1996 IADC/SPE Asia Pacific Drilling Technology held in Kuala Lumpur, 9-11 September 1996.
6. Azar, J.J. and Sanchez, R.A.: "Important Issues in Cuttings Transport for Drilling Directional Wells," SPE Paper 39020 presented at the 5<sup>th</sup> Latin America and Caribbean Petroleum Engineering Conference, Rio de Janeiro, Brazil, Aug. 30 – Sept. 3, 1997.
7. Sample, K.J. and Bourgoyne, A.T.: "An Experimental Evaluation of Correlations Used for Predicting Cutting Slip Velocity," SPE Paper 6645 presented at the 52<sup>nd</sup> Annual Fall Technical Conference, Denver, Colorado, Oct. 9-12, 1977.
8. Sample, K.J. and Bourgoyne, A.T.: "Development of Improved Laboratory and Field Procedures for Determining the Carrying Capacity of Drilling Fluids," SPE Paper 7497 presented at the 53<sup>rd</sup> Annual Fall Technical Conference, Houston, Texas, Oct. 1-3, 1978.
9. Tomren, P.H.: The Transport of Drilled Cuttings in an Inclined Eccentric Annulus, MS Thesis, U of Tulsa, Oklahoma, 1979.
10. Ford, J.J., Peden, J.M., Oyenevin, E.G., Zarrouh, R.: "Experimental Investigation of Drilled Cuttings Transport in Inclined Boreholes," SPE Paper 20421 presented at the 65<sup>th</sup> Annual Technical Conference, New Orleans, Sept. 23-26, 1990.

11. Gavignet, A.A. and Sobey, I.J.: "Model Aids Cuttings Transport Prediction," JPT, September 1989, p.916-921.
12. Walton, I.C.: "Computer Simulator of Coiled Tubing Wellbore Cleanouts in Deviated Wells Recommends Optimum Pump Rate and Fluid Viscosity," SPE Paper 29491 presented at the Production Operations Symposium, Oklahoma City, April 2-4, 1995.
13. Tomren, P.H., Iyoho, A.W. and Azar, J.J.: " An Experimental Study of Cuttings Transport in Directional Wells," SPE DE, Feb. 1986, p.43-56.
14. Okrajini, S.S. and Azar, J.J.: " The Effects of Mud Rheology on Annular Hole Cleaning in Directional Wells," SPE DE, Aug. 1986, p.297-308.
15. Becker, T.E., Azar, J.J., Okrajini, S.S.: "Correlations of Mud Rheology Properties with Cuttings Transport Performance in Directional Drilling," SPE DE Mar. 1991, p.16-24.
16. Clark, R.K. and Bickman, K.L.: "A Mechanistic Model for Cutting Transport," SPE Paper 28301 presented at the 69<sup>th</sup> Annual Technical Conference, New Orleans, 25-28 September 1994.
17. Rasi, M.: "Hole Cleaning in Large-Angle Wellbores," SPE Paper 27464 presented at the 1994 SPE/IADC Drilling Conference held in Dallas, Texas, 15-18 1994.
18. Hacıislamoglu, M.: Non-Newtonian Flow in Eccentric Annuli and Its Application to Petroleum Engineering Problems, Ph.D. Dissertation, Louisiana State University, Baton Rouge, Louisiana, 1989.
19. Azouz, I., Shirazi, S.A., Pilehvari, A. and Azar, J.J.: "Numerical Simulation of Laminar Flow of Yield-Power Law Fluids in Conduits," of December 1993, p.710-716.
20. Vinod, P.S.: "Rheology Effects on Laminar and Turbulent Flow of Model Drilling Fluids Deviated Wells," SPE Paper 28287 presented Arbitrary Cross-Section", Transactions of the ASME, vol. 15, at the 1994 IADC/SPE Drilling Conference held in Dallas, Texas, February 15-18.
21. Sanchez, R.A., Azar, J.J., Bassal, A.A. and Martins, A.L.: "Effect of Drillpipe Rotation on Hole Cleaning During Directional-Well Drilling," SPEJ, June 1999, p.101-107.
22. Martins, A.L., Santana, C.C.: "Evaluation of Cutting Transport in Horizontal and Near Horizontal Wells - A Dimensionless Approach," SPE Paper 23643 presented

at the 2<sup>nd</sup> Latin American Petroleum Engineering Conference, Caracas, Venezuela, March 8-11, 1992.

23. Doron, P. and Barnea, D.: "A Three-Layer Model for Solid-Liquid Flow in Horizontal Pipes," *International Journal of Multiphase Flow*, Vol. 19, No. 6, 1993, p.1029-1043.
24. Iyoho, A.W. and Takahashi, H.: "Modeling Unstable Cuttings Transport in Horizontal, Eccentric Wellbores," *SPE Paper 27416*, July 23, 1993.
25. Cho, H., Shah, S.N., and Osisanya, S.O.: "A Three-Layer Modeling for Cuttings Transport with Coiled Tubing Horizontal Drilling," *SPE Paper 63269* presented at the 2000 SPE Annual Technical Conference and Exhibition held in Dallas, Texas, 1-4 October 2000.
26. Cho, H., Shah, S.N., and Osisanya, S.O.: "A Three-Segment Hydraulic Model for Cuttings Transport in Horizontal and Deviated Wells," *SPE Paper 65488* presented at the 2000 SPE/CIM International Conference on Horizontal Well Technology held in Calgary, Canada, 6-8 November 2000.
27. Sifferman, T.R. and Becker, T.E.: "Hole Cleaning in Full-Scale Inclined Wellbores," *SPE DE*, June 1992, p.115-120.
28. Peden, J.M., Ford, J.T. and Oyeneyin, M.B.: "Comprehensive Experimental Investigation of Drilled Cuttings Transport in Inclined Wells Including the Effects of Rotation and Eccentricity," *SPE Paper 20925* presented at the Europec 90, Hague, Netherlands, October 22-24, 1990.
29. Leising, L.J. and Walton, I.C.: "Cuttings Transport Problems and Solutions in Coiled Tubing Drilling," *SPE Paper 39300* presented at the 1997 IADC/SPE Drilling Conference held in Dallas, Texas, March 3-6.
30. Martin, M., George, C., Bison, P. and Konirsch, O.: "Transport of Cuttings in Directional Wells," *SPE Paper 16083* presented at the 1987 IADC/SPE Drilling Conference held in New Orleans, March 15-18.
31. Gao, E. and Young, A.C.: "Hole Cleaning in Extended Reach Wells," *SPE Paper 29425* presented at the 1995 IADC/SPE Drilling Conference held in Amsterdam, February 28-March 2, 1995.
32. Li, J. and Walker, S.: "Sensitivity Analysis of Hole Cleaning Parameters in Directional Wells," *SPE Paper 54498* presented at the 1999 SPE/ICoTA Roundtable held in Houston, Texas, May 25-26.
33. Crouse, P.C. and Lunan, W.B.: "Coiled Tubing Drilling-Expanding Application Key to Future," *SPE Paper 60706* presented at the 2000 SPE Annual Technical Conference and Exhibition held in Dallas, Texas, 1-4 Oct. 2000.

34. Sas-Jaworsky II, A.: Coiled Tubing – Operations and Services, Part 4, World Oil, Coiled Tubing Handbook, Gulf Publishing Company, 1993.
35. Gu, H., Walton, I.C. and Brady, B.H.G.: “ A Computer Wellbore Simulator for Coiled Tubing Cleanout Operations” Computer Methods and Advances in Geomechanics, Balkema, Rotterdam, 1994.
36. “Coiled Tubing Consortium Report,” Well Construction Technology Center, The University of Oklahoma, Unpublished, December 31, 1999.
37. Azouz, A., Shah, S.N., Vinod, P.S., and Lord, D.L.: “Experimental Investigation of Friction Pressure Losses in Coiled Tubing,” SPE Production & Facilities, May 1998, p. 91-98.
38. Medjani, B. and Shah, S.N.: “A New Approach for Predicting Frictional Losses of Non-Newtonian Fluids in Coiled Tubing,” SPE Paper 60319 presented at the 2000 SPE Rocky Mountain Regional/Low Permeability Reservoir Symposium held in Denver, CO, 12-15, March 2000.
39. Shah, S.N.: “Correlation Predict Pressure of Fracturing Fluids”, Oil and Gas J. 16 Jan. 1984.
40. “Coiled Tubing Consortium Report,” Well Construction Technology Center, The University of Oklahoma, Unpublished, June 21, 2000.
41. Shah, S.N.: “Effects of Pipe Roughness on Friction Pressure of Fracturing Fluids,” SPE PE, May 1990.
42. Willingham, J.D., Shah, S.N.: “Friction Pressure of Newtonian and Non-Newtonian Fluids in Straight and Reeled Coiled Tubing,” SPE Paper 60719 presented at the 2000 SPE/ICoTA Coiled Tubing Roundtable held in Houston, TX, 5-6 April 2000.
43. Bourgoyne, A.T. Jr., Millheim, K.K., Chenevert, M.E., and Young, F.S. Jr.: Applied Drilling Engineering, SPE Text Book Series Vol. 2, SPE, Richardson, Texas, 1991.
44. Colebrook, C.F.: “Turbulent Flow in Pipes, with Particular Reference to the Transition Region Between the Smooth and Rough Pipe Laws,” Journal of Inst. of Civil Engineer, London, 1939.
45. Hanks, R.W. and Pratt, D.R.: “On the Flow of Bingham Plastic Slurries in Pipes and Between Parallel Plates,” Society of Petroleum Engineer J. Transaction of AIME, December 1967, p. 342-46.

46. Cullender, M.H. and Smith, R.V.: "Practical Solution of Gas-Flow Equations for Wells and Pipelines with large Temperature Gradients," Transaction, AIME vol. 207, 1956, p. 281-87.
47. Reed, T.D., and Pilehvari, A.A.: "A New Model for Laminar, Transient, and Turbulent Flow of Drilling Muds," SPE Paper 25456 presented at the Production Operation Symposium, Oklahoma City, 21-23 March 1993.
48. Silva, M.A. and Shah, S.N.: "Frictional Pressure Correlations of Newtonian and Non-Newtonian Fluids Through Concentration and Eccentric Annuli," SPE Paper 60720 presented at the 2000 SPE/ICoTA Coiled Tubing Roundtable held in Houston, TX, 5-6 April 2000.
49. Sifferman, T.R., Myers, G.M., Haden, E.I., and Wahl, H.A.: "Drill-Cuttings Transport in Full-Scale Vertical Annuli," J. Pet Tech., Nov. 1974, p.1295-1302.
50. Johnson, V.K., and Sparrow, E.M. "Experiments on Turbulent Flow Phenomena in Eccentric Annular Ducts," J. of Fluid Mechanics, vol 25, 1966, p.65.
51. Brown, N.P., and Weaver, A.: "Cleaning Deviated Holes: New Experimental and Theoretical Studies," SPE Paper 18636 presented at the 1989 SPE/IADC Drilling Conference held in New Orleans, LA, Feb. 28-March 3, 1989.
52. Aguilera, A. et al: Horizontal Wells, Gulf Publishing Company, Houston, TX, 1991.
53. Shah, S.N., and Lord, D.L.: "Critical Velocity Correlations for Slurry Transport with Non-Newtonian Fluids," AIChE Journal Vol. 37, No. 6, June 1991, p.863-870.
54. Iyoho, A.W., Horeth II, J.M., and Veenkant, R.L.: "A Computer Model for Hole-Cleaning Analysis," JPT, September, 1988, p.1183-1192.
55. Chien, S.F.: "Settling Velocity of Irregularly Shaped Particles," SPE Paper 26121 presented at the 69<sup>th</sup> Annual Technical Conference and Exhibition held in New Orleans, Louisiana, September 25-28, 1994.
56. Chabra, R.P.: "Motion of Spheres in Power Law Fluids of Intermediate Reynolds Numbers: A Unified Approach," Chem. Eng. Process, Vol. 28, 1990, p. 89-94.
57. Shah, S.N.: "Proppant Settling Correlations for Non-Newtonian Fluids Under Static and Dynamic Conditions," Society of Petroleum Engineers Journal, April 1982, p.164-170.
58. Shah, S.N.: "Proppant-Settling Correlations for Non-Newtonian Fluids," SPE PE Nov. 1986, p. 446-448.



59. Peden, J.M. and Luo, Y.: "Settling Velocity of Various Shaped Particles in Drilling and Fracturing Fluids," SPE Paper 16243, 1987.
60. Fang, G.: "An Experimental Study of Free Settling of Cuttings in Newtonian and Non-Newtonian Drilling Fluids," SPE Paper 26125, November 1992.
61. Salama, A.I.A., and Mikula, R.J.: Suspensions: Fundamentals and Applications in the Petroleum Industry, Chapter II: Particle and Suspension, American Chemical Society, Washington DC, 1996.
62. Thomas, D.G.: "Transport Characteristics of Suspensions: Relation of Hindered Settling Floc Characteristics to Rheological Parameters," AIChE Journal, Vol. 9, 1963, p.310-316.
63. El-Samni, E.A.: Hydraulic Forces Acting on Particles in the Surface of a Stream Bed, Ph.D. Dissertation, University of California, 1949, pp.1-13.
64. Einstein, H.A., and El-Samni, E.A.: "Hydrodynamic Forces on a Rough Wall," Review of Modern Physics, Vol. 21, No. 3, 1949, p. 520-524.
65. Collins, R.E.: Flow of Fluids Through Porous Materials, Research & Engineering Consultants, Inc., Englewood, Colorado, 1990.
66. Amyx, J., Bass, D.M. Jr., and Whiting, R.L.: Petroleum Reservoir Engineering Physical Properties, McGraw-Hill Publishing Company, New York, 1988, p.36-56.
67. Aremu, K.J.: Evaluation of Shale-Drilling Fluid Interaction Using Specific Surface Area Approach, MS Thesis, The University of Oklahoma, 1998.
68. Nasr-El-Din, H.A.: Suspensions: Fundamentals and Applications in the Petroleum Industry, Chapter I: Flow of Suspension in Pipe Lines, American Chemical Society, Washington DC, 1996.
69. Shah, S.N.: Suspensions: Fundamentals and Applications in the Petroleum Industry, Chapter XI: Suspensions in Hydraulic Fracturing, American Chemical Society, Washington DC, 1996.
70. Mysels, K.J.: Introduction to Colloid Chemistry, Interscience, New York, 1959.
71. Lake, L.W.: Enhanced Oil Recovery, Prentice Hall, Englewood Cliffs, NJ, 1989, p.47-48.
72. Walton, I.C.: "Eddy Diffusivity of Solid Particles in a Turbulent Liquid Flow in a Horizontal Pipe," AIChE Journal, Vol. 41, No. 7, July 1995, p. 1815-1820.

73. Pigott, R.J.S.: "Mud Flow in Drilling," Drilling and Production Proceeding, API, Washington, DC, 941, p.91-103.
74. Hopkin, E.A.: "Factors Affecting Cuttings Removal During Rotary Drilling," JPT, June 1967, p. 807-814.
75. Doron, P., Granica, D., and Barnea, D.: "Slurry Flow in Horizontal Pipes-Experimental and Modeling," International Journal of Multiphase Flow, Vol. 13, No. 4, 1987, p.535-547.
76. Doron, P., Simkhis, M., and Barnea, D.: "Flow of Solid-Liquid Mixtures in Inclined Pipes," International Journal of Multiphase Flow, Vol. 23, No. 2, 1997, p.313-323.
77. Martin, A.L., Sa, C.H.M., Lourencs, A.M.F. and Fieire, L.G.M.: "Experimental Determination of Interfacial Friction Factor in Horizontal Drilling With a Bed of Cuttings," SPE Paper 36075 presented at the 4<sup>th</sup> Latin American and Caribbean Petroleum Engineering and Conference, Port of Spain, Trinidad, April 23-26, 1996.
78. Pilehvari, A.A., Azar, J.J., and Shirazi, S.A.: "State-of-the-Art Cuttings Transport in Horizontal Wellbores," SPE DC, Vol. 14, No. 3, September 1999.
79. Walker, S. and Li, J.: "The Effects of Particles Size, Fluid Rheology, and Pipe Eccentricity on Cuttings Transport," SPE paper 60755 presented at the 2000 SPE/ICoTA Coiled Tubing Roundtable held in Houston, TX, 5-6 April 2000.
80. Jones, T.G.J. and Hughes, T.L.: Suspensions: Fundamentals and Applications in the Petroleum Industry, Chapter X: Drilling Fluid Suspensions, American Chemical Society, Washington DC, 1996.
81. Luo, Y.J. and Bern, P.A.: "Flow-Rate Predictions for Cleaning Deviated Wells," SPE Paper 23884 presented at the 1992 IADC/SPE Drilling Conference held in New Orleans, LA, Febuary 18-21.
82. Bain, A.G. and Bonnington, S.T.: The Hydraulic Transport of Solids by Pipeline, Pergamon Press Inc., New York, 1970, p.7-32.
83. Hemphill, T. and Larsen, T.I.: "Hole-Cleaning Capabilities of Water-and Oil-Based Drilling Fluids: A Comparative Experimental Study", SPE DC, December, 1996. p.201-207.
84. Zamora, M, Jefferson, D.T., and Powell, J.W.: "Hole-Cleaning Study of Polymer-Based Drilling Fluids", SPE Paper 26329 presented at the 68<sup>th</sup> Annual Technical Conference and Exhibition of the SPE held in Houston, Texas, 3-6 October 1993.

85. North, F.K.: Petroleum Geology, Unwin Hyman, Inc. Winchester, Massachusetts, 1985, p. 132.
86. Martins, A.L., Sa, C.H.M., Lourenco, A.M.F., and Campos, W.: "Optimizing Cuttings Circulation in Horizontal Well Drilling", SPE Paper 35341 presented at the International Petroleum Conference and Exhibition of Mexico held in Villahermosa, Mexico, 5-7 March 1996.
87. Cho, H., Shah, S.N., and Osisanya, S.O.: "Selection in Optimum Coiled Tubing Drilling Parameters Through the Cuttings Bed Characterization," SPE Paper 68436 presented at the SPE/ICoTA Coiled Tubing Roundtable held in Houston, Texas, 7-8 March 2001.
88. Quigley, M.C.: "Advanced Technology for Laboratory Measurements of Drilling Fluid Friction Coefficient," SPE Paper 19537 presented at the 64<sup>th</sup> Annual Technical Conference and Exhibition held in San Antonio, TX, October 8-11, 1989.
89. Televantos, Y., Shook, C.A., Carleton, A., and Streat, M.: "Flow of Slurries of Coarse Particles at High Solids Concentrations," Canadian Journal of Chemical Engineering, Vol. 57, 1979, pp. 255-62.
90. Bagnold, R.A.: "Experiments on a Gravity-Free Dispersion of Large Solid Spheres in a Newtonian Fluid Under Shear," Proc. R. Soc. Vol. A225, 1954, pp.49-63.
91. Bird, R.B., Stewart, W.E., and Lightfoot, E.N.: Transport Phenomena, John Wiley & Sons, New York, 1976, p. 180-200.
92. Gibilaro, L.G., Felice, R.D., and Waldram, S.P.: "Generalized Friction Factor and Drag Coefficient Correlation for Fluid-Particle Interactions," Chemical Eng. Science, Vol. 40, No. 10, 1985, p. 1817-1823.
93. Cho,H., Shah, S.N., and Osisanya, O.S.: "Effects of Fluid Flow in a Porous Cuttings-Bed on Cuttings Transport Efficiency and Hydraulics," SPE Paper 71374 presented at the 2001 SPE Annual Technical Conference and Exhibition held in New Orleans, Louisiana, 30 September – 3 October 2001.
94. Doron, P and Barnea, D.: "Effect of the No-Slip Assumption on the Prediction of Solid-Liquid Flow Characteristics," Int. J. of Multiphase Flow, Vol. 18, No. 4, 1992, p. 617-622.
95. Didday, R., and Page, R: Fortran for Humans, Fourth Edition, West Publishing, New York, 1984.

96. Dodson, C.R. and Standing, M.B.: "Pressure-Volume-Temperature and Solubility Relations for Natural Gas Water Mixtures," Drilling and Production Proceeding, API (1944), 1973.
97. Perry, R.H. and Green, D.W.: Perry's Chemical Engineer's Handbook, Sixth Edition, McGraw-Hill, New York, 1984.
98. Meyer, B.R.: "Generalized Drag Coefficient Applicable for All Flow Regimes," Oil and Gas Journal, May 26, 1986, p.71-77.

## **APPENDIX A**

### **Drag Coefficient and Particle Reynolds Number**

In this appendix, particle Reynolds number and drag coefficient of a single spherical particle under static conditions are provided in detail for both Newtonian and non-Newtonian fluids.

### 1. Drag force

Two expressions may be written for the force, which act on a sphere falling at a terminal velocity  $v_p$  in a quiescent fluid of infinite extent. From Newton's second law the drag and gravitational forces deducted by buoyancy force must be equal:

$$F_D = F_G - F_B \quad (\text{A-1})$$

where

$$F_D = \frac{1}{8} C_D \rho_L v_p^2 (\pi d_p^2) \quad (\text{Drag Force}) \quad (\text{A-2})$$

$$F_G = \frac{1}{6} g_s \rho_s \pi d_p^3 \quad (\text{Gravitational Force}) \quad (\text{A-3})$$

$$F_B = \frac{1}{6} g \rho_L \pi d_p^3 \quad (\text{Buoyancy Force}) \quad (\text{A-4})$$

Rearranging Eq.(A-1) in terms of drag coefficient  $C_D$ :

$$C_D = \frac{4}{3} \frac{g d_p}{v_p^2} \left( \frac{\rho_s - \rho_L}{\rho_L} \right) \quad (\text{A-5})$$

- where,  $g$  = acceleration of gravity  
 $d_p$  = equivalent diameter of particle  
 $v_p$  = particle terminal settling velocity  
 $\rho_s$  = density of solid particle  
 $\rho_L$  = fluid density

## 2. Drag coefficient

### Newtonian fluids

Basically, the drag coefficient represents the fraction of the kinetic energy of the settling velocity that is used to overcome the drag force on the particle, while Reynolds number is a ratio between the inertial force and the viscous force of a fluid.<sup>55</sup> The particle's Reynolds number for Newtonian flow is defined as:

$$Re_p = \frac{\rho v_p d_p}{\mu_L} \quad (A-6)$$

where,  $\mu_L$  = fluid viscosity.

The drag coefficient  $C_D$  is a function of Reynolds number and is usually presented for creeping, intermediate, and turbulent regions. Three regions of flow are defined by the relevant Reynolds number as follows:

$$\text{Stokes region:} \quad Re_p < 0.1 \quad (A-7)$$

$$\text{Intermediate region:} \quad 2 < Re_p < 500 \quad (A-8)$$

$$\text{Newton region:} \quad 500 < Re_p < 2 \times 10^5 \quad (A-9)$$

In these three regions, the drag coefficients are given by Shah.<sup>57</sup>

$$C_D = \frac{24}{Re_p} \quad (\text{Stokes}) \quad (A-10)$$

$$C_D = \frac{18.5}{Re_p^{3/5}} \quad (\text{Intermediate}) \quad (A-11)$$

$$C_D \cong 0.44 \quad (\text{Newton-turbulent}) \quad (A-12)$$

### Non-Newtonian fluids

Generalized particle's Reynolds number for non-Newtonian power law is usually defined as:

$$N_{Re\ p} = \frac{\rho v_p^{2-n} d_p^n}{k} \quad (A-13)$$

The effect of viscous flow in drag coefficient and particle settling velocity with the irregular shape is quite comprehensive. Therefore, simple equations and correlation are included in this study. Similarly, the drag coefficients based on Shah's work<sup>57</sup> are given by Meyer.<sup>98</sup>

$$C_D = \frac{24X}{N_{Re\ p}} \quad (\text{Stokes}) \quad (A-14)$$

$$C_D = \left[ \frac{24}{N_{Re\ p}^{1.1}} \left( \frac{24}{N_{Re\ p}^{0.9}} X^2 + 7.5 \right) \right]^{1/2} \quad (\text{Intermediate } 0.1 < N_{Re\ p} < 100) \quad (A-15)$$

$$C_D = \frac{18.2}{N_{Re\ p}^{0.6}} \quad (\text{Intermediate } 100 < N_{Re\ p} < 500) \quad (A-16)$$

$$C_D \cong 0.44 \quad (\text{Newton } 500 < N_{Re\ p}) \quad (A-17)$$

The following boundaries are used<sup>98</sup>: when  $X < 1$  and  $n < 1$  then;

$$\text{low boundary } X = 3^{n-1} [(n+2)/3n]^n \quad (A-18)$$

when  $n > 1$  and  $X > 1$  then;

$$\text{high boundary } X = 1.0 + 0.8(1-n)^{0.7} \quad (A-19)$$

### 3. Moving bed velocity for horizontal wells

The lift force acting on a particle is a function of lift coefficient, defined as follows:



$$C_L = 5.82 \left( \frac{\alpha'_p}{N'_{Re p}} \right)^{1/2} \quad (2.25)$$

$$F_L = C_L \frac{\pi d_p^2}{8} \rho_L U^2 \quad (2.27)$$

The perpendicular distances to the line of action are defined as: (Refer to Fig. 3.3)

$$L_D = \frac{d_p}{2} \cos\left(\frac{\pi}{6}\right) \quad (A.20)$$

$$L_{Gi} = L_L = \frac{d_p}{2} \sin\left(\frac{\pi}{6}\right) \quad (A.21)$$

Substituting Eqs. A-2 – A.4, A.20, A.21, 2.25 and 2.27 for Eq. 2.28, it becomes:

$$\begin{aligned} & \frac{1}{2} \rho_L U_{mb}^2 C_D \left[ \frac{1}{4} \pi d_p^2 - \frac{1}{8} d_p^2 \left( \frac{\pi}{3} - \sin \frac{\pi}{3} \right) \left( \frac{d_p}{2} \cos \frac{\pi}{6} \right) \right] + \\ & \frac{1}{2} \rho_L U_{mb}^2 C_L \left( \frac{1}{4} \pi d_p^2 \right) \frac{d_p}{2} \sin \frac{\pi}{6} - \\ & \frac{1}{6} \pi \rho_L g d_p^3 \left[ C'_{mb} \frac{y_{mb}}{d_p} + (1 - C'_{mb}) \right] \frac{d_p}{2} \sin \frac{\pi}{6} \\ & \frac{1}{6} \pi \rho_s g d_p^3 \left[ C'_{mb} \frac{y_{mb}}{d_p} + (1 - C'_{mb}) \right] \frac{d_p}{2} \sin \frac{\pi}{6} = 0 \end{aligned} \quad (A.22)$$

Equation A.22 can be rearranged and simplified as:

$$C'_{mb} = \sqrt{\frac{0.1309(\rho_s - \rho_L) g d_p \left[ C'_{mb} \frac{y_{mb}}{d_p} + (1 - C'_{mb}) \right]}{\rho_L (0.16515 C_D + 0.0982 C_L)}} \quad (3.20)$$

The details of derivation of moving bed velocity for a horizontal segment are described in Appendix D.

## **APPENDIX B**

### **Solution of Diffusivity Equation**

Particles are held in suspension against the gravitational force by a combination of viscous resistance and diffusion by turbulent eddies. The mechanism, which governs the dispersion of the solid particle in the upper layer, is represented by the well-known diffusion equation:

$$\varepsilon_p \frac{d^2C}{dy^2} + v_p \frac{dC}{dy} = 0 \quad (\text{B.1})$$

where,  $C$  is the cuttings volumetric concentration (fraction),  $y$  is the vertical coordinate (perpendicular to the pipe axis),  $\varepsilon_p$  is the diffusion coefficient and  $v_p$  is the particle terminal settling velocity. Hindered settling velocity,  $v_h$ , is used instead of  $v_p$  in this study. Since  $\varepsilon_p$  and  $v_p$  are both constants and independent of  $y$ -coordinate, the partial derivatives in Eq. B.1 can be replaced by a total derivative and expressed as:

$$\frac{d^2C}{dy^2} + \frac{v_h}{\varepsilon_p} \frac{dC}{dy} = 0 \quad (\text{B.2})$$

Integrate Eq. B.2 with respect to  $y$ , it becomes:

$$\frac{dC}{dy} + \frac{v_h}{\varepsilon_p} C(y) = C_1 \quad (\text{B.3})$$

where  $C_1$  is a arbitrary constant. Eq. B.3 is a first order, linear ordinary differential equation with constant coefficients. The integrating factor for Eq. B.3 is:

$$\text{Int factor} = \exp \int \left( \frac{v_h}{\varepsilon_p} \right) dy = \exp \left( \frac{v_h}{\varepsilon_p} y \right) \quad (\text{B.4})$$

Multiplying Eq. B.3 with Eq. B.4, it becomes:

$$e^{(v_h/\varepsilon_p)y} \frac{dC}{dy} + e^{(v_h/\varepsilon_p)y} \frac{v_h}{\varepsilon_p} C(y) = C_1 e^{(v_h/\varepsilon_p)y} \quad (\text{B.5})$$

or

$$\frac{d}{dy} \left\{ e^{(v_h \cdot y \cdot \varepsilon_p)} C'(y) \right\} = C_1 e^{(v_h \cdot y \cdot \varepsilon_p)} \quad (\text{B.6})$$

Integrating both sides of Eq. B.6, it becomes:

$$\left\{ e^{(v_h \cdot y \cdot \varepsilon_p)} C'(y) \right\} = C_1 e^{(v_h \cdot y \cdot \varepsilon_p)} \left\{ \frac{\varepsilon_p}{v_h} \right\} + C_2 \quad (\text{B.7})$$

where C2 is another arbitrary constant. Eq. B.7 can be re-written as:

$$C'(y) = C_1 \left\{ \frac{\varepsilon_p}{v_h} \right\} + C_2 e^{-(v_h \cdot y \cdot \varepsilon_p)} \quad (\text{B.8})$$

Eq. B.8 is a general solution of Eq. B.1. In order to solve for the constants C1 and C2, the following boundary conditions are used.

$$\left| \begin{array}{l} y = D \text{ (diameter of casing)} \quad C'(y) = 0 \\ y = y_h \text{ (bed height)} \quad C'_{sd} = C'_h \end{array} \right| \quad (\text{B.9})$$

When boundary conditions are applied to the Eq. B.8, the general solutions are:

$$0 = C_1 \left\{ \frac{\varepsilon_p}{v_h} \right\} + C_2 e^{(-v_h D \cdot \varepsilon_p)} \quad (\text{B.10})$$

$$C'_h = C_1 \left\{ \frac{\varepsilon_p}{v_h} \right\} + C_2 e^{(-v_h y_h \cdot \varepsilon_p)} \quad (\text{B.11})$$

Combining Eqs B.10 and B.11 and solving for C2, it becomes:

$$C_2 = \left\{ \frac{C'_h}{e^{(-v_h y_h \cdot \varepsilon_p)} - e^{(-v_h D \cdot \varepsilon_p)}} \right\} \quad (\text{B.12})$$

Substituting Eq. B.12 for Eq. B.9, the following equation is obtained.

$$0 = C_1 \left\{ \frac{\varepsilon_p}{v_h} \right\} + \left\{ \frac{C'_h}{e^{(-v_h y_h \cdot \varepsilon_p)} - e^{(-v_h D \cdot \varepsilon_p)}} \right\} e^{(-v_h D \cdot \varepsilon_p)} \quad (\text{B.13})$$

Eq. B.13 can be re-written as:

$$C_1 \left\{ \frac{\varepsilon_p}{v_h} \right\} = \frac{C_b}{\left\{ e^{(-v_h D / \varepsilon_p)} - e^{(-v_h v_b / \varepsilon_p)} \right\}} e^{(-v_h D / \varepsilon_p)} \quad (\text{B.14})$$

Substituting Eqs B.12 and B.14 for Eq. B.8, the local cuttings volumetric concentration in the suspension layer can be expressed as:

$$C(y) = \frac{C_b}{\left\{ e^{(-v_h D / \varepsilon_p)} - e^{(-v_h v_b / \varepsilon_p)} \right\}} e^{(-v_h D / \varepsilon_p)} + \frac{C_b}{\left\{ e^{(-v_h v_b / \varepsilon_p)} - e^{(-v_h D / \varepsilon_p)} \right\}} e^{(-v_h v_b / \varepsilon_p)} \quad (\text{B.15})$$

Re-arranging Eq. B.15 will be:

$$C(y) = C_b \frac{e^{(-v_h v_b / \varepsilon_p)} - e^{(-v_h D / \varepsilon_p)}}{e^{(-v_h D / \varepsilon_p)} - e^{(-v_h v_b / \varepsilon_p)}} \quad (\text{B.16})$$

Alternately, when only the homogeneous solution of Eq. B.8 is considered, the local volume fraction of cuttings can be expressed as:

$$C(y) = C_b \exp \left\{ \frac{-v_h}{\varepsilon_p} (D - y_b) \right\} \quad (\text{B.17})$$

A negative sign of hindered settling velocity comes from the fact that the particle settling velocity has a component in the negative radial direction.

## **APPENDIX C**

### **Wellbore Geometry**

The important parameters in hydrodynamics are the heights of cuttings beds and the areas (a stationary bed and a moving bed) under the given pumping velocity with its rheological characteristics. The objective of this section is to define the relationships of wellbore geometry to eccentricity, diameter of casing and coiled tubing, and each bed height and area. Fig. C.1 illustrates the typical wellbore geometry for a three-layer flow model. This wellbore geometry also works for a two-layer flow model, in that a moving bed layer should be zero.

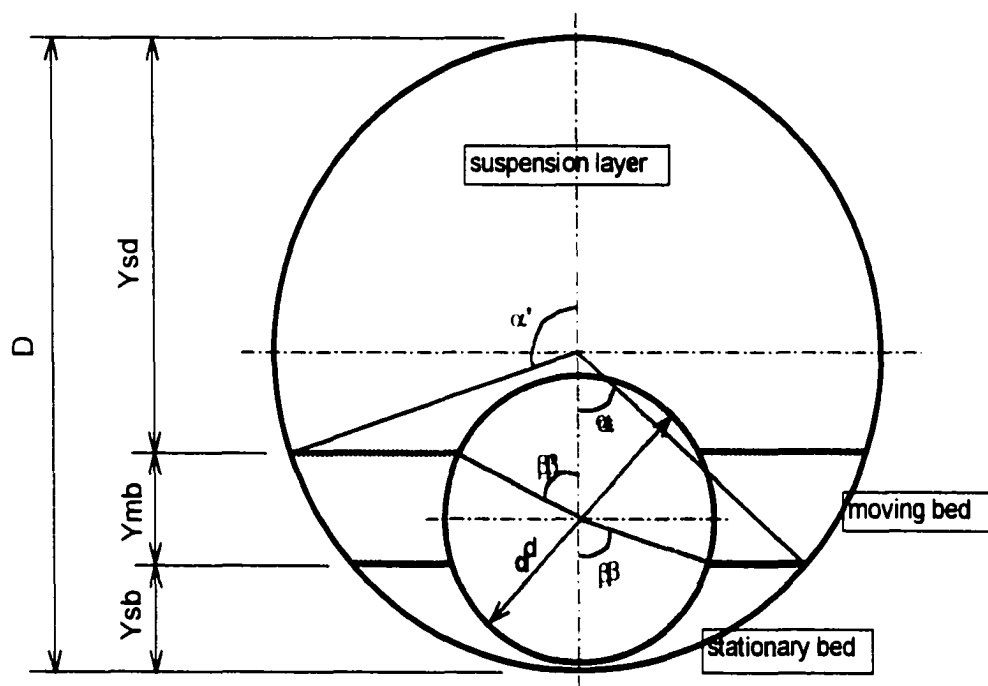


**Fig. C.1 – Typical wellbore geometry**

The angles between the center point of a wellbore and the upper contact point of a stationary bed, and the lower part of a suspension layer are defined as  $\alpha$ , and  $\alpha'$ ,

respectively. In the same manner, the angles between the center point of a coiled tubing and the upper contact point of a stationary bed, and the lower part of a suspension layer are also defined as  $\beta$  and  $\beta'$ , respectively. The following equations are developed based on those factors relationships. These equations are directly applied to the iterative calculation for the model solution.

***For Stationary Bed:***

**Case 1)**  $y_{sb} \leq \frac{d}{2}$

$$\cos \alpha = \left( \frac{D}{2} - y_{sb} \right) \frac{2}{D} \quad (\text{C.1})$$

$$\alpha = \cos^{-1} \left( \frac{D - 2y_{sb}}{D} \right) \quad (\text{C.2})$$

$$\cos \beta = \frac{d - 2y_{sb}}{d} \quad (\text{C.3})$$

$$\beta = \cos^{-1} \left( \frac{d - 2y_{sb}}{d} \right) \quad (\text{C.4})$$

$$y_{sb} = \frac{D}{2}(1 - \cos \alpha) = \frac{d}{2}(1 - \cos \beta) \quad (\text{C.5})$$

$$A_{sb} = \frac{D^2}{8}(2\alpha - \sin 2\alpha) - \frac{d^2}{8}(2\beta - \sin 2\beta) \quad (\text{C.6})$$

$$S_{sb} = D\alpha + d\beta \quad (\text{C.7})$$

**Case 2)**  $\frac{d}{2} < y_{sb} \leq d$

$$\cos \alpha = \frac{D - 2y_{sb}}{D} \quad (\text{C.8})$$



$$\alpha = \cos^{-1}\left(\frac{D - 2Y_{sb}}{D}\right) \quad (\text{C.2})$$

$$\cos(\pi - \beta) = \frac{2y_{sb} - d}{d} \quad (\text{C.9})$$

$$\beta = \pi - \cos^{-1}\left(\frac{2y_{sb} - d}{d}\right) \quad (\text{C.10})$$

$$y_{sb} = \frac{D}{2}(1 - \cos\alpha) = \frac{d}{2}\{1 + \cos(\pi - \beta)\} \quad (\text{C.11})$$

$$A_{sb} = \frac{D^2}{8}(2\alpha - \sin 2\alpha) - \frac{\pi d^2}{4} + \frac{d^2}{8}\{2\pi - 2\beta - \sin(2\pi - 2\beta)\} \quad (\text{C.12})$$

$$S_{sb} = D\alpha + d\beta \quad (\text{C.13})$$

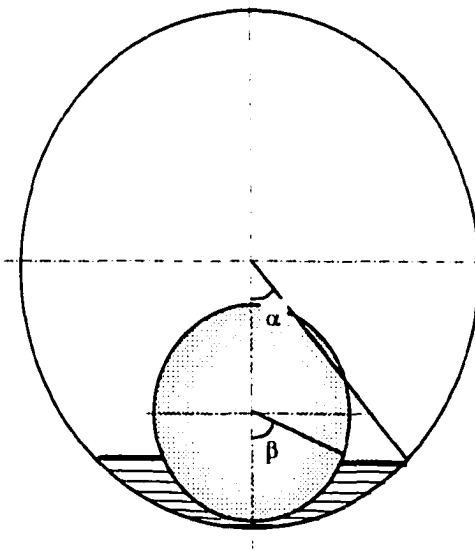


**Fig. C.2 – Stationary bed case 1**

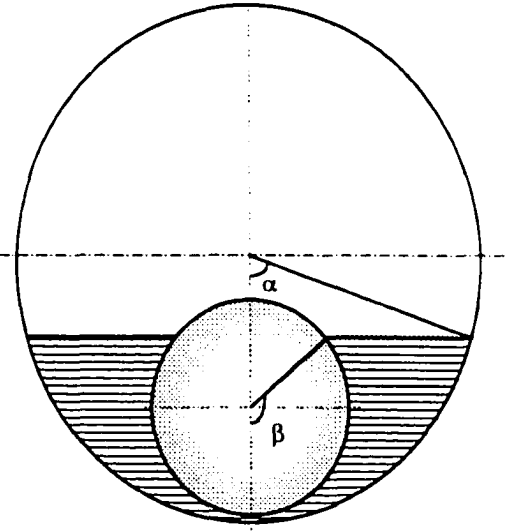


**Fig. C.3 – Stationary bed case 2**

$$\textbf{Case 3)} \quad d < y_{sb} \leq \frac{D}{2}$$

$$\cos \alpha = \frac{D - 2y_{sb}}{D} \quad (\text{C.8})$$

$$\alpha = \cos^{-1} \left( \frac{D - 2y_{sb}}{D} \right) \quad (\text{C.2})$$

$$y_{sb} = \frac{D}{2} (1 - \cos \alpha) \quad (\text{C.14})$$

$$A_{sb} = \frac{D^2}{8} (2\alpha - \sin 2\alpha) - \frac{\pi d^2}{4} \quad (\text{C.15})$$

$$S_{sb} = D\alpha + d\pi \quad (\text{C.16})$$

$$\textbf{Case 4)} \quad \frac{D}{2} \leq y_{sb}$$

$$\cos(\pi - \alpha) = \frac{2y_{sb} - D}{D} \quad (\text{C.17})$$

$$\alpha = \pi - \cos^{-1} \left( \frac{2y_{sb} - D}{D} \right) \quad (\text{C.18})$$

$$y_{sb} = \frac{D}{2} \{1 + \cos(\pi - \alpha)\} \quad (\text{C.19})$$

$$A_{sb} = \frac{\pi D^2}{4} - \frac{D^2}{8} \{2\pi - 2\alpha - \sin(2\pi - 2\alpha)\} - \frac{\pi d^2}{4} \quad (\text{C.20})$$

$$S_{sb} = D\alpha + d\pi \quad (\text{C.21})$$

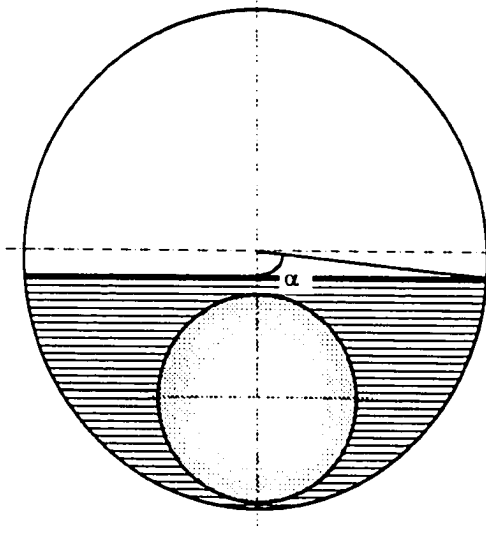


**Fig. C.4 – Stationary bed case 3**

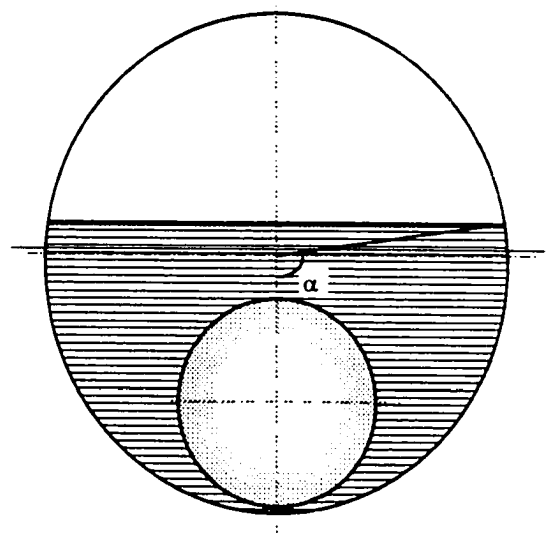


**Fig. C.5 – Stationary bed case 4**

*For Suspension layer:*

**Case 1)**  $y_{sh} \leq \frac{D}{2}$

$$\cos \alpha' = \frac{D - 2y_{sd}}{D} \quad (C.22)$$

$$\alpha' = \cos^{-1} \left( \frac{D - 2y_{sd}}{D} \right) \quad (C.23)$$

$$y_{sd} = \frac{D}{2} (1 - \cos \alpha') \quad (C.24)$$

$$A_{sd} = \frac{D^2}{8} (2\alpha' - \sin 2\alpha') \quad (C.25)$$

$$S_{sd} = D\alpha' \quad (C.26)$$

$$S_{sdmb} = D \sin \alpha' \quad (C.27)$$

**Case 2)**  $\frac{D}{2} < y_{sd} \leq (D - d)$

$$\cos(\pi - \alpha') = \frac{2y_{sd} - D}{D} \quad (\text{C.28})$$

$$\alpha' = \pi - \cos^{-1}\left(\frac{2y_{sd} - D}{D}\right) \quad (\text{C.29})$$

$$y_{sd} = \frac{D}{2} \{1 + \cos(\pi - \alpha')\} \quad (\text{C.30})$$

$$A_{sd} = \frac{\pi D^2}{4} - \frac{D^2}{8} \{2\pi - 2\alpha' - \sin(2\pi - 2\alpha')\} \quad (\text{C.31})$$

$$S_{sd} = D\alpha' \quad (\text{C.32})$$

$$S_{sdmb} = D \sin(\pi - \alpha') \quad (\text{C.33})$$

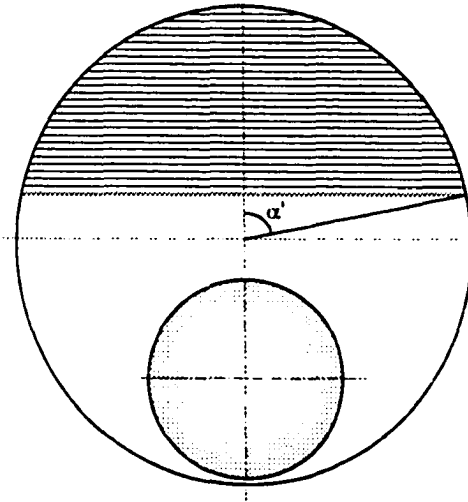


**Fig. C.6 – Suspension layer case 1**

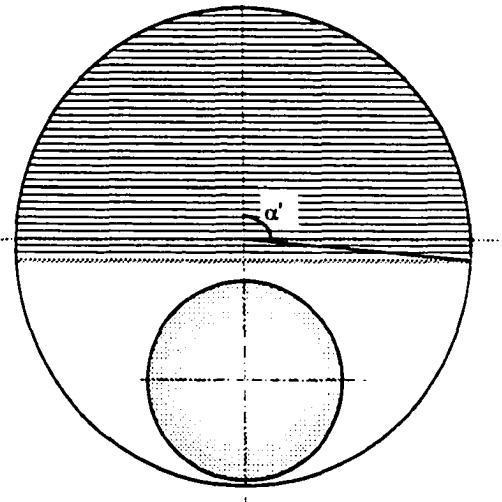


**Fig. C.7 – Suspension layer case 2**

$$\textbf{Case 3)} \quad (D-d) < y_{sd} \leq \left(D - \frac{d}{2}\right)$$

$$\cos(\pi - \alpha') = \frac{2y_{sd} - D}{D} \quad (\text{C.28})$$

$$\alpha' = \pi - \cos^{-1}\left(\frac{2y_{sd} - D}{D}\right) \quad (\text{C.29})$$

$$\cos(\pi - \beta') = \frac{D - y_{sd} - d/2}{d/2} \quad (\text{C.34})$$

$$\beta' = \cos^{-1}\left(\frac{2D - 2y_{sd} - d}{d}\right) \quad (\text{C.35})$$

$$y_{sd} = \frac{D}{2} \{1 + \cos(\pi - \alpha')\} = D - \frac{d}{2} (1 + \cos \beta') \quad (\text{C.36})$$

$$A_{sd} = \frac{\pi D^2}{4} - \frac{D^2}{8} \{2\pi - 2\alpha' - \sin(2\pi - 2\alpha')\} - \frac{d^2}{8} (2\beta' - \sin 2\beta') \quad (\text{C.37})$$

$$S_{sd} = D\alpha' + d\beta' \quad (\text{C.38})$$

$$S_{sdb} = D\sin(\pi - \alpha') - d\sin \beta' \quad (\text{C.39})$$

$$\textbf{Case 4)} \quad D - \frac{d}{2} < y_{sd} \leq D$$

$$\cos(\pi - \alpha') = \frac{2y_{sd} - D}{D} \quad (\text{C.28})$$

$$\alpha' = \pi - \cos^{-1}\left(\frac{2y_{sd} - D}{D}\right) \quad (\text{C.29})$$

$$\cos(\pi - \beta') = \frac{y_{sd} - D + d/2}{d/2} \quad (\text{C.40})$$

$$\beta' = \pi - \cos^{-1}\left(\frac{2y_{sd} - 2D + d}{d}\right) \quad (\text{C.41})$$

$$y_{sd} = \frac{D}{2} \{1 + \cos(\pi - \alpha')\} \quad (C.42)$$

$$A_{sd} = \frac{\pi D^2}{4} - \frac{D^2}{8} \{2\pi - 2\alpha' - \sin(2\pi - 2\alpha')\} - \frac{\pi d^2}{4} + \frac{d^2}{8} \{2\pi - 2\beta' - \sin(2\pi - 2\beta')\} \quad (C.43)$$

$$S_{sd} = D\alpha' + d\beta' \quad (C.44)$$

$$S_{imb} = D \sin(\pi - \alpha') - d \sin(\pi - \beta') \quad (C.45)$$

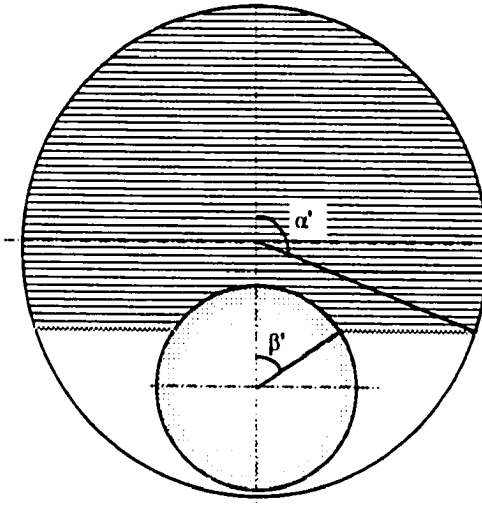


**Fig. C.6 – Suspension layer case 3**

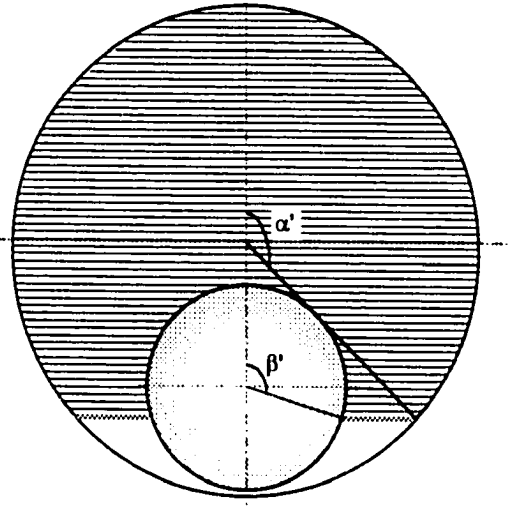


**Fig. C.7 – Suspension layer case 4**

## **APPENDIX D**

### **Derivation of Minimum Moving Bed Velocity for Horizontal Segment**

The moment, due to forces summed around acting point “A”, is described in the following equation.

$$F_D L_D - (F_G - F_B) L_G + F_L L_L \geq 0 \quad (4.5)$$

where,  $F_D$  is drag force,  $F_L$  is lift force,  $F_G$  is the gravitational force, and  $F_B$  is the buoyancy force.  $L$  with different subscript is the length of each forces acting on the particle. The cutting will move up into the suspension region when the fluid velocity is higher enough to move up cutting from the bed due to the lift force. In the case of lifting, the radial forces in the radial direction gives:

$$F_L \sin \theta - F_G + F_B \geq 0 \quad (D.1)$$

The drag force,  $F_D$ , is exerted by the surrounding medium (the moving bed layer):

$$F_D = \frac{1}{2} \rho_L U_{mb}^2 C_D A_p \quad (D.2)$$

where  $\rho_L$  is the density of the carrier fluid,  $U_{mb}$  is the minimum moving bed velocity,  $C_D$  is the drag coefficient for the particle.  $A_p$  is the area upon which the drag force acts, i.e., the projection of the particle's exposed area onto a plane, normal to the flow direction.

$$A_p = \frac{1}{4} \pi d_p^2 - \frac{1}{8} d_p^2 \left( \frac{\pi}{3} - \sin \frac{\pi}{s} \right) \quad (D.3)$$

The momentum balance is acted on the contact point of the particle and it's neighbors in the downstream direction denoted, “A” in Figure D.1. Hence, the perpendicular distance from the line of action of this force through point “A” is:

$$L_D = \frac{d_p}{2} \cos \left( \frac{\pi}{6} \right) \quad (D.4)$$

The drag force in Eq. D.2 can be re-written as:



$$F_D = \frac{1}{2} \rho_L U_{mb}^2 C_D \left\{ \frac{\pi}{4} d_p^2 - \frac{1}{8} d_p^2 \left[ \frac{\pi}{3} - \sin \left( \frac{\pi}{3} \right) \right] \right\} \quad (D.5)$$

The opposing moment is due to the normal force exerted by the column of particles lying above the particle. The average number of solid particles whose weight is to be considered is:[32]

$$N = C_{mb} \frac{y_{mb} - d_p}{d_p} \sin \theta \quad (D.6)$$

where,  $y_{mb}$  is the height of the moving bed layer and  $C_{mb}$  is the moving bed concentration.

The submerged weight of a particle is:

$$W_p = \frac{1}{6} \pi (\rho_p - \rho_L) g d_p^3 \quad (D.7)$$

where  $g$  is the gravitational acceleration,  $\rho_p$  and  $\rho_L$  are particle density and fluid density respectively. The normal force due to gravitational force and buoyancy force is:

$$F_G - F_B = W_p \left( C_{mb} \frac{y_{mb}}{d_p} \sin \theta \right) \quad (D.8)$$

The acting distance,  $LG$ , for both the gravitational force and buoyancy force can be calculated from the descriptive geometry shown in Fig. D.1.

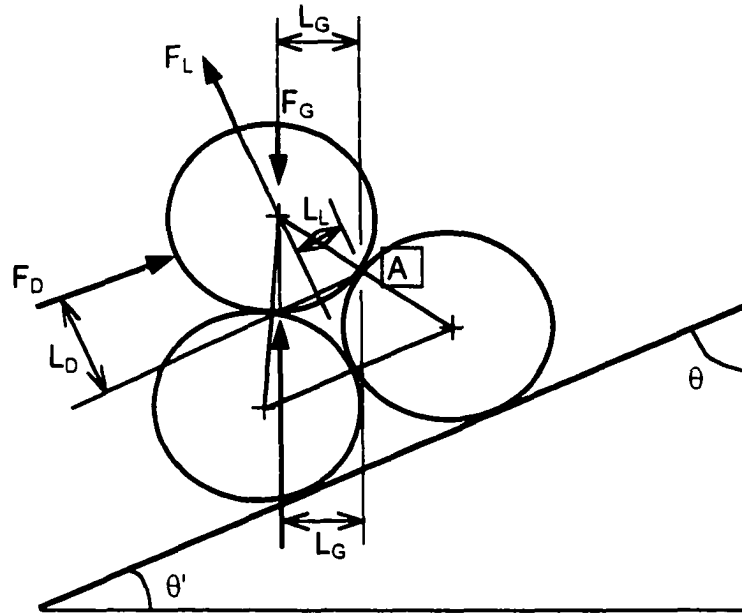


**Fig. D.1 – Forces acting on a particle**

$$L_G = \frac{d_p}{4} \left[ 1 + 2 \sin\left(\frac{\pi}{3}\right) \tan \theta' \right] \sin \theta \quad (\text{D.9})$$

The lift force can be obtained as:

$$F_L = \frac{1}{2} \rho_L U_{mb}^2 C_L A_p' \quad (\text{D.10})$$

where  $A_p'$  is the projection area of the particle. It is assumed that the cutting is a sphere

for this calculation. The projection area of a sphere,  $A_p'$ , is:

$$A_p' = \frac{\pi}{4} d_p^2 \quad (\text{D.11})$$

The acting distance for lift force,  $L_L$ , can be calculated from Fig. D.1..

$$L_L = \frac{d_p}{4} \quad (\text{D.12})$$

The minimum moving bed velocity can then be calculated by equating the driving torque and the opposing torque, specified in Eq. 4.5. Each part of this equation is described below.  $FDLD$  is:

$$\frac{1}{2}\rho_L U_{mb}^2 C_D \left[ \frac{\pi}{4} d_p^2 - \frac{1}{8} d_p^2 \left( \frac{\pi}{3} - \sin \frac{\pi}{s} \right) * \frac{d_p}{2} \cos \left( \frac{\pi}{6} \right) \right] = 0.1651 \rho_L U_{mb}^2 C_D d_p^3 \quad (D.13)$$

The term of  $(F_G - F_B)L_G$  is:

$$\begin{aligned} \frac{1}{6}\pi(\rho_c - \rho_L)gd_p^3 \left[ C_{mb} \frac{y_{mb}}{d_p} \sin \theta \right] * \frac{d_p}{4} \left[ 1 + 2 \sin \left( \frac{\pi}{3} \right) \tan \theta' \right] \sin \theta = \\ 0.131(\rho_c - \rho_L)gd_p^3 \left[ C_{mb} \frac{y_{mb}}{d_p} \sin \theta \right] [1 + 1.732 \tan \theta'] \sin \theta \end{aligned} \quad (D.14)$$

$$\text{The term of } F_L L_L \text{ is: } \frac{1}{2}\rho_L U_{mb}^2 C_L \frac{\pi}{4} d_p^2 * \frac{d_p}{4} = 0.0982 \rho_L U_{mb}^2 C_L d_p^3 \quad (D.15)$$

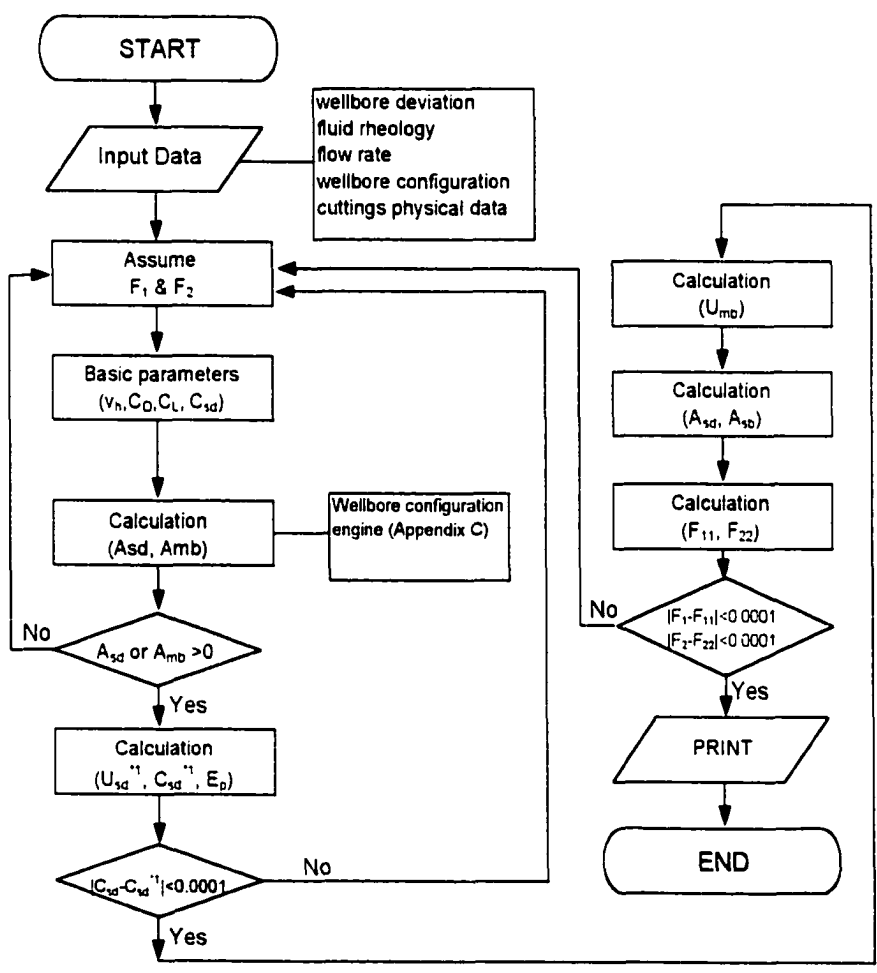
Combining Eqs. D.13, D.14, and D.15 and solving for  $U_{mb}$ , it becomes:

$$U_{mb} = \sqrt{\frac{0.131(\rho_s - \rho_L)g \left[ C_{mb} \frac{y_{mb}}{d_p} \sin \theta \right] [1 + 1.732 \tan \theta'] \sin \theta}{\rho_L (0.1651 C_D + 0.0982 C_L)}} \quad (4.6)$$

## **APPENDIX E**

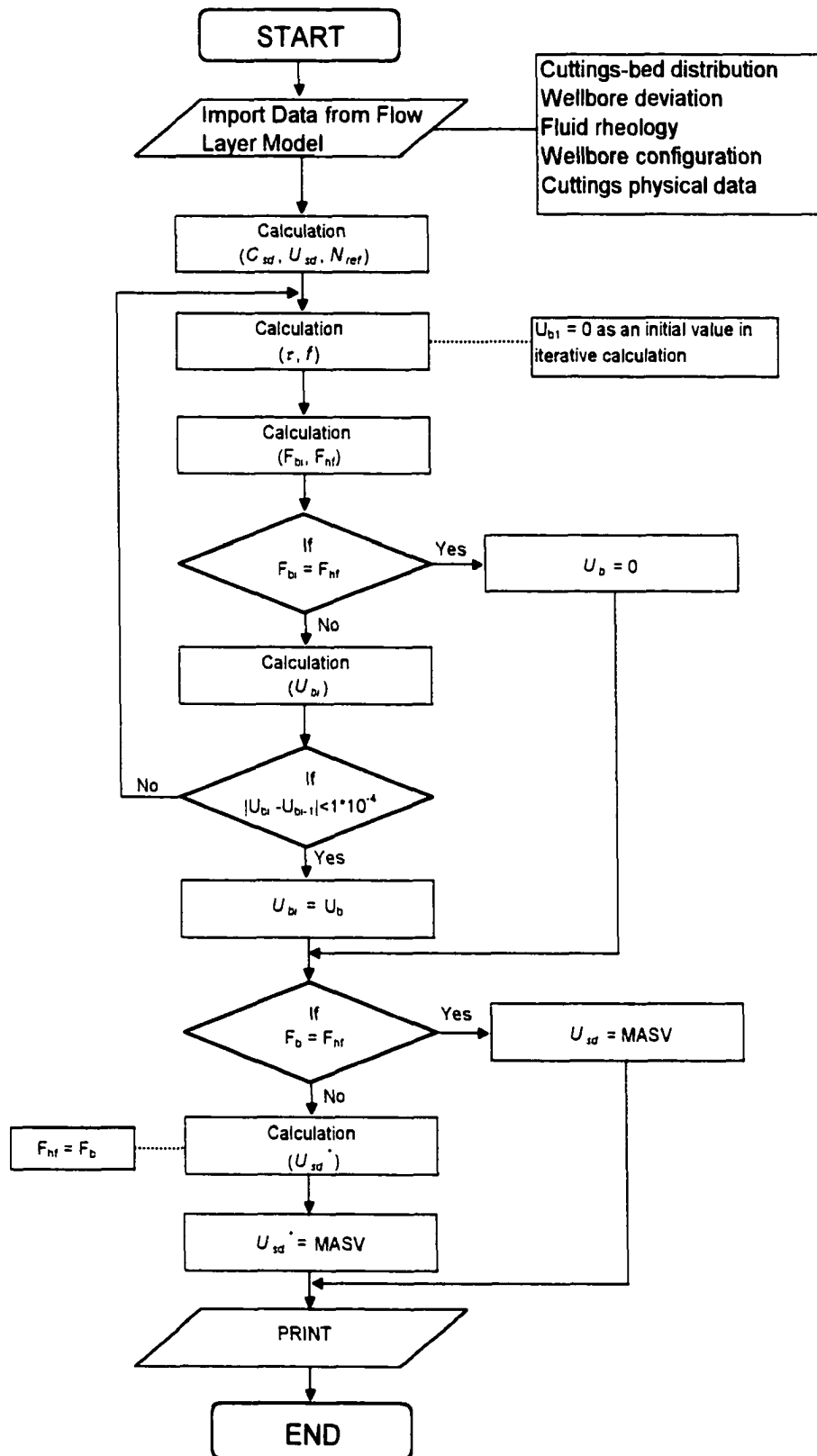
### **Hierarchy Chart to Solve Cuttings Bed Distribution**

# Hierarchy chart to solve cuttings bed distribution



## **APPENDIX F**

### **Hierarchy Chart for the Calculation of a Cuttings-bed Velocity and its Minimum Anti-Sliding Velocity**



## **APPENDIX G**

### **Hierarchy Chart to Estimate Frictional Pressure Losses**



# Hierarchy chart for the calculation of pressure gradient

